Application of Instrumental Analysis Methods to Characterisation of Monoclonal Antibody-Based
Formulations

A thesis submitted to the University for the degree of Doctor of Philosophy

2019

Research School of Biosciences

Application of Instrumental Analysis Methods to Characterisation of Monoclonal Antibody-Based Formulations

Declaration

No part of this thesis has been submitted in support of any other application for a degree of qualification of the University *** or any other University of institute of learning

………

……………
Date

Abstract

Monoclonal antibodies (mAbs) are a dominant class of protein-based drugs used in multiple therapeutic contexts. These drugs have revolutionised the management of a number conditions and are positioned as an important strategy in tailored pharmaceutical approaches (targeted therapy) for immunomodulation and oncological management. The *in vivo* formulation of proteins, including antibodies, is a complex process tightly regulated through environmental factors and homeostatic mechanisms. Reproduction of these conditions is essential during *ex vivo* manufacture of mAbs to ensure the stability of proteins and to prevent aggregation, which may impact on the efficacy of the agent in biological tissue. Among these environmental factors, temperature pH, buffer characteristics, and the use of excipients, including salts, sugars, surfactants and amino acids are of paramount importance. The focus of the present paper was to provide an overview of contemporary literature, with a focus on key studies performed by the author and colleagues, focusing on how excipient use and instrumental monitoring of stability and aggregation in mAbs could have the potential to influence future drug design and protein formulation practice.

Analysis of the data set suggested that the regulation of these features during the formulation of mAbs is a complex process and there is a need to ensure that all processes within the manufacture of mAbs are controlled according to the relevant environmental factors influencing protein stability and aggregation. This paper highlights the use of adherent and non-adherent cell lines to investigate the ability of excipients to maintain mAb stability. The specific excipients analysed including amino acids (arginine and glutamate), and combinations/comparison of ionic excipients in solution, pH and dynamics of solutions, including protein-protein interactions, concentrations and agglomeration. It was demonstrated in these studies that excipients have specific and contrasting effects on mAb stability and aggregation potential. Furthermore, characterisation of the effects of excipients and formulation techniques provided a key insight into the role of these factors in maintaining mAb stability, while instrumental techniques were evaluated during the characterisation of stability and agglomeration in a variety of contexts.

The majority of this paper reflects the culmination of six published papers, in which the author has actively participated, focusing on the application of instrumental analysis methods to the characterisation of mAb formulations. These studies highlight a broad range of techniques used to characterise protein formulations and which may be applied to mAbs, including nuclear magnetic resonance (NMR) spectroscopy and orthogonal techniques. Characterisation of the size of protein/mAb aggregates has been demonstrated, with pharmaceutical relevance, including in the design of pro-drugs. Furthermore, key characteristics of mAb formulation, stability and aggregation have been characterised

using multiple models, providing a comprehensive insight into this topic. The included studies indicate that additives that disrupt protein-protein interactions and prevent aggregation can influence mAb stability and that the stabilisation characteristics of these proteins can be measured using instrumental techniques. These studies have clear implications for the use of instrumental analysis in the development of therapeutic mAbs, highlighting the need for further research in this field, including further investigation of the value of NMR spectroscopy and orthogonal techniques.

Acknowledgements

I would like to express my sincere gratitude to Professor Mark Smales for his amazing support, guidance and patience during the writing of this thesis. He has pushed me to be able to achieve a qualification that I thought was past me.

I would like to express a huge thank you to all the academic PI's and co-authors of the papers that form the basis of this thesis. They have all been amazing and it's been a wonderful scientific journey with them in the quest of enhancing formulation knowledge.

Thank you for all supporting my application for this degree.

Final thanks go to family and friends for their support, help and encouragement. Thank you!

Contents

Table of Figures

1.0 Background to the Thesis

This thesis is submitted for consideration based upon a track record of work and publication over a period of time around the broad area of stabilising biotherapeutic protein formulations destined for use in the clinic to treat a range of diseases. The papers put forward for consideration under this, and the contributions I made to each of these studies, are as follows (full versions of the papers are included in Appendix A);

1. "*Characterizing monoclonal antibody formulations in arginine glutamate solutions using ^1H NMR spectroscopy*" by Kheddo and co-workers (Kheddo, et al., 2016)
Candidates Contribution: I initiated the project and was one of the main industrial supervisors for this project. NMR is a unique innovative technique that has not been fully utilised for full antibodies. Work was directed from a formulation standpoint by myself to understand the impact of the technique as well as impact of the Arg-Glu formulation. Study design, student supervision, data decision, and research direction as well as manuscript review was carried out by me.

2. *"The effects of arginine glutamate, a promising excipient for protein formulation, on cell viability: Comparisons with NaCl"* by Kheddo and co-workers (Kheddo, et al., 2016)
Candidates Contribution: My group is always on the lookout for novel excipients. This research explored arg-glu as a novel stabilising excipient. I drove the research application from a formulation perspective, directing, supervising, teaching the student. The awareness and direction also related to the academic PI, the science behind formulation and stability. Student was additionally supervised by myself in my lab at MedImmune.

3. "*Characterisation of Stress-Induced Aggregate Size Distributions and Morphological Changes of a Bi-Specific Antibody Using Orthogonal Techniques*" by Hamrang and co-workers (Hamrang, et al., 2015, p. 2473)
Candidates Contribution: Supervised the student from an industrial perspective. Making the student and academic PI aware of the impact of their research and relevance. The direction included, study design, data interrogation, manuscript review as well future study requirements.

4. "*Controllin the bioactivity of a peptide hormone in vivo by reversible self-assembly"* by Myriam M. Ouberai and co-workers (Ouberai et al., 2017)
Candidates' contribution: student was guided on different ways through which bioactivity of peptide hormones can be controlled from a laboratory point of view. Use of peptides with hopes of developing

a new drug with high levels of efficacy and safety was explained. Through in-depth experiments, the student was in a good position to understand every aspect and was guided in the laboratory which enhanced clear understanding of different concepts.

5. "*The effect of protein concentration on the viscosity of a recombinant albumin solution formulation*" by Goncalves and co-workers (Goncalves, et al., 2013, p. 1)

Candidates Contribution: Primary industrial supervisor for this project. Again directed the research in relation to its applicability to the formulation sector. Direction of project ranged from study design, data interpretation and interrogation, presentation and manuscript review and approval. Student was also supervised in my lab, which required hands-on support as well as direction.

6. "*A pH-Induced Switch in Human Glucagon-like Peptide-1 Aggregation Kinetics*" by Zapadka and co-workers (Zapadka, et al., 2016).

Candidates Contribution:

Evidence to confirm my contribution is provided in Appendix B, which includes an email from the corresponding author of each paper outlining their interpretation of my contribution. These were obtained independent from myself and by my academic supervisor for this thesis. The remainder of this thesis provides a general introduction to the area of formulation sciences and developments within this and then explains the findings of each of the papers above. A general discussion is then provided that attempts to place the findings of these studies in the wider context of the primary literature. The papers to be considered towards this PhD submission are all provided in full in Appendix A.

1.1 General Introduction to Monoclonal Antibodies

Monoclonal antibodies (mAb) are of paramount importance in modern biomedical research and for the treatment of an ever-widening number of diseases (Clark & Pazdernik, 2015, p. 74). These reagents are employed during diagnosis of diseases as well as in treatment of cancer, autoimmune diseases, rheumatoid arthritis and other diseases and infections. Monoclonal antibodies can be characterised as antibodies generated from a single cell line or a single clone, forming identical antibody molecules. A schematic diagram of an antibody is presented in Figure 1.1 below.
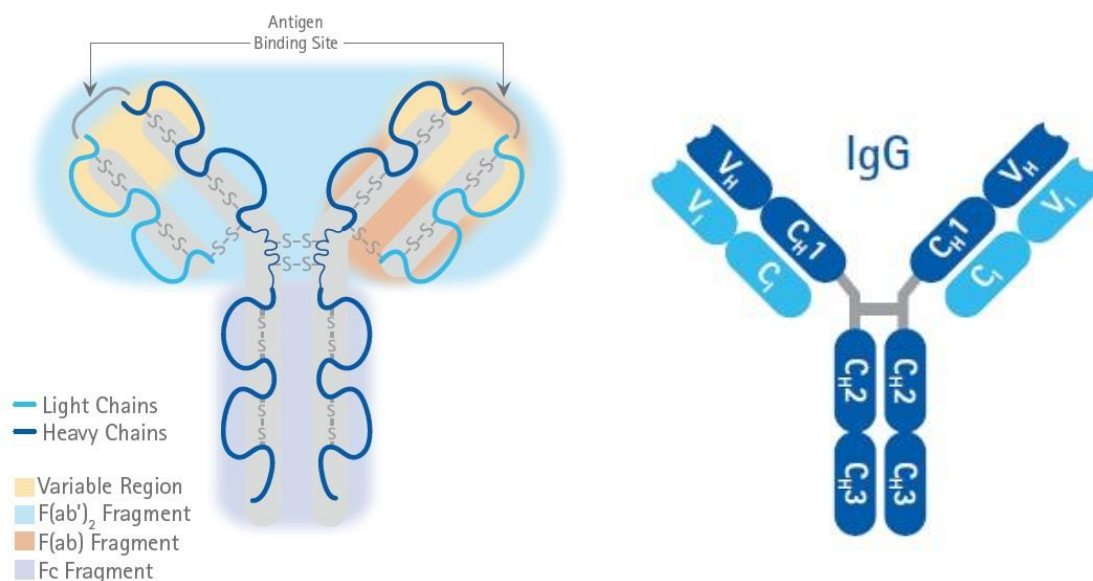
Figure 1.1: Antibody structure. Schematic representation of an antibody (left) and immunoglobulin G (right), adapted from (Merck KGaA, 2015, p. 9)

The use of mAbs in biomedical research has proven to be important in providing reagents for the identification of nucleic acids, proteins, carbohydrates as well as other biologically active molecules in numerous basic science studies. Application of mAbs in biomedical investigations has resulted in the identification of molecules that control replication of cells, differentiation processes and advanced general knowledge in the corresponding relationship between structures of biologically active molecules and their functions (Weiner et al., 2010, p.317). Such advances in biological sciences have improved our understanding of host responses to toxins and disease agents, to tumours (spontaneously transformed cells), to transplanted tissues and organs and to autoimmunity forming molecules.

Formulation development is vital in proteins as it ensures excellent stability, supporting chemical and physiochemical process. Also, biologics are susceptible to structural instabilities due to their complex structure and also being very sensitive to environmental factors. Each protein is distinct in its way. Therefore, this makes it hard for them to guess or have an optimum formulation condition. Any structural perpetration can also disrupt proteins causing it to lose its biological activity or even immunological response. This phenomenon can be experienced when or during the production, storage,

transportation and its delivery to patients. There are several conditions one has to consider when developing optimum formulation conditions. These conditions or factors might include:

- Protein concentration
- Delivery options
- Container or closure systems
- Stresses
- Lyophilization involves freeze-drying or freezing the product, lowering its pressure and later removing the ice through sublimation
- Stability indicating assays
- Degradation pathways

Proteins formulation is a critical step which is overly overshadowed and can easily hinder drugs development. Many developers do not take into consideration the amount of time needed to formulate and can result in a diminished product and choosing too long might as well hinder the ability of the drug to make it to the market before completion. Failure to understand the protein properties thoroughly and nature will delay the formulation and result in poor results from the start, resulting in a commodity not fit for commercialization. As a way of formulating a drug, some responsibilities need to be adhered to develop a viable drug that is clinically and commercially viable. Drugs require at least two years of shelf life, some requiring as long as three years, 100-150 mg/ml for RIA with lower concentrations being okay for oncology, requires high potent immunotherapy, and mostly required as a liquid for RIA with lyophilized drugs mostly recommended for oncology. For a product or a prescription to be commercially viable, there must be a formulated and appropriate way or mode of delivery and their presentations should be specified by TPPs like vials and other devices. The drug should then have a manufacturing process and plans for clinical trials.

Biopharmaceutical technology is a new model of drug development that has led to the shifting of drug development from small molecule to abundant molecules proteins. The drugs have caused a shift in diseases to cure enhancing the quality of health and life in general, more so to patients with diseases like refractory cancer, and other autoimmune diseases. Since USFDA approved the first biopharmaceutical product in 1982, the number of products has increased rapidly with monoclonal antibodies like zenapax and proleukin being introduced in successive years. However, production is very stressful; the process involves several processes that are critical a very time-consuming. From fermentation, purification and harvesting, the methods are time-consuming and very expensive. The procedures are usually therapeutic recombinant proteins that are obtained through biotechnological process. There is anticipation that in the ten years, 50% of all drugs produced will involve the process biopharmaceuticals. The method of purification involves cation exchange, anion exchange,

Nanofiltration and concentration and diafiltration from where the products are primarily harvested. This consists in isolating the product from microorganisms, making the product and finding a viable patient, putting the product in the patient and learning how the patient reacts to the product, if the product cures the particular problem the patient was suffering from, full development is then met, and the product is put on sale. The whole process can take from 10-15 years before completion, requiring substantial investment.

Lead identification is one of the vital processes during drug development. The process is also called lead optimization. Chemical properties of lead are used in improving potency, pharmacokinetics, and selectivity parameters of the developing drug. Once the molecule has been identified, its adsorption, distribution, metabolism, excretion and toxicity properties are determined. If the product has no toxicity or is not mutagenic, it can be used as a lead molecule. Therefore, a leading compound or a lead compound is a biologically or pharmacological activity is likely to have a therapeutic effect but maybe having suboptimal structure requiring a modification that will make it better fit for the target. For a lead compound with the developmental focus to be selected, it must be chemically stable and PTMs, be able to form solutions and also have physical stability. Chemical stability is in the form of colloidal, conformational and interfacial stabilities. Selecting a lead compound that has both the properties of functionality and the developmental compound is not easy as the collaborative approach witnessed between R and D is very critical for its success. Finally, developmental screening is essential as it enables one to select a better drug candidate. This is achieved by identifying molecules that have optimal functional and biophysical characteristics and having platforms with compatible leads. Developability screening is performed in lead candidates before evaluation of preclinical evaluation.

In addition to the outlined features, the exquisite specificity of monoclonal antibodies allows their application in disease diagnosis and treatment, encountered in both humans and animals. Animals are widely employed in the production of monoclonal antibodies. It was established that under adequate production conditions, mAb-generating hybridomas are able to survive indefinitely. For this reason, continuous production of monoclonal antibodies is associated with reducing the number of required animals during *in vitro* experiments. Nevertheless, despite current advancements in the production of monoclonal antibodies, current methods can be highly distressing to host animals, underlying the necessity of optimising mAb production technologies (Yamada, et al., 2017, p. 111) (Santos & Galvao, 2017, p. 696).

Alfaleh and co-workers describe how mAbs can be effectively generated with the aid of phage display technology (Alfaleh, et al., 2017, p. 2). This method of generating mAbs was initially described in 1985 by G. Smith (Smith, 1985, p. 1315). Currently, phage display technology is a powerful technique for displaying required peptides or proteins on filamentous phage through the utilisation of a viral coat

protein. It was found that each phage clone corresponding to an antibody phage library displayed a specific antigen-binding site. This site was formed by random combinations of both light and heavy chain variable fragments, produced through cloning from B-cell pools. A range of binding entities, including Fab (Fragment antigen binding), scFv (single-chain variable domain), VL (variable light chain regions), VH (Variable heavy chain regions) as well as a series of peptides that could be employed in the production of novel biopharmaceuticals were isolated from the described phage display libraries. The indicated antibody regions are summarised in the figures 1.2 and 1.3 below:
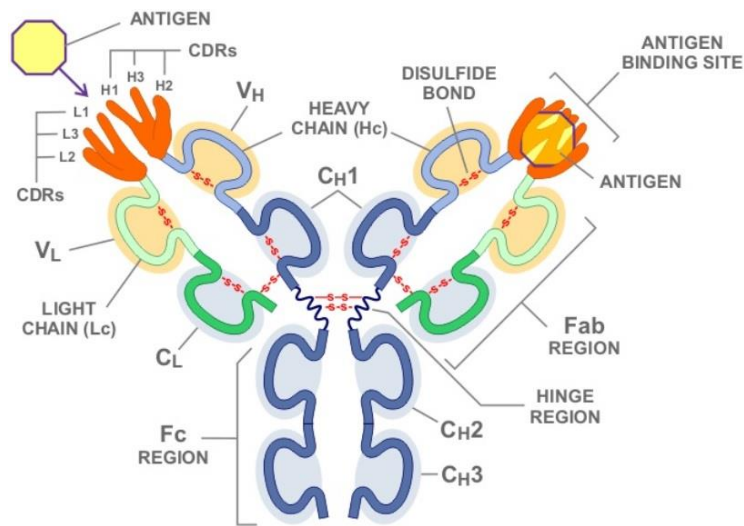
Figure 1.2: Antibody Fab region. Fragment antigen binding (Fab region) in antibodies, adapted from (Merck KGaA, 2015, p. 10)
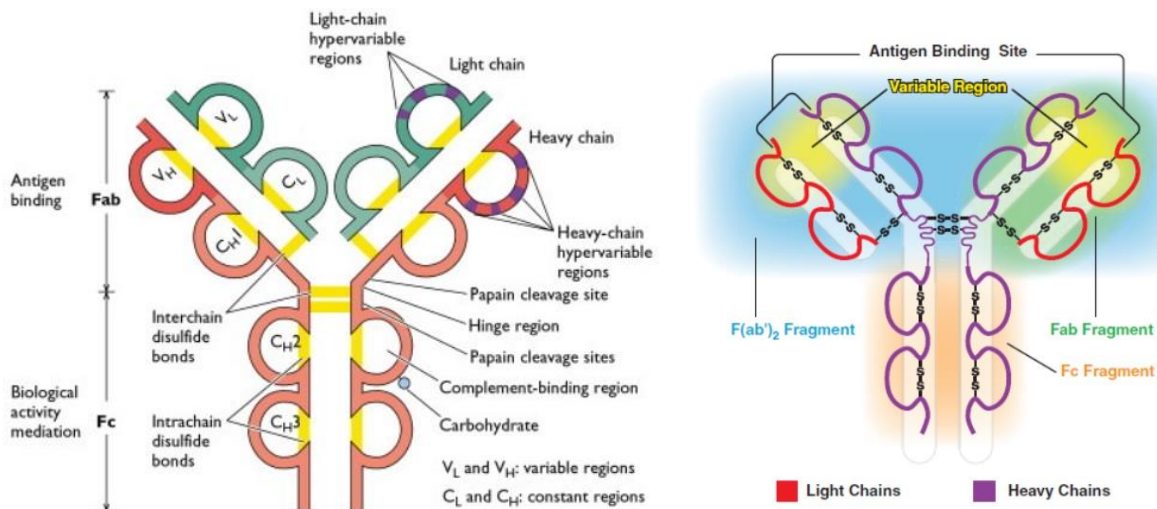
Figure 1.3: Additional antibody structures. scFv (single-chain variable domain), VL (variable light chain regions), VH (Variable heavy chain regions) in antibodies, adapted from (Merck KGaA, 2015, p. 17)

Antibody phage libraries are based on mRNA that was extracted from natural sources, including bone marrow, the spleen or peripheral lymphocytes. Alternatively, in order to enhance the required properties of antibodies, it is possible to produce the required phage libraries using synthetic methods. For instance, combinatorial antibody libraries were produced by using VL- and VH-domains combined populations, joined with the aid of protease-resistant (Gly4Ser)$_3$ linkers resulting in the formation of a DNA sequence. Comparing various types of displays it was established that monovalent display was among the most popular systems due to its ability for selection of antibodies with high affinity (Alfaleh, et al., 2017, p. 7).

Considering recent advancements in this type of technology, it can be stated that antibody generation and display utilises a range of new methodologies that harness mammalian and yeast display. Literature sources report that a range of various antibodies has been effectively isolated against various targets by using yeast display. Also, in addition to the described procedures, mammalian cells were employed to display IgGs (Immunoglobulin G) or scFvs, making it possible to isolate high affinity antibodies with predetermined biological functions. The various display systems have their own advantages and disadvantages, however, a description of every individual system and its areas of applications are beyond the goal of this work and the reader is referred to the following for a good overview (Farhadfar & Litzow, 2016, p. 14).

From a manufacturing/production perspective, isolation of various antibody fragments is carried out with the aid of panning or affinity enrichment. The purpose of this synthetic technique is to isolate mAbs from the corresponding phage library based on the ability of a given mAb to interact with the desirable biological target(s). The process consists of three major steps: 1) exposure of the tested library to the corresponding target with capturing of the required phage binders; 2) washing of the test solution with the purpose of eliminating the presence of low affinity or non-selective binders; 3) elution of specific binders with amplification. The described process is repeated from three to six iterations, resulting in the overall reduction of the phage diversity along with amplification in the quantity of selective binders. The obtained antibodies are subsequently employed in various therapeutic applications, such as cancer treatment, autoimmunity and asthma (Ren, et al., 2017, p. 76) (Teo, et al., 2016, p. 73).

When considering specific applications of mAbs in modern biotechnology, mAbs are extensively employed in the characterisation and classification of tumours and tissues based on the expression of defined markers. For instance, implementation of mAbs against various organs associated antigens (placental alkaline phosphatase, prostate specific antigen and human chorionic gonadotropin) may be employed by pathologists during the identification and characterisation of primary tumours (Ordonez, 1999, p. 313). Monoclonal antibodies have been found to be particularly useful to distinguish

structurally similar formations, such as adenocarcinoma and mesothelioma (Ferri, et al., 2016, p. 592). These materials are also useful for the identification of tissues or organs where undifferentiated metathesis originates. Thus, the detection of metathesis processes through immunocytological analysis of tissue samples obtained from bone marrow, lymph nodes as well as other tissues has proven to be highly effective by using specific monoclonal antibodies. In cases when axillary lymph nodes are investigated for metastatic breast cancer, implementation of monoclonal antibodies to test cytokeratin results in the elevation of the detection efficiency by approximately 10% (Ferri, et al., 2016, p. 592).

In addition to the described above applications of mAbs in cancer treatment, mAbs can also be used in the treatment of autoimmune diseases and asthma. Thus, considering the treatment of autoimmune conditions, Bruno and co-workers (2011, p.83) indicated that by knowing the immunological movements corresponding to autoimmunity, it becomes possible to target all steps of the process. In particular, therapeutic applications are focused on activating T lymphocytes in the corresponding lymph nodes, the production of immunological synapses, T cell differentiation and production of cytokines (Bruno, et al., 2011, p. 283). Finally, monoclonal antibodies may also be employed in asthma treatment. As indicated by Byrne (2013, p.23), patients suffering from refractory asthma were a considerable burden to the modern system of healthcare. Novel treatment approaches presumed the use of humanized monoclonal antibodies or hMabs for the mitigation of the condition. In the corresponding publication, Byrne indicated that by using anti-IgE it was possible to considerably reduce asthma symptoms in the study group of patients. It was also shown that hMabs were able to block IL-5, which was highly beneficial for patients, manifesting in elevated levels of periostin in blood (Byrne, 2013, p. 23).

Monoclonal antibodies are basically distributed cells that are actively divided through the biological process of cell division from a single and active ancestral cell. They form a class of antibodies with identical off springs of a given hybridoma. In their function, they are very specific in terms of location in the human body and are derived from a single biological clone. In addition, the cells can be grown indefinitely. Monoclonal antibodies have the ability of recognizing and instantly binding to antigens within the human body. The main reason for this process is to actively discriminate between specific existing epitopes within the human system responsible for providing protection against disease organisms within the human body.

Monoclonal antibodies function by targeting specific proteins in human system that influences cell activities such as receptors. In addition, monoclonal antibodies also target other proteins that exist on the surface of both normal and cancer cells. Through their specificity, the antibodies are able to bind tightly to cancerous cells. This process is achieved through the help of a cytotoxic agent like a strong radioactive component which is aggressive enough to seek out and destroy the specific cancer cells

while at the same time protecting the healthy cells within the human system. This is very critical especially when it comes to managing the health of a cancer patient. Most recorded deaths come as a result of strong chemo rays that are directed to the area with which the cancer cells have attacked in the human body. In the process, many healthy cells are damaged making it difficult from an individual to fully recover from the ailment.

An interesting part of dealing with monoclonal antibodies is tumour cells. There are specific tumour cells that display the ability of replicating in an endless manner and are fused with mammalian cells that produce specific types of antibodies. The process leads to fusion referred to as hybridoma, an action that constantly produces antibodies within the human system. The specific types of antibodies that are formed as a result of this process are referred to as monoclonal because they are generated from on type of cell. The single cell factor in this case makes it possible to refer to the antibodies that are generated as mono. In addition, there are specific types of antibodies that are produced as a result of conventional biological methods. These types of cells are then referred to as polyclonal antibodies. They are basically derived from a series of preparations that contain many kind of cells and not only one as it is for monoclonal cells.

Monoclonal antibodies are unique in nature based on the manner in which they are produced. In this case, they are artificially produced based on a given type of antigen in order to enable the process of binding to their target antigens within the human body. There are unique instances where monoclonal antibodies are produced in the laboratory. For this case, laboratory production of monoclonal antibodies is initiated through clones of a single cell which suggests that every monoclonal antibody in the human body is produced by the same human cell.

Biological fusion of cell culture myeloma cells takes place within the mammalian spleen cells antibodies. This process results in hybrid cells that are generally referred to as hybridomas. Hybridoma cells have the ability of producing large amounts of monoclonal antibodies which are very crucial in the human body when it comes to enhancing protection against infectious diseases. The process of cell fusion in this case results in two different types of cells. One of the cells in this case is characterized with the ability to grow in a continuous manner. On the other hand, the other cell is characterized with the ability of producing large amounts of purified antibodies in the human body. Further research on the same suggests that hybrid cells have the ability of producing only 1 exact antibody that is pure in nature than any other type of polyclonal antibody. Monoclonal antibodies are more effective in their function when compared to conventional types of drugs. These types of drugs have the character of attacking foreign substance. They also attack the healthy human cells in the body and for that reason, they have certain side effects that may be completely dangerous to use. Side effects would also vary based on the type of genes and specific allergic factors that vary with different human systems.

Abnormal protein comes as a result of presence of large amounts of specific types of monoclonal antibody in the blood. In this case, the protein is detected through physical examination and identified via screening blood test referred to as protein electrophoresis. Basically, abnormal production of monoclonal antibodies in the human system is considered as a small population of plasma cells that are found in large amounts in the bone marrow.
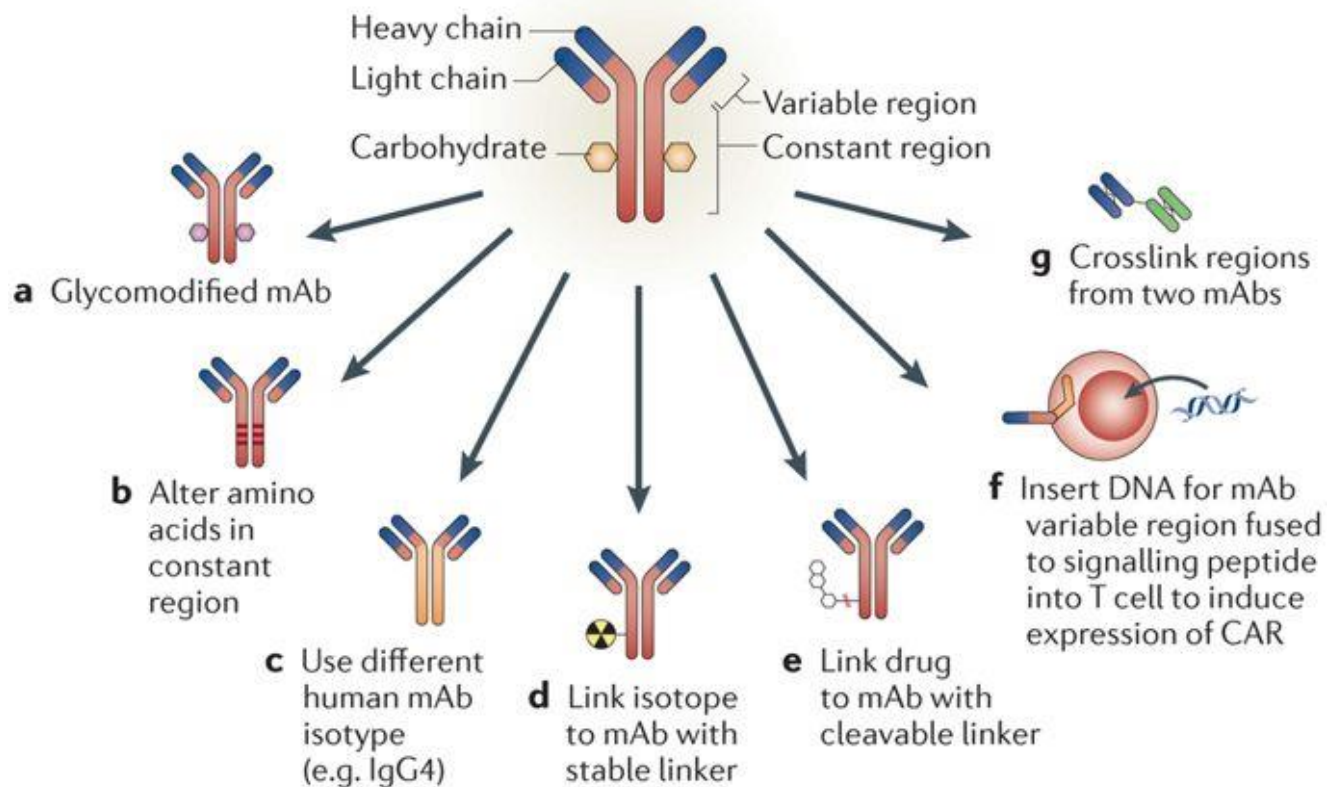
Nature Reviews | Cancer

Reflecting at the overall process of production of monoclonal antibodies indicates that it is a complex cycle. The process involves bulk production of monoclonal antibodies that work against a specific type of antigen produced at the same time. In this case, monoclonal antibodies are produced through multiple and identical copies of a given type of cell referred earlier as hybridoma. Hybridoma in this case is created as a result of fusion of two types of cells. The cells actively combine with individual characteristics at hand contributing to the final identity of the product that is generated. Therefore, it is critical to understand that formation of each type of cell comes back to the nature of the individual cells that initially interacted. It also depends on the type of fusion that took place in order to generate a given type of cell. During formation, the formed cells would undergo biological process of cell division to generate and spread to other parts of the body. Protection against diseases in the human system would prioritize distribution of the cells based on urgency. For instance, in situations where the

human body is weak in specific organs, the antibodies would be distributed around the area in large amounts to ensure that infections that would compromise health of a human being are completely addressed before the situation becomes complicated.

1.2 Aims and objectives of the work described in this thesis

The work described here is aimed at summarising current developments in the area of monoclonal antibody therapy and the work undertaken over a period of time by the author in the field as evidenced via the publications presented and discussed, specifically describing factors that affect stability and integrity of mAb-based formulations destined for use in humans. It is also aimed at discussing the findings presented in the published work in the context of the larger field of recent papers in the area, their main findings and implications. The contribution of the author here, to each of the highlighted publications, is also described.

The objectives of the work are to:

1. Provide an introduction to the concept of mAb-based treatment and discuss this therapy in relation to other types of treatment.
2. Give emphasis to the most significant findings in the area of monoclonal antibodies.
3. Establish fundamental hypothesises between various areas of monoclonal antibody development and the corresponding mAb-based formulations.
4. Outline a possible theoretical framework for the development of monoclonal antibodies-based formulations using relevant recent publications.
5. Provide a summary of the key publications submitted by the candidate for consideration towards a PhD, the main findings and implications and the contribution of the author to the studies.

1.3 Literature review, including published work by the candidate

Considering the properties and application areas of monoclinal antibodies described under section 1.1 above, it is clear that investigations in the area of mAb formulation stability is of paramount importance to the development of novel mAb based drugs. For a protein based medicine, such as a mAb, to reach the clinic it must be able to be formulated in an appropriate manner that can maintain the stability and activity of the molecule for a specified shelf-life, ensuring its safety, but also so that the practitioner can deliver the required dose in an appropriate manner.

As a general introduction to the concept of monoclonal antibodies as therapies and reagents, it can be stated that during the first half of the twentieth century antibody-mediated immunity was determined to be fundamentally important for specific immune responses (Merck KGaA, 2015, p. 8). Since their initial introduction during 1970s, immunolabelling antibody technologies were substantially

improved and antibodies were adopted as critical components in life science research. The main principle of all investigations in the area was the fact that specific antibodies would be able to interact with specific antigens with the formation of exclusive antibody-antigen complexes. The presented work is focused on a range of selected publications, covering various aspects of monoclonal antibody formulations, such as characterisation of the corresponding solutions, their stability and the nature of chemical interactions between individual peptide molecules. Nevertheless, ScienceDirect indicated that the number of publications in the area (Search term: "Monoclonal Antibodies" 1995 – 13.271 publications - 2017 - 16.203 publications) increased over the past decade what highlighted the importance of the topic to the world science (ScienceDirect, 2018).

The notion antigen presents antibody generation. This term describes any compound that is able to produce immune responses, such as generation of specific molecules of antibodies. The definition of antigen presumes the possibility of combining with specific antibodies that are generated in its presence. In general terms, antigens present foreign proteins as well as their fragments that are introduced in the host body through infections. In addition to foreign nature, proteins of various organisms are also able to perform the same functions what results in the corresponding autoimmune responses. Viruses and bacteria contain antigen molecules on their surfaces and insides. As the consequence, these antigens can be chemically isolated for the corresponding development of vaccines. Antibodies are characterised as immunoglobulin molecules, capable of specific interactions with antigens. Antibodies are generated as a form of response to invasions of foreign molecules. Antibodies are commonly described as immunoglobulins (Igs). From the structural perspective human immunoglobulin is similar to glycoproteins with 82-96% forms by proteins and the remaining part by carbohydrates (Merck KGaA, 2015, p. 9). These molecules are of paramount importance to human immunity, what underlines the necessity of investigations in the area.

Detailed description of all recent publications in the area is beyond the goal of the work, however it is clear that effective purification of the corresponding monoclonal antibodies is fundamentally important to any type of research in the area. Thus, Yamada and co-workers described an efficient flow-through mode of monoclonal antibody purification (Yamada, et al., 2017, p. 110). The research group indicated that employed in various biopharmaceutical applications, such as production of new drugs and modification of the existing ones. It was found that buffer exchanges would be able to substantially improve impurities removal during depth filtration. Yamada and co-workers demonstrated that by using various depth filters it was possible to obtain the necessary level of protein purification. Based on the obtained results, a flow-through operation mode was suggested as an effective antibody manufacturing process (Yamada, et al., 2017, p. 110). The following sections of the review are focused on selected publications, discussing properties of monoclonal antibodies under various conditions and

characterisation of the corresponding formulations. Protein formulation is a vital component in biological development. Formulation of proteins entails of conducting a series preformation trials to determine the solubility at various ionic strengths or pH conditions. After establishing the solubility properties, conduct the new iteration to test the pH conditions, salts, ionic strengths and buffering agents. This is followed by performing ability screening approach to enable selection of optimal conditions by use of proprietary formulation development technique. Stability of proteins refers to the net balance of forces, which determine whether proteins are in their denatured or native folded stage. Interactions between disulphide, Van der Waals, hydrophobic, hydrogen bonding and electrostatics are factors that determine stability of proteins. Denatured state of proteins is characterised by entropic and non-entropic free energies.

1.3.1 General Approach to Formulation of Biotherapeutic Proteins, Particularly mAbs

The formulation of mAbs can be considered from the perspective of a standard manufacturing process, using mammalian cell culture (Li and Amanullah, 2010, p.2). Cells are grown in culture over a period of weeks to provide a seed culture (also called inoculum) for fermentation (Vazquez-Rey and Lang, 2011, p.1495). Subsequent culture techniques lead to dramatic expansion of the cell population and culminate in cell harvesting through centrifugation or microfiltration methods. The following stage involves 'capturing' the protein, using chromatography (Protein A or ion exchange), often combined with additional purification stages to remove host proteins and other impurities, including a stage of membrane filtration and nanofiltration (Bee et al., 2009, p.940). During this process, there is an important emphasis on the conditions used to generate cells, as well as during the analysis and purification of proteins, including mAbs, captured from these cells.

Under standard biological condition *in vivo*, the cellular and extracellular environment is tightly regulated through a diverse range of homeostatic mechanisms (Vazquez-Rey and Lang, 2011, p.1495). The regulation of factors such as pH, temperature, and ionic concentrations provides the basis for creating a biologically stable environment for a range of biological activities, including the formation and processing of proteins (Wang et al., 2007, p.2). As deviations in any of these parameters may render proteins unstable or dysfunctional it is necessary to consider the effects of the environment when formulating proteins *ex vivo* and in pharmaceutical or biomedical contexts.

One of the most concerning aspects of protein formulation is the potential for aggregation (oligomerisation) of proteins, which was first described in the Lumry-Eyring model (1954). Aggregation events are commonplace, although the underlying mechanisms for aggregation are not completely understood in all drug manufacturing contexts. Adding to the complexity of understanding these mechanisms is the differential classification of protein aggregates, including soluble/insoluble

aggregates, covalent/non-covalent aggregates, native/denatured aggregates, and reversible/non-reversible aggregates (Wang et al., 2007, p.6). It is beyond the scope of this paper to consider the aspects of formulation associated with all of these aggregation definitions. However, it is apparent that aggregation removal and/or control is essential to ensure the biological activity of the resulting proteins (including mAbs) and to ensure no harmful effects occur in the recipient of the drug due to the effects of aggregates (Vazquez-Rey and Lang, 2011, p.1497).

Aggregation during the production of mAbs may occur at multiple stages, providing a basis for tight regulation of the formulation process throughout the production of mAbs. Aggregation can occur during initial cell culture, both within the cell and following secretion of the protein in the cell culture medium (Vazquez-Rey and Lang, 2011, p.1497). A large amount of aggregation also occurs during the purification process of mAb production, whereby the environmental characteristics of the process have a particularly important effect on aggregation potential (Iacob et al., 2013, p.4316). Modulation and control of the environment, including the addition of excipients to stabilise proteins again aggregation and denaturation, is commonplace in biomedical manufacturing as a consequence (Iacob et al., 2013, p.4316).

The remainder of this section will consider the excipients used for protein stability and formulation, with a specific focus on excipients relevant to mAb formulation. These excipients include: pH and buffering agents, salts, sugars, amino acids, and surfactants.

1.3.2 Excipients in mAb formulation

1.3.2.1 pH and buffer characteristics

Buffer solutions are used throughout the process of mAb manufacturing and can have complex effects on the stability of proteins (Cleland et al., 1993, p.307). Aggregation of mAbs has been associated with interactions between the Fc domain of immunoglobulins (Igs), particularly IgG (Wang et al., 2007, p.7), while it has also been noted that some buffers have little or no effect on protein stability (Daugherty and Mrsny, 2006, p.700). The purpose of buffers is to provide some regulation over the solution pH, among other characteristics, as pH is considered an important determinant of protein formulation, stability and ultimate function (Vazquez-Rey and Lang, 2011, p.1497).

The effect of pH influences the ionic features of the protein molecule, which can influence protein-protein interactions, the three-dimensional conformation of the protein structure, and the interaction of the protein with other molecules (Zheng and Janis, 2006, p.47). Carboxyl groups and amino groups are ionisable and are particularly influenced by molecular pH of the solution and pH

values close to the isoelectric point (pI) of the protein can lead to the formation of diploes (Wang et al., 2007, p.14). The pI is achieved when the protein exhibits equal positive and negative charge in the carboxyl and amino groups, which promotes the degree of interaction between proteins (Zheng and Janis, 2006, p.49). Therefore, when the pH is close to the pI of the protein, aggregation is more likely to occur. The formulation of mAbs is typically performed with pH values lower than the pI, leading to disruption of the dipole state and the generation of a clear overall charge on the protein molecule (Liu et al., 2008, p.2427). Consequently, protein monomers are more likely to repel each other (due to identical electrostatic charges), making aggregation a less energetically favourable process (Wang et al., 2007, p.15). Therefore, regulation of pH in order to reduce aggregation is an important aspect of mAb production and can involve the use of buffering solutions such as histidine, phosphate, acetate and citrate.

1.3.2.2 Salts

As with the pH of a solution, the importance of buffer characteristics is also evident in determining the effects of salts on protein stability (Shire et al., 2004, p.1392). Salt ions can interact with proteins in a number of ways and to varying degrees, depending on the overall pH of the solution and the types of salts present in the buffer/solution. Salts form a large amount of the ionic strength of the solution and the use of polyvalent salts in particular has the potential to promote aggregation through an increase in ionic strength of the solution (Ohtake et al., 2011, p.1055). When ionic strength of the solution is increased due to the dissolution of salts with high valence, ionic accumulation adjacent to the surface of proteins is common (Ohtake et al., 2011, p.1055). This leads to an increase in the potential interactions between proteins and subsequent aggregation, due to presence of counter-charged salt ions close to the protein surface. The use of trivalent, bivalent or monovalent salts may reduce the potential for aggregation.

High concentrations of salts can also act to stabilise protein formulations through a mechanism of preferential exclusion (Vazquez-Rey and Lang, 2011, p.1498). Preferential exclusion refers to the deficiency of co-solvent molecules in the vicinity of the protein/mAb and is also termed preferential hydration, as water molecules dominate the region around the protein molecule (Arakawa et al., 1991, p.287). The result of preferential exclusion is that protein stability increases, and solubility decreases due to the energetically unfavourable nature of salt-protein interactions and the stable conformation of the protein as a consequence (Vazquez-Rey and Lang, 2011, p.1498). Different anions have a different effect on precipitating out proteins and have been classified according to the Hofmeister series, which is indicative of the stable hydration shells in anions and the stabilisation of interactions between salts

and water molecules: citrate > phosphate > OAc-, F- > Cl- > Br- > I- > ClO$_4$- (Kendrick et al., 2002, p.65).

1.3.2.3 Sugars

Sugars may also be used to stabilise proteins, specifically sugars that are non-reducing, including sucrose and trehalose (Wang, 1999, p.133). The use of reducing sugars is not considered suitable in biomedical protein stabilisation due to the potential for the Maillard reaction (amino acid deprotonation) (Wang, 1999, p.133). However, non-reducing sugars have been shown to reduce the activation energy of protein unfolding, with stability in proteins induced through preferential exclusion (Daugherty and Mrsny, 2006, p.688). For the stabilisation of mAb proteins during freeze-drying, sugars and polyols may act by stabilising protein kinematics within a matrix or by acting as water substitutes, maintaining thermodynamic stabilisation in the place of water molecules lost during the freeze-drying process.

1.3.2.4. Amino acids

The role of amino acids in the stabilisation of proteins has been recognised for many decades, although the precise mechanism of this stabilising effect is a matter of on-going debate, while varying to some extent between the use of different specific amino acids (Frokjaer and Otzen, 2005, p.298). However, there is a general suggestion in the literature that amino acids stabilise protein formulations by interfering with protein-water interactions and adjusting the thermodynamic properties of the medium (Wang et al., 2007, p.14). The use of arginine (Arg) and glutamic acid/glutamate (Glu) is common in the context of drug manufacturing and protein stabilisation for biomedical purposes (Golovanov et al., 2004, p.8935). These amino acids have been shown to stabilise the thermodynamic properties of protein-water interactions, reducing the potential for aggregation and enhancing stability in solution (Frokjaer and Otzen, 2005, p.298). However, the precise mechanisms of these amino acids will be considered later in this paper.

1.3.2.5 Surfactants

The use of surfactants in the stabilisation of proteins is also commonplace and is particularly important where formulation involves stages such as mixing, shaking or repeated freeze-thaw cycles (Kerwin, 2008, p.2924). Surfactants (e.g. polysorbate 80) reduce the tension in the air-water interface, reducing the potential for mAbs to interact at this interface, which may be associated with protein

unfolding and aggregation (Kerwin, 2008, p.2924). Surfactants may act in numerous ways to promote mAb stability, including through competition with the protein at the air-water interface, shielding of hydrophobic regions of the protein, or serving as a chaperone for protein folding (Wang et al., 2007, p.17).

The following sections contain a brief introduction as to the rationale for each of the publications discussed in this submission in more detail.

1.3.3 Paper 1: Kheddo P, Cliff MJ, Uddin S, van der Walle CF, Golovanov AP (2016) Characterizing monoclonal antibody formulations in arginine glutamate solutions using 1H NMR spectroscopy, MAbs 8(7):1245-1245.

The characterisation of various mAb-based formulations, and the impact of the formulations on the mAb, was undertaken by H^1 NMR as part of one of the publications submitted by the candidate for consideration within this thesis submission (Kheddo, et al., 2016, p. 1245). The necessity of the research described is supported by the fact that monoclonal antibodies are heavily utilised as biotherapeutics and as reagents in a substantial number of clinical investigations. However, it was established that increasing therapeutic concentrations of monoclonal antibodies increases self-association and aggregation of proteins, thus promoting their instability. In addition to the outlined negative effects it is expected that elevated therapeutic protein concentrations will result in the formation of soluble clusters that, in turn, may have a negative impact on the viscosity of the corresponding formulations. The outlined negative effects generally take place at protein concentrations >100 mg/ml and it was hypothesised that the addition of excipients should be considered, and able, to minimise such undesired instability (Kheddo, et al., 2016, p. 1245).

After analysing recent developments in the area of excipient formulations, it was established that arginine glutamate was effective and safe for routine implementation in the design of new formulations (Kheddo, et al., 2014, p. 127). Arginine has been shown to protect proteins against aggregation by slowing protein-protein association reactions and protein folding (Baynes et al., 2005, p. 4919). However, when combined with glutamate (glutamic acid), the Arg-Glu effect is synergistic and provides a stronger reduction in intermolecular interactions and subsequent aggregation compared to Arg alone (Vedadi et al., 2006: 15835). As a result of the study by Kheddo et al., (2014, p.127), it was expected that new synergistically working excipients would and could be developed in order to improve stability of novel monoclonal antibody-based reagents and drugs. However, in order to estimate mAb self-association that may take place at elevated protein concentrations, novel orthogonal analytical techniques are necessary. Currently, sample dilution is necessary to effectively carry out protein characterisation by standard analysis methods (e.g. mass spectrometry, chromatography, dynamic light scattering), thus orthogonal analytical techniques are required that allow the user to monitor changes in physical parameters associated with alterations in the chemical nature of the tested product without

sample dilution, at the formulated concentration and ambient temperature. Sample dilution results in concentration changes that will alter protein-protein interactions, self-association and stability of the molecule in question. Dilution of protein samples presents an intrinsic component of sample preparation for NMR investigations. The potential primary impact of the sample preparation procedure is to avoid slow protein precipitation, formation of a mixture containing both folded and unfolded proteins, reduce aggregation problems and degradation. It is clear that with the aid of sample dilution it is possible to produce uniform solutions, containing the same configurations of protein molecules (Cavanagh, et al., 2006, p. 76). Kheddo and co-workers indicated that by investigating the corresponding protein-based drugs at their target concentrations, it should be possible to establish the most effective stabilising agent (Kheddo, et al., 2016, p. 1246).

Kheddo and co-workers demonstrated that NMR spectroscopy was a powerful but underutilised approach in the analysis of mAb-based formulations (Kheddo, et al., 2016, p. 1246). It was suggested that when NMR was applied to the analysis of proteins it was possible to quickly and efficiently monitor signal changes as the result of functional group dynamics in solutions (Cavanagh, et al., 2006, p. 77). Nevertheless, while applying NMR to solutions containing monoclonal antibodies, broad and overlapping signals were observed. The indicated observation is associated with the large molecular sizes of the investigated mAbs (approx. 145 kDa) and complex interactions between various molecular groups. Further, traditional analysis techniques associated with NMR analysis, such as isotopic labelling, could not be applied to these systems due to production difficulties in natural systems. Nevertheless, characterisation was possible under elevated temperatures, which resulted in reduced water viscosity, allowing formation of proton NMR spectrum with distinguishable signals, corresponding to different function groups of the protein. Kheddo and co-workers show that common NMR-detectable parameters including signal intensities, deuterium exchange rates, relaxation times as well as rotational and translational diffusion were heavily depended on protein stability, aggregation and self-association in the corresponding tested solution (Kheddo, et al., 2016, p. 1246). This reinforces the need to be able to investigate formulations without diluting the samples beforehand to understand their behaviour under the concentrations at which they will be formulated. The results of this study are discussed in section 3.1 below.
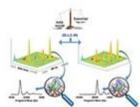
Characterizing monoclonal antibody formulations in arginine glutamate solutions using ^{1}H NMR spectroscopy

Priscilla Kheddo, Matthew J. Cliff, Shahid Uddin, Christopher F. van der Walle & Alexander P. Golovanov

Taylor & Francis
Taylor & Francis Group

REPORT

∂ OPEN ACCESS

Characterizing monoclonal antibody formulations in arginine glutamate solutions using ^{1}H NMR spectroscopy

Priscilla Kheddo[a,b], Matthew J. Cliff[a], Shahid Uddin[c], Christopher F. van der Walle[c], and Alexander P. Golovanov[a,b]

[a]Manchester Institute of Biotechnology, University of Manchester, Manchester, UK; [b]School of Chemistry, University of Manchester, Manchester, UK; [c]Formulation Sciences, MedImmune Ltd, Granta Park, Cambridge, UK

ABSTRACT

Assessing how excipients affect the self-association of monoclonal antibodies (mAbs) requires informative and direct *in situ* measurements for highly concentrated solutions, without sample dilution or perturbation. This study explores the application of solution nuclear magnetic resonance (NMR) spectroscopy for characterization of typical mAb behavior in formulations containing arginine glutamate. The data show that the analysis of signal intensities in 1D ^{1}H NMR spectra, when compensated for changes in buffer viscosity, is invaluable for identifying conditions where protein-protein interactions are minimized. NMR-derived molecular translational diffusion rates for concentrated solutions are less useful than transverse relaxation rates as parameters defining optimal formulation. Furthermore, NMR reports on the solution viscosity and mAb aggregation during accelerated stability study assessment, generating data consistent with that acquired by size-exclusion chromatography. The methodology developed here offers NMR spectroscopy as a new tool providing complementary information useful to formulation development of mAbs and other large therapeutic proteins.

Introduction

Monoclonal antibodies (mAbs) are increasingly being approved as therapeutics, and a substantial number are undergoing evaluation in clinical studies.[1-3] However, as proteins, mAbs suffer from instabilities, such as aggregation and self-association, during preparation, formulation and storage, especially at the higher concentrations (>100 mg/ml) often needed to deliver a therapeutic dose as a single injection.[4,5] Highly concentrated proteins also may form soluble clusters,[6,7] which may affect the viscosity of solutions,[8] an important consideration for using such solutions for injections. To minimize the unwanted instabilities, mAbs are formulated in the presence of excipients.[9-19] New, safe and effective combinations of excipients working synergistically, such as arginine glutamate (Arg·Glu), have been recently described and validated,[20-25] suggesting that new excipient combinations even within the generally-regarded-as-safe category can significantly improve the storage stability and injectability properties of mAbs.[26] To assess the suitability of excipients, new orthogonal analytical techniques that are able to report on mAb stability and self-association *in situ* at very high concentrations are needed[27] because many existing analytical techniques may suffer from observable signals out of scale, thus requiring sample dilution (in turn distorting understanding, e.g., self-association properties). Monitoring such measured physical parameters as a function of excipient type and concentration *in situ*, at the target mAb concentration and temperature (e.g., during accelerated stability studies), would be a direct and undistorted way to choose the best excipients and buffer conditions.

One of the analytical methods currently greatly underused for the formulation characterization of mAbs is solution nuclear magnetic resonance (NMR) spectroscopy. NMR is a very powerful technique capable of observing and monitoring signals from individual groups and types of atoms in a protein molecule, and reporting on the structure and dynamics of proteins in solution.[28-30] The obvious difficulty of applying solution NMR spectroscopy to mAbs is their large molecular size (ca 145 kDa), which generally leads to broad signals in the spectra and significant signal overlap. Common strategies applied in protein NMR, such as using deuteration or the introduction of isotopic labels, are not generally applicable to full-length native mAbs due to the difficulties with production of such labeled material in the standard expression systems (typically, mammalian cells). The native mAbs solutions that can be characterized have 2 favorable properties: they are generally highly-concentrated, and they allow for higher temperature to be used during the experiments, where the viscosity of water is reduced and molecular tumbling is faster, often leading to NMR spectra of sufficiently good quality. Indeed, recent reports have suggested use of proton NMR and natural-abundance ^{1}H-^{13}C–correlation spectra to fingerprint mAbs.[31-37] Because the NMR-observable parameters such as translational and rotational diffusion, transverse relaxation times, deuterium exchange rates and observed signal intensities[28,38,39] depend

strongly on the self-association, aggregation and stability of protein in solution, we explored how such measurable parameters would depend on the concentration and state of a typical industrially relevant IgG1 mAb (identified as "mAb2" in our previous studies[24]) in various solution conditions.

The two aims of the current study were: 1) exploration of the applicability of NMR methodology for typical tasks in protein formulation, and 2) identification of the optimal concentration of Arg·Glu that minimizes mAb self-association and solution viscosity. Here, we used solution NMR spectroscopy to measure a number of experimental parameters for mAb solutions to explore their sensitivity to the changes in the solution environment. The apparent viscosities of solutions derived from NMR measurements were compared with macroscopic solution viscosities measured using the m-VROC viscometer. Accelerated stability studies were also conducted, with NMR detection compared with conventional technique using size-exclusion chromatography (SEC). We suggest a pragmatic approach to interpreting the NMR measurables for optimal formulation development.

Results

Using 1D ^{1}H NMR spectroscopy to assess mAb stability upon addition of Arg·Glu

Proton NMR signals, which reflect the state of a protein in solution, can be characterized by a number of measurable parameters. Signal integral is generally proportional to the concentration of soluble protein. Protein aggregation increases the rate of transverse relaxation, causing signals to broaden and intensity to decrease. Larger aggregates (e.g., solid sub-micron protein particles) can lead to such a fast signal relaxation that the signals from this sub-species of the sample will not be observable. Therefore, in principle, measuring the intensities of protein signals vs different solution environment is expected to report on the aggregation state of protein in solution.

To assess the effect of solvent conditions on 1D ^{1}H NMR spectra of a chosen test mAb (called here mAb2 for consistency with our previous study[24]), we first recorded 1D ^{1}H spectra (with identical experimental parameters) for 3 different protein concentrations (40, 100 and 200 mg/ml) at pH 6 and 7, with varying concentrations of Arg·Glu added (between 0 and 200 mM). Respectable spectral quality was achieved at 40°C (see Fig. S1) due to increased molecular tumbling rate at this higher temperature; this temperature is far below the first melting transition temperature for mAb2,[24] ensuring that the molecule is not significantly destabilized. Results of these experiments are presented on Fig. 1. Several useful observations can be made from looking at the trends (Fig. 1A): the self-association is low when protein is at low concentration (40 mg/ml), and the signal intensities (both at pH 6 and 7,Fig 1A,B) decrease marginally with increased concentrations of Arg·Glu added. This decrease, however, is proportional to the increase in the buffer viscosity (due to Arg·Glu, see below). When the signal intensities are corrected for buffer viscosity (I_η^N), they
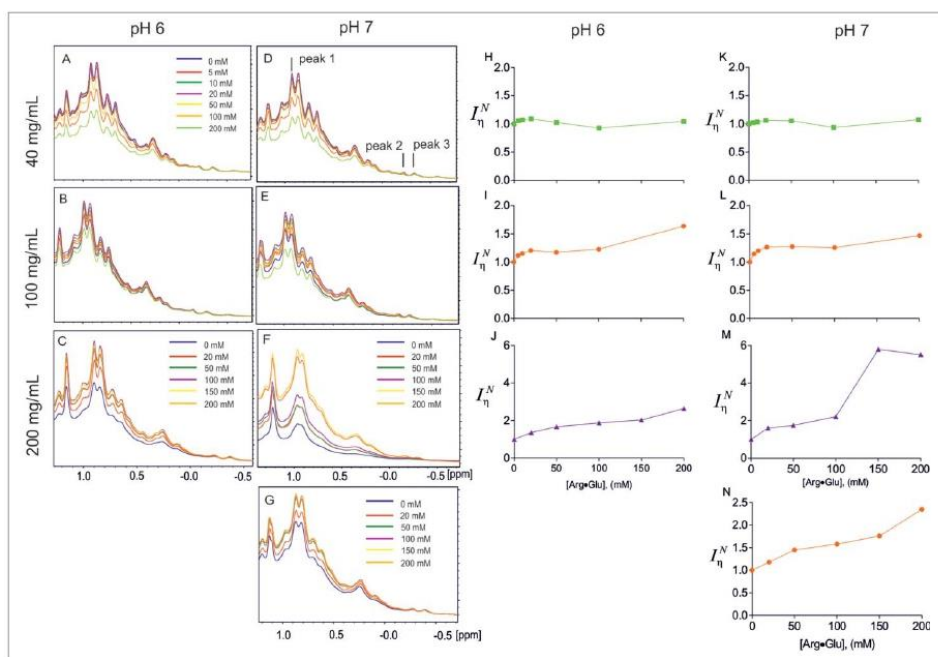
Figure 1. Effect of Arg·Glu addition on NMR signal intensities of mAb2 in different solutions, as labeled. Panels A-G show overlays of selected high-field region of ^{1}H NMR spectra of mAb2, with concentrations of components as labeled. In (A)–(F) 10 mM CP buffer was present. Panel (G) includes spectra of 100 mg/ml mAb2 recorded in the absence of any salt apart from Arg·Glu added as indicated. Dependences of viscosity-corrected normalized signal intensities I_η^N measured for peak 1 upon increase in Arg·Glu concentration are shown on correspondent right-hand panels (H)–(N). (Color version of this figure is available online)

stay fairly flat when mAb2 is at low concentration (Fig 1H, K). For larger concentrations of mAb2 (e.g., 200 mg/ml), the signal behaviors clearly change: despite the increase in buffer viscosity, signal intensities increase with the addition of Arg·Glu (Fig 1C, F). The values of viscosity-corrected normalized signal intensities I_η^N increase even more and grow almost 3-fold and 6-fold at pH 6 (Fig 1J) and pH 7 (Fig 1H), respectively. At the intermediate mAb2 concentration (100 mg/ml), I_η^N show initial faster growth followed by slower growth, with an overall increase of around 1.5-fold when 200 mM Arg·Glu was added (Fig 1I, L). To check if such spectral effects depend on the type and the ionic strength of the base buffer, a control experiment was run for mAb2 dissolved at 100 mg/ml in only de-ionized (Milli-Q) water, where the electrostatic repulsion between the protein molecules is not screened by salt and hence should be at its maximum.[18] The NMR spectra clearly show that both raw (Fig 1G) and viscosity-corrected normalized I_η^N (Fig 1N) signal intensities increase significantly upon addition of Arg·Glu. The increase of signal intensities in NMR spectra recorded under the identical experimental conditions can be unambiguously interpreted as an increase in the population of monomeric or lower-oligomeric protein species and a decrease of concentration-dependent protein self-association[7] upon the addition of Arg·Glu. Interestingly, addition of Arg·Glu also caused concentration-dependent perturbations of well-resolved high-field mAb2 signals (marked peak 2 and peak 3 on Fig. 1D) from which the disassociation constant K_d for this interaction can be estimated as 90 mM (Fig. S2).

Similar analysis of 1D spectra acquired in the temperature-dependent manner can be used, as well as relative normalized integral parameter L_η^N that we suggest, to assess how excipients or sample conditions affect the melting temperature and amount of soluble mAbs (see Supplemental Information, and Fig. S3). Moreover, by recording the 1D spectra before and after the brief sample exposure to elevated temperature, and using an easily quantifiable NMR-derived parameter that we introduce, a short-term storage stability factor F, it is possible to assess the short-term sample stability in different formulations under thermal stress (Supplemental Information, and Fig. S4). We conclude that, as NMR signal intensities are very sensitive to both protein self-association and solution viscosity, finding a formulation that maximizes the signal intensity is expected to coincide with the beneficial formulation leading to stable monomeric mAb solution with minimum overall solution viscosity.

Accelerated stability studies of mAb2 using NMR and size-exclusion chromatography

Having established that proton NMR signals reflect the amount of monomeric or lower-oligomeric protein remaining in solution, we further explored how NMR can be used to monitor mAb2 physical degradation over time, with concentrated samples (300 mg/ml) stored at 40°C in 4 different formulations. Additionally, to assess the relative exposure of amide groups to the solvent by monitoring the deuterium exchange, NMR samples were formulated in ^2H_2O. These long-term storage experiments were also repeated, with the fraction of monomeric protein remaining in solution F^{mono} assessed by SEC, a traditional method used in industry. The raw spectra for 4 different sample conditions are presented on Fig. 2A–D. The reporter region chosen for monitoring the decrease in peak intensity includes amide region 8–10.5 ppm (region additionally affected by the exchange of protons for deuterons) and region 6–8 ppm, which is mostly populated by the aromatic signals that are not prone to exchange, but with some contribution from exchanging amide signals. These regions were chosen because protein signals here are not obscured by strong signals from the excipients and buffer components used for these formulations. As can be seen from the spectra, with time the signal intensities generally decrease, but the rate of the decrease varies between the 4 chosen formulations. Fig. 2E–H presents the fractions of the initial signal intensities of aromatic signals (F^{AR}) and amide signals (F^{NH}), or of monomer present in solution derived using SEC analysis (F^{mono}), versus time, which all reflect the rate of protein degradation due to sample aggregation and precipitation. It can be seen that monitoring the aromatic signal intensities over time slightly overestimates the rate of apparent sample degradation: signals decrease their intensities with time faster than the monomer is lost in the solution according to SEC analysis.

It should be noted that for the SEC analysis the protein sample needs to be diluted, which is expected to shift the solution equilibrium for reversible self-association toward monomeric species, thus probably overestimating the amount of monomeric protein in the original concentrated solution. This is unlike NMR, which assesses aggregation *in situ*. The difference in the degradation rate also can be explained by additional contribution from deuterium exchange on intensities of amide signals overlapping in the aromatic region. As the rate of deuterium exchange of labile groups (which indirectly reflect on the increase protein dynamics and structure perturbation) is strongly dependent on pH, and is inherently accelerated at higher pH, it is not possible to compare the rates of decay at different pH; however, it is possible to do that at an identical pH. This comparison reveals that adding 200 mM of Arg·Glu significantly increases storage stability at pH 6 (Fig. 2E,F) as reported both by F^{mono} and F^{AR}, with the rate of deuterium exchange also reduced, as reported by F^{NH}, likely due to more shielding from the solvent in a more stable folded structure. At pH 7, the effect of Arg·Glu was compared with the effect of Arg·HCl. Here, Arg·HCl apparently had more a stabilizing effect than Arg·Glu according to F^{AR} and F^{NH}, whereas according to F^{mono} there was not much difference in the long-term stability (Fig. 2G,H). At this point, NMR analysis highlighted the differences in stability between formulations that were not evident from the SEC analysis.

In order to understand the reasons for faster decays of F^{AR} compared to F^{mono}, the solution viscosity needs to be taken into account because its increase (e.g., with time) can also lead to signal decay and additional decrease in measured F^{AR}. To check this hypothesis, the macroscopic viscosities of these 4 formulations were also monitored with time using the m-VROC viscometer (Fig. 3). The measurements reveal that the addition of Arg·Glu leads to much lower mAb2 solution viscosity. Although use of Arg·HCl lead to an apparently stable formulation at pH 7 (Fig. 2H), the viscosity of this formulation was the highest, ∼3–4 times higher than the mAb2 viscosity with
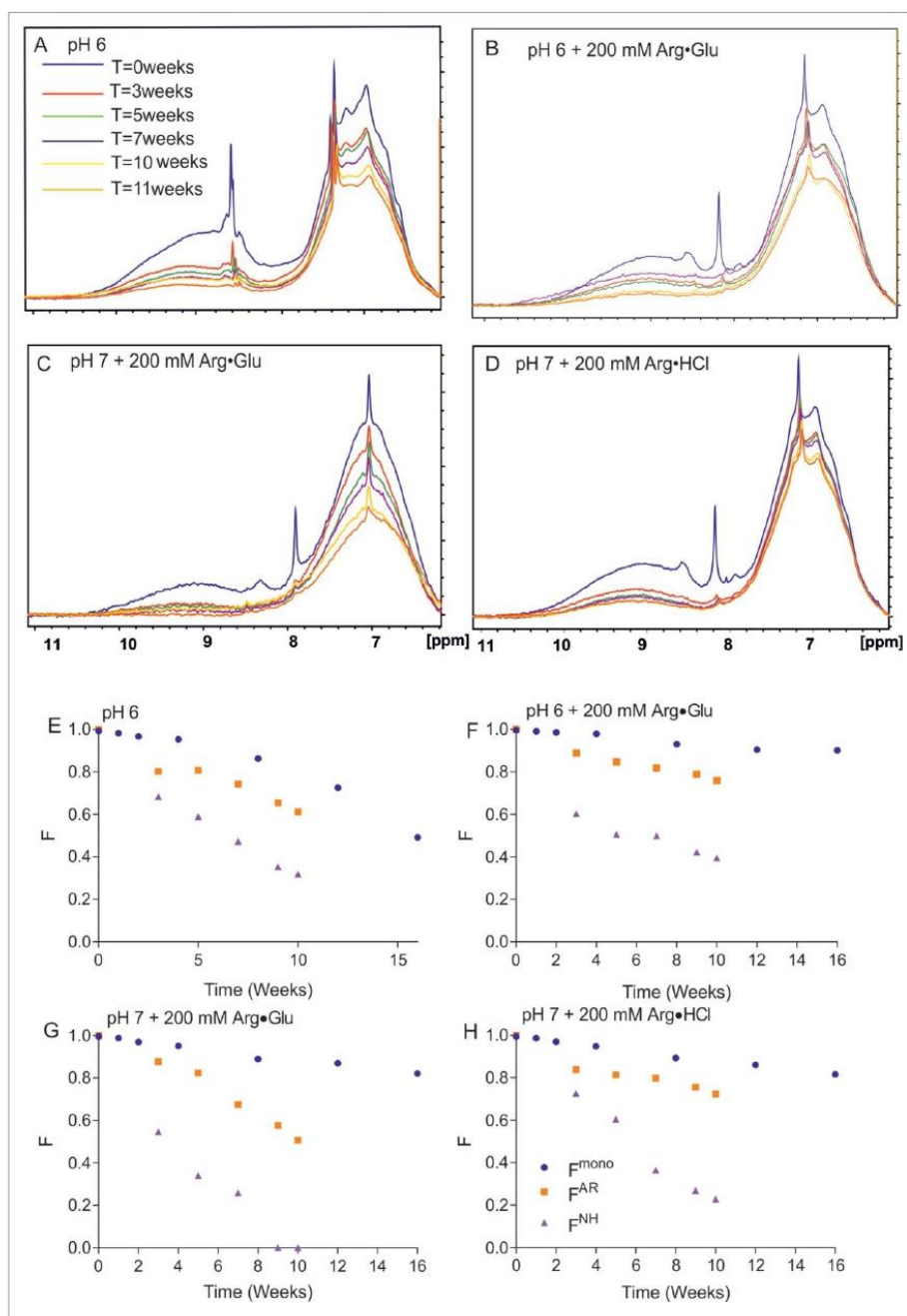
Figure 2. Assessing by NMR and SEC the long-term storage stability of mAb2 at 40°C in selected formulations. The 1D ^{1}H NMR spectral overlays (amide and aromatic region) for 4 different formulations of 300 mg/ml mAb2 in 10 mM citrate-phosphate buffer are shown, as a function of time: at pH 6 in the absence of additives (A); in the presence of 200 mM Arg·Glu (B); at pH 7 in the presence of 200 mM Arg·Glu (C); and in the presence of 200 mM Arg·HCl (D). Correspondent panels (E)-(H) show for the same 4 formulations the time-dependence of relative fractions of aromatic (F^{AR}) and amide (F^{NH}) signals remaining in the spectra vs time, reporting on soluble protein loss. Independently, the fraction of monomeric protein F^{mono} was assessed using SEC and plotted. (Color version of this figure is available online)
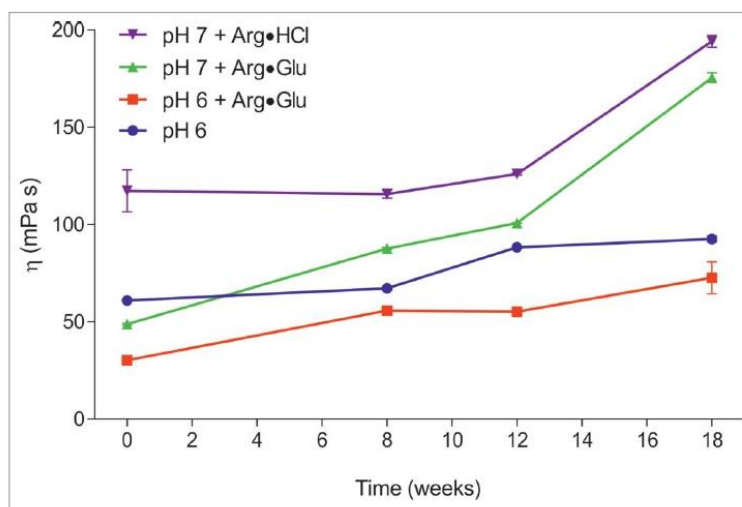
Figure 3. Assessing the macroscopic solution viscosity, using mVROC, during long-term accelerated mAb2 stability studies. mAb2 were formulated at 300 mg/ml in 10 mM citrate-phosphate buffer at pH 6 and further additives, as labeled, and stored at 40°C for prolonged period of time. (Color version of this figure is available online)

Arg·Glu added at pH 6. Interestingly, all formulations tested here showed a tendency to increase in viscosity after prolonged storage. The rate of this increase is not precisely mirrored by the loss of monomer content F^{mono}. The reason for this is unclear, but may reflect the transient nature of reversible self-association of protein oligomers. We suggest that it is this increase in solution viscosity with time that is responsible for the additional decay in F^{AR}, compared with the benchmark F^{mono} values. As solution viscosity and aggregation are primary considerations in developing mAb formulations, we suggest that monitoring a simple NMR-measurable parameter such as F^{AR} with time can be a valuable orthogonal criterion for optimizing such formulations. Minimizing the rate of F^{AR} decay over time should ensure that the maximum amount of soluble un-aggregated protein remains in solution, and solution viscosity is not increased during prolonged storage.

Assessing viscosity and aggregation state of mAb2 solutions using rheometry and translational self-diffusion measured by SE-PFG NMR spectroscopy

This and previous studies[20,21,23,24] suggest that addition of Arg·Glu reduces protein aggregation in a concentration-dependent manner. To explore further the effect of Arg·Glu on the apparent protein cluster size and solution viscosity, we employed stimulated echo pulsed-field-gradient (SE-PFG) diffusion-ordered NMR spectroscopy (DOSY)[39-41] to measure the translational self-diffusion coefficients of both mAb2 and citrate, which served as a small probe molecule in the buffer, at 3 mAb2 concentrations (40, 100 and 200 mg/ml) at pH 6 and 7, in the presence of increasing concentrations of Arg·Glu added up to 200 mM (Fig. S5). Measured diffusion coefficients D were plotted as a function of Arg·Glu concentrations (Fig. 4A, B), or for convenience, as a function of mAb2 concentration (Fig. 4C, D). Apart from the observed significant decrease in the values of D with increased protein concentration (which was expected

due to increased protein crowding, excluded volume effects and protein self-association at higher concentration) the plots of Fig. 4A, B reveal a marginal dependence of diffusion coefficients D on concentration of Arg·Glu added. As the translational molecular diffusion rate is dependent on solvent viscosity, and the solvent viscosity inherently increases with the addition of Arg·Glu, this effect needs to be taken into account when interpreting the changes of D under different conditions.

The concentration-dependence of the apparent viscosity of the buffer itself, as well as of mAb2 solutions, was measured by following the diffusion of the small probe molecule inherently present in the sample buffer, citric acid (see Materials and Methods). The 'microscopic' solution viscosities thus measured by NMR (Fig. 5A, B) were compared to the 'macroscopic' solution viscosities measured using the m-VROC viscometer (Fig. 5C, D; due to limited sample availability, the macroscopic viscosity of the 200 mg/ml mAb2 sample was not assessed). The graphs for microscopic and macroscopic viscosities generally follow similar trends, with microscopic viscosities measured for mAb2 solutions by NMR being generally systematically smaller. The macroscopic and microscopic viscosities of the buffer itself upon the addition of Arg·Glu were, however, very similar, showing a steady increase in viscosity (Fig. 5A, C). Despite this increase in the underlying buffer viscosity, the addition of Arg·Glu noticeably decreased the overall viscosity of mAb2 solutions, which was particularly evident at higher protein concentrations (100 and 200 mg/ml), where the solution viscosity was initially very high, with the largest effect observed with 100–150 mM Arg·Glu. This relative decrease in the mAb2 solution viscosity upon addition of Arg·Glu was detected by both NMR and viscometer. We conclude that addition of Arg·Glu to highly concentrated solutions of mAbs can be used not only to increase their stability in storage, but also to reduce viscosity of solutions.

To explore further the observed effect of Arg·Glu on NMR signal intensities and protein viscosity, we used the Stokes-Einstein Equation 4 (see Materials and Methods) to assess an
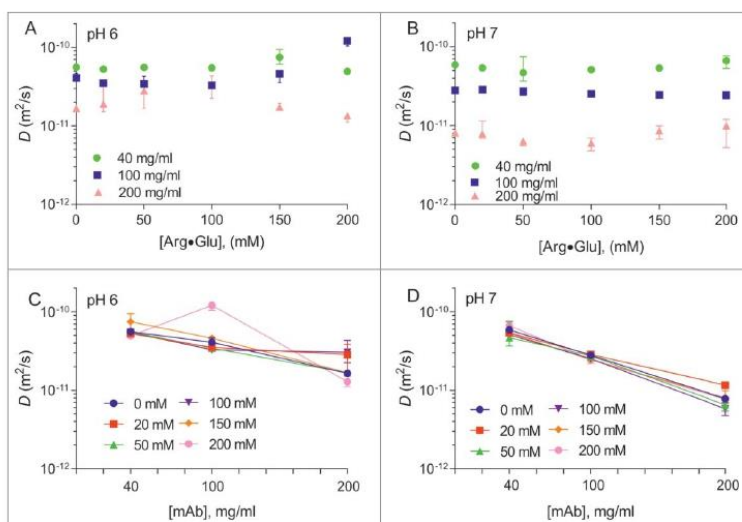
Figure 4. Translational diffusion coefficients D of mAb2 measured by DOSY. The values of D for mAb2 formulated at pH 6 (A) and pH 7 (B) are shown vs the concentration of Arg·Glu added. The same data is also presented in different coordinates on panels (C) and (D), respectively. (Color version of this figure is available online)

apparent radius of protein clusters (R_h) diffusing in solution, knowing the translational diffusion coefficient D, and the measured viscosity of the buffer with Arg·Glu added. Although a crude approximation, the values of R_h may reflect on the apparent changes in the effective cluster size of mAbs forming at higher concentrations, which can be modulated by the addition of Arg·Glu. The results are presented in Fig. 6A, B. At low mAb2 concentration, when self-association of the protein is minimal, the values of R_h appear steady and only marginally decrease upon addition of Arg·Glu, up to the value close to 4 nm expected for a typical monomeric mAb[18] (Fig. 6A, B). With increased mAb2 concentrations the apparent R_h also increases, but addition of Arg·Glu in the region of 50–100 mM (at pH 6) and 200 mM (at pH 7) caused R_h to drop significantly. For convenience, the same data is presented in different coordinates (Fig. 6C, D), showing more clearly the mAb2-concentration-dependent increase in R_h, as well as a partial negation of this effect by addition of Arg·Glu. The reduction in the apparent size of the transient mAb2 clusters upon adding Arg·Glu, revealed here from diffusion measurements, agrees well with the viscosity-reducing effect of Arg·Glu, and matches with the increase in signal intensities in 1D ^{1}H spectra described above.

Measuring the effect of Arg·Glu on proton transverse relaxation rate R_2

In addition to translational diffusion, proteins in solution undergo molecular tumbling. The rate of molecular tumbling depends on the size of the cluster, and therefore can report on protein self-association state. The tumbling rate is generally reflected in the value of transverse relaxation rates of the protons R_2: the larger the cluster, the faster the rate. However, local polypeptide chain flexibility can reduce the values of R_2

for particular signals. Increased relaxation rate R_2 makes NMR signals appear broader and decreases signal intensity.

To explore in more detail the effect of Arg·Glu addition on mAb2 signal intensities (Fig. 1), or on the apparent mAb2 radius R_h (Fig. 6), the R_2 values were measured for 40 and 100 mg/ml mAb2 solutions at pH 6 and 7, upon addition of increasing concentrations of Arg·Glu. Due to significant overlap between individual proton signals, possible effect of local mobility on relaxation rates of individual protons, and difficulty of tracking the same signals in a titration series, the relaxation data was measured for multiple proton signals in the aliphatic part of the spectra. Thus, the trends in the typical population behavior of R_2 values upon addition of Arg·Glu to mAb2 formulated at 40 and 100 mg/ml can be analyzed (Fig. 7A–D). Generally, a significant shift of R_2 population was observed toward lower values upon the addition of increasing concentrations of Arg·Glu (Fig. 7A–D), with typical values decreasing around 3-fold upon addition of 200 mM Arg·Glu. Such a dramatic decrease in relaxation rates R_2 was unexpected, also taking into account that the inherent increase in buffer viscosity upon an addition of Arg·Glu should slow down molecular tumbling, and contribute toward an increase of R_2. It is unlikely that addition of Arg·Glu leads to structure destabilization and increased polypeptide chain flexibility, as mAb2 is equally thermally stable in the presence of Arg·Glu.[24] To help interpret the significant decrease in transverse relaxation rates R_2, we used an empirical observation that, for protein molecules of this size range, the values of R_2 are generally proportional to the molecular mass and hence to the effective volume occupied by the molecule or cluster of molecules, as well as to the viscosity of the solution. Using this simple approximation, the averaged relative effective volume (aggregation number) of the mAb2 cluster at each concentration of Arg·Glu was calculated, and these are presented on Fig. 7E–H. The relative values give an estimate of the required change in apparent aggregation number needed
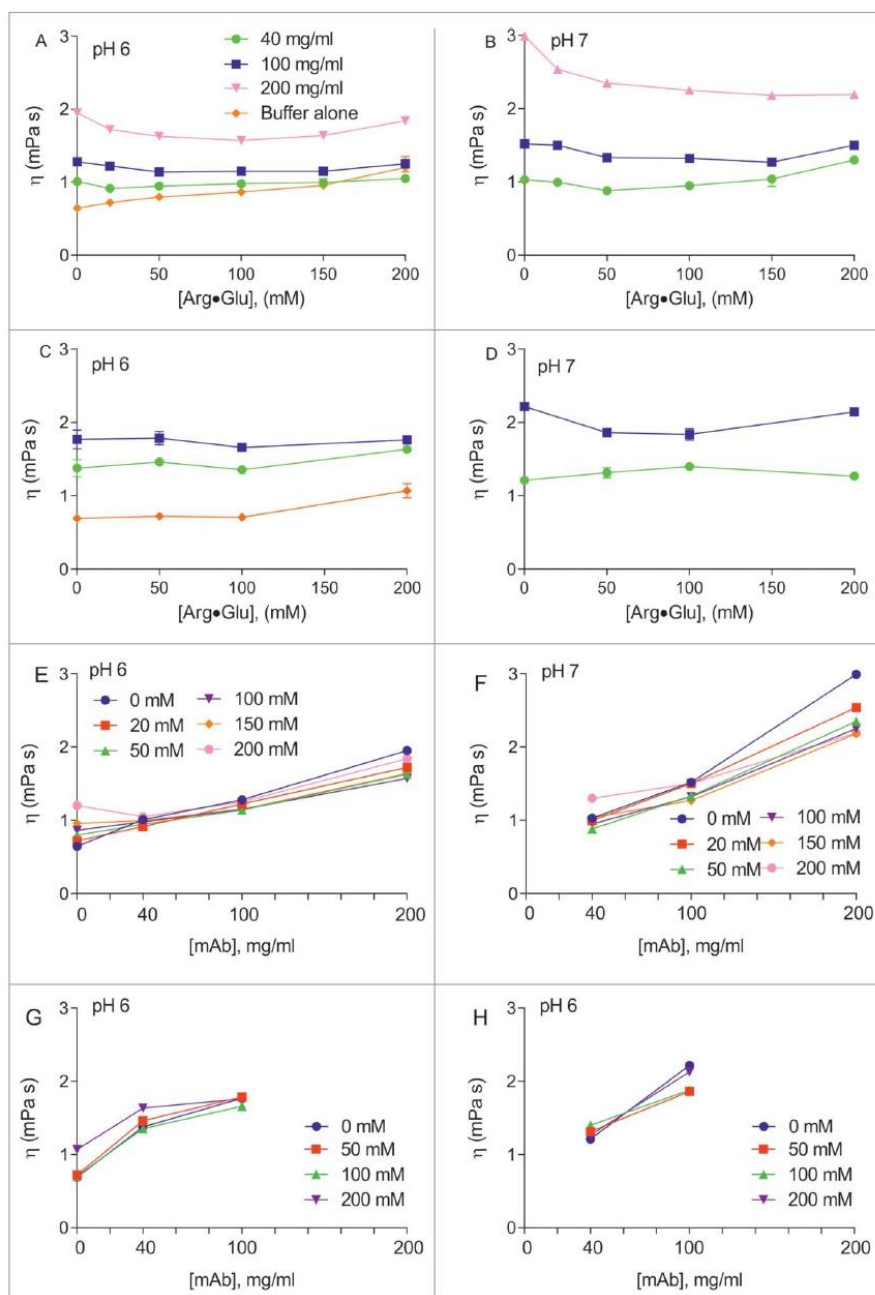
Figure 5. Viscosity of Arg·Glu solutions with and without mAb2 measured by NMR and m-VROC viscometer. Viscosity was measured from NMR-derived diffusion coefficients of citrate ions in solutions at pH 6 (A) and pH 7 (B) in the presence of mAb2 (concentrations as indicated) or buffer alone. Viscosities measured by m-VROC viscometer used the same conditions at pH 6 (C) and pH 7 (D). The NMR data (E, F) and viscometer data (G,H) are re-drawn to highlight the solution viscosity dependence on mAb2 concentration. (Color version of this figure is available online)

to achieve the observed reduction in the measured transverse relaxation rate R_2 upon addition of Arg·Glu. We speculate that the estimated typical 6-fold reduction in the apparent aggregation number may reflect the reduction in reversible self-association of mAb2 oligomers, with a concomitant increase in the overall molecular tumbling rate. It should be also noted that the 6-fold reduction in cluster volume can be achieved by only a 1.8-fold decrease in radius, approximating the change in
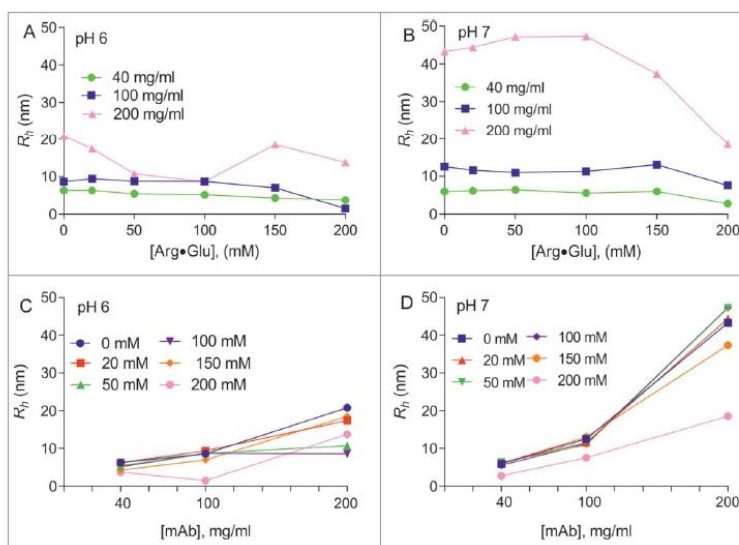
Figure 6. Assessing the changes in the apparent hydrodynamic radius R_h of mAb2 upon addition of Arg·Glu. The values of R_h were assessed vs concentration of Arg·Glu added, using Stokes-Einstein equation for solutions with different concentrations of mAb2 (as labeled) formulated at pH 6 (A) and pH 7 (B). Same dependences are also presented vs mAb2 concentrations, with concentrations of Arg·Glu added color-coded, for pH 6 (C) and pH 7 (D). (Color version of this figure is available online)

R_h estimated from the translational diffusion measurements (Fig. 6A, B).

Discussion

It had been long established that the unwanted high viscosity of some mAb formulations originate from reversible self-association that becomes more prominent at higher concentrations.[7,9,16,27] Reversible self-association can also be a first step toward formation of irreversible aggregates and particles. Therefore, it is essential to monitor and assess the extent of such self-association, and influence of the sample conditions (pH and excipients), *in situ*, without sample dilution.[27] Solution NMR spectroscopy is a powerful analytical technique that is used routinely in structural biology, especially for smaller proteins that can be labeled with stable isotopes, ^{15}N, ^{13}C and ^{2}H. This technique is sensitive to even transient interactions between proteins. Ironically, sample optimization to provide the best spectral properties by fine-tuning sample conditions (pH, temperature, additives) to minimize undesired protein aggregation and increase monomeric content, has long been a first standard step in setting up any protein NMR experiment.[42] Protein NMR typically uses quite high protein concentrations (above mM range), with self-association, increased viscosity and long-term instability of samples all causing problems. The quality, stability and reproducibility of NMR spectra were always used as a criteria for choosing the "best" buffer conditions for a given protein (albeit, usually of small size).

In this study, we explored whether this 'traditional' NMR approach can be useful for very large and unlabeled 145 kDa proteins, mAbs, which are normally considered too complex for proton NMR to resolve. We have described a pragmatic approach to NMR data analysis and interpretation, using NMR parameters as criteria for mAb formulation screening, and shown that simply maximizing the signal intensity of the mAb in 1D ^{1}H NMR spectra ensures that the size of transient protein clusters, as well as overall solution viscosity, is minimized. The necessary experimental setup, placing mAb samples in NMR tubes in different formulations and running the spectra, followed by the analysis of signal intensities, can be easily automated. Although more high-throughput traditional assays may be beneficial at the early stages of formulation screening, NMR can play a role in later stages where detailed understanding of solution behavior may be beneficial, as well as for orthogonal validation of chosen formulations.

Apart from 1D signal intensities, other NMR measurables, such as translational diffusion and relaxation rates, provide a further insight into mAb behavior in different formulations; analysis of these, however, may require more manual input into the experimental setup and data analysis. We found that, although parameters such as translational diffusion coefficients and transverse relaxation rates may be difficult to interpret in the absolute quantitative sense (as no theory currently adequately addresses the self-interaction of proteins at very high protein concentrations and molecular crowding), these parameters still enable the comparison of different formulation conditions. The unique ability of NMR spectroscopy to provide diverse information about the sample *in situ* and to report on the quantities of monomeric and lower-oligomeric species in solution, as well as their conformational state, is ideally complementary to existing methods such as light scattering and chromatography.

The pragmatic approach taken in this work builds on long-accepted assumptions and simplifications. First, the proton transverse relaxation rate R_2 (and hence, signal linewidth) is proportional to the apparent weight-averaged molecular
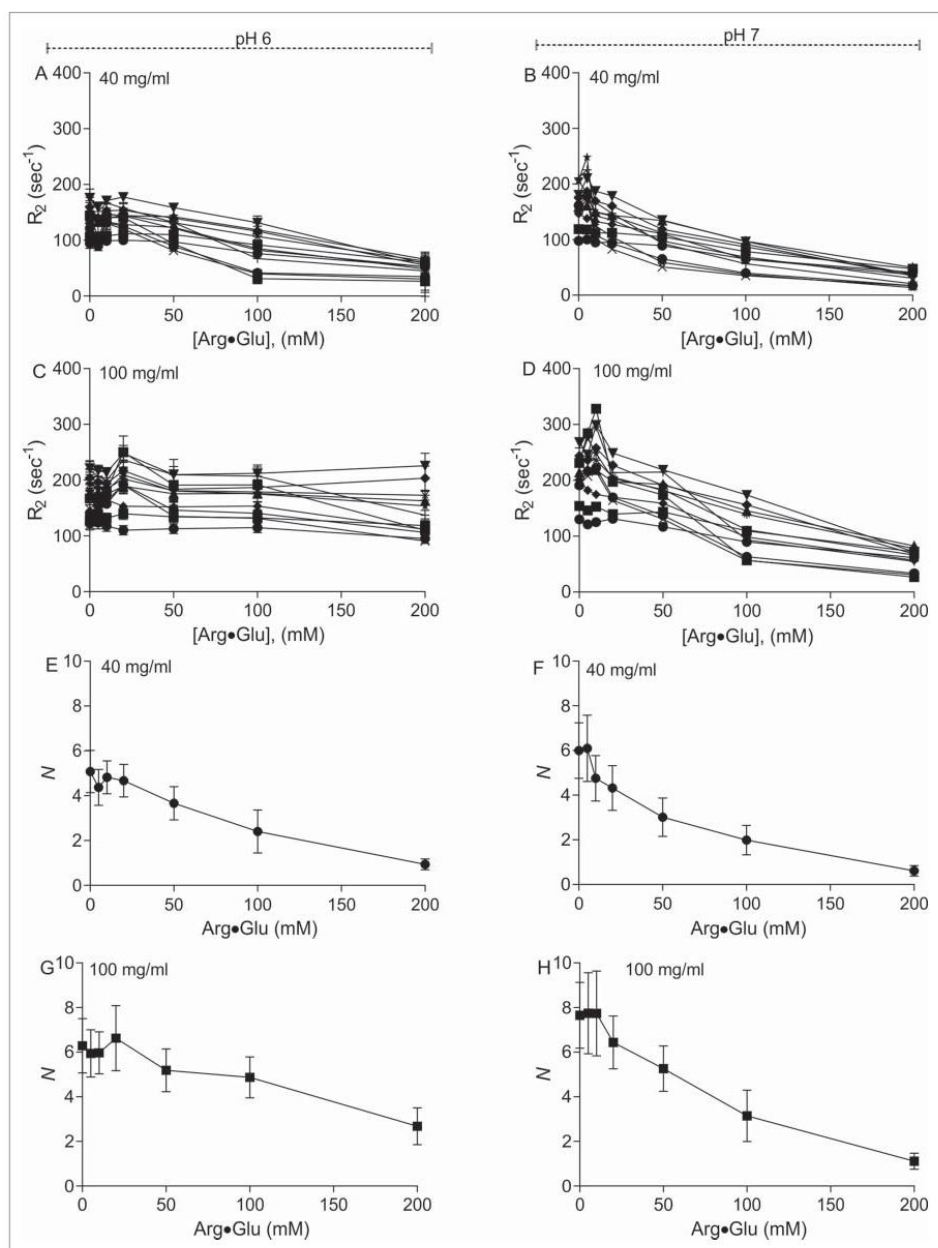
Figure 7. Transverse relaxation rates R_2 of mAb2 protons are generally reduced upon addition of Arg·Glu, which can be interpreted as a relative reduction in the effective protein cluster volume. The panels on the left and right correspond to data obtained at pH 6 and pH 7, respectively. Manifolds of the measured dependencies of R_2 for a selection of signals of mAb2 formulated at 40 mg/ml (A,B) and 100 mg/ml (C,D) show general downward drift upon addition of increasing concentrations of Arg·Glu. The population average values of R_2 were then used to estimate (see Equation 6) the expected relative reduction in the effective aggregation number N, for mAb2 formulated at 40 mg/ml (E,F) and 100 mg/ml (G,H). The error bars represent the expected variability of the data in the manifold.

mass.[42,43] Another implicit assumption, based on the current practice and experience in the protein NMR field, is that observed signal intensities for folded stable proteins in solution are proportional to the concentration of monomeric and lower-oligomeric species, signals from larger aggregates being too broad and unobservable. The decrease in molecular tumbling rate, due to increased viscosity or even transient self-association, will increase transverse relaxation rate and cause signal broadening with concomitant decrease in their intensity. One widely used parameter, protein self-diffusion coefficient, is

linked via the Stokes-Einstein equation (4) to the hydrodynamic size of a molecule and solution viscosity. We found that diffusion of small probe molecules, such as citrate present in the buffer, was sensitive to the apparent viscosity of a solution, even when it contained mAbs: correlation was found with the macroscopic solution viscosity. Protein self-diffusion in crowded (concentrated) solutions is well-known to be strongly affected and attenuated by inter-protein collisions during the PGSE diffusion experiment.[40] In highly-concentrated solutions, this self-diffusion, however, becomes severely limited by the excluded volume and 'caging' effect[44] wherein the diffusion of protein molecules is limited by a high inter-molecular collision rate, although data may still be useful in regard to the relative behavior of comparable solutions.[43] The translational diffusion may also be a poor reporter of protein association if it is affected by factors such as long-distance electrostatic repulsion.[45] This may limit the usefulness of protein diffusion coefficient D measured at high concentration as a criterion for choosing the 'best' formulation condition.

Here, we found that D of mAb2 depended strongly on protein concentration, but the effect of Arg·Glu addition on D was only marginal, although this excipient addition did have a strong effect judging by the signal intensities and R_2 relaxation rates. For interpretation of the changes in D (e.g., transforming them into effective changes in radius of hydration R_h), the knowledge of solution viscosity is required, but for high-concentration mAbs solutions micro- and macro-viscosity may differ significantly, and adding excipient may further modulate viscosity both directly (usually, increasing micro-viscosity of the buffer) and indirectly (often, decreasing overall mAb solution viscosity). Taking into account that the validity of the Stokes-Einstein equation will be limited for concentrated solutions, deriving the reliable values of R_h from D can be open to interpretations and may not be straightforward. The situation with rotational diffusion, which governs R_2, is very different: protein can tumble in crowded conditions with a tumbling time τ_c dependent on the species size (association state) and transient interactions with neighboring molecules, all of which are sensitive to addition of excipients. Mutual electrostatic steering, which may manifest as transient clusters leading to increased viscosity, would also lead to an increase in R_2 rate.[46] Reduction in such steering by addition of excipients therefore can also be detected.

It should be noted that mAb2 used in this study, which is the same as mAb2 we presented previously,[24] is an example of an intrinsically stable and soluble antibody. Despite this, at a very high mAb2 concentration the measurable NMR parameters registered quite significant differences as solvent conditions were varied, highlighting the inherent sensitivity of this NMR technique. It can be anticipated that other, less stable mAbs, which require more careful formulation to achieve satisfactory solubility and stability profile, would show even greater variation in NMR measurables. This study also demonstrated that in the NMR experiments it is possible to use significant concentrations (up to 200 mM) of non-deuterated excipients in the samples, without causing noticeable problems with dynamic range, or strong signal overlap. Use of modern NMR spectrometer equipment allows the measurement of relatively weak mAbs signals (with typical concentration 0.26 to 2.0 mM used

in this study) on the background of large signals from excipients (e.g., 200 mM), without a necessity to selectively suppress these strong signals. Importantly, the general large dispersion of protein signals allows signals to be picked for analysis that are not obscured by the strong signals from the excipients used. Any baseline distortion introduced can be subtracted from each individual spectrum using the standard spectral processing tools. Moreover, use of existing NMR approaches, for example diffusion-based filtering of signals originating from low-molecular weight excipients, may allow further adaptation of pulse sequences for formulation studies of these large proteins. Introducing the existing tools for automation of sample preparation, spectral acquisition and analysis would allow streamlining of the process and adaptation of this technique for medium-throughput screening environment.

Materials and methods

Monoclonal antibody and sample preparation

The monoclonal antibody, mAb2 (IgG1 with MW 145 kDa, pI of 7.9–8.3) was supplied by Medimmune and was identical to mAb2 described in our earlier paper.[24] Solutions of mAb2, 500 μl each, were prepared in 10 mM citrate-phosphate (CP) buffer at pH 6 and 7 with final concentrations of 40, 100 and 200 mg/mL. To each sample, 5% D_2O was added for NMR lock. For NMR measurements, parts of these samples (ca 180 μl) were temporarily transferred to 3 mm NMR tubes. To achieve accurately defined addition of Arg·Glu (5–200 mM) without sample dilution, pre-measured aliquots freeze-dried in Eppendorf tubes were successively reconstituted with 500 μl mAb2 solutions. The freeze-dried aliquots of Arg·Glu were prepared from a 0.5 M stock solution containing equimolar mixture of the free amino acids L-Arg (Analytical grade, Sigma–Aldrich) and L-Glu (Analytical grade, Sigma–Aldrich) in MilliQ water, with pH adjusted where necessary. For the long-term stability studies, 4 formulations were prepared by first dialyzing mAb2 in appropriately diluted formulations, freeze-drying the formulations and then reconstituting them in D_2O in 8-times smaller volume in 180 μl, to achieve the final 300 mg/mL concentration of mAb2 and 10 mM CP buffer in all of them, with additional 200 mM Arg·Glu at pH 6 or pH 7, or 200 mM Arg·HCl at pH 7, or buffer alone at pH 6. Samples were supplemented with 0.01% NaN_3 to prevent bacterial growth, sealed in 3 mm NMR tubes and stored in a controlled temperature incubator at 40°C for the duration of the study. Final mAb2 concentrations were confirmed based on their absorbance at 280 nm.[24] For SE-HPLC, mAbs were diluted to 10 mg/mL in the appropriate buffer, with the monomer content quantified as described previously.[24]

General NMR experiments

All NMR experiments were run on Bruker 800 MHz Avance III spectrometer equipped with 5 mm TCI cryoprobe with temperature control unit, using standard pulse programs and parameters from Bruker library, at 40 °C, unless stated otherwise. Proton 1D spectra were recorded using p3919gp pulse program using 16.0194 ppm spectral width and applying EM window

function with typical 10 Hz broadening. Using one 90°-pulse experiment with water presaturation lead to similar changes in signal intensities upon excipient addition, but was not used for quantitative measurements because of more prominent spectral distortions. Spectra were processed and analyzed using Topspin 3.1 and Dynamics Center 2.2.4 (Bruker).

Analysis of viscosity-corrected signal intensities in 1D ^{1}H NMR spectra

To compensate for the increase in buffer viscosity upon addition of Arg·Glu, which slows down molecular tumbling and reduces apparent spectral intensities, the viscosity-corrected normalized signal intensities in NMR spectra I_η^N were calculated as:

$$I_\eta^N = \frac{I_{[RE]}}{I_{[RE=0]}} \frac{\eta_{[RE]}}{\eta_{[RE=0]}} \tag{1}$$

where $I_{[RE]}$ and $I_{[RE=0]}$ are signal intensities and $\eta_{[RE]}$ and $\eta_{[RE=0]}$ are buffer viscosities in the presence and absence of Arg·Glu, respectively. The buffer viscosity values were derived from the diffusion coefficients of citrate ions measured using PFG-NMR spectroscopy (see below). The flat dependencies of I_η^N over [Arg·Glu] would show that the concentration of soluble monomeric or lower-oligomeric protein species is not affected by Arg·Glu addition.

Analysis of temperature dependence of NMR spectra and short-term and long-term thermal stress studies

For these studies, mAb2 at 40 and 100 mg/mL were formulated at pH 6 and 7 with and without 200 mM Arg·Glu, These were subjected to increased temperatures T between 40–75 °C, incremented in 5°C steps, with 10 min equilibration after each temperature increase. A pair of 1D NMR spectra (p3919gp pulse program) was then acquired at each temperature with 45 min interval. To assess the dependence of concentration of monomeric or lower-oligomeric soluble species on the temperature T, relative increase in viscosity upon addition of 200 mM Arg·-Glu, if appropriate, were additionally taken into account. Temperature-dependent normalized integral parameters L_η^N were calculated as:

$$L_\eta^N(T) = \frac{L^T}{L_{[RE=0]}^{40}} \frac{\eta_{[RE]}}{\eta_{[RE=0]}} \tag{2}$$

where L^T is the signal integral at a particular temperature T, $L_{[RE=0]}^{40}$ is the integral measured at 40 °C in the absence of Arg·-Glu, and $\frac{\eta_{[RE]}}{\eta_{[RE=0]}}$ is the ratio of the buffer viscosity (with or without 200 mM Arg·Glu, as appropriate) to the viscosity without Arg·Glu. Flat and level dependence of L_η^N over T would show that there is no temperature-dependent change in the population of monomeric or lower-oligomeric species.

The fraction of soluble protein F preserved in solution after exposure to high temperature for time period t were calculated as:

$$F = \frac{I^t}{I^0} \tag{3}$$

where I^0 and I^t are the intensities of the same signal before and after 45 min exposure at a high temperature. The value F is the measure of short-term sample stability at increased temperature, and shows the fraction loss of monomeric or lower-oligomeric species in solution over an arbitrarily set time period t (here, $t = 45$ min). For the long-term stability studies, the samples were stored at 40°C and 1D NMR spectra recorded at the same temperature regularly over 10 weeks. The fraction of soluble monomeric or lower-oligomeric protein preserved in solution after time exposure was calculated using Equation (3) for a number of peaks integrated in the aromatic (F^{AR}) and amide (F^{NH}) regions (7 ppm and 9 ppm respectively), and presented as the fractions of the initial values.

Measuring diffusion rates by pulsed field gradient (PFG) NMR spectroscopy

Changes in the translational diffusion coefficient (D) were monitored using SE-PFG (stimulated echo- pulsed-field gradient) with bipolar gradients pulses with water suppression (Bruker's standard pulse program stebpgp1s19). The diffusion time (Δ) and the gradient length (δ) were set to 250 ms and 4.0 ms, respectively. The acquisition time and relaxation delay were 640 ms and 2.0 s, respectively, with a gradient pulse of 45 G/cm. The diffusion spectra were recorded with 32 scans over a spectral width of 16 ppm with 16 linear gradient steps, 10–98% gradient intensity. Each sample was allowed to equilibrate within the NMR spectrometer for 5 minutes after the completion of experimental setup. Translation diffusion coefficients D were derived using standard diffusion-ordered spectroscopy (DOSY) analysis offered in Topspin. The errors in D were calculated based on the upper and lower error limits for each DOSY peak. The gradients were calibrated to achieve the tabulated values for dioxan diffusion in water,[39] and then to calibrate the diffusion of citrate ions present in the buffer. Dioxan could not be used as a diffusion probe for buffers containing Arg·Glu due to signal overlap. DOSY experiments allowed to measure diffusion coefficients simultaneously of both probe molecule, citrate, and mAb2, when present, upon addition of Arg·Glu. Thus, measured diffusion coefficient D was related to the apparent size of the molecule and apparent viscosity using the Stokes-Einstein equation:

$$\frac{kT}{6\pi R_h \eta} \tag{4}$$

where T is the absolute temperature, k is the Boltzmann constant; R_h is the hydrodynamic radius and η is the viscosity. Diffusion rates of citrate ions in CP buffer at 40°C measured by DOSY without and with Arg·Glu added were used, together with the Equation (4), to determine the values of buffer viscosity in the presence of Arg·Glu, $\eta_{[RE]}$. Parameters were calibrated so that the measured $\eta_{[RE=0]}$ matched the dynamic viscosity of

water at 40°C in the absence of Arg·Glu (0.65 mPa s). Using the measured diffusion coefficients D of mAb2, and knowing buffer viscosities, the apparent hydrodynamic radius (R_h) of mAb2 was calculated using rearranged Equation (4).

Controlled temperature long-term storage stability studies with HPLC-SEC analysis

Accelerated stability studies were set up at 40°C for 300 mg/mL mAb2 formulated similarly as for NMR long-term stability studies. The final mAb formulations were transferred to 3 ml glass vials and stored for 16 weeks. The samples were tested by SE-HPLC for percentage of mAb2 monomer remaining in solution every week for the first month and then monthly up to 4 months, using the methodology described previously.[24]

Viscosity measurements

The viscosity of the mAb solutions was determined using the m-VROC viscometer (RheoSense Inc., San Ramon, CA, USA). Solutions of mAb2 at concentrations 40 and 100 mg/ml were measured with a B05-chip at a shear rate of 6000 1/s for 30 sec. Viscosity of 300 mg/ml samples from long-term accelerated stability series was measured using a D05-chip at a shear rate of 5000 1/s for 15 sec. Measurement temperature was set at 40°C and was controlled by an external water bath. Samples were filled in to a 1 ml syringe and triplicate measurements were acquired where possible due to the limitation of sample volumes. Between each measurements the system was washed with 1% tergazyme followed by 1% aquet and then water each with 750 μL/min flow rate for 60 sec (for B05-Chip) or 1000 μL/min for 45 sec (D05-chip).

Measurement of transverse relaxation rates R_2

Non-selective proton transverse relaxation rates R_2 were measured using a series of standard Carr-Purcell-Meiboom-Gill (CPMG) experiments, with the number of echoes varied (pulse program cpmgpr1d, Bruker). The relaxation delay was 5 sec, and the majority of protein signal decay was occurring between 4 and 66 spin echoes applied (with corresponded times from 2.48 to 40.92 ms). The data was processed using the T1/T2 Relaxation analysis tool in Topspin 3.1 and/or Dynamics Center 2.2.4 (Bruker) and fitted to the mono-exponential decay. To track the changes in the characteristic R_2 population behavior upon adding Arg·Glu, 12 prominent proton signals were selected for analysis between -0.5 and 1 ppm and followed throughout the titration. Assuming that R_2 of the signals (in the absence of internal motions and chemical exchange) are generally proportional to the rotational correlation time τ_c,[42] which in turn is proportional to the effective spherical volume V (or molecular weight) of the protein cluster[39]:

$$R_2 \propto \tau_c = \frac{V\eta}{kT} \qquad (5)$$

Further assuming that the lowest value R_2^m, which was observed at the lowest protein concentration 40 mg/ml in the presence of 200 mM of Arg·Glu (with microscopic viscosity η^m), corresponds to the minimum cluster volume V^m (i.e., mAb2 monomer), the apparent aggregation number N (i.e, the effective number of mAb2 molecules in a cluster) in all other conditions can be estimated from R_2 and known microscopic viscosity η as:

$$N = \frac{V}{V^m} = \frac{R_2\eta^m}{R_2^m\eta} \qquad (6)$$

The value of aggregation number N gives an indication of what should be the expected change in the apparent size of the mAb2 cluster to explain the observed decrease in relaxation rate R_2 for a rigid molecule.

Disclosure of potential conflict of interest

SU and CFvdW are full time employees of MedImmune Ltd.

References

1. Ecker DM, Jones SD, Levine HL. The therapeutic monoclonal antibody market. MAbs 2015; 7:9-14; PMID:25529996; http://dx.doi.org/10.4161/19420862.2015.989042
2. Elvin JG, Couston RG, van der Walle CF. Therapeutic antibodies: market considerations, disease targets and bioprocessing. Int J Pharm 2013; 440:83-98; PMID:22227342; http://dx.doi.org/10.1016/j.ijpharm.2011.12.039
3. Fajardo-Ramirez OR, Ascacio-Martinez JA, Licea-Navarro AF, Villela-Martinez LM, Barrera-Saldana HA. Technological Evolution in the Development of Therapeutic Antibodies. Rev Invest Clin 2015; 67:158-69; PMID:26202739
4. Cromwell ME, Hilario E, Jacobson F. Protein aggregation and bioprocessing. AAPS J 2006; 8:E572-9; PMID:17025275; http://dx.doi.org/10.1208/aapsj080366
5. Mahler HC, Friess W, Grauschopf U, Kiese S. Protein aggregation: pathways, induction factors and analysis. J Pharm Sci 2009; 98:2909-34; PMID:18823031; http://dx.doi.org/10.1002/jps.21566
6. Stradner A, Sedgwick H, Cardinaux F, Poon WC, Egelhaaf SU, Schurtenberger P. Equilibrium cluster formation in concentrated protein solutions and colloids. Nature 2004; 432:492-5; PMID:15565151; http://dx.doi.org/10.1038/nature03109
7. Yearley Eric J, Godfrin Paul D, Perevozchikova T, Zhang H, Falus P, Porcar L, Nagao M, Curtis JE, Gawande P, Taing R, et al. Observation of Small Cluster Formation in Concentrated Monoclonal Antibody Solutions and Its Implications to Solution Viscosity. Biophys J 2014; 106:1763-70; PMID:24739175; http://dx.doi.org/10.1016/j.bpj.2014.02.036
8. Johnston KP, Maynard JA, Truskett TM, Borwankar AU, Miller MA, Wilson BK, Dinin AK, Khan TA, Kaczorowski KJ. Concentrated dispersions of equilibrium protein nanoclusters that reversibly dissociate into active monomers. ACS Nano 2012; 6:1357-69; PMID:22260218; http://dx.doi.org/10.1021/nn204166z
9. Kanai S, Liu J, Patapoff TW, Shire SJ. Reversible self-association of a concentrated monoclonal antibody solution mediated by Fab-Fab interaction that impacts solution viscosity. J Pharm Sci 2008; 97:4219-27; PMID:18240303; http://dx.doi.org/10.1002/jps.21322
10. Shire SJ. Formulation and manufacturability of biologics. Curr Opin Biotechnol 2009; 20:708-14; PMID:19880308; http://dx.doi.org/10.1016/j.copbio.2009.10.006

11. He F, Woods CE, Becker GW, Narhi LO, Razinkov VI. High-throughput assessment of thermal and colloidal stability parameters for monoclonal antibody formulations. J Pharm Sci 2011; 100:5126-41; PMID:21789772; http://dx.doi.org/10.1002/jps.22712

12. Kopec J, Schneider G. Comparison of fluorescence and light scattering based methods to assess formation and stability of protein-protein complexes. J Struct Biol 2011; 175:216-23; PMID:21536135; http://dx.doi.org/10.1016/j.jsb.2011.04.006

13. Sule SV, Cheung JK, Antochshuk V, Bhalla AS, Narasimhan C, Blaisdell S, Shameem M, Tessier PM. Solution pH that minimizes self-association of three monoclonal antibodies is strongly dependent on ionic strength. Mol Pharmaceut 2012; 9:744-51; PMID:22221144; http://dx.doi.org/10.1021/mp200448j

14. Bhambhani A, Kissmann JM, Joshi SB, Volkin DB, Kashi RS, Middaugh CR. Formulation design and high-throughput excipient selection based on structural integrity and conformational stability of dilute and highly concentrated IgG1 monoclonal antibody solutions. J Pharm Sci 2012; 101:1120-35; PMID:22147527; http://dx.doi.org/10.1002/jps.23008

15. Saito S, Hasegawa J, Kobayashi N, Tomitsuka T, Uchiyama S, Fukui K. Effects of ionic strength and sugars on the aggregation propensity of monoclonal antibodies: influence of colloidal and conformational stabilities. Pharm Res 2013; 30:1263-80; PMID:23319172; http://dx.doi.org/10.1007/s11095-012-0965-4

16. Kamerzell TJ, Pace AL, Li M, Danilenko DM, McDowell M, Gokarn YR, Wang YJ. Polar solvents decrease the viscosity of high concentration IgG1 solutions through hydrophobic solvation and interaction: formulation and biocompatibility considerations. J Pharm Sci 2013; 102:1182-93; PMID:23359242; http://dx.doi.org/10.1002/jps.23453

17. Roberts D, Keeling R, Tracka M, van der Walle CF, Uddin S, Warwicker J, Curtis R. The role of electrostatics in protein-protein interactions of a monoclonal antibody. Mol Pharm 2014; 11:2475-89; PMID:24892385; http://dx.doi.org/10.1021/mp5002334

18. Roberts D, Keeling R, Tracka M, van der Walle CF, Uddin S, Warwicker J, Curtis R. Specific ion and buffer effects on protein-protein interactions of a monoclonal antibody. Mol Pharm 2015; 12:179-93; PMID:25389571; http://dx.doi.org/10.1021/mp500533c

19. Wang SJ, Zhang N, Hu T, Dai WG, Feng XY, Zhang XY, Qian F. Viscosity-Lowering Effect of Amino Acids and Salts on Highly Concentrated Solutions of Two IgG1 Monoclonal Antibodies. Mol Pharmaceut 2015; 12:4478-87; PMID:26528726; http://dx.doi.org/10.1021/acs.molpharmaceut.5b00643

20. Golovanov AP, Hautbergue GM, Wilson SA, Lian LY. A simple method for improving protein solubility and long-term stability. J Am Chem Soc 2004; 126:8933-9; PMID:15264823; http://dx.doi.org/10.1021/ja049297h

21. Hautbergue GM, Golovanov AP. Increasing the sensitivity of cryoprobe protein NMR experiments by using the sole low-conductivity arginine glutamate salt. J Magn Reson 2008; 191:335-9; PMID:18207440; http://dx.doi.org/10.1016/j.jmr.2007.12.017

22. Blobel J, Brath U, Bernadó P, Diehl C, Ballester L, Sornosa A, Akke M, Pons M. Protein loop compaction and the origin of the effect of arginine and glutamic acid mixtures on solubility, stability and transient oligomerization of proteins. Eur Biophys J 2011; 40:1327-38; PMID:21390527; http://dx.doi.org/10.1007/s00249-011-0686-3

23. Shukla D, Trout BL. Understanding the synergistic effect of arginine and glutamic acid mixtures on protein solubility. J Phys Chem B 2011; 115:11831-9; PMID:23831612; http://dx.doi.org/10.1021/jp204462t

24. Kheddo P, Tracka M, Armer J, Dearman RJ, Uddin S, van der Walle CF, Golovanov AP. The effect of arginine glutamate on the stability of monoclonal antibodies in solution. Int J Pharm 2014; 473:126-33; PMID:24992318; http://dx.doi.org/10.1016/j.ijpharm.2014.06.053

25. Kheddo P, Golovanov AP, Mellody KT, Uddin S, van der Walle CF, Dearman RJ. The effects of arginine glutamate, a promising excipient for protein formulation, on cell viability: Comparisons with NaCl.

26. Pifferi G, Restani P. The safety of pharmaceutical excipients. Farmaco 2003; 58:541-50; PMID:12875883; http://dx.doi.org/10.1016/S0014-827X(03)00079-X

27. Liu J, Nguyen MD, Andya JD, Shire SJ. Reversible self-association increases the viscosity of a concentrated monoclonal antibody in aqueous solution. J Pharm Sci 2005; 94:1928-40; PMID:16052543; http://dx.doi.org/10.1002/jps.20347

28. Cavanagh J, Fairbrother WJ, Palmer AG, Rance M, Skelton NJ. Protein NMR Spectroscopy: Principles and Practice, 2nd Edition. Elsevier, Inc.: Amsterdam, 2007.

29. Marion D. An introduction to biological NMR spectroscopy. Mol Cell Proteomics 2013; 12:3006-25; http://dx.doi.org/10.1074/mcp.O113.030239

30. Wang G, Zhang ZT, Jiang B, Zhang X, Li C, Liu M. Recent advances in protein NMR spectroscopy and their implications in protein therapeutics research. Anal Bioanal Chem 2014; 406:2279-88; PMID:24309626; http://dx.doi.org/10.1007/s00216-013-7518-5

31. Wishart DS. Characterization of biopharmaceuticals by NMR spectroscopy. Trac-Trend Anal Chem 2013; 48:96-111; http://dx.doi.org/10.1016/j.trac.2013.03.009

32. Poppe L, Jordan JB, Lawson K, Jerums M, Apostol I, Schnier PD. Profiling Formulated Monoclonal Antibodies by H-1 NMR Spectroscopy. Anal Chem 2013; 85:9623-9; PMID:24006877; http://dx.doi.org/10.1021/ac401867f

33. Poppe L, Jordan JB, Rogers G, Schnier PD. On the Analytical Superiority of 1D NMR for Fingerprinting the Higher Order Structure of Protein Therapeutics Compared to Multidimensional NMR Methods. Anal Chem 2015; 87:5539-45; PMID:25929316; http://dx.doi.org/10.1021/acs.analchem.5b00950

34. Chen K, Freedberg DI, Keire DA. NMR profiling of biomolecules at natural abundance using 2D 1H-15N and 1H-13C multiplicity-separated (MS) HSQC spectra. J Magn Reson 2015; 251:65-70; PMID:25562571; http://dx.doi.org/10.1016/j.jmr.2014.11.011

35. Arbogast LW, Brinson RG, Marino JP. Mapping monoclonal antibody structure by 2D 13C NMR at natural abundance. Anal Chem 2015; 87:3556-61; PMID:25728213; http://dx.doi.org/10.1021/ac504804m

36. Arbogast LW, Brinson RG, Formolo T, Hoopes JT, Marino JP. 2D H-1 (N), N-15 Correlated NMR Methods at Natural Abundance for Obtaining Structural Maps and Statistical Comparability of Monoclonal Antibodies. Pharm Res 2016; 33:462-75; PMID:26453189; http://dx.doi.org/10.1007/s11095-015-1802-3

37. Arbogast LW, Brinson RG, Marino JP. Application of Natural Isotopic Abundance (1)H-(13)C- and (1)H-(15)N-Correlated Two-Dimensional NMR for Evaluation of the Structure of Protein Therapeutics. Methods Enzymol 2016; 566:3-34; PMID:26791974; http://dx.doi.org/10.1016/bs.mie.2015.09.037

38. James TL. Fundamentals of NMR. In Selected Topics in Biophysics, Biophysical Society, Rockville, MD 1998; Chapter 1:1-31

39. Yao S, Babon JJ, Norton RS. Protein effective rotational correlation times from translational self-diffusion coefficients measured by PFG-NMR. Biophys Chem 2008; 136:145-51; PMID:18583018; http://dx.doi.org/10.1016/j.bpc.2008.06.002

40. Price WS, Tsuchiya F, Arata Y. Lysozyme aggregation and solution properties studied using PGSE NMR diffusion measurements. J Am Chem Soc 1999; 121:11503-12; http://dx.doi.org/10.1021/ja992265n

41. Dehner A, Kessler H. Diffusion NMR spectroscopy: Folding and aggregation of domains in p53. Chembiochem 2005; 6:1550-65; PMID:16138303; http://dx.doi.org/10.1002/cbic.200500093

42. Anglister J, Grzesiek S, Ren H, Klee CB, Bax A. Isotope-edited multidimensional NMR of calcineurin B in the presence of the non-deuterated detergent CHAPS. J Biomol Nmr 1993; 3:121-6; PMID:8383554; http://dx.doi.org/10.1007/BF00242480

43. Inoue T, Akasaka K. Self Association of Streptomyces Subtilisin Inhibitor - Sedimentation Equilibrium and H-1-NMR Studies. J Biochem-Tokyo 1987; 102:1371-8; PMID:3329195

Toxicol Vitro 2016; 33:88-98; PMID:26873863; http://dx.doi.org/10.1016/j.tiv.2016.02.002

44. Roos M, Link S, Balbach J, Krushelnitsky A, Saalwachter K. NMR-detected brownian dynamics of alphaB-crystallin over a wide range of concentrations. Biophys J 2015; 108:98-106; PMID:25564856; http://dx.doi.org/10.1016/j.bpj.2014.11.1858

45. McGuffee SR, Elcock AH. Atomically detailed simulations of concentrated protein solutions: the effects of salt, pH, point mutations, and protein concentration in simulations of 1000-molecule systems. J Am Chem Soc 2006; 128:12098-110; PMID:16967959; http://dx.doi.org/10.1021/ja0614058

46. Roos M, Hofmann M, Link S, Ott M, Balbach J, Rossler E, Saalwächter K, Krushelnitsky A. The "long tail" of the protein tumbling correlation function: observation by (1)H NMR relaxometry in a wide frequency and concentration range. J Biomol NMR 2015; 63:403-15; PMID:26582718; http://dx.doi.org/10.1007/s10858-015-0001-1

The importance of stabilising monoclonal antibodies-based formulations was outlined in a further publication by Kheddo and co-workers (Kheddo, et al., 2016, p. 88). This study established that the mAb product must have an adequate shelf-life under common shipping conditions and storage temperatures. Currently, by changing pH and ionic strength of the mAb solution, it is possible to change the necessary stability parameters, however more recently a particular focus has been placed on the possibility of adding various excipients (Watts, et al., 2005, p. 521). These compounds were found to substantially increase product stability through prevention of aggregation as well as enhanced protein optimisation in the corresponding pharmaceutical products. Stabilising compounds include glycine, histidine, arginine as well as other amino acids. In addition to the indicated excipients, sugars were also found to provide a stabilising effect. A range of theories is suggested to explain the observed protein stabilisation in the presence of these excipients. These theories include prevention of protein aggregation through excluded volume as well as preferential interactions and hydration (Bye, et al., 2014, p. 869). Selection of excipients in the industrial settings in carried out using biophysical assays where a range of possible candidates is initially identified and screened to compare the impact of these on the product stability.

When comparing the stabilising effects of various excipients, Arakawa and co-workers found that arginine was particularly effective in supressing aggregation of proteins (Arakawa, et al., 2007, p. 2). The exact mechanism of action was not established, however it was determined that arginine was able to form reversible bonds with protein side chains that was compensated by repulsion from other chains and groups (Arakawa, et al., 2007, p. 3). The concentration of arginine determines the total stabilisation effect and the difference between repulsion/attraction that is observed upon producing arginine-stabilised products. Computer based simulations suggested that arginine cations produce clusters at certain protein regions, rich with carboxylate and guanidinium side chains. It was also established that stabilisation was substantially affected by the presence of ion-ion pairs as well as other charged groups. Thus, it was found that arginine citrate, phosphate and sulphate were the most active forms of arginine with the strongest aggregation suppression effect.

In addition to arginine and arginine-based salts, the possibility of using other amino acids in protein stabilisation was explored. Thus, equimolar mixtures of arginine and glutamate were prepared, and their stabilisation properties tested. The described amino acids are intrinsic components of cells, they can be found in the diet of both humans and animals. For this reason, arginine and arginine/glutamate-based excipients present a highly attractive stabilising component of monoclonal antibody-based formulations. Kheddo and co-workers suggested that initial experiments on monoclonal

antibody stabilisation with arginine-based excipients indicated that it was possible to achieve solution stabilisation under elevated temperatures and broad pH range (Kheddo, et al., 2016, p. 89). The results of this study are discussed in section 3.1 below.

CrossMark

The effects of arginine glutamate, a promising excipient for protein formulation, on cell viability: Comparisons with NaCl

Priscilla Kheddo [a,b], Alexander P. Golovanov [a,b], Kieran T. Mellody [b], Shahid Uddin [c], Christopher F. van der Walle [c], Rebecca J. Dearman [b,*]

[a] Manchester Institute of Biotechnology, University of Manchester, Manchester M1 7DN, UK
[b] Faculty of Life Sciences, University of Manchester, Manchester M13 9PL, UK
[c] MedImmune Ltd, Granta Park, Cambridge CB21 6GH, UK

ARTICLE INFO

ABSTRACT

The effects of an equimolar mixture of L-arginine and L-glutamate (Arg·Glu) on cell viability and cellular stress using in vitro cell culture systems are examined with reference to NaCl, in the context of monoclonal antibody formulation. Cells relevant to subcutaneous administration were selected: the human monocyte cell line THP-1, grown as a single cell suspension, and adherent human primary fibroblasts. For THP-1 cells, the mechanism of cell death caused by relatively high salt concentrations was investigated and effects on cell activation/stress assessed as a function of changes in membrane marker and cytokine (interleukin-8) expression. These studies demonstrated that Arg·Glu does not have any further detrimental effects on THP-1 viability in comparison to NaCl at equivalent osmolalities, and that both salts at higher concentrations cause cell death by apoptosis; there was no significant effect on measures of THP-1 cellular stress/activation. For adherent fibroblasts, both salts caused significant toxicity at ~400 mOsm/kg, although Arg·Glu caused a more precipitous subsequent decline in viability than did NaCl. These data indicate that Arg·Glu is of equivalent toxicity to NaCl and that the mechanism of toxicity is such that cell death is unlikely to trigger inflammation upon subcutaneous injection in vivo.

1. Introduction

Since the licencing by the US Food and Drug Administration (FDA) in 1986 of the first monoclonal antibody therapy, a murine IgG2a anti-CD3 antibody for the treatment of solid organ transplant rejection, the field has expanded rapidly (Hooks et al., 1991; Singleton, 2014; Walsh, 2010). These targeted biological therapies are now used for the treatment of a range of diseases including rheumatoid arthritis, psoriasis, inflammatory bowel disease and cancer (Lynch et al., 2014; Sedger and McDermott, 2014; Pandey and Mahadevan, 2014). Indeed, in 2012 three monoclonal antibodies that target the proinflammatory cytokine tumor necrosis factor (TNF)-α (adalimumab, infliximab and entanercept) were the world's top selling medicines in that year (Ho and Chien, 2012).

The formulation process in the biopharmaceutical industry requires the quantitative characterization of several potential degradation pathways, both covalent (e.g. oxidation, deamidation, proteolysis) and non-covalent (e.g. aggregation, unfolding-denaturation, phase separation) (Razinkov et al., 2015). The formulation that is selected must impart a long term stability to the product, at least over the required shelf-life, storage temperature and shipping conditions. It is the composition of the aqueous environment (buffer pH, ionic strength, excipient, etc.) that plays a critical role in maintaining the colloidal stability of an antibody in solution (Roberts et al., 2015). Various excipients (additives) have been used to optimize protein stability of pharmaceutical products and to minimize the extent of aggregation (Kamerzell et al., 2011). These include amino acids, such as histidine, arginine, and glycine (Arakawa et al., 2007a), sugars, such as trehalose (Kaushik and Bhat, 2003). There are several mechanisms by which small molecule excipients are proposed to stabilize proteins, including preferential interaction, preferential hydration and excluded volume (Bye et al., 2014). It is currently not possible to select excipients for a particular mAb formulation a priori, although platform approaches in the industry may favour

one particular solution condition. The identification of one or more excipients to be included in a buffer in order to stabilize the protein formulation may be carried out by analysis of data generated by high throughput biophysical assays (Cheng et al., 2012).

Arginine is of particular interest as an excipient used to suppress protein aggregation, with several groups working on the elucidation of its mechanism of action. The weak interactions of arginine with the protein surface are due to its affinity for some amino acid side chains and the peptide backbone, but this is balanced by repulsion from the protein surface on account of an increase in the surface tension and volume exclusion effects (a complete review is given by Arakawa et al. (2007b)). The net effect of the preferential inclusion versus exclusion of arginine from the protein surface is dependent on its concentration, with an apparent saturation of the protein surface at around 0.5 M, above which arginine is considered to be excluded (Schneider and Trout, 2009). In silico modelling suggests that arginine cations cluster at certain protein surface patches via interaction with guanidinium and carboxylate amino acid side chains (Vagenende et al., 2013). However, the salt forms of excipients containing charged groups (or ion–ion pairs) are also known to play an important role in determining the mechanism of action in regard to protein stabilization. This is especially true for various salt forms of arginine, whose ability to suppress protein aggregation was shown to follow the empirical Hofmeister series; phosphate, sulphate and citrate more strongly interacting with the arginine cation and suppressing aggregation (Schneider et al., 2011). Given the importance of the salt form of arginine, one such excipient currently being explored in the area of biopharmaceutics is an equimolar mixture of amino acids L-arginine and L-glutamate (Arg·Glu salt). This excipient has been shown to increase protein solubility and stability and has been used in the fields of structural biology and vaccine development for some time (Blobel et al., 2011; Golovanov et al., 2004; Mistilis et al., 2015; Vedadi et al., 2006). These amino acids are a natural constituent of organisms and cells, they are part of human diet, and therefore inherently are non-toxic. Initial experiments have indicated that Arg·Glu can suppress aggregation of monoclonal antibody preparations induced by increased temperatures or pH and was also effective under accelerated stability conditions at weakly acidic to neutral pH (Kheddo et al., 2014).

In practice, excipients used for patient-injected formulations, including L-Arg and L-Glu, are chosen from the Generally Recognized as Safe (GRAS) category (US Food and Drugs Agency [FDA], 1982; Ogaji et al., 2011; Pifferi and Restani, 2003). However, the higher Arg·Glu concentrations (e.g. ≥200 mM in the final formulation, Kheddo et al., 2014), which may be necessary for optimal protein solubility, increase osmolality and hence may affect cell viability in vitro or in vivo or cause cellular stress (Vázquez-Rey and Lang, 2011). Indeed, the tolerability of hypertonic injectables has been reviewed recently (Wang, 2015). For drug products intended for subcutaneous injection, the main potential adverse effects were identified as enhanced site pain, local irritation and possible tissue damage and it was recommended that for drug products intended for subcutaneous injection, the upper osmolality limit should be 600 mOsm/kg (Wang, 2015). Changes to tissue osmolality may also cause activation of local dendritic cells (DC), sentinel cells of the immune system, acting as a trigger for inflammation (Gallo and Gallucci, 2013). These cells are activated by so-called "danger signals" which may derive directly from pathogens or dying host cells and also may be associated with perturbations of tissue/cell homeostasis such as changes in osmolality. Hypotonicity has been shown to act as a danger signal (Compan et al., 2012) and there are also reports that osmotic shock due to hypertonicity induced the production of the proinflammatory cytokine interleukin (IL)-8 by human peripheral blood mononuclear cells (Shapiro and Dinarello, 1997) and upregulation of macrophage caspase-1 (Ip and Medzhitov, 2015).

The aim of the current investigations was to examine the effects of increased concentrations of Arg·Glu on cell viability and cellular stress using in vitro cell culture systems. Similar studies have been conducted previously to investigate the impact of excipients within formulations on cell viability (Gursoy et al., 2003; Lee et al., 2013; Ménard et al., 2012; Nogueira et al., 2011). Cells of relevance to the subcutaneous route of administration have been selected (Kagan, 2014): the human monocyte cell line THP-1 (a surrogate DC line; Megherbi et al., 2009), grown as a single cell suspension, and human primary fibroblasts, cultured as an adherent monolayer. Thus, the impact on cell viability of increasing osmolalities of L-Arg and L-Glu solutions (together and separately) has been examined in comparison with the reference standard NaCl. In addition, for THP-1 cells, the mechanism of cell death which these different salts cause at relatively high concentrations has been investigated by flow cytometry, allowing differentiation between death by necrosis and death by apoptosis (otherwise known as programmed cell death) (Kabakov et al., 2011). More subtle effects of the presence of Arg·Glu on cell activation have been assessed as a function of changes in membrane marker expression on activated THP-1 cells (Megherbi et al., 2009).

2. Methods

2.1. Cell line maintenance

The THP-1 human monocytic leukaemia cell line (Sigma-Aldrich Chemical Co.; Poole, Dorset, U.K.) was cultured in RPMI-1640 medium (Sigma) supplemented with 400 µg/mL streptomycin, 400 µg/mL penicillin (both from Sigma), 2 mM L-glutamine (GIBCO; Paisley, Renfrewshire, UK) and 10% fetal calf serum (FCS; GE Healthcare, Cambridge, UK). THP-1 cells were maintained in vented T75 flasks at 37 °C in an atmosphere of 5% CO_2 and split every 3–4 days when confluent ($>2 \times 10^6$ cells/mL). Primary fibroblasts from human explants were cultured in DMEM medium (high glucose [4.5 g/L] with 2 mM L-Glutamine; GIBCO) supplemented with 400 µg/mL streptomycin, 400 µg/mL penicillin, 2 mM GlutaMax (GIBCO), 0.25 µg/mL amphotericin B (Sigma) and 10% FCS. Fibroblasts were maintained in 10 cm culture dishes at 37 °C/5% CO_2 and passaged every 3–4 days when >80% confluent. Cell number was assessed by exclusion of 0.5% trypan blue using a hemocytometer.

2.2. Salts used for generating changes in osmolality

Stock solutions of cell culture grade arginine glutamate (Arg·Glu) from equimolar mixtures of L-Arg (CAS number 74–79–3) and L-Glu (CAS number 142–47–2), NaCl (CAS number 7647–14–5), L-arginine hydrochloride (Arg·HCl; CAS number 1119–34–2) and sodium glutamate (NaGlu; CAS number 56–86–0) (all from Sigma-Aldrich) were prepared at 2.24 M, 4.96 M, 4.32 M and 3.9 M, respectively, in RPMI-1640 medium supplemented as described above without FCS. The salts of the amino acids (rather than the free bases) were used to keep the pH of L-Arg and L-Glu amino acid solutions within physiological range, whereas to prepare Arg·Glu, free bases of these amino acids were mixed together. Solutions were filtered using a 0.22 µm syringe filter and stored at 4 °C until use.

2.3. Determination of osmolality of salt solutions

The osmolality of Arg·Glu, NaCl, Arg·HCl and NaGlu solutions was measured using an Osmomat 030-D Cryoscopic Osmometer (Gonotec GmbH, Berlin, Germany) following standard operating procedures. A 1 M stock solution formulated in RPMI media was prepared for each salt and final concentrations of 5, 100, 150 and 200 mM were prepared for each compound for analysis and construction of a standard curve.

2.4. Cell treatments

Confluent THP-1 cells were harvested by centrifugation at room temperature (RT) (1000 g for 5 min) and re-suspended at

1×10^6 cells/mL in RPMI-1640 medium without FCS in flat-bottomed 24 well tissue culture plates. Salts were prepared in the same medium at stock concentrations and added to cell cultures to achieve the required osmolalities (280–680 mOsm/kg). Control cells were treated with medium alone. In initial experiments, dose responses were conducted. In subsequent experiments, cells were treated with Arg·Glu, NaCl, Arg·HCl or NaGlu to achieve the osmolality range (280–680 mOsm/kg) or the equivalent concentration range 50–200 mM. In some experiments, positive control cells were treated with 0.1 μg/mL lipopolysaccharide (LPS) from *Escherichia coli* 055:B5 (Sigma). Cells were incubated for 4 h or for 24 h at 37 °C in an atmosphere of 5% CO_2. Following the incubation, the cells were spun at 1000 g at RT for 5 min and re-suspended in 100 μL phosphate buffered saline (PBS; Sigma) without calcium and magnesium salts, for determination of cell viability. For phenotypic marker expression the cells were re-suspended in 2% bovine serum albumin (BSA; Sigma) in PBS. Supernatants and lysates were also harvested for nitric oxide determination. Lysates were obtained by lyzing the cell pellets in 100 μl of 0.01% Triton X 100 (Sigma).

Confluent fibroblast cells were washed once with PBS and trypsinized with 0.05% trypsin–ethylenediaminetetraacetic acid (EDTA; Sigma) for 3–4 min at 37 °C until the cells detached from the plate. Cells were re-suspended in complete DMEM medium and were centrifuged at 1000 g RT for 5 min. Cells were re-suspended at 2×10^5 cells/mL in complete DMEM medium in flat-bottomed 24 well tissue culture plates for 6 h at 37 °C/5% CO_2. The cells were then washed with PBS and treated with the salts formulated as described above but in DMEM medium without FCS to achieve the required osmolalities for 24 h. Following the incubation, the cells were trypsinized with 0.05% trypsin–EDTA and re-suspended in 5% FCS/PBS to determine cell viability.

2.5. Measurement of viability

Cell viability of both fibroblasts and THP-1 cells was routinely determined by staining of cells with 5 μg/mL propidium iodide (PI) immediately prior to analysis. Cells (10^4) were analyzed using a FACSCalibur flow cytometer (Becton Dickinson, Mountain View, CA) and FlowJo software (Tree Star Inc., Ashland, OR, USA). Dose response curves were obtained and IC50 values (the concentration/osmolality required to cause a 50% loss in viability) calculated using the inbuilt dose–response fitting function with a nonlinear fit analysis in the OriginPro software version 9.0.

2.6. Measurement of phenotypic marker expression by flow cytometry

Following treatment of THP-1 cells, phenotypic marker expression was assessed. Cells were re-suspended in 2% BSA in PBS. Approximately 2×10^5 cells were transferred to individual wells in round bottomed 96 well tissue culture plates and incubated at 4 °C for 15 min. The cells were washed at 1000 g for 5 min and incubated with the following monoclonal antibodies at 4 °C for 30 min: anti-human leukocyte antigen antibody (HLA-DR; DAKO, Glostrup, Denmark), anti-human CD54 antibody and allophycocyanin (APC)-conjugated anti-human CD86 antibody (BD PharMingen, Oxford, UK) at a 1 in 50 dilution. Isotype controls used were mouse IgG2aκ for anti-human HLA-DR and IgG1κ (BD PharMingen) for anti-human CD54 antibody and anti-human CD86 antibody. After incubation, cells were washed twice with PBS (1000 g for 5 min) followed by a further 30 min incubation at 4 °C with fluorescein isothiocyanate (FITC)-conjugated F(ab′)$_2$ goat anti-mouse IgG at a 1 in 50 dilution (DAKO) for anti-human CD54 and anti-human HLA-DR antibody stained samples; cells stained with APC-conjugated anti-human CD86 antibody were incubated with 2% BSA in PBS. Cells were washed as previously described and finally re-suspended in 5% FCS/PBS, and analyzed by FACSCalibur. Dead cells were excluded from all analyses by staining with 5 μg/mL PI immediately prior to analysis for cells stained for CD54 and HLA-DR; for CD86 staining dead cells were excluded following 5 min incubation with 2 μg/mL of 7-aminoactinomycin D (7-AAD; BD PharMingen). For each sample, a total of 10^4 viable cells was analyzed.

Flow cytometry data were analyzed using FlowJo v10. Cell debris was eliminated by gating on the forward scatter (FSC-H) and side scatter (SSC-H) parameters and gates for marker expression were defined on the basis of isotype control staining. The mean fluorescence intensity (MFI) and the percentage positive cells were both used as separate indicators of the extent of surface marker expression.

2.7. Flow cytometric analyses for apoptosis and cytotoxicity

The levels of apoptosis/necrosis induced were investigated by staining of THP-1 cells for annexin V (TACS™ Annexin V-FITC Apoptosis Detection kits, R&D Systems Europe, Abingdon, UK). Following 4 h or 24 h incubation at 37 °C, the cells were incubated with PI and annexin V-FITC as described in the manufacturer's protocol and 10^4 cells were analyzed by FACSCalibur and FlowJo. The combination of annexin V-FITC and PI staining allows for the differentiation between early apoptotic cells (annexin V$^+$/PI$^-$), late apoptotic cells (annexin V$^+$/PI$^+$), necrotic cells (annexin V$^-$/PI$^+$) and viable cells (annexin V$^-$/PI$^-$) (Dearman et al., 2008; Kabakov et al., 2011).

2.8. Analysis of nitric oxide release by Griess assay

The nitrite concentration from supernatants and lysates harvested at 24 h after initiation of THP-1 cell culture was measured by the Griess assay (Tsikas, 2007) according to the manufacturer's instructions (Promega, Southampton). A 6-fold dilution series using the nitrite standard (1.56 to 100 μM) was prepared and added to Maxisorb plastic microtiter plates (Nunc, Copenhagen, Denmark). Supernatants and lysate samples were added to the plate and 1% sulfanilamide in 5% phosphoric acid was added to every well. This was incubated for 10 min in the dark. N-1-napthylethylenediamine dihydrochloride (0.1%) in milliQ water was then added to every well and incubated for a further 10 min in the dark. Optical density at 550 nm was measured using an automated reader (Multiskan, Flow Laboratories, Irvine, Ayrshire, UK). The nitrite concentrations were determined by plotting the nitrite standard reference curve and using the associated computer software for microplate-based assays (Genesis, Life Sciences International Ltd., Basingstoke, UK).

2.9. Analysis of IL-8 secretion by enzyme-linked immunosorbant assay (ELISA)

The IL-8 content of culture supernatants harvested 24 h after initiation of culture of THP-1 cells was measured by sandwich ELISA (Duoset mouse IL-8 kit; R & D Systems, Abingdon, UK). Maxisorb plastic microtiter plates (Nunc, Copenhagen, Denmark) were used for these assays. Briefly, 96-well plates were coated with 0.1 μg/ml mouse anti-human IL-8 antibody and incubated overnight at 4 °C. 1% BSA in PBS was added to all wells to prevent nonspecific binding and the plates were placed on an orbital shaker (300 rpm) for 1 h at room temperature. Doubling dilutions of recombinant human IL-8 standard (0.008 to 2 ng/mL) were added to triplicate wells and supernatant samples diluted to various extents were added in duplicate and plates were incubated for a further 2 h with shaking. Goat anti-human IL-8 antibody (diluted 1 in 5000) was added to each well and the plates were incubated for 2 h. Streptavidin–horseradish peroxidase (diluted 1 in 1000) was added to each well and the plates incubated for 30 min in the dark. Between each step, the plates were washed three times with 0.05% PBS/Tween-20. Optical density at 450 nm was measured using an automated reader (Multiskan). A standard curve derived with murine recombinant cytokine and associated computer software for microplate-based assays (Genesis) were used to calculate the cytokine concentration in supernatants.

2.10. Statistical analyses

The statistical significance of differences in chemical or LPS induced changes in membrane marker expression, cytokine secretion and cell viability between experimental and control groups were calculated using one-way analysis of variance (ANOVA) with a P-value of <0.05 being considered significant.

3. Results

3.1. Effect of Arg·Glu on THP-1 and primary fibroblast cell viability

In initial experiments, the ion-specific impact of changes in osmolality on viability of the THP-1 human monocyte cell line (grown as a cell suspension) was investigated. The excipients Arg·Glu, NaCl, Arg·HCl and NaGlu were used over a range of concentrations in order to achieve solution osmolalities in the range of 280–525 mOsm/kg (Fig. 1E). In these experiments the salts were added to the standard isotonic cell culture media, bringing the cumulative osmolality of solution into the hypertonic range. Cell viability was determined using flow cytometry (PI exclusion) and is illustrated as percentage viable cells for each treatment with respect to both solution osmolality (Fig. 1A) and solution concentration (Fig. 1B). Baseline viability (in the presence of media alone) for THP-1 cells was ~90%. Increasing the cumulative osmolality of the culture media with Arg·Glu, NaCl and NaGlu caused a decrease in cell viability, with toxicity profiles that were virtually superimposable with ~50% toxicity recorded at 450 mOsm/kg. However, treatment with Arg·HCl caused a more marked loss in cell viability at much lower cumulative osmolalities, with ~45% toxicity observed at 380 mOsm/kg. To facilitate direct comparison of the relative amount of each ion required to cause significant toxicity, the same cytotoxicity data are displayed also as a function of the concentrations of the individual salts added to the isotonic media (Fig. 1B). This comparison shows that on a mole per mole basis, the toxicity profiles of NaGlu and Arg·Glu are superimposable, whereas Arg·HCl and NaCl cause losses in cell viability at lower concentrations (~50% toxicity at 100 mM). In contrast, the impact on cell viability of addition of Arg·Glu at concentrations below 100 mM is minimal.

A somewhat different picture was seen when parallel experiments were conducted with adherent primary human fibroblasts. Fibroblast cells were cultured at 2×10^5 cells/mL with a range of osmolalities (280–620 mOsm/kg) of the various salts for 24 h and the cell viability was determined by PI staining using flow cytometry; data are illustrated with respect to osmolality (Fig. 1C) and concentration (Fig. 1D). For all salts there was a dose dependent decrease in cell viability (reaching statistical significance between 385 and 425 mOsm/kg) and for some salts (Arg·Glu and NaCl) there was a residual population of ~20% that remained viable. With respect to osmolality changes, the cytotoxicity profiles of Arg·Glu and Arg·HCl showed a rapid decrease in viability from 400 mOsm/kg and above, which was very similar to the dose response observed for THP-1 cells. Fibroblasts were more resistant to the effects of NaCl and NaGlu, where a slower decline in viability was observed until ~525 mOsm/kg, which was followed by a very rapid drop in viability (Fig. 1C). However, on a molar concentration basis, all salts with the exception of NaGlu displayed equivalent toxicity over the range of concentrations examined (50–200 mM) (Fig. 1D). These data indicate that for the adherent fibroblast cell line, Arg·Glu and Arg·HCl have some effects on cell viability due to factors in addition to osmolality.

An alternative way of representing these data for comparative purposes is to calculate the concentration/osmolality that results in a 50% loss of viability, an IC50 value (Table 1) for each salt. For THP-1 cells, the IC50 values confirmed that with respect to osmolality, Arg·Glu, NaCl, and NaGlu had similar effects on viability (values ranging from 449.1 and 474.3 mOsm/kg) whereas the IC50 value for Arg·HCl was considerably lower (360.6 mOsm/kg). With respect to molar

concentration, however, IC50 values for NaCl and Arg·HCl were considerably lower (<100 mM) than those recorded for NaGlu and Arg·Glu. For fibroblast cells, IC50 values for osmolality confirmed that these cells were more susceptible to Arg·Glu and Arg·HCl than to NaCl and NaGlu. On a mole for mole basis, similar IC50 values (ranging from 119.1 to 128.0 mM) were recorded for all of the salts with the exception of NaGlu (171.1 mM).

Interestingly, as the independent osmolality measurements show (Fig. 1E), in practice the increase in osmolality versus concentration of salt added (Arg·Glu, NaCl, Arg·HCl and NaGlu) is highly dependent on the nature of the salt, likely due to differences in their degree of dissociation at equal concentrations. The NaCl salt results in the highest increase in osmolality of the solution, and the Arg·HCl salt the least, for each given concentration of salt. Thus, considerably higher concentrations of Arg·Glu, Arg·HCl and NaGlu are required to achieve osmolalities equivalent to NaCl (Fig. 1E).

In summary, the key findings here were that the effects on cell viability were largely consistent with changes in osmolality. However, for Arg·Glu and Arg·HCl with the adherent cells and for Arg·HCl with the THP-1 cells, the effects were not solely attributable to osmolality changes. In subsequent experiments, the focus was on THP-1 cells due to the ability of these cells to act as indicator cells and to respond to danger signals (Gallo and Gallucci, 2013; Megherbi et al., 2009).

3.2. Toxicity of L-Arg salts for THP-1 cells is not due to nitric oxide production

A potential mechanism for the additional impact of hypertonic Arg·HCl on THP-1 cell viability, over and above the effects of changes in osmolality, was explored. It was hypothesized that the more profound cytotoxic effect of Arg·HCl could be due to the release of nitric oxide by the cells in the presence of Arg·HCl, as arginine is a substrate for the formation of nitric oxide (Chen et al., 2013; Chou et al., 2010; Pekarova et al., 2013). Therefore, the effects of the addition of Arg·Glu, NaCl, Arg·HCl and NaGlu on nitric oxide production by THP-1 cells were examined (Fig. 2). Cells were cultured for 24 h in the presence of 50 or 100 mM concentrations of the salts, the latter condition under which Arg·HCl caused marked toxicity, and supernatants and cell lysates analyzed for secreted and intracellular levels of nitric oxide, respectively, by Greiss assay. Although the nitric oxide content of supernatants derived from cells following treatment with the various salts was variable (~60% to 140% of control values of 1 μM), such differences were not statistically significant. In contrast, statistically significant decreases in the nitric oxide content of lysates (intracellular nitric oxide content) were recorded for all treatments (ranging from ~30% to 40% of control values of 1.2 μM). However, the divergent cytotoxicity profile recorded for Arg·HCl compared to the other salts could not be reconciled on the basis of nitric oxide production.

3.3. Mechanism of cell death caused by hypertonic addition of salts to THP-1 cells

In initial experiments (cf Fig. 1) cell viability was assessed using PI staining which distinguishes dead (necrotic) cells from live cells. In those experiments, Arg·Glu and NaGlu showed very similar toxicity profiles with respect to solution osmolality and cell death to that which was observed for the reference excipient, NaCl. However, to further characterize the extent and pattern of cell death occurring, and to confirm that the mechanism of cell death was indeed similar between Arg·Glu and NaCl, a combination of PI and annexin V-FITC staining was used. This combination allows for the distinction between early apoptotic cells (annexin V-FITC positive), late apoptotic cells (annexin V-FITC and PI positive), necrotic cells (PI positive) and viable cells (unstained) (Kabakov et al., 2011). THP-1 cells were treated with 50–200 mM concentrations of the salts, or with medium alone, for 4 h or 24 h, stained with annexin V-FITC and PI and analyzed using a
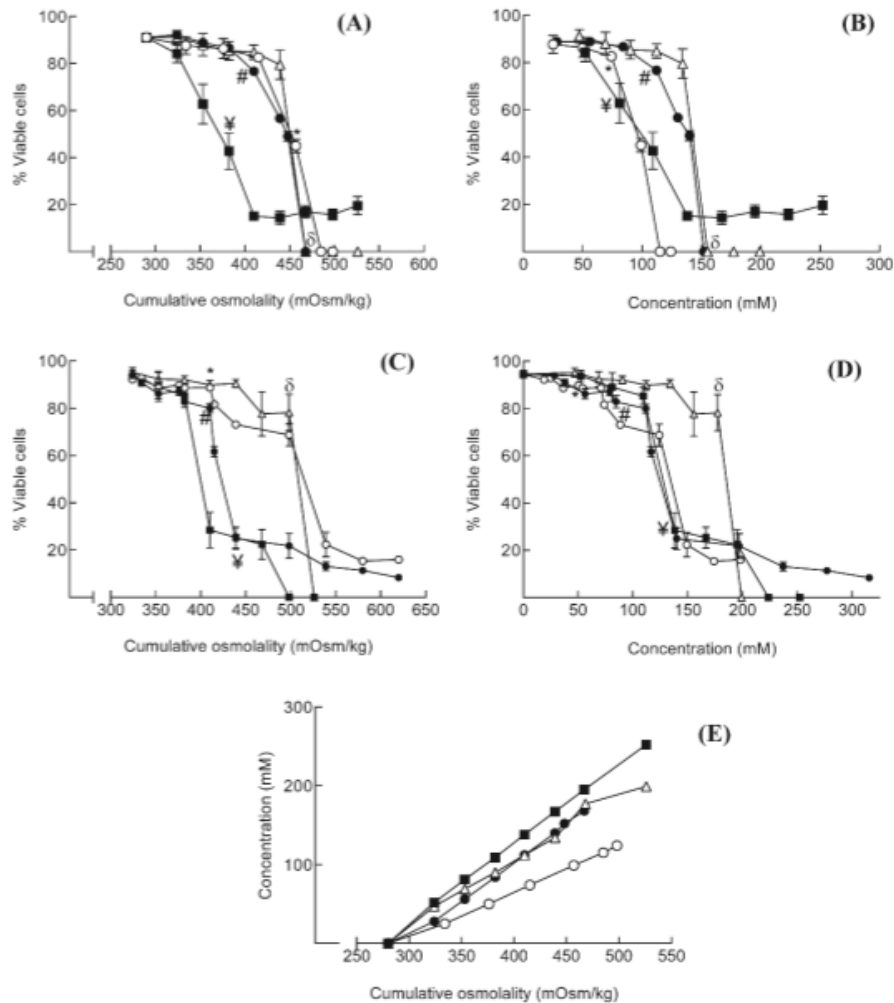
Fig. 1. Effect of changes in osmolality on THP-1 cell or fibroblast viability: comparisons of different salts THP-1 cells were seeded into 24-well plates at 10^6 cells/mL. in serum free RPMI media (A, B) or human primary fibroblasts were seeded at 2×10^5 cells/mL in complete DMEM medium in flat-bottomed 24 well plates for 6 h at 37 °C (C, D). Cells were cultured in serum free media for 24 h at 37 °C with varying concentrations of NaCl (O), Arg·Glu (●), Arg·HCl (■) and NaGlu (△) spanning a range of osmolalities from 280 to 525 mOsm/kg (A) or from 280 to 625 mOsm/kg (C) and a range of concentrations from 0 to 250 mM (B) or from 0 to 325 mM (D). Control cells were cultured with medium alone (280 mOsm/kg). Following culture, fibroblasts were trypsinized and THP-1 and fibrobalsts were harvested and cell viability was determined using PI. Cells (10,000) were analyzed by flow cytometry using a FACSCalibur flow cytometer for PI staining (FL2 channel; viability) against forward scatter (FSC; size). Data are displayed as % cell viability for n = 3–6 experiments (mean and SE) versus excipient with respect to cumulative osmolality (A, C) and the concentrations of each excipient required to achieve the required osmolality (B, D). The statistical significance of differences between cells cultured in medium alone (isotonicity) and cells treated with various concentrations of salts was assessed by one way ANOVA ($p < 0.05$; * = NaCl, # = Arg·Glu, ¥ = Arg·HCl, δ = NaGlu). For clarity of presentation, only the first concentration of each salt preparation at which there was a significant loss of cell viability is illustrated. The relationship between each individual salt concentration as formulated in RPMI media and cumulative osmolality as measured using an osmometer is illustrated in (E).

Table 1

IC50 values calculated additive concentrations and osmolalities required to achieve 50% drop in viability for THP-1 cells or fibroblasts for each of the salts; raw data displayed in Fig. 1.

Additives	THP-1 cells		Fibroblast	
	[Salt], mM	mOsm/kg	[Salt], mM	mOsm/kg
Arg·Glu	141.1	449.1	119.1	417.4
NaCl	99.6	456.4	114.7	482.9
Arg·HCl	94.3	360.6	128.0	400.7
NaGlu	158.6	474.3	171.1	489.7

FACSCalibur flow cytometer (Figs. 3 and 4). These time points were chosen on the basis of preliminary kinetics experiments that revealed that after 2 h incubation there was little impact on THP-1 cell viability or apoptosis, whereas after 4 h, significant effects were observed at concentrations of >150 mM (data not shown). The 24 h time point was utilized to determine whether lower concentrations (<100 mM) of salts that were without effect on cell viability as measured by PI exclusion at this time point (cf Fig. 1) had more subtle effects on apoptosis. Representative quadrant plots are displayed in Fig. 3, illustrating the gating strategy and showing examples of predominantly viable cells (Fig. 3A, 94.5% cells in lower left quadrant), populations of early and late apoptotic cells (Fig. 3B; 33% and 42%, respectively, in the lower
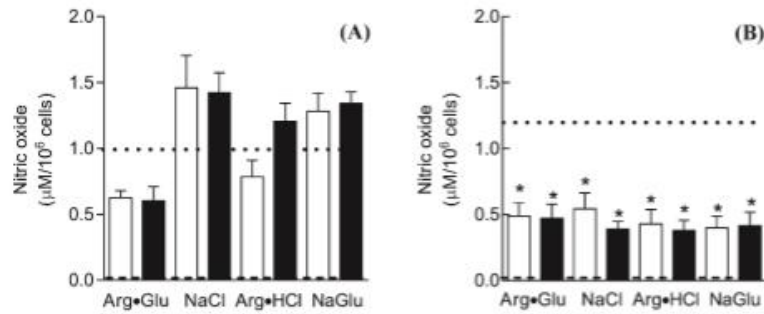
Fig. 2. Impact of Arg·Glu and other salts on THP-1 cell nitric oxide production THP-1 cells were seeded into 24-well plates at 10^6 cells/mL in serum free RPMI media and were cultured for 24 h at 37 °C in medium alone (represented by the dashed line) or in the presence of 50 mM (open column) or 100 mM (closed column) Arg·Glu, NaCl, Arg·HCl or NaGlu. Supernatants (A) and lysates (B) were collected after the 24 h incubation and the nitrite concentration was determined by the Griess assay. The nitric oxide content of the media (with supplements) in the absence of cells was also determined (dotted line). The nitrite concentrations were determined using a nitrite standard reference curve and the associated computer software for microplate-based assays and data are displayed as nitrite concentration (μM; mean and SE). The statistical significance of differences in the nitrite content of samples from cells cultured in medium alone and cells treated with various concentrations of salts was assessed by one way ANOVA (*$p < 0.05$).

and upper right quadrants), predominantly late apoptotic cells (Fig. 3C; 85.5% of cells in upper right quadrant) and populations containing necrotic cells (Fig. 3D; 15.5% cells in the upper left quadrant).

Culture of THP-1 cells with 50 or 100 mM of the salts for 4 h had little impact on cell viability (Fig. 4A-D), although there was a significant loss in viability for all 4 salts at concentrations of 150 mM and above. This
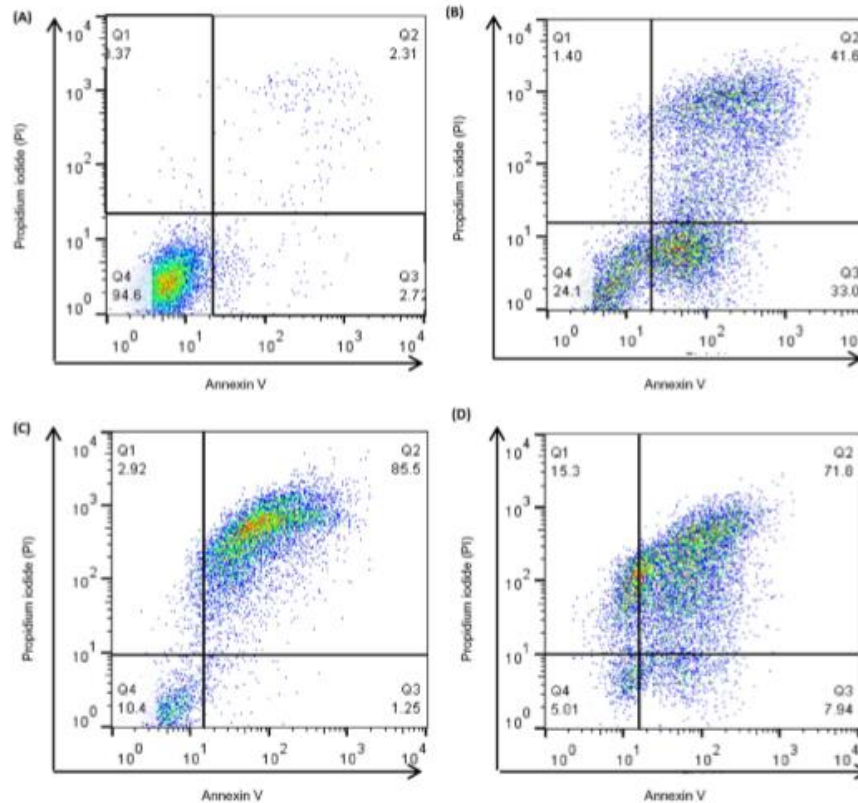
Fig. 3. The gating strategy for the characterization of the mechanism of cell death (representative FACS histograms) THP-1 cells were seeded into 24-well plates at 10^6 cells/mL and cultured for 24 h in serum free RPMI media alone (A), or in the presence of 150 mM NaGlu (B), 200 mM Arg·Glu (C), 200 mM NaCl (D). Following incubation, cells were stained with annexin V-FITC (FL-1 channel) and PI (FL-2 channel) and 10,000 cells were analyzed using a FACSCalibur flow cytometer. Data are displayed as representative quadrant analyses showing the pattern of cytotoxicity for each treatment group; in each case the lower left quadrant represents Annexin V-ve/PI-ve (viable) cells, the lower right quadrant represents annexin V + ve/PI-ve (early apoptotic) cells, the upper right quadrant represents annexin V + ve/PI + ve (late apoptotic) cells and the upper left quadrant represents annexin V-ve/PI + ve (necrotic) cells. The percentage of cells in each quadrant is indicated.
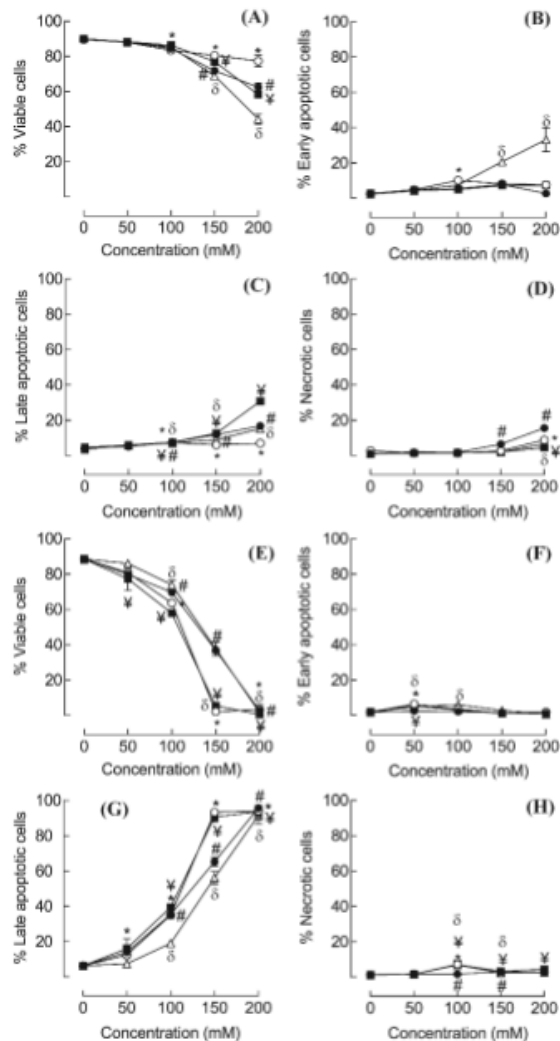
Fig. 4. Characterization of the mechanism of cell death THP-1 cells were seeded into 24-well plates at 10^6 cells/mL in serum free RPMI media and were cultured for 4 h (A–D) or 24 h (E–H) at 37 °C in the presence of 50–200 mM NaCl (O), Arg·Glu (●), Arg·HCl (■) or NaGlu (Δ). Control cells were cultured with medium alone. To characterize the extent and pattern of induced cytotoxicity, cells were stained with Annexin V–FITC (FL-1 channel) and PI (FL-2 channel) and 10,000 cells were analyzed using a FACSCalibur flow cytometer. The results are displayed as the percentages of cells that are Annexin V-ve/PI-ve (viable) (A, E), Annexin V + ve/PI-ve (early apoptotic) (B, F), Annexin V + ve/PI + ve (late apoptotic) (C, G), Annexin V-ve/PI + ve (necrotic) (D, H). In each case, data are shown as % total cells in each category (mean and SE for n = 3 experiments, where for clarity SE > 2% only are shown). The statistical significance of differences between cells cultured in medium alone and cells treated with various concentrations of salts was assessed by one way ANOVA ($p < 0.05$; * = NaCl, # = Arg·Glu, ¥ = Arg·HCl, δ = NaGlu).

was generally paralleled by increased numbers of late apoptotic and necrotic cells, with the exception of NaGlu, which caused a more marked loss in viability than did the other salts, and this was paralleled by an increased frequency of early apoptotic cells (Fig. 4B). After 24 h in culture, only the 50 mM concentration of each of the salts was without significant effects on cell viability. In each case at doses of 100 mM and above there was a significant drop in the frequency of viable cells

which was reflected by a corresponding significant increase in late apoptotic cells, with no marked changes in early apoptotic or necrotic cells (Fig. 4E–H). Consistent with the previous data (cf Fig. 1B) where viability was assessed simply as a function of PI exclusion, for a given concentration of salt, NaCl and Arg·HCl were considerably more cytotoxic than NaGlu or Arg·Glu and this resulted in increased numbers of late apoptotic cells.

These data demonstrate that the mechanism of cell death is very similar between NaCl and Arg·Glu, with loss of viability being paralleled in both cases by increased frequency of late apoptotic cells with little evidence of early apoptotic or necrotic cells.

3.4. Impact of hypertonic concentrations of salts on markers of THP-1 cell activation

It is clear from the experiments described thus far that high concentrations (>150 mM) of Arg·Glu and other ions impact markedly on cell viability over a 24 h culture period. In subsequent experiments, more subtle effects on the activation status of the cells were explored under conditions where the impact on cell viability was marginal. Changes in membrane marker (CD54, HLA-DR and CD86) expression were measured on resting THP-1 cells and cells stimulated with the toll-like receptor (TLR) 4 ligand LPS, a polyclonal activator of monocytes (Rossol et al., 2011). Resting THP-1 cells were ~20% CD54 + ve, 60% HLA-DR + ve and <5% CD86 + ve. Treatment with LPS increased significantly the frequency of CD54 + ve cells (to ~90%) and also upregulated the level of expression (increasing MFI from ~60 au to 360 au) but was without marked effect on levels of the other markers. The presence of the various salts was also without impact on resting levels of HLA-DR and CD86 (data not shown). With respect to CD54 expression, 50 mM of the salts were largely without effect on either the frequency of positive cells or the extent of expression, whereas 100 mM of each of the salts tended to cause a small increase (to ~40%) in the proportion of CD54 + cells and a slight increase in MFI to ~120 au for NaCl. However, none of these small changes reached statistical significance (Fig. 5A and B). Finally, the impact of Arg·Glu and NaCl on production of the proinflammatory cytokine IL-8 was examined. Cells cultured with medium alone did not secrete detectable levels of IL-8 (<0.1 ng/mL) whereas culture in the presence of LPS induced detectable cytokine expression (~1 ng/mL) (Fig. 5C). There was some inter-experimental variation, but treatment with a range of concentrations of Arg·Glu or NaCl did not result in significant cytokine production.

4. Discussion

The impact of the excipient Arg·Glu and other related salts on cell viability and cellular stress using in vitro cell culture systems has been examined. These studies have demonstrated that Arg·Glu does not have any further detrimental effects on viability of the monocyte (DC surrogate) THP-1 cell line in comparison to NaCl at equivalent osmolalities, and that relatively high concentrations of both salts cause cell death by apoptosis. In contrast, Arg·HCl was more toxic to this cell line at equivalent osmolalities. For human primary fibroblasts that grow as an adherent monolayer, all salts caused significant toxicity at 385 and 425 mOsm/kg, although Arg·Glu and Arg·HCl caused a more precipitous subsequent decline in viability than did NaCl or NaGlu. These data suggest that salts containing arginine have an impact on cell viability of adherent cells that is in addition to effects due to hypertonicity and that in the case of Arg·Glu can only be partially ameliorated by the presence of Glu. There was some indication that the arginine containing salts affected cell adherence/morphology of the primary human fibroblasts (data not shown). Indeed there is some precedent for hypertonicity impacting on the cytoskeleton, with adherent human monocytes and macrophages showing changes in microtubule organisation upon hypertonic stress (400 mOsm/kg NaCl) (Nunes et al., 2013). It is of interest that the polystyrene tissue culture plates in which the primary human
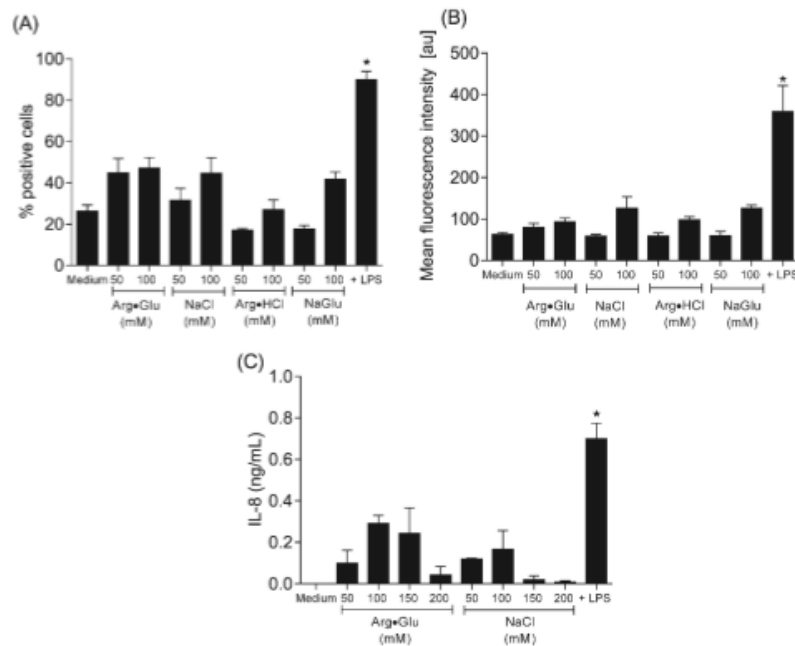
Fig. 5. Effects of Arg·Glu and other salts on CD54 expression and IL-8 production THP-1 cells were seeded into 24-well plates at 10^6 cells/mL in serum free RPMI media and were cultured for 24 h at 37 °C with medium alone or in the presence of 50–200 mM of Arg·Glu, NaCl, Arg·HCl or NaGlu. Positive control cells were cultured with LPS (0.1 µg/mL). At the end of the culture period, cells were stained for expression of CD54 or with isotype control (mouse IgG1κ) antibody and dead cells were excluded with PI. Data (10,000 cells) were acquired using a FACSCalibur flow cytometer and results are displayed as percentage positive cells (A) and mean fluorescence intensity (arbitrary units; au) (B) (mean and SE for six independent experiments). Following culture, samples were centrifuged at 1000 rpm for 5 min and supernatants were collected and analyzed for IL-8 content by ELISA (C). Results are displayed as mean and SEM of 3 independent experiments. The statistical significance of differences between cells cultured in medium alone and cells treated with various concentrations of salts or LPS was assessed by one way ANOVA (*$p < 0.05$).

fibroblasts are cultured are treated to increase hydrophilicity of the polystyrene and ensure a negative charge, conditions which promote cell adherence (Curtis et al., 1983). It may be that the positively charged arginine ion in the Arg·Glu and Arg·HCl preparations interfere with this interaction through salt screening of the net surface charge.

It is of interest that in the nonadherent indicator cell line (THP-1), Arg·HCl was more toxic than the other salts, for a given osmolality. For the nonadherent cell line, the presence of Glu in the Arg·Glu preparation reduced this toxicity. One possible explanation for this increased toxicity was that arginine was acting as a substrate for the formation of nitric oxide (Chen et al., 2013; Chou et al., 2010; Pekarova et al., 2013), which interacts with superoxide radicals to form peroxynitrite, causing oxidative damage to cells (Calcerrada et al., 2011). Clearly the THP-1 cells were able to secrete detectable nitric oxide (~1 µM was measured in the supernatants, levels some 50-fold higher than that recorded in the absence of cells), amounts similar to those recorded previously for the same cell line under the same culture conditions (~2.5 M) (Garg et al., 2005). Interestingly, there was no differential effect of arginine on nitric oxide production. However, all salts caused a significant decrease in intracellular nitric oxide, even under conditions (50 mM) where there was no effect on viability, suggesting that this may be due to hypertonicity. Indeed, it has been reported previously in other cell types (muscle cells and in cartilage) that exposure to hypertonic concentrations of NaCl and sucrose or mannitol results in reduced levels of nitric oxide and the enzyme inducible nitric oxide synthase (Le et al., 2006; Pingle et al., 2003). Thus, hypertonicity per se may trigger decreases in expression of nitric oxide. It should be noted that the assay utilized herein is an approximation of nitric oxide content, as it measures nitrite (NO^{2-}) only, which is one of two primary, stable and non-volatile breakdown products of nitric oxide, the other being nitrate (NO^{3-})(Tsikas, 2007). The mechanism by which Arg·HCl is more toxic for the nonadherent cell line than the other salts is unclear at present, however, the presence of Glu in the Arg·Glu mixture appears to ameliorate this toxicity.

The experiments conducted herein have demonstrated that hypertonic stress induced by all 4 salts tested resulted in cell death by apoptosis (with the majority of cells in the late apoptotic stage by 24 h) with very little necrosis occurring at any concentration. This is a key finding given the fact that cells that die by necrosis expel their contents when they lyse, including inflammatory cytokines that stimulate further pro-inflammatory responses (Rock and Kono, 2008). In contrast, cells that die by apoptosis are compacted into apoptotic bodies as a mechanism to avoid immune activation and instead are phagocytosed (Biermann et al., 2013). One of the earliest signs of apoptosis is the translocation of the membrane phospholipid phosphatidylserine from the inner to the outer leaflet of the plasma membrane. This molecule is recognized by phagocytes, triggering phagocytosis and also the production of anti-inflammatory cytokines, resulting in efficient removal of the dying cell without inflammation. In the flow cytometric analyses of apoptosis, it is the expression of this cell surface phosphatidylserine that is detected by the binding of the fluorescently labelled ligand annexin V (Kabakov et al., 2011). Although there have been suggestions that late apoptotic cells more closely resemble necrotic cells, due to their compromised cell membranes, in fact it has been shown that both early and late apoptotic cells induce the differential signalling pathways in macrophages compared with necrotic cells and that intracellular contents released from late apoptotic cells are neutral and not proinflammatory (Patel et al., 2006). The fact that all of the salts examined caused death by apoptosis is not simply a feature of the target THP-1 cell, as it has been demonstrated previously that under the right

conditions, such as stimulation with bacterial toxins, THP-1 cells undergo necrosis (Melehani et al., 2015). It is of interest that all of the salts caused cell death by the same mechanism and with similar kinetics. This suggests that induction of apoptosis is a common feature of hypertonic insult which is consistent with previous studies in which hyperosmotic stress has been shown to induce apoptosis, particularly in kidney cells (Alfieri and Petronini, 2007). There are fewer studies in which monocyte or DC populations have been investigated, but here too the mechanism of monocyte cell death induced by osmolytes such as NaCl and mannitol at 500 mOsm/kg has been shown to be apoptosis (Gastaldello et al., 2008). To our knowledge there have been no previous studies on the mechanism of Arg·Glu induced cytotoxicity. Thus, all the salts including Arg·Glu induce the THP-1 cells to undergo apoptosis, in which case this is not expected to result in inflammation.

More subtle effects of the salts on the THP-1 indicator cell line were explored: the impact on markers of cellular stress/cell maturation such as changes in expression of the membrane marker CD54 (intercellular adhesion molecule–1; ICAM-1) and production of the pro-inflammatory cytokine IL-8. ICAM-1 is an adhesion molecule that is a member of the immunoglobulin superfamily with functions that relate to its role in cell adhesion and migration (Simmons, 1995). Its ligands include the matrix factor hyaluronan and lymphocyte function-associated antigen-1 on T cells; interaction with its T cell ligand provides costimulation and therefore activation of the adaptive immune response (Simon et al., 1991). IL-8 is an inducible chemokine whose production is stimulated in various cell types by other proinflammatory cytokines such as IL-1 and TNF-α. IL-8 plays a key role in acute inflammation, being the main chemotactic factor for neutrophils, the most important phagocytic cell in many different types of inflammatory reaction and may also play a role in macrophage and fibroblast chemotaxis (Harada et al., 1994). These two markers have been shown to be indicative of the activation of DC-like cells such as the THP-1 cell line. Thus, TLR ligands including TLR1, TLR2 and TLR4 each caused increased ICAM-1 expression and IL-8 secretion by THP-1 cells (Lee et al., 2011; Spachidou et al., 2007). Furthermore, less vigorous stimuli, such as chemicals that have the ability to cause contact allergy, a T cell mediated delayed type hypersensitivity in the skin, upregulate the same markers on THP-1 cells in culture (Megherbi et al., 2009; Tuschl and Kovac, 2001). In the experiments described herein, consistent with the published data, stimulation of THP-1 cells with the TLR4 ligand LPS resulted in the expected up-regulation of these markers, with increases in both the number of ICAM-1 positive cells and the amount expressed per cell. In contrast, treatment with the salts was without marked effects on expression of the membrane marker or cytokine expression; for both Arg·Glu and NaCl there were similar, but variable, low level effects on both markers that did not reach statistical significance. There is some evidence with other cell lines that hyperosmolality may impact on cytokine expression, particularly for endothelial and epithelial cell lines. Thus, hypertonic concentrations of NaCl and mannitol increased IL-8 expression by Caco-2 and HT-29 cells (human intestinal epithelial cell lines) and by bronchial epithelial cells (NCI-H$_{292}$) (Hashimoto et al., 1999; Hubert et al., 2004; Németh et al., 2002). In both cell types, induction of IL-8 was via a p38 mitogen-activated protein kinase. Interestingly, for the human intestinal epithelial cell lines, hypo-osmolality (163 mOsm/L NaCl) was considerably more stimulatory than was hyperosmolality (496 mOsm/L NaCl) with respect to cytokine induction (Hubert et al., 2004). It could be argued that for tissues such as the gastrointestinal tract, exposure to marked fluctuations in osmolarity is a feature of normal physiology and as such these cells are required to sense and respond to such changes (Brocker et al., 2012). In contrast, there are far fewer reports regarding the response of monocytes/macrophages or DC to hyperosmotic stress (induced by either NaCl or glycerol/mannitol), and conflicting results have been generated. It has been reported that hypertonicity had no impact on basal IL-8 release and inhibited LPS-induced expression of this cytokine by freshly isolated human blood monocytes (Brulez et al., 1999), whereas others report

that human peripheral blood mononuclear cells respond to NaCl by up-regulating IL-8 and IL-1β, the latter at the level of message only (Shapiro and Dinarello, 1997). Furthermore, it has been demonstrated that hypotonicity, but not hypertonicity, activates macrophage and monocyte caspase 1 (IL-1β processing enzyme) and induces IL-1β release as a result of cell swelling (Compan et al., 2012; Perregaux et al., 1996). Conflicting data have been reported, with hyper-osmotic stress upregulating caspase 1, but here macrophages were primed with LPS (Ip and Medzhitov, 2015). As such, the experiments reported herein confirm that in the absence of priming, hypertonicity caused by Arg·Glu or NaCl fails to impact significantly on monocyte IL-8 production, over a range of doses that spanned concentrations that impacted on cell viability. In regard to excipient concentrations, it should be remembered that immediately following subcutaneous injection the vehicle in which the drug is formulated disperses. This exchange into a physiological medium, with concomitant decrease in excipient concentration, may have biophysical consequences and the in vivo local cellular response is yet to be determined (Kinnunen and Mrsny, 2014).

In conclusion, adherent and nonadherent cell lines exhibit very similar toxicity profiles for Arg·Glu, and for the nonadherent cell line, the data are consistent with the toxicity being due to changes in osmolality. In common with hypertonic concentrations of NaCl, the mechanism of cell death is via apoptosis and is thus not pro-inflammatory, which is confirmed by the negative findings for markers of cellular stress or activation (membrane marker and proinflammatory cytokine expression). Taken together these data indicate that Arg·Glu is of equivalent toxicity to NaCl and that the use of Arg·Glu as an excipient for subcutaneous injection is not expected to result in atypical inflammation.

Transparency document

The Transparency document associated with this article can be found, in the online version.

Acknowledgements

References

Alfieri, R.R., Petronini, P.G., 2007. Hyperosmotic stress response: comparison with other cellular stresses. Pflugers Arch. 454, 173–185. http://dx.doi.org/10.1007/s00424–006-0195-x.

Arakawa, T., Ejima, D., Tsumoto, K., Obeyama, N., Tanaka, Y., Kita, Y., Timasheff, S.N., 2007a. Suppression of protein interactions by arginine: a proposed mechanism of the arginine effects. Biophys. Chem. 127, 1–8. http://dx.doi.org/10.1016/j.bpc.2006.12.007.

Arakawa, T., Tsumoto, K., Kita, Y., Chang, B., Ejima, D., 2007b. Biotechnology applications of amino acids in protein purification and formulations. Amino Acids 33, 587–605. http://dx.doi.org/10.1007/s00726-007-0506-3.

Biermann, M., Maueröder, C., Brauner, J.M., Chaurio, R., Janko, C., Herrmann, M., Muñoz, L.E., 2013. Surface code–biophysical signals for apoptotic cell clearance. Phys. Biol. 10, 065007. http://dx.doi.org/10.1088/1478-3975/10/6/065007.

Blobel, J., Brath, U., Bernadó, P., Diehl, C., Ballester, L., Sornosa, A., Akke, M., Pons, M., 2011. Protein loop compaction and the origin of the effect of arginine and glutamic acid mixtures on solubility, stability and transient oligomerization of proteins. Eur. Biophys. J. 40, 1327–1338. http://dx.doi.org/10.1007/s00249-011-0686-3.

Brocker, C., Kuhlee, A., Gatsogiannis, C., Balderhaar, H.J., Honscher, C., Engelbrecht-Vandre, S., Ungermann, C., Raunser, S., 2012. Molecular architecture of the multisubunit homotypic fusion and vacuole protein sorting (HOPS) tethering complex. Proc. Natl. Acad. Sci. U. S. A. 109, 1991–1996. http://dx.doi.org/10.1073/pnas.1117797109.

Brulez, H.F., ter Wee, P.M., Snijders, S.V., Donker, A.J., Verbrugh, H.A., 1999. Mononuclear leucocyte function tests in the assessment of the biocompatibility of peritoneal dialysis fluids. J. Clin. Pathol. 52, 901–909. http://dx.doi.org/10.1136/jcp.52.12.901.

Bye, J.W., Platts, L., Falconer, R.J., 2014. Biopharmaceutical liquid formulation: a review of the science of protein stability and solubility in aqueous environments. Biotechnol. Lett. 36, 869–875. http://dx.doi.org/10.1007/s10529-013-1445-6.

Calcerrada, P., Peluffo, G., Radi, R., 2011. Nitric oxide-derived oxidants with a focus on peroxynitrite: molecular targets, cellular responses and therapeutic implications. Curr. Pharm. Des. 17, 3905–3932. http://dx.doi.org/10.2174/138161211798357719.

Chen, F., Lucas, R., Fulton, D., 2013. The subcellular compartmentalization of arginine metabolizing enzymes and their role in endothelial dysfunction. Front. Immunol. 4, 184. http://dx.doi.org/10.3389/fimmu.2013.00184.

Cheng, W.Q., Joshi, S.B., He, F., Brems, D.N., He, B., Kerwin, B.A., Volkin, D.B., Middaugh, C.R., 2012. Comparison of high-throughput biophysical methods to identify stabilizing excipients for a model IgG2 monoclonal antibody: conformational stability and kinetic aggregation measurements. J. Pharm. Sci. 101, 1701–1720. http://dx.doi.org/10.1002/jps.23076.

Chou, S.Y., Hsu, C.S., Hsu, M.Y., Liang, S.J., Yeh, C.L., Yeh, S.L., 2010. Effects of different arginine concentrations on angiogenic protein production induced by HeLa cells. Nutrition 26, 818–822. http://dx.doi.org/10.1016/j.nut.2009.08.004.

Compan, V., Baroja-Mazo, A., López-Castejón, G., Gomez, A.I., Martínez, C.M., Angosto, D., Montero, M.T., Herranz, A.S., Bazán, E., Reimers, D., Mulero, V., Pelegrín, P., 2012. Cell volume regulation modulates NLRP3 inflammasome activation. Immunity 37, 487–500. http://dx.doi.org/10.1016/j.immuni.2012.06.013.

Curtis, A.S., Forrester, J.V., McInnes, C., Lawrie, F., 1983. Adhesion of cells to polystyrene surfaces. J. Cell Biol. 97, 1500–1506.

Dearman, R.J., Cumberbatch, M., Portsmouth, C., Maxwell, G., Basketter, D.A., Kimber, I., 2008. Synergistic effects of chemical insult and toll-like receptor ligands on dendritic cell activation. Toxicol. In Vitro 222, 1927–1934. http://dx.doi.org/10.1016/j.tiv.2008.09.012.

Gallo, P.M., Gallucci, S., 2013. The dendritic cell response to classic, emerging, and homeostatic danger signals. Implications for autoimmunity. Front. Immunol. 4, 138. http://dx.doi.org/10.3389/fimmu.2013.00138.

Garg, R., Gupta, S.K., Tripathi, P., Naik, S., Sundar, S., Dube, A., 2005. Immunostimulatory cellular responses of cured Leishmania-infected patients and hamsters against the integral membrane proteins and non-membranous soluble proteins of a recent clinical isolate of Leishmania donovani. Clin. Exp. Immunol. 140, 149–156. http://dx.doi.org/10.1111/j.1365-2249.2005.02745.x.

Gastaldello, K., Husson, C., Dondeyne, J.P., Vanherweghem, J.L., Tielemans, C., 2008. Cytotoxicity of mononuclear cells as induced by peritoneal dialysis fluids: insight into mechanisms that regulate osmotic stress-related apoptosis. Perit. Dial. Int. 28, 655–666.

Golovanov, A.P., Hautbergue, G.M., Wilson, S.A., Lian, L.Y., 2004. A simple method for improving protein solubility and long-term stability. J. Am. Chem. Soc. 126, 8933–8939. http://dx.doi.org/10.1021/ja049297h.

Gursoy, N., Garrigue, J.S., Razafindratsita, A., Lambert, G., Benita, S., 2003. Excipient effects on in vitro cytotoxicity of a novel paclitaxel self-emulsifying drug delivery system. J. Pharm. Sci. 92, 2411–2418. http://dx.doi.org/10.1002/jps.10501.

Harada, A., Sekido, N., Akahoshi, T., Wada, T., Mukaida, N., Matsushima, K., 1994. Essential involvement of interleukin-8 (IL-8) in acute inflammation. J. Leukoc. Biol. 56, 559–564.

Hashimoto, S., Matsumoto, K., Gon, Y., Nakayama, T., Takeshita, I., Horie, T., 1999. Hyperosmolarity-induced interleukin-8 expression in human bronchial epithelial cells through p38 mitogen-activated protein kinase. Am. J. Respir. Crit. Care Med. 159, 634–640. http://dx.doi.org/10.1124/jpet.107.135871.

Ho, R.J., Chien, J.Y., 2012. Drug delivery trends in clinical trials and translational medicine: growth in biologic molecule development and impact on rheumatoid arthritis, Crohn's disease, and colitis. J. Pharm. Sci. 101. http://dx.doi.org/10.1002/jps.23154 (2668–1074).

Hooks, M.A., Wade, C.S., Millikan, W.J., 1991. Muromonab CD-3: a review of its pharmacology, pharmacokinetics, and clinical use in transplantation. Pharmacotherapy 11, 26–37. http://dx.doi.org/10.1875-9114.1991.tb03595.x.

Hubert, A., Cauliez, B., Chedeville, A., Husson, A., Lavoinne, A., 2004. Osmotic stress, a proinflammatory signal in Caco-2 cells. Biochimie 86, 533–541. http://dx.doi.org/10.1016/j.biochi.2004.07.009.

Ip, W.K., Medzhitov, R., 2015. Macrophages monitor tissue osmolarity and induce inflammatory response through NLRP3 and NLRC4 inflammasome activation. Nat. Commun. 6, 6931. http://dx.doi.org/10.1038/ncomms7931.

Kabakov, A.E., Kudryavtsev, V.A., Gabai, V.I., 2011. Determination of cell survival or death. Methods Mol. Biol. 787, 231–244. http://dx.doi.org/10.1007/978-1-61779-295-3_17.

Kagan, L., 2014. Pharmacokinetic modeling of the subcutaneous absorption of therapeutic proteins. Drug Metab. Dispos. 42, 1890–1905. http://dx.doi.org/10.1124/dmd.114.059121.

Kamerzell, T.J., Esfandiary, R., Joshi, S.B., Middaugh, C.R., Volkin, D.B., 2011. Protein-excipient interactions: mechanisms and biophysical characterization applied to protein formulation development. Adv. Drug Deliv. Rev. 63, 1118–1159. http://dx.doi.org/10.1016/j.addr.2011.07.006.

Kaushik, J.K., Bhat, R., 2003. Why is trehalose an exceptional protein stabilizer? An analysis of the thermal stability of proteins in the presence of the compatible osmolyte trehalose. J. Biol. Chem. 278, 26458–26465. http://dx.doi.org/10.1074/jbc.M300815200.

Kheddo, P., Tracka, M., Armer, J., Dearman, R.J., Uddin, S., van der Walle, C.F., Golovanov, A.P., 2014. The effect of arginine glutamate on the stability of monoclonal antibodies in solution. Int. J. Pharm. 473, 126–133. http://dx.doi.org/10.1016/j.ijpharm.2014.06.053.

Kinnunen, H.M., Mrsny, R.J., 2014. Improving the outcomes of biopharmaceutical delivery via the subcutaneous route by understanding the chemical, physical and physiological properties of the subcutaneous injection site. J. Control. Release 182, 22–32. http://dx.doi.org/10.1016/j.jconrel.2014.03.011.

Le, D., Hofbauer, M.A., Towle, C.A., 2006. Differential effects of hyperosmotic challenge on interleukin-1-activated pathways in bovine articular cartilage. Arch. Biochem. Biophys. 445, 1–8. http://dx.doi.org/10.1016/j.abb.2005.11.012.

Lee, S.M., Kim, E.J., Suk, K., Lee, W.H., 2011. CD300F blocks both MyD88 and TRIF-mediated TLR signaling through activation of Src homology region 2 domain-containing phosphatase 1. J. Immunol. 186, 6296–6303. http://dx.doi.org/10.4049/jimmunol.1002184.

Lee, J., Lin, E.W., Lau, U.Y., Hedrick, J.L., Bat, E., Maynard, H.D., 2013. Trehalose glycopolymers as excipients for protein stabilization. Biomacromolecules 14, 2561–2569. http://dx.doi.org/10.1021/bm501365a.

Lynch, M., Kirby, B., Warren, R.B., 2014. Treating moderate to severe psoriasis — best use of biologics. Expert. Rev. Clin. Immunol. 10, 269–279. http://dx.doi.org/10.1586/1744666X.2014.873701.

Megherbi, R., Kiorpelidou, E., Foster, B., Rowe, C., Naisbitt, D.J., Goldring, C.E., Park, B.K., 2009. Role of protein haptenation in triggering maturation events in the dendritic cell surrogate cell line THP-1. Toxicol. Appl. Pharmacol. 238, 120–132. http://dx.doi.org/10.1016/j.taap.2009.05.001.

Melehani, J.H., James, D.B., DuMont, A.L., Torres, V.J., Duncan, J.A., 2015. Staphylococcus aureus leukocidin A/B (LukAB) kills human monocytes via host NLRP3 and ASC when extracellular, but not intracellular. PLoS Pathog. 11 (6), e1004970. http://dx.doi.org/10.1371/journal.ppat.1004970.

Ménard, N., Tsapis, N., Poirier, C., Arnauld, T., Moine, L., Lefoulon, F., Péan, J.M., Fattal, E., 2012. Drug solubilization and in vitro toxicity evaluation of lipoamino acid surfactants. Int. J. Pharm. 423, 312–320. http://dx.doi.org/10.1016/j.ijpharm.2011.11.030.

Mistilis, M.J., Bommarius, A.S., Prausnitz, M.R., 2015. Development of a thermostable microneedle patch for influenza vaccination. J. Pharm. Sci. 104, 740–749. http://dx.doi.org/10.1002/jps.24283.

Németh, Z.H., Deitch, E.A., Szabó, C., Haskó, G., 2002. Hyperosmotic stress induces nuclear factor-kappaB activation and interleukin-8 production in human intestinal epithelial cells. Am. J. Pathol. 161, 987–996. http://dx.doi.org/10.1016/S0002-9440(10)64259-9.

Nogueira, D.R., Mitjans, M., Infante, M.R., Vinardell, M.P., 2011. The role of counterions in the membrane-disruptive properties of pH-sensitive lysine-based surfactants. Acta Biomater. 7, 2846–2856. http://dx.doi.org/10.1016/j.actbio.2011.03.017.

Nunes, P., Ernandez, T., Roth, I., Qiao, X., Strebel, D., Bouley, R., Charollais, A., Ramadori, P., Foti, M., Meda, P., Féraille, E., Brown, D., Hasler, U., 2013. Hypertonic stress promotes autophagy and microtubule-dependent autophagosomal clusters. Autophagy 9, 550–567. http://dx.doi.org/10.4161/auto.23662.

Ogaji, I.J., Nep, E.I., Audu-Peter, J.D., 2011. Advances in natural polymers as pharmaceutical excipients. Pharm. Anal. Acta 3, 146. http://dx.doi.org/10.4172/2153-2435.1000146.

Pandey, M., Mahadevan, D., 2014. Monoclonal antibodies as therapeutics in human malignancies. Future Oncol. 10, 609–636. http://dx.doi.org/10.2217/fon.13.197.

Patel, V.A., Longacre, A., Hsiao, K., Fan, H., Meng, F., Mitchell, J.E., Rauch, J., Ucker, D.S., Levine, J.S., 2006. Apoptotic cells, at all stages of the death process, trigger characteristic signaling events that are divergent from and dominant over those triggered by necrotic cells: implications for the delayed clearance model of autoimmunity. J. Biol. Chem. 281, 4663–4670. http://dx.doi.org/10.1074/jbc.M508342200.

Pekarova, M., Kubala, L., Martiskova, H., Papezikova, I., Kralova, S., Baldus, S., Klinke, A., Kuchta, R., Kadlec, J., Kuchtova, Z., Kolarova, H., Lojek, A., 2013. The unique role of dietary L-arginine in the acceleration of peritoneal macrophage sensitivity to bacterial endotoxin. Immunol. Res. 56, 73–84. http://dx.doi.org/10.1007/s12026-012-8379-2.

Perregaux, D.G., Laliberte, R.E., Gabel, C.A., 1996. Human monocyte interleukin-1beta posttranslational processing. Evidence of a volume-regulated response. J. Biol. Chem. 1996 (271), 29830–29838. http://dx.doi.org/10.1074/jbc.271.47.29830.

Pifferi, G., Restani, P., 2003. The safety of pharmaceutical excipients. Farmaco 58, 541–550. http://dx.doi.org/10.1016/S0014-827X(03)00079-X.

Pingle, S.C., Sanchez, J.F., Hallam, D.M., Williamson, A.L., Maggirwar, S.B., Ramkumar, V., 2003. Hypertonicity inhibits lipopolysaccharide-induced nitric oxide synthase expression in smooth muscle cells by inhibiting nuclear factor kappaB. Mol. Pharmacol. 63, 1238–1247. http://dx.doi.org/10.1124/mol.63.6.1238.

Razinkov, V.I., Treuheit, M.J., Becker, G.W., 2015. Accelerated formulation development of monoclonal antibodies (mAbs) and mAb-based modalities: review of methods and tools. J. Biomol. Screen. 20, 468–483. http://dx.doi.org/10.1177/1087057114565593.

Roberts, D., Keeling, R., Tracka, M., van der Walle, C.F., Uddin, S., Warwicker, J., Curtis, R., 2015. Specific ion and buffer effects on protein-protein interactions of a monoclonal antibody. Mol. Pharm. 12, 179–193. http://dx.doi.org/10.1021/mp500533c.

Rock, K.L., Kono, H., 2008. The inflammatory response to cell death. Annu. Rev. Pathol. 3, 99–126. http://dx.doi.org/10.1146/annurev.pathmechdis.3.121806.151456.

Rossol, M., Heine, H., Meusch, U., Quandt, D., Klein, C., Sweet, M.J., Hauschildt, S., 2011. LPS-induced cytokine production in human monocytes and macrophages. Crit. Rev. Immunol. 31, 379–446. http://dx.doi.org/10.1186/1476-9255-9-1.

Schneider, C.P., Trout, B.L., 2009. Investigation of cosolute-protein preferential interaction coefficients: new insight into the mechanism by which arginine inhibits aggregation. J. Phys. Chem. B 113, 2050–2058. http://dx.doi.org/10.1021/jp808042w.

Schneider, C.P., Shukla, D., Trout, B.L., 2011. Arginine and the Hofmeister series: the role of ion-ion interactions in protein aggregation suppression. J. Phys. Chem. B 115, 7447–7458. http://dx.doi.org/10.1021/jp111920y.

Sedger, L.M., McDermott, M.F., 2014. TNF and TNF-receptors: from mediators of cell death and inflammation to therapeutic giants — past, present and future. Cytokine Growth Factor Rev. 25, 453–472. http://dx.doi.org/10.1016/j.cytogfr.2014.07.016.

Shapiro, L., Dinarello, C.A., 1997. Hyperosmotic stress as a stimulant for proinflammatory cytokine production. Exp. Cell Res. 231, 354–362. http://dx.doi.org/10.1006/excr.1997.3476.

Simmons, D.L., 1995. The role of ICAM expression in immunity and disease. Cancer Surv. 24, 141–155.

Simon, J.C., Cruz Jr., P.D., Tigelaar, R.E., Sontheimer, R.D., Bergstresser, P.R., 1991. Adhesion molecules CD11a, CD18, and ICAM-1 on human epidermal Langerhans cells serve a functional role in the activation of alloreactive T cells. J. Investig. Dermatol. 96, 148–151. http://dx.doi.org/10.1111/1523-1747.ep12515946.

Singleton, C.A., 2014. MS in the analysis of biosimilars. Bioanalysis 6, 1627–1637. http://dx.doi.org/10.4155/bio.14.110.

Spachidou, M.P., Bourazopouloum, E., Maratheftism, C.I., Kapsogeorgoum, E.K., Moutsopoulos, H.M., Tzioufas, A.G., Manoussakis, M.N., 2007. Expression of functional

In addition to NMR based techniques, reports in the area suggest that orthogonal methods (e.g. such as Dynamic Light Scattering (DLS), Micro-Flow Imaging (MFI), Raster Image Correlation Spectroscopy (RICS)) could also be used for characterisation of monoclonal antibodies and the corresponding mAb-based formulations (Hamrang, et al., 2015, p. 2473). As described in the sections above, stabilisation of mAb drugs is of paramount importance to the development of safe and effective formulations. Kheddo and co-workers indicated that protein self-association and aggregation may be observed under physiological conditions, however in the work by Hamrang and co-workers it was indicated that various stress (changes in temperature, pH, addition of buffers) conditions might result in the formation of protein aggregates characterised by different formation mechanisms and morphologies (Hamrang, et al., 2015, p. 2474). For instance, it was described that freeze-thaw can result in partial protein unfolding as a result of changes in cryo-concentration of the tested solutes and pH changes, observed as the result of buffer crystallisation. In addition to the described experimental conditions, increased temperatures may also have a negative impact on conformational changes in the investigated proteins. Thus, a gradual increase in temperature may result in protein unfolding which, in turn, may trigger additional partial unfolding of different areas of the protein molecule. The outlined processes mediate conformational changes, which promote aggregation as described in the manuscript (Hamrang, et al., 2015, p. 2475). The results of this study are discussed in section 3.2 below.

Recent publications indicated that during particle characterisation more emphasis should be placed on the determination of particles in the 0.5-5 µm range, due to possible production of novel pharmaceuticals. Aggregates in this size range can be classified as sub-visible and novel characterisation methods should be developed to characterise particles in this size range. Currently, the majority of experimental challenges encountered during the analysis of protein aggregates are associated with the inability of the employed techniques to characterise a considerable range of particles sizes and discriminate between foreign/protein-based particles (Hamrang, et al., 2015, p. 2476). Modern analytical methods that are employed in the characterisation of various aggregates are graphically represented in Figure 1.4 below.
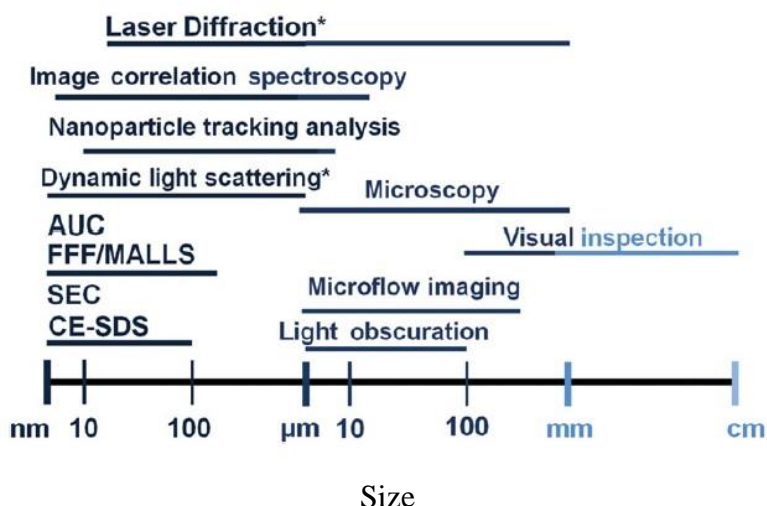
Size

Figure 1.4: Modern analytical methods employed in particle characterisation and the range of sizes over which these can be used to measure particles, adapted from (Hamrang, et al., 2015, p. 2474). MALLS refers to multi-angle laser light scattering technique, FFF refers to field-flow fractionation, AUC is analytical ultracentrifugation, CE-SDS is capillary electrophoresis-sodium dodecyl sulphate and SEC is size exclusion chromatography (Hamrang, et al., 2015, p. 2474).

Figure 1.4 suggests that multiple methods can be applied to characterise protein particles of the same size, however in all cases a lack of discrepancy of the methods to differentiate between protein-based particles and foreign contaminants presents a considerable disadvantage. It can also be observed that possible characterisation methods may fundamentally employ different characterisation principles, but the outlined above disadvantages will be intrinsic to all of the applied techniques. In figure 1.4 above, analysis methods marked with an asterisk represent techniques that are unable to perform quantification of particle size absolute distributions.

Taking into consideration the outlined above disadvantages associated with traditional analysis techniques and the importance of preventing protein aggregation that was discussed in publications by Kheddo and co-workers, the development and use of alternative analysis methods needs to be investigated. In particular, Hamrang and co-workers suggested that implementation of RICS (Raster Image Correlation Spectroscopy) can be highly effective in the analysis of particle morphology (Hamrang, et al., 2015, p. 2475). The same research group also indicated that by combining RICS with other analytical techniques, such as DLS (Dynamic light scattering) and MFI (micro-flow imaging) it was possible to analyse particles across a considerable size range that were generated as the result of freeze-thaw and thermal stresses. Literature sources indicate that RICS is a well-established analytical tool, that has been employed in various situations to measure particle mobility and size through the utilisation of diffusion coefficients and the Stokes-Einstein equation (Hamrang, et al., 2015, p. 2476).

From a practical perspective, during the collection of confocal fluorescent images, intensity of fluorescence gradually changes due to diffusion of the analysed molecules across the corresponding confocal volume and subsequent recording of the produced raster scan. In turn, particle size and yield information can be produced based on correlations between fluctuations of fluorescence intensities, observed within confocal data. It is clear that the described methods can be employed in conjunction with the technique developed by Kheddo and co-workers to investigate particle size distributions in monoclonal antibody-based formulations (Kheddo, et al., 2016, p. 89).

& Mark E. Welland1

Characterisation of Stress-Induced Aggregate Size Distributions and Morphological Changes of a Bi-Specific Antibody Using Orthogonal Techniques

ZAHRA HAMRANG,[1] MARYAM HUSSAIN,[1] KATIE TINGEY,[2] MALGORZATA TRACKA,[2] JOSÉ R. CASAS-FINET,[3] SHAHID UDDIN,[2] CHRISTOPHER F. VAN DER WALLE,[2] ALAIN PLUEN[1]

[1]Manchester Pharmacy School, University of Manchester, Manchester M13 9PT, UK
[2]MedImmune, Formulation Science, Granta Park, Cambridge CB21 6GH, UK
[3]MedImmune LLC, Analytical Biochemistry, Gaithersburg Maryland 20878

ABSTRACT: A critical step in monoclonal antibody (mAb) screening and formulation selection is the ability of the mAb to resist aggregation following exposure to environmental stresses. Regulatory authorities welcome not only information on the presence of micron-sized particles, but often any information on sub-visible particles in the size range obtained by orthogonal sizing techniques. The present study demonstrates the power of combining established techniques such as dynamic light scattering (DLS) and micro-flow imaging (MFI), with novel analyses such as raster image correlation spectroscopy (RICS) that offer to bridge existent particle sizing gaps in this area. The influence of thermal and freeze–thaw stress treatments on particle size and morphology was assessed for a bi-specific antibody (mAb2). Aggregation of mAb2 was confirmed to be concentration- and treatment-dependent following thermal stress and freeze–thaw cycling. Particle size and count data show concentration- and treatment-dependent behaviour of aggregate counts, morphological descriptors and particle size distributions. Complementarity in particle size output was observed between all approaches utilised, where RICS bridged the analytical size gap (~0.5–5 μm) between DLS and MFI. Overall, this study highlights the potential of orthogonal image analyses such as RICS (analytical size gap) and MFI (particle morphology) for formulation screening. © 2015 Wiley Periodicals, Inc. and the American Pharmacists Association J Pharm Sci 104:2473–2481, 2015

Keywords: protein aggregation; microscopy; fluorescence spectroscopy; image analysis; particle size

INTRODUCTION

The development of safe and potent monoclonal antibody (mAb) therapeutics requires the design of rational processes and formulations yielding products with sufficient physicochemical stability over the desired shelf life. During manufacture and bioprocessing, a therapeutic protein will be subjected to a range of potentially destabilising environmental conditions that could result in the loss of native protein structure and subsequent protein aggregation.[1] Extensive loss of native structure and aggregation may lead to loss of therapeutic efficacy and potentially adverse effects following administration.[2]

Different stress types are recognised to give rise to distinct aggregation mechanisms[3] and the formation of aggregates of various sizes and morphologies. For example, freeze–thaw conditions can lead to the partial unfolding of a protein[4] as a consequence of cryo-concentration of solutes,[1] pH changes arising from buffer crystallisation (e.g., phosphate buffers),[5] formation and subsequent exposure of the protein to ice–liquid interfaces,[6] or adsorption to container walls.

In the case of exposure to elevated temperatures, several sequential conformational changes may ensue (i.e., unfolding) that trigger the formation of multiple partially unfolded intermediates and eventually undergo irreversible conformational changes that lead to aggregation.[7]

Experimental challenges associated with the analytical characterisation of aggregates generated by various stresses relate to the inability of a single approach to characterise a broad particle size range (see Fig. 1) or lack of discrimination between foreign particulate contaminants and proteinaceous particles. Hence, multiple complementary orthogonal technologies are often implemented. These technologies may be based on different principles for size measurement or suffer from experimental artefacts during sample preparation that can further complicate comparison of aggregate size data between samples.[8,9]

Recently, more emphasis has been placed on the characterisation of sub-visible aggregates in the gap size range (i.e., 0.5–5 μm) stimulating the need for development of novel technologies capable of size measurement overlapping with this range.[13]
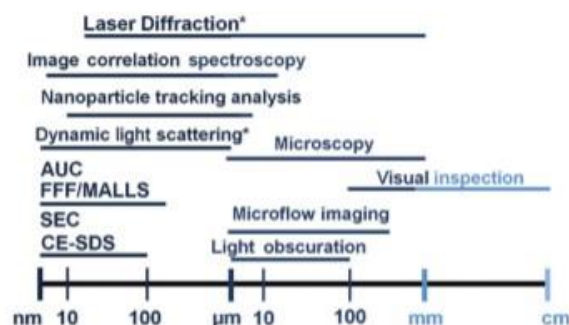
Herein, the intention of the present case study is to assess the capability of raster image correlation spectroscopy (RICS) as a new particle metrology tool for the analysis of a broad particle size range in combination with micro-flow imaging (MFI), dynamic light scattering (DLS) and data visualisation

Figure 1. Schematic depicting the relative particle size ranges characterised by several analytical techniques. Asterisk (*) denotes methods that are unable to quantify absolute particle size distributions. SEC refers to size-exclusion chromatography, CE-SDS to capillary electrophoresis-sodium dodecyl sulphate, AUC to analytical ultracentrifugation, FFF to field-flow fractionation and MALLS to multi-angle laser light scattering. Adapted from Hamrang et al.,[10] Singh et al.[11] and Zölls et al.[12] with permission from Elsevier, John Wiley & Sons and John Wiley & Sons, respectively.

(i.e., radar chart array) for analysis of aggregate size ranges and concentrations generated by thermal and freeze–thaw stresses.

Raster image correlation spectroscopy is an image analysis tool originally developed by Digman et al.[14] that enables measurement of mobility (diffusion coefficients) and size (through the application of the Stokes–Einstein equation). During acquisition of fluorescent confocal images, fluorescence intensity fluctuations resulting from the diffusion of fluorescently-labelled molecules across the confocal volume is captured through a raster scan. Subsequent correlation of inherent fluorescence intensity fluctuations within confocal image time series can yield concentration and size information. Spatial resolution offered at pixel level for raster-scanned images enables the determination of information contained in successive pixels (microseconds), lines (milliseconds) and frames (seconds), that for a high-resolution image can generate a statistically significant number of regions for analysis of particle size distributions.

MATERIALS AND METHODS

Materials

A bi-specific antibody, hereafter referred to as mAb2, with a theoretical molecular weight of 204 kDa (and experimentally measured pI of ~9.1) was provided by MedImmune (Cambridge, UK). mAb2 was provided formulated in a 25-mM histidine and 235-mM sucrose buffer (pH 6.0) and filtered (0.2 μm pore-sized filter) prior to sample preparation.

Histidine and sucrose were obtained from Sigma–Aldrich UK (Dorset, UK) and were of analytical grade.

SYPRO® red (Molecular Probes, Oregon) was prepared as a 50× stock solution in pre-filtered histidine–sucrose buffer and diluted to a final working concentration of 2.5× for fluorescence studies immediately prior to experimentation (all solutions were prepared freshly).

Methods

Sample Preparation

Thermal Stress Protocol

In order to generate aggregates formed by protein unfolding, a series of thermal stress experiment were performed. Aliquots (0.5 mL) of mAb2 (final concentration of 1 and 10 mg/mL) were pre-filtered (0.2 μm syringe filter) and transferred into 1.5 mL low-binding polypropylene micro-centrifuge tubes (cat no. E1415-2600; StarLab, Milton Keynes, Buckinghamshire, UK) on a heat plate. Samples were incubated on the heat plate at 58°C overnight (a temperature below the first melting point of mAb2 as determined by calorimetry, see Supplementary Information Fig. S1) to generate particulates. Following heating experiments, samples were allowed to cool to room temperature prior to characterisation of particle size and morphology.

Freeze–Thaw Protocols

1. Uncontrolled freeze–thaw (rapid): Pre-filtered aliquots (0.5 mL) of mAb2 (final concentration 1 and 10 mg/mL) were placed in micro-centrifuge tubes supported on an open rack (to prevent direct contact with surfaces), stored in a −80°C freezer for 1 h and thawed for 30 min at 37°C on a heat plate.
2. Controlled freeze–thaw protocol (slow): To represent repeated freeze–thaw effects on particle generation during transportation, the following protocol was utilised; a Bio-Cool® controlled-rate freezer (SP Scientific, Suffolk, UK) was utilised for all controlled freeze–thaw experiments. Cycles were programmed so that a 1°C/min reduction in temperature up to −80°C, with subsequent ramping up to 25°C and retention at this temperature for 30 min (the process was repeated till three and five freeze–thaw cycles were performed).

All samples were handled in a manner as to prevent contamination with airborne particles.

Image Acquisition with Confocal Microscopy

A Zeiss 510 Confocor 2 confocal microscope with a LSM tube lens and c-Apochromat 40×/1.2NA water-immersion objective lens was utilised for image acquisition. Samples (non-covalently) labelled with SYPRO® red dye were excited with a Helium-Neon laser at 543 nm and the emitted fluorescence was collected using a Long pass filter set (LP585).

Confocal image time series of 1024 × 1024 pixel resolution were captured over 100 frames with a corresponding pixel time of 6.4 μs for both stressed and non-treated samples that were subjected to labelling with SYPRO® red using the aforementioned approach.

Analysis of Size Distributions with RICS

An in-house RICS software (ManICS) was used for the analysis of images acquired using confocal microscopy. A full description of the RICS algorithm has previously been described elsewhere.[14,15] Stressed samples of the aggregated (and labelled) bi-specific antibody were transferred to a 96-well plate. Image time series (1024 × 1024 pixels) were sub-divided into 32 × 32 pixel sub-regions and the respective diffusion coefficients (D) generated as output for the entire image. All fits

possessing a R^2 below 0.7 were discarded from the fit data prior to the generation of particle size distributions.

Raster image correlation spectroscopy-derived diffusion coefficients were subsequently converted to particle diameter using the Stoke–Einstein equation (following the determination of sample viscosity):

$$D = \frac{k_B T}{3\eta\pi a} \tag{1}$$

where D refers to the diffusion coefficient, k_B refers to the Boltzmann constant, T is the temperature at which the measurements were performed, η is solvent viscosity and a is the hydrodynamic diameter. Particle size distributions were subsequently generated from this data and compared with MFI and DLS.

Dynamic Light Scattering

Analysis of aggregate size distributions for non-treated and stressed samples was performed using a Zetasizer Nano ZS (Malvern Instruments Ltd., Malvern, Worcestershire, UK) for mAb2 (1 and 10 mg/mL) samples. Samples were equilibrated for 2 min at 20°C and all measurements performed in triplicate. The number of runs was optimised for each sample prior to the initiation of measurements (a minimum of 13 runs were performed per measurement). The size distribution data for mAb2 samples including Z-average, polydispersity and size distributions were determined following correlation of data using the Dispersion Technology Software version 5.0 for protein characterisation (Malvern). Z-average values were determined through cumulant analysis of the correlation function (Eq. (2))[16]:

$$C(\tau) = A \exp\left(-2\Gamma\tau + \mu_2\tau^2 - \ldots\right) \tag{2}$$

where $C(\tau)$ represents the baseline-subtracted correlation function and τ represents the delay time. Values A, μ_2 and Γ are determined by least squares fitting of the correlation function $[C(\tau)]$. The intensity-weighted average diffusion coefficient $(D_{t,avg})$ is determined from $D_{t,avg}.q^2$ where q is the scattering vector. Equation 1[17] is subsequently applied to determine $D_{t,avg}$ to determine the intensity-weighted mean harmonic particle size distribution.

Micro-Flow Imaging

All MFI experiments were performed using a Brightwell Micro-Flow Imaging™ instrument (Brightwell Technologies, Ottawa, Canada). The system model was a DPA4200 with a depth of field of 100 μm, resolution of 0.25 μm and nominal size range of 1–70 μm at a magnification of 14×. Particle free buffer (i.e., 5 mL) was purged through the system to remove any residual particulates from previous measurements and reduce the baseline prior to data acquisition for each sample. Millipore-filtered pure water was used to check for any background particulates and provide a clear baseline. Subsequently, the sample was introduced (0.1 mL sample at a rate of 0.1 mL/min), the illumination optimised and 0.5 mL of sample analysed at a corresponding flow rate of 0.1 mL/min.

Brightfield images, morphometric (i.e., equivalent circle diameter, aspect ratio and circularity) and particle data (e.g., transparency) obtained from the analysis of non-treated and stressed samples were subjected to analysis of particle concentration, morphology and size distribution.

Data Analysis

Unless otherwise stated, a non-parametric paired sample Wilcoxon signed rank test was performed to assess the influence of stress type on resultant size distribution. A calculated probability (i.e., p value) equal or less than 0.05 was considered to be statistically significant.

Radar charts of MFI data were constructed for each stress type to aid visual assessment of the influence of stress treatment on aggregate size, concentration and morphology.[17,18] The mean, mean + SD and mean − SD were determined for each corresponding parameter to aid visualisation of data variability following exposure to each stress. Corresponding data were plotted in Microsoft Excel as a radar chart plot on a logarithmic scale (for each of the five particle categories) for particle concentration charts and on a linear scale for aspect ratio, mean intensity (i.e., mean intensity/1000) and intensity SD.

RESULTS

The Influence of Thermal Stress Treatment on Aggregate Morphology, Concentration and Particle Size Distribution

Bi-specific antibody samples were stored at 58°C overnight to assess the influence of thermal stress on aggregate size range, particle concentration and morphology. Samples were subsequently subjected to analysis with RICS, MFI and DLS.

Dynamic Light Scattering

Analysis of intensity-based light scattering data for thermally stressed samples revealed the presence of predominantly monomeric peaks (see Supplementary Information Fig. S2 and Table S1). However, the presence of larger aggregates (i.e., micron sized) was confirmed within these samples.

Relative to non-treated mAb2 samples (i.e., 25°C), a significant increase in Z-average from 14.6 ± 0.74 and 10.7 ± 0 nm (mean ± standard error for 1 and 10 mg/mL samples, respectively) to 33.40 ± 0.20 and 30.23 ± 0.10 nm was observed following thermal stress treatment. For the non-treated samples, although the particle size distributions indicated that mAb2 existed largely as the monomer or small soluble aggregates (peak 1), the presence of peaks at larger diameters (peaks 2 and 3) confirmed the presence of micron-sized aggregates within the samples.

The Influence of Thermal Stress on Particle Concentration

In order to determine the influence of thermal stress on the generation of sub-visible particles, the concentration of particles in samples (i.e., counts per mL) were compared between stressed and non-treated mAb2 at two different concentrations (1 and 10 mg/mL). Representative particle images for each size range and corresponding radar chart plots for particle counts are presented in Figure 2.

Aggregate types detected by MFI were highly heterogeneous in morphology, ranging from dense and compact small aggregates to ribbon-shaped structures (Fig. 2, top).

Particle concentration data presented in Figure 2 generally show a lower count of detected particles in non-treated mAb2 samples compared with samples that were stressed

2476 RESEARCH ARTICLE – *Pharmaceutical Biotechnology*
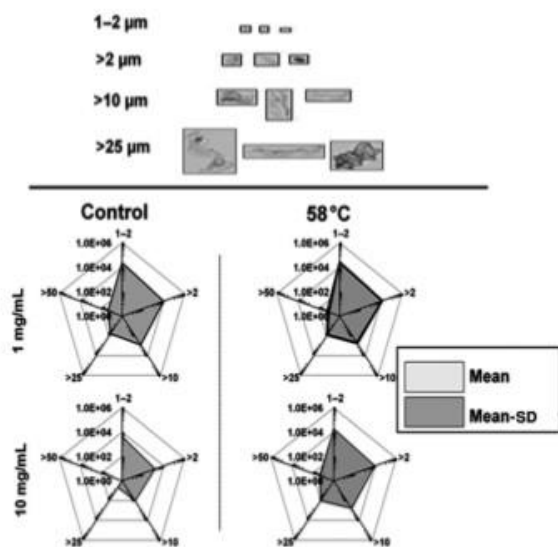
Figure 2. Typical particle images obtained from MFI measurements of 1 and 10 mg/mL mAb2 samples subjected to thermal stress (top) and corresponding radar chart plots of particle concentrations for aggregates with an equivalent circle diameter in the 1–2 μm and greater than 2, 10, 25 and 50 μm size range.

Figure 3. Aggregates from control and thermally-stressed mAb2 samples labelled with SYPRO red (top) and mAb2 aggregate size distributions obtained from RICS and MFI measurements represented by a box plot for 1 and 10 mg/mL samples subjected to thermal stress at 58°C. Sample means are represented by ·, outliers by ♦, medians by horizontal lines, minima/maxima by asterisks, upper and lower range by vertical lines.

overnight at 58°C (across all particle size ranges) indicated by a large grey surface in the radar plots (lower particle concentrations at outermost part of the radar chart). Following treatment, mean particle concentration is observed to increase at both concentrations with a higher incidence of particles in the 1–10-μm size range and emergence of particles larger than 50 μm in size.

The Influence of Thermal Stress on Particle Size Distribution

Particle size distributions generated from RICS and MFI measurements were compared to assess the influence of thermal stress type and concentration of mAb2 on resultant size output (Fig. 3).

Statistically significant differences ($p < 0.05$) were observed between size distributions calculated from RICS analysis of stressed 1 and 10 mg/mL samples (the cut-off minimum size for MFI is 1 μm and hence no data points are reported below this value).

It should be noted that the number of regions generated following performance of RICS on image time series acquired from labelled non-treated (control) samples generated insufficient numbers of fits to be incorporated. This was consistent with an observed small number of fluorescently labelled aggregates in the confocal micrographs.

Dynamic Light Scattering

In order to characterise particle size over a broad range (nm–μm), DLS measurements were utilised to provide an insight into aggregate size distributions formed as a consequence

Table 1. Z-Average (Mean ± Standard Error) Data Obtained from DLS Measurements Performed on 1 and 10 mg/mL Control and Freeze–Thaw Stressed mAb2 Samples

Concentration (mg/mL)	1	10
Treatment	Z-Average Diameter (nm)	
NT	14.6 ± 0.74	10.7 ± 0.0
Controlled F–T		
3×	56.2 ± 6.00	106.0 ± 26.98
5×	118.8 ± 4.47	111.5 ± 78.48
Uncontrolled F–T		
3×	11.30 ± 0.29	11.44 ± 0.13
5×	24.71 ± 5.34	19.86 ± 5.77

of freeze–thaw stress and any inherent differences between controlled and uncontrolled freeze–thaw of mAb2 samples (Table 1). Data obtained from the DLS analysis of mAb2 samples subjected to freeze–thaw cycling indicate an increase in the Z-average for both 1 and 10 mg/mL samples upon increasing the number of freeze–thaw cycles. This was further supported by the emergence of a second peak for the intensity-based light scattering measurements that was observed at larger
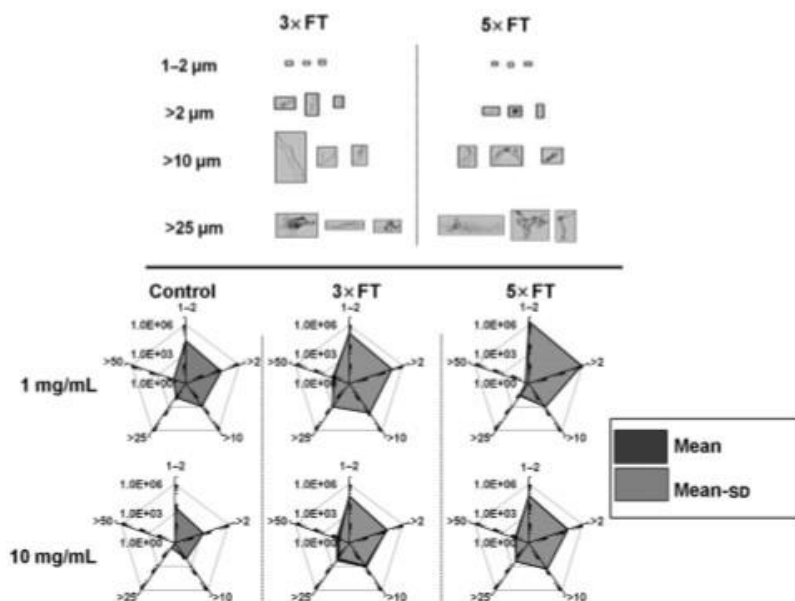
Figure 4. Typical particle images obtained from MFI measurements of 10 mg/mL mAb2 samples subjected to the controlled freeze–thaw (F–T) stress protocol (top) and corresponding cumulative particle counts (mean and mean − SD) for aggregates of 1 and 10 mg/mL mAb2 samples subjected to controlled F–T stress with an equivalent circle diameter in the 1–2 µm, and greater than 2, 10, 25 and 50 µm size range (bottom).

particle sizes in the sub-visible size range (see Supplementary Information Fig. S3 and Table S2). In the case of uncontrolled freeze–thaw cycling smaller changes were observed in both the Z-average diameter and the principle peak diameter size, indicating predominant formation of small soluble aggregates as opposed to sub-visible particles. The presence of micron-sized particles that increased in size following five freeze–thaw cycles was confirmed.

Characterisation of Particle Concentration as a Function of Freeze–Thaw Treatment with MFI

Particle counts obtained from MFI analysis were compared against all freeze–thaw treatments (controlled and uncontrolled versus non-treated mAb2 samples) that demonstrated significant differences in the number of generated particles and their corresponding size ranges.

Micro-flow imaging measurements of various particle size ranges following the application of controlled freeze–thaw stress revealed a consistent increase in particle counts (per mL) from no freeze–thaw treatment (control) up to five cycles (see Fig. 4).

Concentration-dependent behaviour was observed following uncontrolled freeze–thaw stress, such that 1 mg/mL samples consistently contained a higher particle count in comparison to 10 mg/mL mAb2 samples (except for particles >25 and >50 µm after 5× freeze–thaw).

Concentration-dependent behaviour was observed following uncontrolled freeze–thaw stress, such that 10 mg/mL samples consistently contained a higher particle count in comparison to 1 mg/mL mAb2 samples (see Fig. 5).

Uncontrolled freeze–thaw of mAb2 samples led to the formation of a significantly higher particle concentration in the

1–2-µm size range compared with controlled freeze–thaw stress, in all cases except for the 1 mg/mL sample following 5× freeze–thaw.

MFI and RICS

Controlled and uncontrolled freeze–thaw stress treatments were performed on mAb2 samples and subjected to analysis with MFI and RICS in order to evaluate the influence of stress type and complementarity in sizing between the approaches utilised.

Performance of a paired sample Wilcoxon signed rank test ($p < 0.05$) for each sample set revealed no statistically significant differences in size distributions obtained between subsequent freeze–thaw cycles for both controlled and uncontrolled freeze–thaw treatments. Data presented in Figure 6 demonstrates typical aggregates observed in a single confocal images and overlap in the particle size ranges detected by MFI and RICS analysis of samples subjected to freeze–thaw stress.

As aforementioned, control samples contained a small number of micron-sized aggregates labelled by SYPRO® red and were omitted from representation of particle size data because of a small sample size.

Assessment of Particle Morphology Changes following Stress Treatments with MFI

Radar chart arrays were utilised to visualise the variation of morphological descriptors (i.e., aspect ratio, mean intensity and intensity SD) for the five particle size populations (i.e., 1–2, 2–5, 5–10, 10–25 and 25–50 µm) of non-treated and stressed mAb2 samples to enable comparison of stress treatment effects and mAb2 sample concentration.
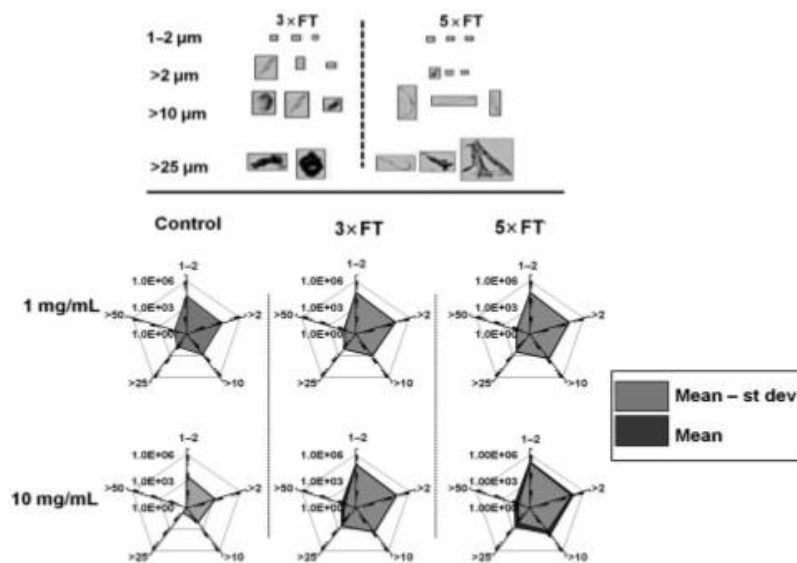
Figure 5. Typical particle images obtained from MFI measurements of 10 mg/mL mAb2 samples subjected to the uncontrolled freeze–thaw (F–T) stress protocol (top) and corresponding particle counts (mean, and mean − SD) for aggregates of 1 and 10 mg/mL mAb2 samples subjected to uncontrolled F–T stress with an equivalent circle diameter in the 1–2 μm, and greater than 2, 10, 25 and 50 μm size range.
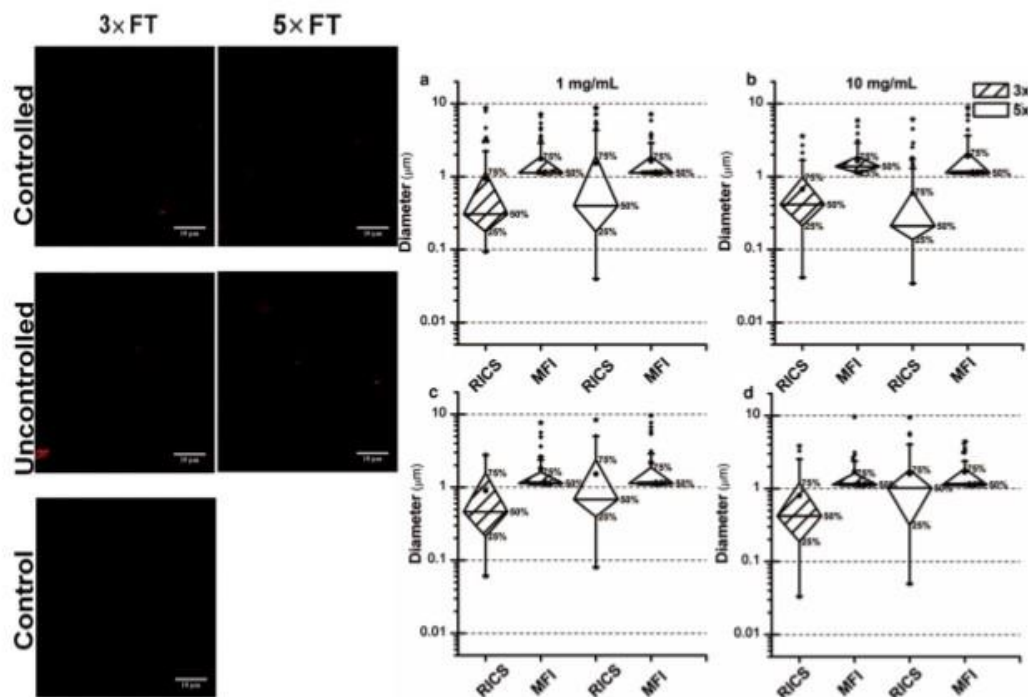
Figure 6. Aggregates from control and freeze-thaw stressed 10 mg/mL mAb2 samples labelled with SYPRO red (left) and mAb2 aggregate size distributions obtained from RICS and MFI measurements represented by a box plot for 1 mg/mL (a) and 10 mg/mL (b) samples subjected to controlled freeze–thaw and 1 mg/mL (c) and 10 mg/mL (d) samples subjected to uncontrolled freeze–thaw stress (right). Sample means are represented by •, outliers by ♦, medians by horizontal lines, minima/maxima by asterisks, upper and lower range by vertical lines.
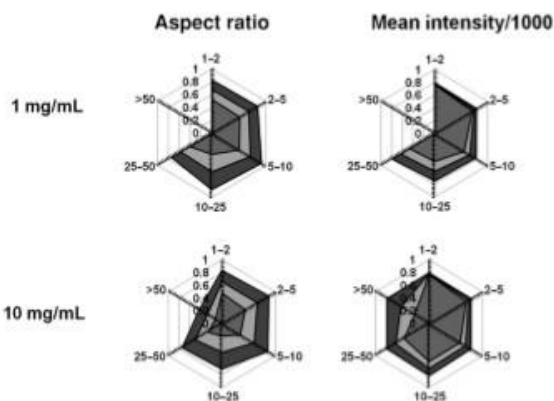
Figure 7. Radar chart plots of morphological parameters obtained from MFI data for mAb2 samples subjected to thermal stress at 58°C overnight across the five particle size classes.

Representative images acquired from aggregates using MFI consisted of particles of varying intensities and shapes. Corresponding radar chart arrays of particle size (i.e., equivalent circle diameter) versus morphological descriptor were constructed across all particle size ranges to aid visualisation of thermal stress treatment effects on particle size and morphology (see Fig. 7).

Radar chart plots presented for mAb2 sub-visible aggregates generated from thermal stress indicated a lower mean intensity for particles in the 10–25-µm size range, whereas mean intensities (divided by 10^3) across all other size ranges were in the

0.8–1-µm range. The mean aspect ratios of particles were found to be consistently similar across all particle size classes for both concentrations of mAb2 subjected to thermal stress. However, significant variation in the mean intensity and the SD of the aspect ratio for each particle class was observed upon increasing the initial mAb2 concentration (i.e., 1 and 10 mg/mL).

Sub-visible aggregates produced from freeze–thaw stress of mAb2 samples were compared between the two protocols (controlled and uncontrolled) utilised in this study (see Fig. 8).

Aspect ratios obtained from MFI measurements of subvisible aggregates obtained following controlled and uncontrolled freeze–thaw stress revealed higher aspect ratios for smaller particle size classes that decreased for aggregates in larger particle size subsets (10–25 and 25–50 µm). Consistent with this observation, smaller particle sizes were found to be more transparent than the longer filamentous particles observed at larger size ranges (higher mean intensity) that exhibited low mean intensities. Changes in aggregate morphology were found to be more pronounced following controlled freeze–thaw stress and upon increasing the number of freeze–thaw cycles. Predominant formation of filamentous aggregates (aspect ratio <0.5) following uncontrolled freeze–thaw effects was observed across all particle size ranges.

DISCUSSION

A current challenge in sizing aggregates in biopharmaceuticals remains to be the diversity of analytical approaches available, limitations associated with their approach and ability to resolve aggregates over a broad size range.[10] Recent research and regulatory attention is being drawn to a consideration of aggregate concentrations across all size ranges that may be insightful in eliciting the underlying mechanism of protein aggregation
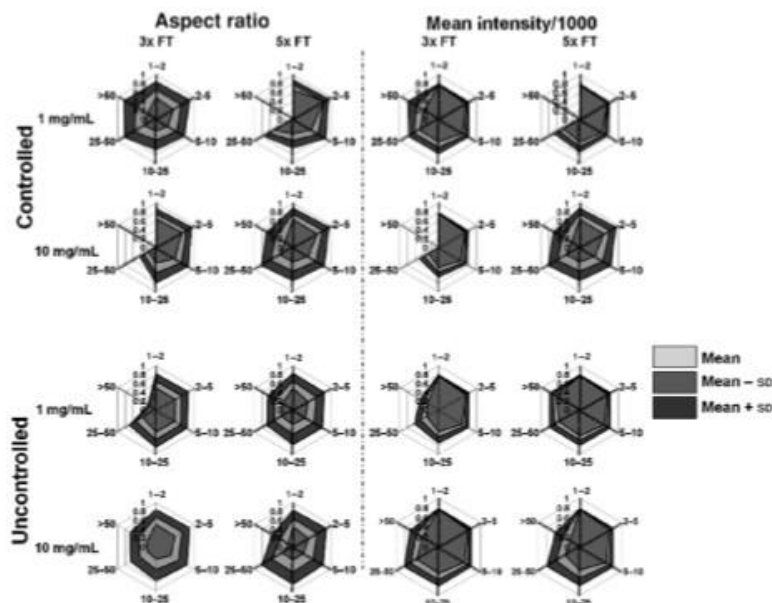
Figure 8. Radar chart arrays of morphological parameters versus particle size for mAb2 sub-visible aggregates generated from controlled and uncontrolled freeze–thaw stress treatment as measured by MFI.

and potential effects following administration. Limitations of well-established sizing methodologies in this analytical gap region has prompted the recent commercialisation of technologies exemplified by nanoparticle tracking analysis (NTA)[19] and resonant mass measurement[20] that offer superior differentiation between non-proteinaceous (e.g., silicone oil droplets) and proteinaceous particles.

Hence, the purpose of this study was to assess the feasibility of RICS application for measuring aggregate size distributions in the analytical gap region as an orthogonal tool in conjunction with MFI. Additionally, the influence of particular stress types on resultant (sub-micron) aggregate size distributions, morphologies and counts were examined through construction of radar charts. Initial screening of aggregate presence with DLS confirmed the formation of both soluble and larger sub-visible aggregates upon thermal and freeze–thaw stress treatment of mAb2.

Heat stress is recognised to contribute to the formation of partially unfolded stable intermediates that are hydrophobic in nature compared with the native (folded) protein. The extent of aggregation following thermal stress treatment below the melting temperature was assessed in this study. This has been reported to be dependent on the stability of aggregate-prone intermediates to form aggregates, as opposed to the melting temperature of the protein in previous reports of thermal stress effects on mAb aggregation.[7,21] Data generated by thermal stress of mAb2 indicated the formation of predominantly small soluble aggregates with DLS and the generation of sub-visible particles with MFI and RICS data relative to non-treated samples. Particle counts measured by MFI confirmed a higher concentration of particles in the 1–50 μm size range for samples heated to 58 °C and following freeze–thaw stress.

Freeze–thaw treatment is a complex and multi-stage process combining stresses from surface denaturation, cryo-concentration, phase separation, crystallisation of buffer components and pH shifts that may contribute to the formation of insoluble aggregates.[19,22,23] In the present study, selection of buffer components prevented the potential for aggregation arising from pH shifts (i.e., the absence of phosphate). Freeze–thaw effects have previously been correlated with the ice-liquid area, therefore, dependent on the concentration of formulated protein. At higher concentrations of protein, the ice-liquid area is smaller and susceptibility to freeze–thaw effects reduced.[24]

Micro-flow imaging as a successful recent particle analysis technology has been extensively applied to multi-parametric characterisation of particles or applied as a custom filter to differentiate between proteinaceous and foreign particulate contamination (data not presented here).[20] However, challenges remain in the accurate differentiation of non-proteinaceous particles from aggregates and the use of other analytical technologies is often required for the detection and quantification of sub-micron particles (not discussed here).[25,26]

Particle counts, aggregate morphological descriptors and relative aggregate size distributions in response to various stress treatments were measured using MFI. As aforementioned, individual micrographs from MFI measurements revealed the formation of particles of various sizes and morphologies induced by freeze–thaw and thermal stress. In all cases, the presence of sub-visible particles increased significantly relative to non-treated samples consistent with previous reports of mAb response to these treatment types.

To further aid qualitative comparison of variation in morphology parameters as a function of particle size, radar chart plots[18] of sub-visible aggregate data were applied to data acquired from stress treatments utilised in this study. Exposure to various stress treatments in this study resulted in the formation of aggregates with various morphologies as represented by radar chart plots. Application of radar chart plots in this context provided a direct means of comparison for the influence of stress types on aggregate formation. Hence, data visualisation tools in this context can support selection of optimal storage conditions and formulation compositions.

The increase in number of sub-visible particles detected by MFI relative to the non-treated mAb2 samples and labelling with extrinsic dyes confirmed both structural changes to the protein and the generation of sub-visible aggregates for further characterisation. Aggregates prepared in this study were labelled with SYPRO red and visualised with confocal microscopy prior to RICS analysis. Comparison of particle size distributions between methodologies revealed complementarity between RICS (hydrodynamic diameter) and MFI (equivalent circle diameter) in all cases with overlapping size ranges (see Figs. 3 and 6) that depended on the resolution associated with each technique (MFI is capable of detecting aggregates >1 μm). In this case, RICS was able to characterise proteinaceous aggregates over a broad size range (i.e., 10 nm to ~100 μm) as demonstrated for each stress type. However, further investigation is required to assess the capability of RICS for particle sizing in overcrowded and polydisperse systems. Extrinsic labelling of stress-induced aggregates has not been observed to further contribute to formation of aggregates in the present study as demonstrated by micrographs of monomeric and aggregated species, and particle size measurements of labelled and unlabelled stressed protein.

Compared with NTA, a particle sizing technique based on the tracking of light scattered (intensity of light scattered in proportional to the sixth power of particle diameter) from particles undergoing Brownian motion, RICS correlates fluorescence intensity fluctuations arising from fluorophore movement within the confocal volume to generate particle size data. Therefore, size data measured by RICS is not susceptible to the presence of a small concentration of large aggregates and dust.[19]

Where NTA relies on the Brownian motion trajectory to be tracked over a sufficient number of frames to enable detection and accurate particle sizing, RICS does not suffer from such biasing, provided the pixel dwell time and frame size are optimised during image acquisition (particles ≥1 μm can also be detected and measured by RICS).[14,27]

However, one of the challenges of sizing fluorescently labelled aggregates (with RICS) remains to be the optimisation and selection of appropriate dyes that are sufficiently photostable, and in a complex system do not label other components (e.g., silicone oil).[15,26]

The majority of reports of aggregate characterisation with microscopy have focused on the use of covalent fluorophores[15,26] to assess the loss of monomeric protein and the formation of higher-order aggregates with limited reports focusing on the quantitative measurement of aggregate sizes following extrinsic aggregate labelling (hydrophobic pocket binding dyes).[28]

To this end, we have demonstrated the applicability of RICS to bridging the analytical size gap in the characterisation of particle size distributions (in this case MFI). As a potential screening tool, RICS may be applied during pre-formulation of

66

protein-based therapeutics for the evaluation of stress effects (e.g., formulation and environmental) on aggregates and their corresponding size distributions.

CONCLUSIONS

In this study, complementarity was demonstrated between aggregate size ranges measured by various particle sizing techniques through overlapping size ranges observed between implemented methods. Particle size data generated by RICS was not biased to a specific particle size range, demonstrating its worth in sizing proteinaceous aggregates. Confocal analysis of aggregates permits direct and selective microscopic examination of changes induced by various stresses.

Techniques such as RICS may be insightful as a tool for the characterisation of aggregate size distributions over a broad size range during pre-clinical formulation studies as requirements for the characterisation of aggregates over broad size ranges become ever-increasingly emphasised by regulatory bodies.

In this study, SYPRO red was successfully utilised as an extrinsic aggregate labelling fluorophore. Further refinement of RICS as a novel particle metrology tool and optimisation of extrinsic aggregate labelling could provide scope for the assessment of stress effects on aggregation during pre-formulation and formulation development studies in more complex specimens.

ACKNOWLEDGMENTS

REFERENCES

1. Kueltzo LA, Wang W, Randolph TW, Carpenter JF. 2008. Effects of solution conditions, processing parameters, and container materials on aggregation of a monoclonal antibody during freeze–thawing. J Pharm Sci 97:1801–1812.
2. Rosenberg A. 2006. Effects of protein aggregates: An immunologic perspective. AAPS J 8:E501–E507.
3. Zhang A, Singh S, Shirts M, Kumar S, Fernandez E. 2012. Distinct aggregation mechanisms of monoclonal antibody under thermal and freeze–thaw stresses revealed by hydrogen exchange. Pharm Res 29:236–250.
4. Privalov PL. 1990. Cold denaturation of protein. Crit Rev Biochem Mol Biol 25:281–306.
5. Pikal-Cleland KA, Rodríguez-Hornedo N, Amidon GL, Carpenter JF. 2000. Protein denaturation during freezing and thawing in phosphate buffer systems: Monomeric and tetrameric β-galactosidase. Arch Biochem Biophys 384:398–406.
6. Chang BS, Kendrick BS, Carpenter JF. 1996. Surface-induced denaturation of proteins during freezing and its inhibition by surfactants. J Pharm Sci 85:1325–1330.
7. Hawe A, Kasper JC, Friess W, Jiskoot W. 2009. Structural properties of monoclonal antibody aggregates induced by freeze–thawing and thermal stress. Eur J Pharm Sci 38:79–87.
8. Filipe V, Hawe A, Carpenter JF, Jiskoot W. 2013. Analytical approaches to assess the degradation of therapeutic proteins. TrAC Trends Anal Chem 49:118–125.
9. Zölls S, Tantipolphan R, Wiggenhorn M, Winter G, Jiskoot W, Friess W, Hawe A. 2012. Particles in therapeutic protein formulations, Part 1: Overview of analytical methods. J Pharm Sci 101:914–935.
10. Hamrang Z, Rattray NJW, Pluen A. 2013. Proteins behaving badly: Emerging technologies in profiling biopharmaceutical aggregation. Trends Biotechnol 31:448–458.
11. Singh SK, Afonina N, Awwad M, Bechtold-Peters K, Blue JT, Chou D, Cromwell M, Krause H-J, Mahler H-C, Meyer BK, Narhi L, Nesta DP, Spitznagel T. 2010. An industry perspective on the monitoring of subvisible particles as a quality attribute for protein therapeutics. J Pharm Sci 99:3302–3321.
12. Zölls S, Gregoritza M, Tantipolphan R, Wiggenhorn M, Winter G, Friess W, Hawe A. 2013. How subvisible particles become invisible—Relevance of the refractive index for protein particle analysis. J Pharm Sci 102:1434–1446.
13. Carpenter JF, Randolph TW, Jiskoot W, Crommelin DJA, Middaugh CR, Winter G, Fan Y-X, Kirshner S, Verthelyi D, Kozlowski S, Clouse KA, Swann PG, Rosenberg A, Cherney B. 2009. Overlooking subvisible particles in therapeutic protein products: Gaps that may compromise product quality. J Pharm Sci 98:1201–1205.
14. Digman MA, Brown CM, Sengupta P, Wiseman PW, Horwitz AR, Gratton E. 2005. Measuring fast dynamics in solutions and cells with a laser scanning microscope. Biophys J 89:1317–1327.
15. Hamrang Z, Pluen A, Zindy E, Clarke D. 2012. Raster image correlation spectroscopy as a novel tool for the quantitative assessment of protein diffusional behaviour in solution. J Pharm Sci 101:2082–2093.
16. Koppel DE. 1972. Analysis of macromolecular polydispersity in intensity correlation spectroscopy: The method of cumulants. J Chem Phys 57:4814–4820.
17. Kalonia C, Kumru OS, Prajapati I, Mathaes R, Engert J, Zhou S, Middaugh CR, Volkin DB. 2015. Calculating the mass of subvisible protein particles with improved accuracy using microflow imaging data. J Pharm Sci 104:536–547.
18. Kalonia C, Kumru OS, Kim JH, Middaugh CR, Volkin DB. 2013. Radar chart array analysis to visualize effects of formulation variables on IgG1 particle formation as measured by multiple analytical techniques. J Pharm Sci 102:4256–4267.
19. Filipe V, Hawe A, Jiskoot W. 2010. Critical evaluation of nanoparticle tracking analysis (NTA) by nanosight for the measurement of nanoparticles and protein aggregates. Pharm Res 27:796–810.
20. Weinbuch D, Zoells S, Wiggenhorn M, Friess W, Winter G, Jiskoot W, Hawe A. 2013. Micro-flow imaging and resonant mass measurement (archimedes)—Complementary methods to quantitatively differentiate protein particles and silicone oil droplets. J Pharm Sci 102:2152–2165.
21. Fesinmeyer RM, Hogan S, Saluja A, Brych S, Kras E, Narhi L, Brems D, Gokarn Y. 2009. Effect of ions on agitation- and temperature-induced aggregation reactions of antibodies. Pharm Res 26:903–913.
22. Cao E, Chen Y, Cui Z, Foster PR. 2003. Effect of freezing and thawing rates on denaturation of proteins in aqueous solutions. Biotechnol Bioeng 82:684–690.
23. Mahler H-C, Friess W, Grauschopf U, Kiese S. 2009. Protein aggregation: Pathways, induction factors and analysis. J Pharm Sci 98:2909–2934.
24. Eckhardt B, Oeswein J, Bewley T. 1991. Effect of freezing on aggregation of human growth hormone. Pharm Res 8:1360–1364.
25. Sharma D, King D, Oma P, Merchant C. 2010. Micro-flow imaging: Flow microscopy applied to sub-visible particulate analysis in protein formulations. AAPS J 12:455–464.
26. Hamrang Z, Zindy E, Clarke D, Pluen A. 2014. Real-time evaluation of aggregation using confocal imaging and image analysis tools. Analyst 139:564–568.
27. Barnard JG, Babcock K, Carpenter JF. 2013. Characterization and quantitation of aggregates and particles in interferon-β products: Potential links between product quality attributes and immunogenicity. J Pharm Sci 102:915–928.
28. Demeule B, Gurny R, Arvinte T. 2007. Detection and characterization of protein aggregates by fluorescence microscopy. Int J Pharm 329:37–45.

Recent publications describe a range of theories that have been developed to describe processes taking place in solutions with increases in macromolecular content (Goncalves, et al., 2013, p. 1). For instance, a range of theories are based on a presumption that protein molecules behave as hard spherical repulsive particles, however instances of successful applications are limited. Thus, it was determined that in addition to molecular shapes and volumes, additional properties such as association kinetics and charge distribution must be taken into consideration in order to accurately predict behaviour of proteins in solutions and estimate viscosity. In addition to the above factors, introduction of additives as well as changes in the pH of the solution and its ionic strength was found to affect production of oligomeric species. This issue is of paramount importance because it was established that viscosity of protein-based formulations substantially affected the biopharmaceutical industry in general and manufacturing/administration of pharmaceutical products in particular. In a considerable number of cases production of protein-based drugs involves generation of highly concentrated protein formulations. The necessity of these procedures is determined by cost reduction requirements and the need to deliver high concentrations of the active component using low volumes of the generated pharmaceutical product. However, elevated concentrations of bio-macromolecules in many cases are associated with poor processing of the material, caused by elevated viscosity and lack of adequate flow abilities (Goncalves, et al., 2013, p. 2).

Loveday and co-workers extensively described the correlation between solution viscosity and protein concentration (Loveday, et al., 2007, p. R101). When the concentration of proteins is low it is possible to study protein viscosity in solutions using models that are focused on the hydrodynamic behaviour of the studied protein. In addition to hydrodynamic based theories a range of other concepts were implemented to describe the behaviour of proteins in solutions and predict changes in viscosity using protein concentration. However, regardless of the implemented model it is assumed that proteins in solutions are hard macromolecular spheres and an increase in concentration correlates with an increase in viscosity.

The number of studies covering a broad range of protein concentrations as well as possible correlations between high protein quantities and viscosity is however, limited. Publications in the area describe changes in viscosity of protein solutions through the perspective of intrinsic viscosity. Intrinsic viscosity presents a hydrodynamic parameter that is dependent on the size of the molecule and its conformation. This parameter also presents the effective molecular volume under the specific analysed conditions. The hydrodynamic parameter can be calculated by using the Ross-Minton's approach or with the aid of the Krieger-Dougherty model (Minton, 2012, p. 9310). Regardless of the employed

model it is assumed that all changes in the protein composition in the analysed solution are negligible. A considerable disadvantage of the employed models is the fact that protein species in solutions are assumed to be uniform with specific size and shape. In order to address this disadvantage binary mixtures were employed, containing proteins of various sizes. With the aid of the developed models it became possible to more accurately predict the behaviour of protein molecules in solutions. Further, recent publications suggest that it was highly effective to estimate the behaviour of protein species in solutions by using controlled quantities of binary protein mixtures in solutions and determination of the resulting viscosity (Goncalves, et al., 2013, p. 3).

Goncalves and co-workers explored the effects that changes in protein concentration had on viscosity in various formulations of recombinant albumin. The conducted study investigated changes in the human serum albumin concentrations from 0.1 to 500 mg/mL. The corresponding human albumin solutions were prepared in a salt-based buffer. Human serum albumin is the most abundant protein that can be found in the human blood. Its concentration is approximately 40 mg/mL and the function of the protein is to transport active pharmaceutical compounds and unesterified fatty acids. The research group showed that by taking into consideration specific biophysical characteristics of the analysed protein, such as shape and size, it was possible to estimate aggregation patterns of protein species and viscosity of the overall solution. It was also showed that viscosity of protein solutions could be predicted at both high and low protein concentrations. Thus, correlations between protein structure, its concentration in solution and viscosity could subsequently be employed in the development of new pharmaceutical products (Goncalves, et al., 2013, p. 3). The results of this study are discussed in section 3.4 below.

This is a repository copy of *The effect of protein concentration on the viscosity of a recombinant albumin solution formulation*.

White Rose Research Online URL for this paper:
http://eprints.whiterose.ac.uk/95292/

Version: Accepted Version

Article:

Gonçalves, A.D., Alexander, C., Roberts, C.J. et al. (3 more authors) (2016) The effect of protein concentration on the viscosity of a recombinant albumin solution formulation. RSC Advances, 6. pp. 15143-15154.

https://doi.org/10.1039/C5RA21068B

ARTICLE

The effect of protein concentration on the viscosity of a recombinant albumin solution formulation [†]

Andrea D. Goncalves,[a§] Cameron Alexander,[a] Clive J. Roberts,[a] Sebastian G. Spain,[a,‡] Shahid Uddin[b] and Stephanie Allen[a,*]

The effect of protein concentration on solution viscosity in a commercially available biopharmaceutical formulation of recombinant albumin (rAlbumin) was studied. The level of protein aggregation with concentration and its impact on solution viscosity was investigated. Theoretical models predicting viscosity with concentration were applied to these data, and a model that accounts for multiple protein species in solution provided the best fit. The results highlight the need to account for heterogeneity in the level of aggregation when addressing the increase of viscosity observed at high concentration of protein solutions, a significant issue for the manufacture and use of protein-based therapeutics.

Introduction

The viscosity of protein formulations is an important issue for the biopharmaceutical industry due to its practical implications in medicine manufacture and administration.[1] Biopharmaceutical liquid formulations are frequently created with high protein concentration, due to the need for high mass delivery to overcome low potency; low volumes are also desirable to allow patient self-administration in cost effective devices.[1,2] However, when biomacromolecules reach high solution concentrations, problems such as high viscosity and poor flow properties, as well as stability issues, can occur.

Theories from colloidal science have been used to model the observed increases in solution viscosities with increased macromolecular content.[3–5] A number of these are based on approximations to hard spherical repulsive particles, and have been applied with some success.[6,7] However, there are more molecular properties, such as shape[8], charge distribution[9,10] or kinetics of association[11–13], which need to be considered for more accurate predictions of protein solution viscosity. Moreover, such properties depend on factors including pH, temperature, ionic strength and the presence of additives in solution, and therefore these and their impact on the formation of higher order oligomeric biomolecular species

and/or aggregates need also to be considered.

The effect of protein concentration on solution viscosity has been discussed previously.[10,14–19] At dilute concentrations, protein solution viscosity has been studied using models that account for the hydrodynamic behaviour of proteins in a fluid.[15] Other theories that account for inter-protein interaction potential and excluded volume have been applied with relative success in predicting the increase of viscosity with protein concentration.[4,7] In general, all these models assume that (globular) proteins are hard spherical or quasispherical macromolecules and, to some extent, are able to explain the increase of viscosity with concentration and allow a comparison with the behaviour of colloidal dispersions. So far, however, there has not been a theoretical model that is capable of predicting the viscosity of protein solutions in a range from dilute to highly concentrated (>200 mg/mL).

Intrinsic viscosity ($[\eta]$) is a hydrodynamic parameter that is related to the conformation and size of a molecule in dilute solution and represents the effective molecular volume at these conditions[20]. It is defined in terms of concentration (c, in mg/mL) by the following equation:

$$[\eta] = \lim_{c \to 0} \left(\frac{\eta - \eta_o}{c\, \eta_o} \right) \qquad (1)$$

where η is the solution viscosity and η_o is the viscosity of the solvent. One of the hard (quasi)-spherical models relating protein viscosity and concentration, is the modified Mooney equation[21] as per Ross-Minton's approach[18], defined by:

$$\eta_{rel} = \frac{\eta}{\eta_o} = e^{\left[\frac{[\eta]c}{1 - \frac{\kappa}{\nu}[\eta]c} \right]} \qquad (2)$$

where relative viscosity (η/η_o) is an exponential function of concentration (c), $[\eta]$, a crowding effect factor (κ) and Simha's shape factor (ν).[15] As the crowding effect is a consequence of the excluded volume when the protein concentration

[a] School of Pharmacy, The University of Nottingham, University Park, Nottingham, NG7 2RD, UK.
[a] Formulation Sciences, MedImmune, LLC, Cambridge, CB21 6GH, UK.
[*]E-mail: stephanie.allen@nottingham.ac.uk
[§] Current address: Particle Sciences, Devices and Engineering, R&D, GSK, Medicines Research Centre, Stevenage, SG1 2NY, UK
[‡] Current address: Department of Chemistry, University of Sheffield, Dainton Building, Sheffield, S3 7HF. UK.

ARTICLE   Journal Name

increases, the model predicts solution viscosity accounting for the protein's shape and its excluded volume.

From colloidal rheology, the Krieger-Dougherty model (eq. 3),[3]

$$\eta_{rel} = \frac{\eta}{\eta_o} = \left(1 - \frac{\phi}{\phi_{max}}\right)^{-\phi_{max}[\eta]} \tag{3}$$

was originally applied to describe infinite dilutions of hard spherical particles. In the case of random close packing of spheres at low deformations[4,22], the intrinsic viscosity ([η]) in equation 3 is fixed to 2.5 and is dimensionless, since it is defined as a function of volume fraction (ϕ), with a maximum packing fraction (ϕ_{max}) of 0.64. Still assuming the spherical shape, this maximum packing fraction has been discussed to be around 0.71, when the particles are exposed to higher shear rates.[4]

The Russel-Saville-Schowalter revision of Batchelor's equation[4] (eq. 4), is a model which predicts the increase of viscosity of hard spherical particles, while taking into account interparticle interactions based on the effective distance between particles.

$$\eta_{rel} = \frac{\eta}{\eta_o} = 1 + 2.5\phi + s\phi^2 + O(\phi^3) \tag{4}$$

where the coefficient s of the quadratic term is defined by,

$$s = 2.5 + \frac{3}{40}\left(\frac{d_{eff}}{a}\right)^5 \tag{5}$$

and is dependent on the effective interparticle distance, d_{eff}, and the radius of particle, a. The factor d_{eff} is dependent on both the hydrodynamic contributions of the particle as well as the interaction potential, relevant to the dispersion conditions. Batchelor showed that for a concentrated dispersion of hard spherical repulsive particles, the value of s is equal to 6.2, where $d_{eff} = 2a$. [4]

The models described above assume that any change in composition of protein species in solution is negligible. Parameters in these models typically account for only one species of a specific shape and size. Some authors have addressed the problem for binary mixtures of different sized particles, to predict the impact of this on the solution viscosity.[5,23–25]. In recent reports, binary blends of proteins have been studied by controlling the content of each protein in solution and understanding the effect of this on the overall solution viscosity.[14,26]

Galush et al.[26] presented a study on the viscosity of mixed protein solutions, using mixtures of different monoclonal antibodies (mAbs) and of one mAb with BSA. Their conclusions derived from measuring the viscosity of both the individual protein solutions and blends. They proposed that the viscosity of protein blends could be predicted by an additive function of the viscosity of each individual protein multiplied by its respective known weight fraction (eq. 6).

$$\ln \eta(w_{tot}, f_2) = (1 - f_2)\ln \eta_1(w_{tot}) + f_2 \ln \eta_2(w_{tot}) \tag{6}$$

where η_1 and η_2 are the viscosities of pure protein 1 and 2, respectively, f_1 and f_2 are the weight fractions corresponding

to the protein 1 and 2 present in the blend and w_{tot} is the total weight/volume concentration of the protein mixture.

Minton[14] has contributed with the generalisation of equation 2 and equation 3 and application to predicting the viscosity of globular protein solutions containing only one protein, but with relatively well-known fractions of its monomeric and higher order associative species. The generalised models of Ross-Minton (eq. 7) and Krieger-Dougherty (eq. 8) models, as proposed by Minton, are as follows:

$$\frac{\eta}{\eta_o} = exp\left[\frac{[\eta]_w w_{tot}}{1 - \frac{w_{tot}}{w^*}}\right] \tag{7}$$

$$\frac{\eta}{\eta_o} = \left(1 - \frac{w_{tot}}{w^*}\right)^{-[\eta]_w w^*} \tag{8}$$

Note that the Krieger-Dougherty equation has been modified to allow the use of weight/volume concentrations (w_{tot}, in [mg/mL]), rather than volume fractions. Both equations 7 and 8 are now represented as functions of w_{tot}, $[\eta]_w$ and w^*. The parameter $[\eta]_w$ is weight-averaged intrinsic viscosity (in [mg/mL]), described in equation 9. The parameter w^* represents an estimated protein concentration above which the solution cannot flow, referred to as jamming concentration.[14,22]

$$[\eta]_w = \sum \frac{w_i [\eta]_i}{w_{tot}} \tag{9}$$

Here a recombinant human albumin (rAlbumin) solution formulated in a buffer containing salt and a surfactant was studied. The rAlbumin studied is expressed in Saccharomyces cerevisiae and has an identical amino acid sequence to human serum albumin (HSA).[27] HSA is the most abundant protein in the blood at a concentration of ~40 mg/mL. It is the major transport protein for unesterified fatty acids, having the capacity to bind numerous metabolites, active pharmaceutical ingredients as well as other organic molecules.[28]

Our study investigated the rheological characteristics of HSA samples with concentrations ranging from 0.1 mg/mL to approximately 500 mg/mL, using steady shear rheology with a torsional rheometer. A detailed biophysical characterisation of these samples was performed to account for the level of aggregation, size and shape of protein species, within higher concentrations of rAlbumin, to probe relationships between aggregation and solution viscosity. The ultimate goal was to predict the viscosity of highly concentrated globular protein solutions, using the abovementioned models to enhance the efficacy of formulated biopharmaceuticals.

Materials and Methods

Materials

Recombinant human albumin (rAlbumin) was donated by Novozymes Biopharma UK Ltd. (Nottingham, UK) in the form of Recombumin® Prime (batches: 1104 and 1101). The product is a liquid formulation of concentration 200 mg/mL, stored at 2-8 °C. All other reagents were obtained from Sigma-Aldrich,

UK and were of analytical grade. The formulation buffer of Recombumin® Prime is composed of NaCl (145 mM), polysorbate-80 (15 mg/L) and sodium octanoate (32 mM) in ultrapure water (pH = 7.0 ± 0.3 at room temperature). Another buffer was prepared containing only NaCl (145 mM) in ultrapure water (pH = 7.0 ± 0.3).

Centrifugal concentrators (Vivaspin 20 – 5 kDa molecular weight cut-off with polyethersulfone membrane; Sartorius Stedim, Ltd., UK) were used to concentrate rAlbumin samples to higher concentrations than the starting material (200 mg/mL). The procedure recommended by the manufacturer was followed, using a fixed 45º rotor centrifuge (Hermle Z400, Labortechnik GmbH, Germany). After centrifugation, samples were collected, mixed and checked for their concentration using UV-Visible spectroscopy. All samples and the respective buffers were stored at 2-8 ºC.

Methods

Quantification of protein concentration by UV-Visible spectroscopy

An Agilent 8453 UV-Vis spectrophotometer (model G1103, Agilent Technologies, Germany) was used to quantify protein concentration via absorbance at 280 nm. A quartz cuvette with 1 cm path length (Hellma, Germany) was used for all measurements.

For all protein solutions at concentrations higher than 50 mg/mL, a double dilution scheme was followed to allow a measurement of sample diluted to 0.5 mg/mL. Each second dilution was produced in triplicate so that the absorbance measurement (and posterior concentration calculation) was reported as an average of 3 measurements.

For the determination of concentration of rAlbumin solutions, the percent extinction coefficient at 280 nm ($A_{1 \%}^{1 cm}$) used was 5.8.[29]

Rheology

The rheometers used were Anton-Paar (Graz, Austria) MCR models 301 and 501. Cone-and-plate geometries used throughout this study were stainless steel CP50-1 (diameter = 50 mm; cone angle = 1° and CP40-0.3 (diameter = 40 mm; cone angle = 0.3°). To prevent evaporation of sample and to maintain a constant temperature of 20 °C ± 0.1 °C throughout the measurements, an evaporation blocking system equipped with a peltier unit was used. Prior to measurements, all samples were allowed to equilibrate to room temperature (~ 23 °C) for at least 40 minutes.

Rotational tests (flow curves and viscosity curves) were performed by controlling the shear rate typically from 0.01 to 1000 s⁻¹, and measuring torque, shear viscosity and shear stress. To increase data validity and sensitivity of the method, each shear rate step had a 60 second duration time during which the instrument was averaging over the collected data. Two shear-rate sweeps (ramping down and up) were performed per sample, without waiting time between sweeps. The tests were always started after a 10 minute waiting time after loading the sample.

Micro-viscometer/rheometer on-a-chip (mVROC)

The mVROC, by Rheosense, Inc. (San Ramon, California, USA) was used for measurement of air-water interface-free bulk viscosity at high shear rates. The mVROC is a microfluidics slit rheometer where the microfluidics chip is composed of a microchannel (rectangular slit) made of borosilicate glass mounted on a gold-coated silicon base. Viscosity is measured as a function of pressure drop as the fluid flows in the microchannel (width = 3.02 mm; depth depends on the chip used). In a typical experiment, the flow rate, Q, is varied using a syringe pump and Hamilton gastight glass syringes (Reno, Nevada, USA). The mVROC device outputs the pressure drop as a function of flow rate, which is used to calculate the nominal or apparent viscosity via $\eta(\dot{\gamma}) = \tau_w / \dot{\gamma}_w$.[30] The true shear rate and true shear viscosities are then calculated, respectively, using the Weissenberg-Rabinowitsch-Mooney equation.[30,31]

Samples analysed were rAlbumin solutions at 200 and 500 mg/mL. For these measurements, the A05 and D05 chips were used and the temperature was kept constant at 20 °C ± 0.1 °C using a water circulation system (ThermoCube, SS cooling systems, USA).

High performance size exclusion chromatography (HPSEC)
Determination of level of protein aggregation

rAlbumin samples were analysed for their level of aggregation on HPSEC. The high performance liquid chromatography (HPLC) system used was from Agilent Technologies 1200 series (Germany) with the following components: degasser, binary pump with a 100 µL injection loop, an autosampler, thermostatted sample tray (at 5 °C), a thermostatted (at room temperature) column holder and a UV detector. The software used for this system was Chemstation for liquid chromatography systems, by Agilent Technologies. A Tosoh Biosciences, LLC (USA), model TSK gel G3000SWxl column was used (7.8 mm (ID) x 30 cm (L)), composed of silica gel particles with mean particle size of 5 µm and pore size of 250 Å. A guard column (silica particles of 7 µm, 6 mm (ID) x 4 cm (L)) was also used with the analytical column.

The mobile phase was an aqueous buffer of 0.1 M sodium sulfate (Na_2SO_4) and 0.1 M dibasic sodium phosphate anhydrous (Na_2HPO_4), titrated to pH 6.8 with 6N HCl. This buffer was filtered with 0.22 µm pore size vacuum-driven filter units (PES membrane, EMD Millipore, USA).

All protein samples were diluted to 10 mg/mL, and injection volume was 25 µL. Run time was 20 minutes at a flow rate of 1 mL/min. Each sample was injected three times. Formulation buffers respective to the protein samples were also injected as blanks.

Bio-Rad gel filtration protein standards (Bio-rad Laboratories, Inc., USA) were used for this method's system suitability test. These were prepared according to the manufacturer's instructions and 25 µL were injected once at the beginning and end of 20 sample injections.

All samples, buffers and Bio-Rad protein standards were filtered through 0.45 µm centrifugal filters (Ultrafree-MC PVDF, EMD Millipore, USA). The obtained chromatograms

followed integration and peak symmetry and resolution were calculated via the method analysis used on the software.

Analysis with multiple detectors for determination of molecular weight and intrinsic viscosity of rAlbumin solutions

To calculate bulk molecular weight and intrinsic viscosity, the chromatography system used was a Polymer Labs GPC 50 Plus (Agilent Technologies, USA) gel permeation unit that comprised an autosampler, a fixed volume injection loop (20 µL), thermostatted column holder, and the following detectors: a 90º light scattering detector, a refractive index detector, and a differential pressure viscometer. Calibration of the system was made with polyethylene oxide (Polymer Labs, UK) solutions in phosphate buffer saline (Lonza, Inc.).

The method details chosen for these experiments were similar to the previous section with exception that samples were diluted to 15 mg/mL, thus injecting 300 µg of total protein. System suitability was still performed with Bio-Rad protein standards and the same buffer was used as mobile phase. Each rAlbumin sample was injected three times, with buffers injected at least once. dn/dc used for protein analysis was 0.185 mL/g.[32]

Dynamic light scattering (DLS)

Sizing measurements were performed using the Zetasizer NanoZS dynamic light scattering instrument (Malvern Instruments, UK). Samples were illuminated by a 633 nm laser and light scattering was detected at 173º by an avalanche photodiode. DLS results were obtained and analysed using the Zetasizer software version 7.01. Protein samples were measured at 1 mg/mL diluted in sample buffer, to reduce non-linearity effects on measurements by increased viscosity of solvent with higher concentrations.

Measurement settings for rAlbumin size readings were at a constant temperature of 20 °C, performing 15 runs of 10 seconds each. An equilibration time of at least 5 minutes was set before the measurement started. Size measurements were made in triplicate with fresh aliquots for each reading.

Results

The rheology of formulated recombinant human albumin solutions

The data in Fig. 1A and 1B show that rAlbumin solutions displayed constant shear viscosities for the increasing shear rates applied (0.01 to 1000 s^{-1}). Fig. 1C shows a linear increase of shear stress with the increasing applied shear rates. For the higher concentration materials (400 - 500 mg/mL) the shear viscosities were from ~1 s^{-1} onwards, while showing slight non-linear increase of viscosities when <1 s^{-1}. However, in general, throughout the range of concentrations of rAlbumin presented and the applied shear rates, it was considered that these solutions exhibited a Newtonian-like behaviour. Each sample was measured using two consecutive shear rate sweeps, ramping down and up (Fig. 1A and 1B). Hysteresis effects were not observed, in agreement with the literature, which suggests

that the protein molecules diffuse rapidly in the fluid once shear is stopped.[7,33,34]

For comparison between the concentration of samples and the obtained shear viscosities, the viscosity values at 1000 s^{-1} were taken from three separate readings per sample and are reported in Fig. 2 as an average with the respective standard deviation. The viscosity values reported here are those at high shear viscosity (η_∞), since the viscosities of these samples were overall shear-rate independent.[7] In Fig. 2 the average viscosity values are reported against the average actual concentrations measured for each sample. It was noted that as the targeted protein concentrations were increasingly higher, it was more difficult to achieve such targets (e.g. ≥ 300 mg/mL; see Table SI-1 from ESI). For clarity within this manuscript therefore, sample concentrations are referred to as the corresponding target concentration.

From Fig. 2A, the viscosity values were similar for lower protein concentrations. An increase of viscosity with increasing concentration was seen, in agreement to what has been reported throughout the literature with regards to serum albumin solutions.[7,10,15] Most importantly, the exponential trend observed from the data in Fig. 2A is also reported for other globular proteins, such as immunoglobulins.[11–13,35]

Characterisation of protein species present in recombinant human albumin solutions

Our aim was to correlate the observed increase in viscosities with the level of aggregation present in the increasing concentrations of rAlbumin samples. Therefore, the identification, relative quantification and size characterisation of the monomeric and oligomeric species present in solution was performed using HPSEC, DLS and microfluidic SDS-PAGE (shown in the ESI).

High-performance size exclusion chromatography (HPSEC)

HPSEC retention times for the protein species typically present were ~7.9, 8.7 and 9.8 minutes, corresponding to trimer, dimer and monomers, respectively (see Fig. SI-1 from ESI). This method of analysis produced good resolution between the different identified species and these were comparable to literature values using a similar setup.[36] No higher molecular weight species other than dimers and trimers were found in any of the solutions analysed. This reflected the high purity of the recombinant albumin material due to its manufacturing process generating only a small percentage of trimers and dimers[27], with the monomer showing the highest relative percentage with a peak area of > 90 %. Samples from 50 to 200 mg/mL had similar peak areas for all protein species. Only when concentrations reached approximately 250 mg/mL and over, a trend could be detected on the increase of dimers and trimers with a corresponding decrease of monomer (Fig. 2B).

Size exclusion chromatography required sample dilution for analysis when concentrations were > 10 mg/mL. Dilution is a limitation of this method since it can influence the material's content in relative percentage of each species, as it can be a factor for some aggregates to disassociate, and therefore be considered reversible.[37,38] It was important to understand if

this was the case with rAlbumin solutions. By comparing injections of proteins at 50 mg/mL and 10 mg/mL concentrations, their respective peak areas were different by factors of < 1 % (see Fig. SI-2 from ESI). Such low differences indicated that dissociation upon dilution of trimers and dimers into monomers was negligible. Moreover, this is in agreement with the irreversibility observed of associated dimer and trimer species reported in prior literature.[39]

Triple-detection HPSEC was used to experimentally determine the intrinsic viscosity and molecular weight (MW) for each of the protein species present in rAlbumin samples: monomer, dimer and trimer. This determination allowed for subsequent analysis discussed ahead in this study.

The results were relative to the two peaks detected corresponding to monomer and dimer, since the differential pressure viscometer could not detect the low percentage of trimers present in solution (see Fig. SI-2 from ESI). Analysis of peak areas per sample showed a trend of increasing rAlbumin dimers, similar to what was observed previously for conventional HPSEC (Table 1).

Dynamic light scattering

The hydrodynamic size analysis of rAlbumin solutions by dynamic light scattering (DLS) was performed for the entire range of solutions after dilution to 1 mg/mL. All solutions were analysed without prior filtration to assess if aggregates were present within the detection limit of DLS (up to 1 μm of hydrodynamic diameter). In all cases, the samples did not show presence of aggregates. For all the analysed samples, the measured average hydrodynamic radii from the size distributions by intensity ranged between 3.8 - 4.5 nm corresponding to values reported in literature[40] for a recombinant human albumin solution (Fig. 3). The hydrodynamic size distribution by volume resulted in one peak, with its mean peak value skewed towards lower sizes, closer to the monomer size.

Surface tension effects on rheology measurements – control experiments

To ensure that the rheological measurements were taken as accurately as possible and were free of artefacts related to the method and the technical specifications of the rheometer, additional experiments were carried out.

The influence of surface tension at the air-water interface of protein solutions in surfactant-free buffers has been shown to present apparent high-viscosities at low shear rates. The use of a conventional rheometer with cone-and-plate geometry has been suggested as not being the most appropriate instrumentation for these types of samples as it is not an air-water interface-free technique.[7] Therefore, a rAlbumin solution at 200 mg/mL (from the original formulation) was analysed with the micro viscometer/rheometer-on-a-chip (mVROC) method, which provides rheometry measurements free of air-water interface. When superimposing the cone-and-plate (CP) rheometer data with mVROC data, the sample at 200 mg/mL showed no difference in its viscosity values. As an example, at shear rate ≈ 1000 s^{-1}, the average viscosities

measured with each instrument were $\eta_{(CP)} \approx 3.5$ mPa.s and $\eta_{(mVROC)} \approx 3.4$ mPa.s (Fig. 4). This clearly showed that the rheometer data were most likely free of air-water interfacial artefacts.

In further experiments, samples were prepared by diluting in an aqueous surfactant-free solution of NaCl 145 mM. rAlbumin solutions at 5, 10, 50 and 100 mg/mL were measured on the rheometer and their level of aggregation was assessed by HPSEC and DLS. HPSEC and DLS data were similar to those of formulated rAlbumin. However, while samples at 5, 10 and 50 mg/mL in NaCl 145 mM showed an increase of viscosities towards low shear rates; only the sample at 100 mg/mL of rAlbumin in NaCl 145 mM presented constant viscosities throughout a similar shear rate range (Fig. 5). Samples at 5 and 10 mg/mL showed a slightly increased high shear viscosity ($\eta\infty$ at $\dot{\gamma} = 1000$ s-1), when compared to the data collected from formulated samples.

Additionally, a test was done to assess if the method of concentrating the protein solution would also concentrate the surfactant (see SI-7). The original sample at 200 mg/mL and the concentrated sample to match 200 mg/mL both presented matching viscosity profiles and values. Therefore, to address the analysis made in this work, the simplest case was considered, where the surfactant would have diffused through the concentrator's membrane during centrifugation for all concentrated samples (> 200 mg/mL).

Effect of high protein concentration on solution viscosity

The intrinsic viscosity of human serum albumin has been reported to be of $4.73\times10^{-3} \pm 1.2\times10^{-4}$ mL/mg, for similar solution conditions to these presented here (temperature at 20 ºC, pH 7.0).[8] Values of intrinsic viscosity for bovine serum albumin, have been reported to be 3.7×10^{-3} mL/mg[15] or similar values.[20,41] Although the albumin here used is fatty-acid bound, it is expected that the presence of fatty acid in serum albumin does not influence the value of intrinsic viscosity.[42] Intrinsic viscosity values in literature for HSA[8] and for bovine serum albumin (BSA)[15] were used to fit the rheometry data (Fig. 6) using Ross-Minton's hard (quasi)-spherical equations relating protein viscosity and concentration (eq. 2).

Our rheology data was fitted to equation 2, with the intrinsic viscosity ([η]) constrained and the κ/v factor freely floating (Fig. 6 – blue and orange line). The computed values for κ/v respective to the fixed intrinsic viscosities chosen from literature were: κ/v = 0.31, using [η]$_{Monkos}$; and κ/v = 0.42, using [η]$_{Tanford}$. These values were comparable to values reported for other globular proteins, such as IgG (κ/v = 0.37 to 0.49) and hemoglobin (κ/v = 0.40).[12,18,35]

The Ross Minton model was fitted to the data allowing free parameters. The best fit computed was using experimental data up to ~350 mg/mL (Fig. 6 – green line). Both the [η] (4.21×10^{-3} mL/mg) and κ/v (0.45) values were in agreement to the values reported in literature.[8,15,20] This fitted intrinsic viscosity value was similar to the intrinsic viscosity value calculated with triple detection HPSEC for the monomer peak of rAlbumin (Table 1). However, the Ross-Minton model did

not predict solution viscosity for the highest concentrations (≥ 350 mg/mL).

The rheology data was fitted to the other hard-sphere model, the Krieger-Dougherty equation (eq. 3). First, the intrinsic viscosity ([η]) was fixed to 2.5, defined for spheres, and setting the maximum packing fraction (ϕ_{max}) to 0.64. Then, the data was fitted defining the maximum packing fraction to 0.71, while still assuming the protein species were spherical ([η] = 2.5). In both cases, fixing intrinsic viscosity to 2.5 and ϕ_{max} could only predict the data up to 100 mg/mL, which is in agreement with the literature[7] (Fig. 7A – orange and magenta lines).

Conversion of weight/volume concentration to volume fraction was calculated via the polymer chemistry equation for volume fraction ($\phi = N_A Vc/MW_h$), taking into account the hydrated molecular weight of the protein - MW_h (eq. 10). The hydrated protein molecular weight was calculated from $MW_h = MW_p(1 + \delta)$, where MW_p is the molecular weight of the protein and δ is the amount of water associated with the macromolecule in g/g.[8,15]

$$\phi = \frac{c}{MW_h}\left(N_A V + \frac{MW_p \delta}{\rho}\right) \quad (10)$$

where c is the concentration in mg/mL, N_A is Avogadro's number, V is the protein's hydrodynamic volume (113.4 nm³), and ρ is the density of water at 20 °C (998.2×10³ mg/mL) and δ = 0.379.[8]

The data was fitted to this model with free parameters, allowing a prediction of viscosity applied to non-spherical particles (Fig. 7A – blue line). The parameters which were best fits using data up to 350 mg/mL, were [η] = 6.94 ± 0.14 and ϕ_{max} = 0.298 ± 0.002 (with r^2 = 0.9996 and χ^2 = 0.26). In this case, the fitted intrinsic viscosity showed a higher value than that corresponding to spheres, indicating that particle aspect ratio had increased and the ϕ_{max} decreased respectively. These values suggest good physical significance, since their product is still within their usual range 1.4 < [η]/ϕ_{max} < 4.[43] The fitted intrinsic viscosity value of ~6.9 agreed with the reported aspect ratio of albumin, known to be a prolate ellipsoid.[8,15,40] Altogether, these observations along with those previously made from the Ross-Minton model, point to a difficulty in prediction of solution viscosity of concentrations > 350 mg/mL (see Fig. 6 (green line) and 7A (blue line)).

The Russel-Saville-Schowalter equation[4] (eq. 4), was used to fit our data since it takes into account the interparticle interaction. To fit the data to this model, s, the term which is defined by the effective distance between particles, was initially chosen to be equal to 6.2, as per Batchelor's proposal applied to repulsive hard spheres.[4] However, Sharma et al.[7] showed that the data of concentrated BSA solutions up to 250 mg/mL could fit with this model (with data up to ~250 mg/mL) using a value s = 10. The authors suggested that this value would correspond to an interaction potential corresponding to a d_{eff} = 2.5a, reflecting BSA's repulsive net negative charge in a saline buffer at pH ~7 10. The comparability between rAlbumin (or HSA) and BSA can be made since these two albumin variants share >75% of their primary structure and many

physical properties (e.g. surface hydrophobicity), having however, slight differences with regards to its thermal stability, electrophoretic behaviour and binding properties.[44,45]

This model could not predict the viscosity of our experimental data at concentrations higher than ~150 mg/mL (ϕ = 0.11), even when fixing s = 10 (Fig. 7B). Since this model fixes the intrinsic viscosity at 2.5 for hard spheres, while it has been previously discussed that rAlbumin (and BSA) are not spherical but prolate ellipsoids, it may well not be the most appropriate albeit the only equation that includes surface charge as determinant to the viscosity of globular protein solutions.

The rheology data was further analysed using the generalised equations of Minton and Krieger-Dougherty for protein viscosity (eq. 7 and 8, respectively), which account for the presence of multiple species of protein in solution. By fitting these two generalised models to the experimental rheology data, it was found that the best fits would be achieved if the concentration range would not include either the last three (for eq. 8) or two data points (for eq. 7) (Fig. 8). The fitted weight-averaged intrinsic viscosity and w^* values suggest conformity between both generalised models. By using these generalised models it is still not possible to predict the higher concentrations above ~350 mg/mL. When fitting the experimental data using all the data points available, the fitted parameters usually presented poor statistical correlations (r2 < 0.9, χ^2 >> 1) as well as higher values for [η]w with no physical significance.

In the study by Galush et al.[26], the protein mixtures were always prepared to a known total weight/volume concentration and known weight fractions of each of the proteins in the mixture. In our case, the presented HPSEC results (Fig. 2B) showed that the monomer, dimer and trimer composition was changing with sample concentration. Therefore, a weight-averaged intrinsic viscosity was calculated per sample (eq. 9), instead of being assumed to remain constant (Table 2), using the data obtained by triple detection HPSEC (Table 1). The weight-averaged intrinsic viscosity values were slightly affected.

Using the calculated weight-averaged intrinsic viscosity, and assuming the different w^* values based on the fitted parameters obtained above, the viscosities were computed for the studied concentrations (Fig. 9A and 9B) for both generalised models. When choosing w^* of higher values (derived from fits using all data points), the viscosities were typically underestimated. On the other hand, using w^* values that were derived from the best fits, 569 mg/mL for the generalised Ross-Minton model (eq. 7), or 399 mg/mL for the generalised Krieger-Dougherty model (eq. 8), the viscosities were correctly predicted for the higher concentrations up to, and including, 450 mg/mL and 350 mg/mL, respectively.

Discussion

The biophysical characterisation reported here aimed at providing a clear characterisation of the rheological behaviour,

and the protein species content, of dilute to highly concentrated solutions of rAlbumin. From the steady shear rheology of these solutions, it was concluded that they showed a Newtonian-like behaviour. This is in clear contrast to previous studies of the rheology of globular proteins[7,33,34,46] where an apparent yield-behaviour has been reported, particularly at lower shear rates (< 10 s⁻¹). The reason for this purely viscous Newtonian-like behaviour is likely due to the presence of polysorbate-80, a well-known surfactant used in biopharmaceutical formulations. This is proposed to negate the effect on rheological properties of surface tension that can occur due to formation of a protein film at the air-water interface.[7] Similar rheological behaviour has been reported for globular protein solutions in a buffer also containing a polysorbate surfactant.[47,48]

Fig. 2A clearly shows the viscosity increase with protein concentration. From the data in the figure, it is clear that a larger increase in viscosity occurred between concentrations ~250 and ~500 mg/mL. The ~500 mg/mL sample reached a high shear rate viscosity of ~10 000 times larger than that of water (1.0016 mPa.s at 20 ºC, as defined by NIST). Although biopharmaceutical formulations are not typically formulated at more than 200 mg/mL, the literature has discussed similar increases of viscosity.[14,26,35] Therefore, analysing the viscosity increase with concentration of rAlbumin solutions as a biopharmaceutical formulation model will help understand what factors govern this exponential rise in viscosity.

To correlate this increase in viscosity with the increase in protein concentration and its level of aggregation, further characterisation with HPSEC was needed. From Fig. 2B it is clear that there is an increase in dimer and trimer content for samples > 250 mg/mL.

Triple-detection HPSEC allowed determination of the intrinsic viscosity and MW of each protein species detected in the conditions used here. Experimentally calculated molecular weight values for monomers and dimers agreed well with the values reported in literature for human serum and bovine serum albumin.[36] The values for intrinsic viscosity detected were however, quantitatively different to those in the literature, possibly due to differences in experimental conditions (e.g. temperature, mobile phase buffer and flow rate), which can affect the working conditions of the differential viscometer. However, our results for intrinsic viscosities were still statistically different (p<0.05, one-way ANOVA) between monomer and dimer at every concentration studied. No variation with concentration was observed for the intrinsic viscosity values within specific molecular weight ranges.

The results obtained by DLS were similar to those described in literature[40] – only one peak was detected, with radii between 3.8 – 4.5 nm corresponding to the hydrodynamic radius of monomeric recombinant human albumin (Fig. 3). The hydrodynamic size distribution by volume showed a slight skew towards monomer size. This reflects the higher relative contribution of monomer in comparison to low relative quantity of dimers and trimers in solution. Data from microfluidic SDS-PAGE (Fig. SI-3) confirmed the presence of

monomers and dimers in the diluted solutions of samples from 200 – 500 mg/mL, and that no other higher molecular weight aggregates were present. This information was in agreement with our data from HPSEC characterisation.

Finally, the rheology results reported in Fig. 4 and Fig. 5 (recorded with mVROC) show that the rheology data of rAlbumin solutions recorded with a cone and plate rheometer, were free from surface-tension effects. When, samples were diluted with surfactant-free buffer it was clear that there were differences in the measured viscosities at high shear, compared to formulated protein solution. These differences are proposed be related to the lower concentration of polysorbate-80 present in the 5 and 10 mg/mL samples, and to some extent those at 50 mg/mL. Polysorbate-80 is present in the formulation to prevent the macromolecule reaching the air/water and solid/water interface.[27] In these samples, as the surfactant was diluted during sample preparation to below its effective concentration, it likely ceased to be sufficient in preventing the protein from reaching the air-water interface present when using the cone-plate geometry. As mentioned before, such surface tension effects have been proposed to influence torque measurements at low shear rates, leading to an apparent yield-behaviour observed as a pronounced increase in the slope of the viscosity function[7], where the sample is no longer Newtonian. Other authors also observed similar differences when adding surfactants to globular protein solutions.[47,48] By studying the rheology of protein samples prepared in surfactant-containing buffer, it is proposed that the values of viscosity and shear stress measured and are similar to a measurement performed with an air-water interface-free instrumentation, such as the mVROC.

The results discussed so far showed that the rAlbumin solutions studied were constituted mainly of monomeric species with a small percentage of dimers and trimers, which increases, at the expense of monomers present in solution, when the solution is concentrated > 250 mg/mL. Since this was also the concentration at which an increase in solution viscosity was noticed, it was important to analyse our rheology data with models that should predict the increase of viscosity with concentration.

In summary, our analysis suggested that concentrations above ~350 mg/mL have a solution viscosity that depends on factors other than those taken into account by the models explored here. These models have been developed based on their application to low concentrations of particle suspensions, where each particle would be far apart from another enough to not influence its flow.[15] Therefore, it is not surprising that these equations always apply well to lower concentrations of albumin.

Although the models presented here are based on hard quasi-spherical repulsive particles and their excluded volume, the predicted data typically suggest that a maximum packing fraction of rAlbumin (based on the best fits) will always be lower than the highest concentrations achieved experimentally (~450 - 500 mg/mL). In addition, viscosity prediction, according to pure hard-sphere particle models,

clearly underestimates the viscosity values for concentrations higher than ~100 - 150 mg/mL.

One possible suggestion to explain such deviation from predictions at high concentration is that the maximum packing concentration could be dependent on solution composition e.g. the relative quantity of monomers and oligomeric species such as dimers and trimers. It is known that suspensions composed of binary sized spherical particles yield a maximum packing fraction approximately larger than the random close packing for a homogenous suspension.[5,23–25] However, albumin is a prolate ellipsoid that has been shown to influence the maximum packing fraction. It has been predicted that for globular protein solutions up to approximately 250 mg/mL with the protein having a 5:1 aspect ratio, the increase of jamming limit would not be significant.[14] The models employed so far assume that associative species remain with the same globular shape, which is clearly not the case.

Apart from shape, it is unlikely that rAlbumin could resemble a hard particle, as its homologue HSA has been reported to exhibit a drop in intrinsic viscosity with temperature increase[8], and its mammalian variant BSA has been shown to have an intrinsic viscosity which is pH-dependent.[49] These studies, along with others from protein hydrodynamic analysis [44,50], point towards the influence of protein conformation in viscosity studies, via a change in intrinsic viscosity depending on the solution conditions. Therefore, as the protein is further concentrated, changes in protein conformation could be a factor to account for the slow increase of viscosity compared to hard sphere model predictions. In addition, this slow increase could also be due to the repulsive nature of inter-protein interactions, which is a phenomenon that has been observed for sterically stabilised colloids.[22]

The deviation from models seen at higher concentrations (≥ 350 mg/mL) could be related to a glass transition similar to that which occurs with colloidal hard spheres. In this case, accounting for repulsive excluded volume, suspensions are expected to approach a glass transition at volume fractions ϕ ≈ 0.58 before approaching the random close packing fraction (ϕ = 0.64).[22] When the concentration approaches a glassy state, the particle is caged by the presence of neighbouring particles, thus slowing down its flow and leading to increased viscosities. In the case of rAlbumin, an analogous glass transition behaviour could be taking place at the concentrations between ~400 to ~500 mg/mL based on similar results seen with highly concentrated solutions of BSA.[51] This would suggest that these concentrations are approaching the jamming limit but does not explain why viscosities cannot be predicted in conventional models. Finally, it is precisely the sample range between 350 mg/mL and 500 mg/mL that showed an increase in the relative quantity of dimers (with a respective decrease of monomers). Therefore, it does suggest that the change of composition and the increase of viscosity with increase of concentration are connected and needs to be addressed in these models.

Conclusions

In this work a range of rAlbumin solutions, in a formulation buffer containing NaCl and a surfactant, were analysed for their rheological behaviour with the aim of understanding the effects of high concentration on solution viscosity. Rheological measurements showed that the solutions behaved as purely viscous fluids in the range of the applied shear rates. It was observed that as the protein concentration increased in solution, the samples presented an increase of viscosity. All samples showed the same oligomeric species were present in solution; monomers, dimers and trimers of rAlbumin. As concentration increased to ~500 mg/mL, the relative quantity of dimers and trimers increased along with a corresponding decrease of monomer. By DLS and microfluidic SDS-PAGE analysis, the solutions showed no other signs of impurities such as other higher order aggregates or protein fragments. Throughout this study several experiments proved that concentrating the rAlbumin ≥ 200 mg/mL did not seem to have any other effect besides the increase of solution viscosity and the change in relative composition of protein species.

A comprehensive theoretical analysis of the rheological experimental data was performed using different models that are commonly applied to predict protein solution viscosity. The Ross-Minton and Krieger-Dougherty equations were demonstrated to predict our experimental data up to 350 mg/mL. When considering the protein inter-distance and thus the effect of interaction potential upon viscosity, the solution viscosity couldn't be predicted for concentrations ≥ 150 mg/mL.

Generalised versions of the Ross-Minton and Krieger-Dougherty equations were also studied and the results showed that the former could successfully fit when using experimental data up to ~400 mg/mL of rAlbumin. Although these models assume that the protein species are hard particles throughout all conditions observed, the equations account for multiple/oligomer species, which determines a weighted approach to intrinsic viscosity suggesting a variation in these species as protein concentration increases. The fact that our analysis produced better fits using these generalised equations further highlights the importance of considering the variation in composition within a protein solution, thus justifying the complete characterisation of oligomeric species present. It is important to note that no other analysis typically accounts for this variation using a sample composed of one protein only. We however suggest that other factors related to highly concentrated solutions may still also need to be considered, particularly since those concentrations not fitted were the most concentrated (> 400 mg/mL), where crowding effects should be more accentuated.

In conclusion, the example of rAlbumin explored here highlights that knowledge of how the protein oligomeric species composition varies between samples of increasing concentration, is a key factor for predicting the viscosity of protein solutions. Application of this knowledge to liquid formulations of therapeutic macromolecules (such as mAbs) would be important to further understand further its solution

Pathak, *Biophys. J.*, 2013, **105**, 2418–26.

50   N. El Kadi, N. Taulier, J. Y. Le Huérou, M. Gindre, W. Urbach, I. Nwigwe, P. C. Kahn and M. Waks, *Biophys. J.*, 2006, **91**, 3397–404.

51   G. J. Brownsey, T. R. Noel, R. Parker and S. G. Ring, *Biophys. J.*, 2003, **85**, 3943–50.

Journal Name

ARTICLE

Figures/ Tables
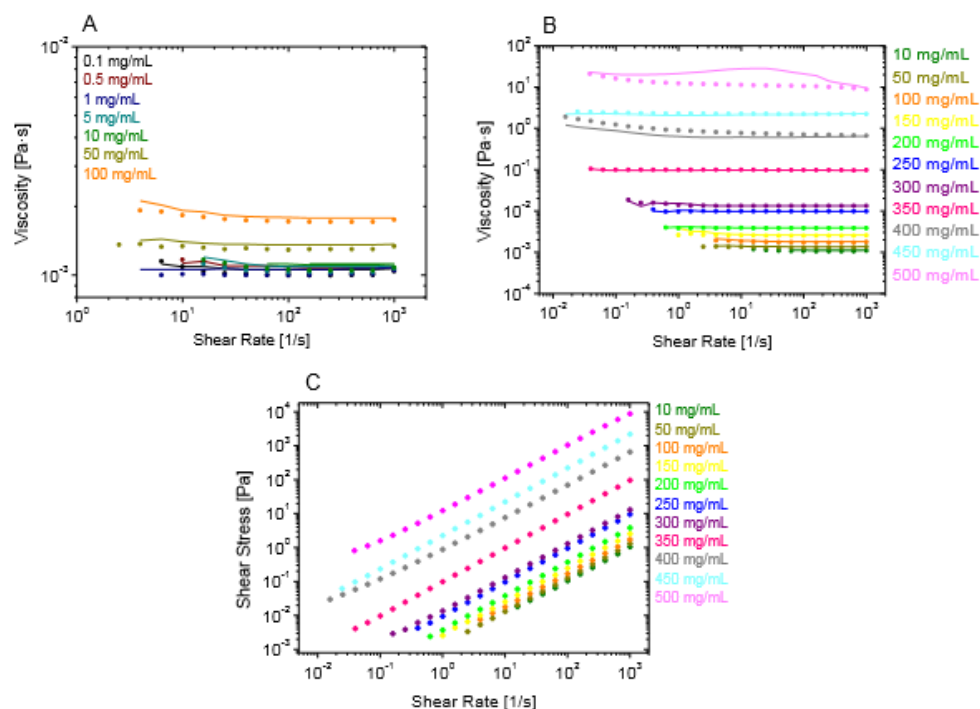
Fig. 1 Experimental steady shear rheology of rAlbumin solutions obtained with cone-plate 50 mm, 1°, or cone-plate 40 mm, 0.3°, at 20 °C. 1A and 1B - Viscosity values are shown for ramping down (closed circles) and ramping up (lines) shear rates. A - Samples from 0.1 to 100 mg/mL. B - Samples from 10 to 500 mg/mL. C - Flow curves for experimental steady shear rheology of rAlbumin solutions from 10 to 500 mg/mL. Shear stress values are shown only for ramping down shear rates.
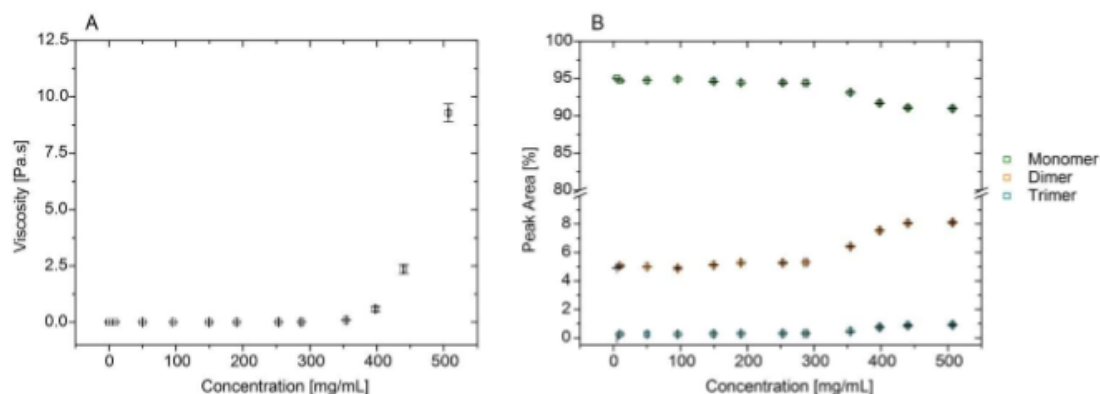
Fig. 2 A Viscosity of rAlbumin solutions ranging from 0.1 mg/mL to 500 mg/mL (target concentrations). Viscosities are taken at high shear (η = 1000 s-1) at 20 °C. Viscosity values are represented as an average and standard deviation (error bars) of 3 separate measurements for each sample. Concentrations are represented as average of 3 measurements and error bars are standard deviation. B HPSEC conventional method for determining level of aggregation of rAlbumin solutions showing relative peak areas in %. Data in squares represent an average of 3 readings per sample. Error bars are standard deviation per sample for peak area % (y-axis) and for concentration (x-axis). All samples were diluted to 10 mg/mL prior to analysis when necessary.

Table 1 HPSEC triple detection values of peak area, bulk molecular weight (MW) and bulk intrinsic viscosity (IV) for monomers and dimers detected in rAlbumin solutions. Average and standard deviations are reported for 3 separate measurements per sample.

Sample (mg/mL)	Monomer			Dimer		
	Peak Area (%)	MW (kDa)	$[\eta]$ (mL/mg)	Peak Area (%)	MW (kDa)	$[\eta]$ (mL/mg)
50	96.11 ± 0.03	64988 ± 297	0.00408 ± 0.00004	3.89 ± 0.02	121239 ±1171	0.00482 ± 0.00014
100	95.97 ± 0.10	65449 ± 933	0.00402 ± 0.00017	4.03 ± 0.10	143044 ± 12519	0.00446 ± 0.00089
200	95.71 ± 0.01	64656 ± 580	0.00408 ± 0.00006	4.29 ± 0.01	130356 ± 1563	0.00477 ± 0.00044
250	95.68 ± 0.01	64791 ± 749	0.00409 ± 0.00006	4.32 ± 0.01	132466 ± 5446	0.00505 ± 0.00072
350	94.69 ± 0.24	66090 ± 1780	0.00412 ± 0.00005	5.31 ± 0.24	138341 ± 8136	0.00441 ± 0.00101
400	94.46 ± 0.02	65290 ± 185	0.00410 ± 0.00003	5.54 ± 0.02	132674 ± 3686	0.00489 ± 0.00050
450	94.33 ± 0.01	65358 ± 184	0.00408 ± 0.00004	5.67 ± 0.01	131680 ± 3886	0.00462 ± 0.00047
500	93.90 ± 0.01	65066 ± 242	0.00412 ± 0.00006	6.10 ± 0.01	132140 ± 4754	0.00467 ± 0.00056
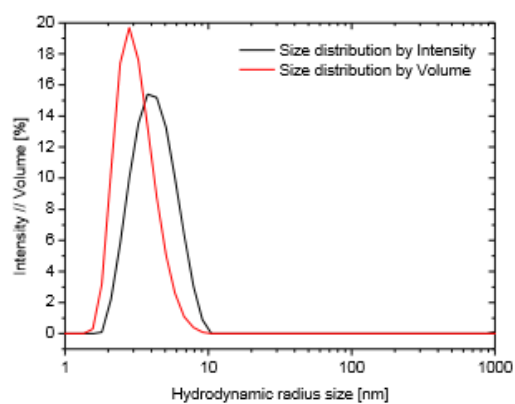
Fig. 3 Dynamic light scattering plots for 200 mg/mL rAlbumin solution diluted to 1 mg/mL. Size distributions by intensity (black line), and by volume (red line).
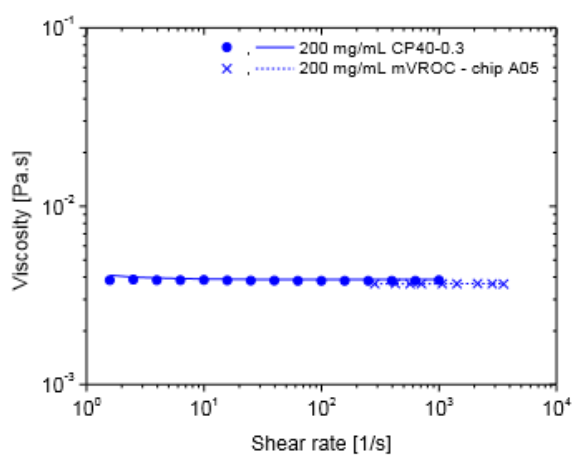
Fig. 4 mVROC data for 200 mg/mL of rAlbumin in comparison to the cone-and-plate rheology data of the same sample. mVROC data: crosses - ramping up shear rates, dashed lines - ramping down shear rates; CP rheology data: closed circles - ramping up shear rates; lines – ramping down shear rates.
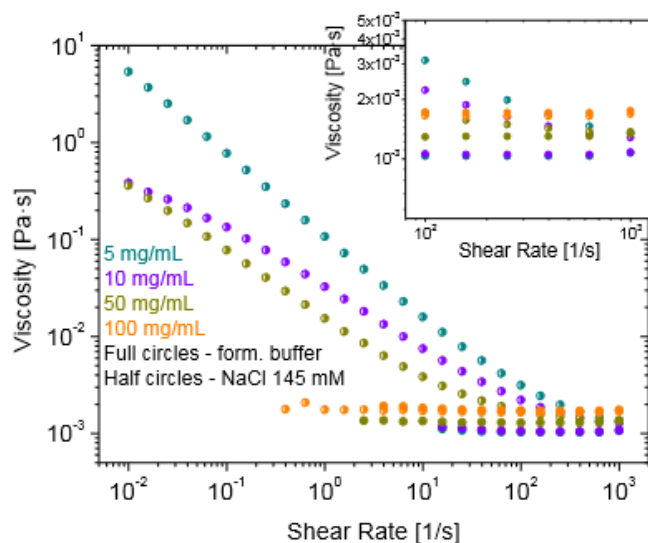
Fig. 5 Viscosity curves for rAlbumin solutions diluted in 145 mM NaCl buffer, in comparison to the material in formulation buffer, at the same concentrations: 5, 10, 50 and 100 mg/mL. Half circles – rAlbumin in 145 mM NaCl only; full circles - rAlbumin in formulation buffer. Inset focuses on the viscosities of these samples at the higher shear rates.
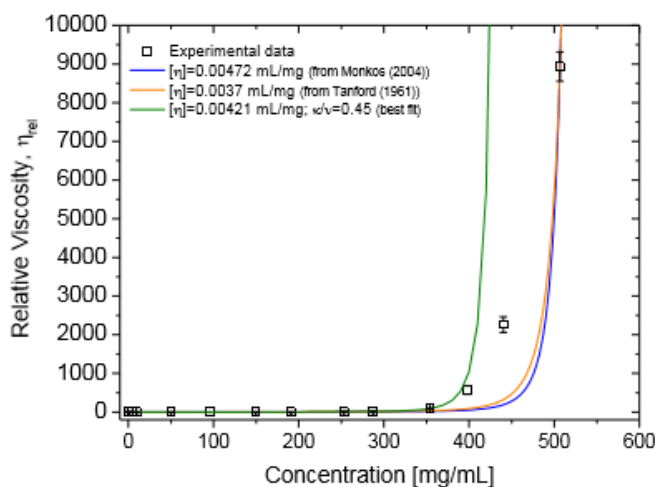
Fig. 6 Experimental cone-and-plate rheometry data (squares) fitted to Ross-Minton's equation (eq. 2). Relative viscosity was obtained by dividing each of the samples high shear viscosity ($\sim$1000s^{-1}) by the averaged buffer viscosity 1.038 $\pm$ 0.013 mPa.s. Fits were calculated by fixing [η] and leaving the parameter κ/v free and are as follows: blue line, [η] = 4.72$\times$10^{-3} mL/mg (from [3]), κ/v = 0.31 $\pm$ 6.6$\times$10^{-4}, r^2 = 0.95; orange line, [η] = 0.0037 mL/mg (from [31]), κ/v = 0.42 $\pm$ 6.9$\times$10^{-4}, r^2 = 0.94. Green line represents best fit of the same equation to experimental data using free parameters. Fit was calculated leaving both [η] and κ/v free: [η] = 4.21$\times$10^{-3} $\pm$ 1.5$\times$10^{-4}; κ/v = 0.45 $\pm$ 0.024; r^2 = 0.999 and χ^2 = 0.40. Experimental data used for this fit was only up to 350 mg/mL.

viscosity. However, in this case, protein structure could also play an important role, where protein-protein interactions between protein domains have been shown to also influence solution viscosity.[11,12]

The relevance of this study to pharmaceutical sciences is that it ultimately shows the importance of better understanding the underlying factors leading to the high viscosity of highly concentrated biopharmaceutical liquid formulations. By using improved models, prediction of protein solution viscosity could eventually bring advantage to early phase development studies, and ultimately help develop better highly concentrated biopharmaceutical formulations, allowing painless sub-cutaneous administration to patients.

Acknowledgements

References

1   S. J. Shire, Z. Shahrokh and J. Liu, *J. Pharm. Sci.*, 2004, **93**, 1390–402.
2   J. Jezek, M. Rides, B. Derham, J. Moore, E. Cerasoli, R. Simler and B. Perez-Ramirez, *Adv. Drug Deliv. Rev.*, 2011, **63**, 1107–17.
3   I. M. Krieger and T. J. Dougherty, *Trans. Soc. Rheol.*, 1959, **III**, 137–152.
4   W. B. Russel, D. A. Saville and W. R. Schowalter, *Colloidal Dispersions*, 1st edn., 1989.
5   R. D. Sudduth, *J. Appl. Polym. Sci.*, 1993, **48**, 25–36.
6   B. Lonetti, E. Fratini, S. H. Chen and P. Baglioni, *Phys. Chem. Chem. Phys.*, 2004, **6**, 1388–1395.
7   V. Sharma, A. Jaishankar, Y. Wang and G. H. Mckinley, *Soft Matter*, 2010, **7**, 5150–5161.
8   K. Monkos, *Biochim. Biophys. Acta*, 2004, **1700**, 27–34.
9   B. A. Salinas, H. A. Sathish, S. M. Bishop, N. Harn, J. F. Carpenter and T. W. Randolph, *J. Pharm. Sci.*, 2009, **99**, 82–93.
10   S. Yadav, S. J. Shire and D. S. Kalonia, *Pharm. Res.*, 2011, **28**, 1973–83.
11   J. Liu, M. D. H. Nguyen, J. D. Andya and S. J. Shire, *J. Pharm. Sci.*, 2005, **94**, 1928–40.
12   S. Kanai, J. U. N. Liu, T. W. Patapoff and S. J. Shire, *J. Pharm. Sci.*, 2008, **97**, 4219–4227.
13   S. Yadav, A. Sreedhara, S. Kanai, J. Liu, S. Lien, H. Lowman, D. S. Kalonia and S. J. Shire, *Pharm. Res.*, 2011, **28**, 1750–64.
14   A. P. Minton, *J. Phys. Chem. B*, 2012, **116**, 9310–5.
15   C. Tanford, *Phyical Chemistry of Macromolecules*, John Wiley & sons, Inc., 1st edn., 1961.
16   S. M. Loveday, L. K. Creamer, H. Singh and M. A. Rao, *J. Food Sci.*, 2007, **72**, R101–7.
17   C. Tanford and J. G. Buzzell, *J. Phys. Chem.*, 1956, **60**, 225–231.
18   P. D. Ross and A. P. Minton, *Biochem. Biophys. Res. Commun.*, 1977, **76**, 971–976.
19   J. Lefevre, *Rheol. Acta*, 1982, **21**, 620–625.
20   S. Harding, *Prog. Biophys. Mol. Biol.*, 1997, **68**, 207–262.
21   M. Mooney, *J. Colloid Sci.*, 1951, **6**, 162–170.
22   J. Mewis and N. Wagner, *Colloidal Suspension Rheology*, Cambridge University Press, UK, 1st edn., 2012.
23   B. Dames, B. R. Morrison and N. Willenbacher, *Rheol. Acta*, 2001, **40**, 434–440.
24   R. D. Sudduth, *J. Appl. Polym. Sci.*, 1993, **48**, 37–55.
25   R. D. Sudduth, *J. Appl. Polym. Sci.*, 1993, **50**, 123–147.
26   W. J. Galush, L. A. N. N. Le and J. M. R. Moore, *J. Pharm. Sci.*, 2012, **101**, 1012–1020.
27   E. Tarelli, A. Mire-Sluis, H. a Tivnann, B. Bolgiano, D. T. Crane, C. Gee, X. Lemercinier, M. L. Athayde, N. Sutcliffe, P. H. Corran and B. Rafferty, *Biologicals*, 1998, **26**, 331–46.
28   S. Curry, H. Mandelkow, P. Brick and N. Franks, *Nat. Struct. Biol.*, 1998, 5, 827–35.
29   M. Dockal, D. C. Carter and F. Rüker, *J. Biol. Chem.*, 2000, **275**, 3042–50.
30   C. J. Pipe, T. S. Majmudar and G. H. McKinley, *Rheol. Acta*, 2008, **47**, 621–642.
31   C. W. ; Macosko, *Rheology: principles, measurements, and applications*, VCH, New York, 1st edn., 1994.
32   H. Zhao, P. H. Brown and P. Schuck, *Biophys. J.*, 2011, **100**, 2309–2317.
33   S. Ikeda and K. Nishinari, *Biomacromolecules*, 2000, **1**, 757–63.
34   S. Ikeda and K. Nishinari, *Food Hydrocoll.*, 2001, **15**, 401–406.
35   S. Yadav, S. J. Shire, D. S. Kalonia and J. U. N. Liu, *J. Pharm. Sci.*, 2010, **99**, 1152–1168.
36   P. Clarke and J.-L. Brousseau, *Pharm. Online Mag.*
37   J. P. Gabrielson, M. L. Brader, A. H. Pekar, K. B. Mathis, G. Winter, J. F. Carpenter and T. W. Randolph, *J. Pharm. Sci.*, 2007, **96**, 268–279.
38   T. Arakawa, D. Ejima, T. Li and J. S. Philo, *J. Pharm. Sci.*, 2010, **99**, 1674–1692.
39   S. J. Burton, A. V Quirk and P. C. Wood, *Eur. J. Biochem.*, 1989, **179**, 379–87.
40   B. Jachimska, M. Wasilewska and Z. Adamczyk, *Langmuir*, 2008, **24**, 6866–72.
41   J. L. Richards, *J. Chem. Educ.*, 1993, **70**, 685.
42   F. Soetewey, M. Rosseneu-motreff, R. Lamote and H. Peeters, *J. Biochem.*, 1972, **71**, 705–710.
43   R. G. Larson, *The Structure and Rheology of Complex Fluids*, Oxford University Press, UK, 1st edn., 1999.
44   L. R. S. Barbosa, M. G. Ortore, F. Spinozzi, P. Mariani, S. Bernstorff and R. Itri, *Biophys. J.*, 2010, **98**, 147–57.
45   A. Michnik, K. Michalik, a. Kluczewska and Z. Drzazga, *J. Therm. Anal. Calorim.*, 2006, **84**, 113–117.
46   S. Ikeda and K. Nishinari, *Int. J. Biol. Macromol.*, 2001, **28**, 315–20.
47   A. Jaishankar, V. Sharma and G. H. Mckinley, *Soft Matter*, 2011, **7**, 7623–7634.
48   T. W. Patapoff and O. Esue, *Pharm. Dev. Technol.*, 2009, **14**, 659–664.
49   P. S. Sarangapani, S. D. Hudson, K. B. Migler and J. a

1.3.7 Paper 5: Ouberai, M.M., Dos Santos, A.L.G., Kinna, S., Madalli, S., Hornigold, D.C., Baker, D., Naylor, J., Sheldrake, L., Corkill, D.J., Hood, J. and Vicini, P., 2017. Controlling the bioactivity of a peptide hormone in vivo by reversible self-assembly. *Nature Communications, 8*(1), p.1026.

Using peptides as therapeutic agents are undergoing research with expectations to discover a new drug that has enhanced levels of efficacy and safety. Peptides full capabilities and potentials will only be understood only if their physiochemical and pharmacokinetics are clearly understood. The research paper is on how a self-assembly strategy for peptides can be used to control and even prolong the bioactivity of another natural peptide hormone in vivo. Having high potency and specificity and also safety structure, peptides are unique and have the potential for the development of therapeutic agents. It is, however challenging as the number of peptides in the market has low solubility, aggregation propensity, chemical instability, little stability against high clearance and short duration of in vivo activity. There are several ways of improving peptide bioavailability with one being engineering peptide analogs that contain unnatural amino acids and conjugate them to polymers, fatty acids, or other abundant proteins. Since the subcutaneous injection is one of the most common ways through which most peptides are administered, there is need to reduce a frequency of dose, have accurate deliver and achieve consistency while applying and these requirements are vital in and needs to be adhered to during treatment where one wants to make and manage chronic diseases effectively. Another different way of approaching the drawbacks, as stated above, would be employing processes that occur naturally like supramolecular self-assembly. The means are solely based on the idea that polypeptide chains align themselves into o β-sheet abundant amyloid-like fibrils.

The Oxi (oxyntomodulin) peptide hormone has been tested as a treatment of obesity by reducing the amount of food ingested increasing energy used in both humans and rodents. Local Oxm is capable of achieving weight loss and glucose control simultaneously, thereby being a suitable agent for the treatment of both diabetes and obesity. Oxfam has a short elimination half-life of 12 minutes in humans, a drawback currently being foreseen by engineers.

Based on this inference, the wide utilization of self-assembling nanofibrils still requires evidence of inclination of natural peptides to be formulated as self-assembling nanostructures (reversibly).

Oxm is capable of self-assembly into nanofibrils since it has 29amino acid glucagon sequence under serene conditions into nanofibrils which dissociate releasing active peptide under physiological states. It is also evident that Oxm administration in mice produces the pharmacological glucose-lowering effect. With these studies, it is an apparent reduction of dose frequency via reversible self-assembly plays a vital role in the treatment of chronic diseases like diabetes and obesity.

Oxi under high yield and mild state can be converted into fibrillary nanostructures estimated at 99% under some optimum conditions depicting amyloid-like properties.

Oxm nanofibrils when incubated under five different media dissociated releasing intact peptide. Electrostatic interactions proved to have a significant impact on the stability of fibrillar Oxm. The different states on equilibrium are hence attained concerning the countries of the solution such as pH, peptide concentration and the various salts available. The full dissociation of glucagon fibrils given time, happen under high dilution.

From the results obtained, it is evident that self-assembled peptide has the capability of releasing helical conformation like peptides which is a crucial fundamental element necessary for cell receptor activation.

DPI (dual polarization interferometry), a technique employed in the dissociation profile of Oxm nanofibrils, was used in the characterization of the dissociation process of the nanostructures in conditions emulating the s.c. Compartment. However, contrary to amyloid-like fibrils known for their stability under several solution conditions, Oxm nanofibrils (under physiological conditions in PBS) dissociate.

The chemically-stable peptide released is found to be active and nontoxic in vitro. In physiological conditions, Oxm can be used as a reservoir where active peptides are kept stored and released with dissociation of nanofibrils. This proves that fibrils in their maturity stage are nontoxic reservoirs of polypeptides and non-fibrillar oligomeric assemblies being toxic.

Oxm nanofibrils, when laced in vivo, produced an effect that lowered glucose level. Furthermore, Oxm when dosed in vivo presented prolonged serum bioactivity. With our study, it is evident that peptide hormones like the Oxm self-assemble in a reverse manner. The data acquired had an inference that Oxm formulation of nanofibril produces an effect of lowering the glucose level. With this data, we are provided with a fundamental basis under which we can create a more in-depth understanding of the possible merits of nanofibril formulation. To improve on the serum stability of the peptide, there would have to be binding of self-assembling nanostructures discretely.

The balance between monomeric and fibrillary states can be managed by enhancing self-assembly conditions to give a more precise fibril structure and peptide confirmation with the corresponding improvement in vivo performance of fibril formulation. The study makes it possible for a concise assessment of the clinical application of self-assembling (reversible) Nano fibrils.

Finally, we can employ this strategy to other peptides to self-assemble into nanostructures, provided that fibrillar condition is exploited to store peptides by the secretory cells.

ARTICLE

Controlling the bioactivity of a peptide hormone in vivo by reversible self-assembly

Myriam M. Ouberai[1], Ana L. Gomes Dos Santos[2], Sonja Kinna[1], Shimona Madalli[3], David C. Hornigold[3], David Baker[3], Jacqueline Naylor[3], Laura Sheldrake[4], Dominic J. Corkill[5], John Hood[6], Paolo Vicini[6], Shahid Uddin[2], Steven Bishop[7], Paul G. Varley[2] & Mark E. Welland[1]

The use of peptides as therapeutic agents is undergoing a renaissance with the expectation of new drugs with enhanced levels of efficacy and safety. Their clinical potential will be only fully realised once their physicochemical and pharmacokinetic properties have been precisely controlled. Here we demonstrate a reversible peptide self-assembly strategy to control and prolong the bioactivity of a native peptide hormone in vivo. We show that oxyntomodulin, a peptide with potential to treat obesity and diabetes, self-assembles into a stable nanofibril formulation which subsequently dissociates to release active peptide and produces a pharmacological effect in vivo. The subcutaneous administration of the nanofibrils in rats results in greatly prolonged exposure, with a constant oxyntomodulin bioactivity detectable in serum for at least 5 days as compared to free oxyntomodulin which is undetectable after only 4 h. Such an approach is simple, cost-efficient and generic in addressing the limitations of peptide therapeutics.

[1] Nanoscience Centre, Department of Engineering, University of Cambridge, Cambridge CB3 0FF, UK. [2] Biopharmaceutical Development, MedImmune Ltd., Granta Park, Cambridge CB21 6GH, UK. [3] Cardiovascular and Metabolic Diseases, MedImmune Ltd., Granta Park, Cambridge CB21 6GH, UK. [4] Invivo Sciences UK, MedImmune Ltd., Granta Park, Cambridge CB21 6GH, UK. [5] Respiratory, Inflammation and Autoimmunity, MedImmune Ltd., Granta Park, Cambridge CB21 6GH, UK. [6] Clinical Pharmacology, Drug Metabolism and Pharmacokinetics, MedImmune Ltd., Granta Park, Cambridge CB21 6GH, UK. [7] Biopharmaceutical development, MedImmune LLC Gaithersburg Headquarters, One MedImmune Way, Gaithersburg, MD 20878, USA. Correspondence and requests for materials should be addressed to M.E.W. (email: mew10@cam.ac.uk)

ARTICLE

Peptides have unique potential as a basis for the development of therapeutic agents owing to their high potency and specificity and their excellent safety profile. In 2013, clinical trials of 128 peptides demonstrated their ability to treat a broad range of conditions, including cancer, autoimmune, cardiovascular, and metabolic diseases[1, 2]. Although there are a number of peptides on the market their full potential as therapeutic agents remains a significant challenge due to their low solubility, chemical instability, aggregation propensity, low stability against proteases, high clearance, and short duration of in vivo activity[2, 3]. Strategies to chemically modify peptides are therefore being developed from native peptide sequences to optimize peptide stability and residence time in serum. One of the common ways of improving peptide bioavailability is to engineer peptide analogs containing unnatural amino acids and conjugate them to fatty acids, polymers, or large proteins[4–6]. Considering that subcutaneous (s.c.) injection is the most common administration route for peptides, reducing the injection frequency and achieving consistent and accurate delivery are requirements for treatment adherence and patient comfort—especially in the effective management of chronic diseases. To this end, the pharmacokinetic properties of peptide analogs can be optimized for long-term controlled release using polymer-based formulations (e.g., the marketed formulations Bydureon®, Zoladex®, and Lupron Depot®)[7].

A very different strategy of addressing the limitations above is to use naturally occurring processes such as supramolecular self-assembly, by which many polypeptides form highly ordered and stable nanostructures[8–13]. This remarkable generic process, which is exploited by living systems, is based on the intrinsic propensity of polypeptide chains to self-assemble into β-sheet rich amyloid-like fibrils via a hydrogen bond network[14]. For instance, various peptide hormones including glucagon are stored in the form of amyloid-like nanofibrils in secretory cells[15], and the concept of an amyloid depot has been applied to the design of an analog of the gonadotropin-releasing hormone degarelix available in the market as Firmagon®[16]. Upon s.c. administration in both rodents and humans, degarelix forms a depot attributed to the formation of amyloid-like fibrils from which the peptide is released into the systemic circulation[16, 17]. Yet, in spite of this very particular example, based on a short (10 amino acids) and chemically modified peptide sequence lacking secondary structure, the broad application of self-assembling nanofibrils as a strategy to address the limitations of peptide therapeutics still needs evidence of the propensity of native peptides to be formulated as reversibly self-assembling nanostructures; the release of active peptide from the nanofibrils which recovers its initial conformation and produces a pharmacological effect; the sufficient in vivo release of active peptide from the nanofibrils to achieve the desired pharmacokinetic profile.

In this study, we investigate a native peptide, oxyntomodulin (Oxm), which is a 37-amino-acid proglucagon-derived peptide hormone with sequence homology to both glucagon and glucagon-like peptide-1 (GLP-1)[18]. As a dual agonist of both glucagon and GLP-1 receptors, Oxm has been shown to be a promising pharmacological agent in the treatment of obesity as it suppresses food intake and increases energy expenditure in both rodents and humans[19–22]. Native Oxm has the advantageous property of simultaneously achieving glucose control and weight loss and consequently is an attractive therapeutic agent to treat both diabetes and obesity[23]. However, the clinical impact of Oxm is currently limited due to its short elimination half-life of 12 min in humans, a limitation which is currently being addressed by complex engineering of analogs. For instance, substantial modification of the Oxm primary sequence is necessary to reduce proteolytic degradation and increase in vivo circulation time[24–27]. This complicated approach to engineer the native peptide sequence in order to both retain activation of glucagon and GLP-1 receptors together with a prolonged residence time in serum is challenging. For example, the recent finding that Oxm analogs increased food intake in rats, exactly the opposite of what is being targeted, illustrates the complexity of achieving the desired therapeutic effect based on peptide sequence modification[28].

We take a much simpler approach. As Oxm contains the 29-amino acid sequence of glucagon we expected it to self-assemble into nanofibrils[19, 29]. Here we show that Oxm readily self-assembles under mild conditions into nanofibrils having intrinsic long-term stability, which can be controlled to subsequently dissociate to release intact and active peptide under physiological conditions. We characterize the reversible self-assembly process using a unique suite of complementary techniques and assays, and describe the in vitro and in vivo bioactivities of fibrillar and released peptides, as well as the pharmacology and pharmacokinetic profile of fibrillar Oxm. After s.c. administration of the nanofibrils in rats, Oxm bioactivity in serum is significantly prolonged with the equivalent of 1 nM Oxm present in serum for at least 5 days after a single s.c. injection of 10 mg kg^{-1}. Following administration of the same dose of free Oxm, serum Oxm bioactivity is undetectable after 4 h. We also show that s.c. administration of fibrillar Oxm in mice produces a pharmacological effect on glucose lowering. These studies demonstrate the potential of reversible self-assembly to reduce dose frequency while maintaining efficacy for peptide therapeutics used to treat chronic diseases such as obesity and diabetes.

Results

Oxm self-assembles into fibrillar nanostructures. Self-assembly of Oxm was carried out at a concentration of 10 mg mL^{-1} in water at an incubation pH of between 7.0 and 7.3 and at a low
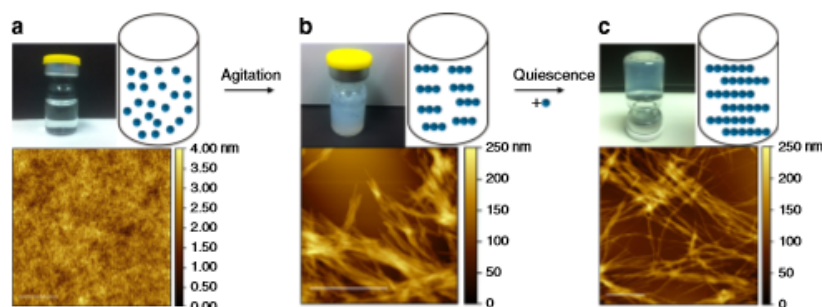
Fig. 1 Self-assembly of Oxm. **a–c** Photographs, schematic representations and AFM images of freshly prepared peptide at 10 mg mL^{-1} in 0.09% saline **a**, after 5 days of incubation with orbital shaking **b** and after incubation of 0.1 mg mL^{-1} fibrils with a 10 mg mL^{-1} free peptide solution in water **c**. Scale bar, 1 μm
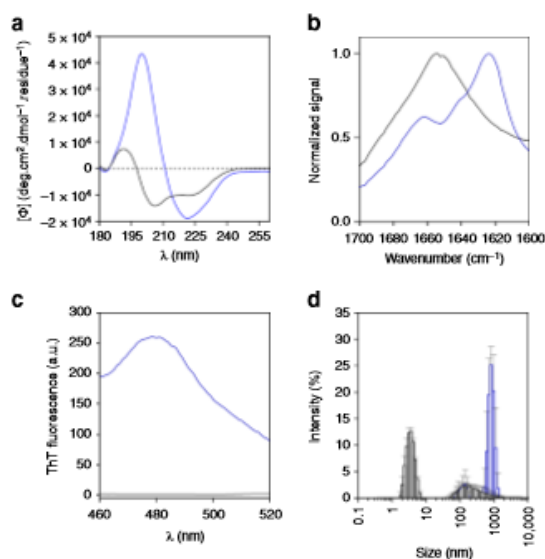
ARTICLE

Fig. 2 Structural properties of free and fibrillar Oxm. **a–d** Free (black) and fibrillar (blue) Oxm at 1 mg mL^{-1} in 0.09% saline. Far-UV CD **a**, ATR-FT-IR, **b** and ThT emission spectra **c**, and DLS analysis (Error bars represent standard deviations obtained from eight measurements of the same sample) **d**

Fig. 3 Characterization of released peptide. **a–d** Schematic of the stability study **a** with examples of a representative AFM image **b**, mass spectrum **c** and far-UV CD spectrum **d** of released Oxm in water. Scale bar, 1 μm

ionic strength (0.09% saline), in order to screen the positive charge (approx. 3+) of the peptide. In order to further promote self-assembly, the solution was incubated at 37 °C and agitated by orbital shaking. The freshly prepared solution was clear, and atomic force microscopy (AFM) analysis showed a homogeneous and smooth layer of peptide that was deposited onto mica (Fig. 1a). No noticeable aggregates were visualized. After incubation for 5 days, the solution turned turbid due to the formation of a suspension of aggregates (Fig. 1b). AFM analysis showed the presence of fibrils with ~10 nm diameter and up to 1 μm length, grouped into bundles. The conversion yield of the self-assembly of Oxm into fibrillar nanostructures was estimated to be 99% under these conditions.

The nanofibrils were next used to seed a solution of free peptide at 10 mg mL^{-1} in water. The solution was incubated without agitation for 1 week and then diluted to 1 mg mL^{-1} in 0.09% saline for another 2–9 days of incubation at 37 °C and then 9 days at room temperature. Most of the free peptide in the solution was converted into nanofibrils with a conversion rate of 94%. The solution took on a gel-like consistency, and the AFM analysis showed a network of nanofibrils with diameters of ~10 nm and lengths between 2 and 9 μm (Fig. 1c).

Structural analysis of free and fibrillar Oxm was performed using far-UV circular dichroism (CD) (Fig. 2a and Supplementary Fig. 1). Free peptides were mainly arranged in an α-helical conformation (36% α-helical and 12% β-sheet content). In contrast, the far-UV spectrum of fibrillar Oxm showed a significant change in the secondary structure, with 57% β-sheet and 14% α-helical content.

A conformational change of the peptide was also assessed by attenuated total reflection (ATR) Fourier transform infrared (FT-IR) spectroscopy (Fig. 2b). The analysis of the ATR-FT-IR data suggests that free Oxm is composed of disordered and α-helix structures as indicated by the band at 1650–1655 cm^{-1} [30, 31]. By contrast, fibrillar Oxm displays a maximum at 1624 cm^{-1} as well
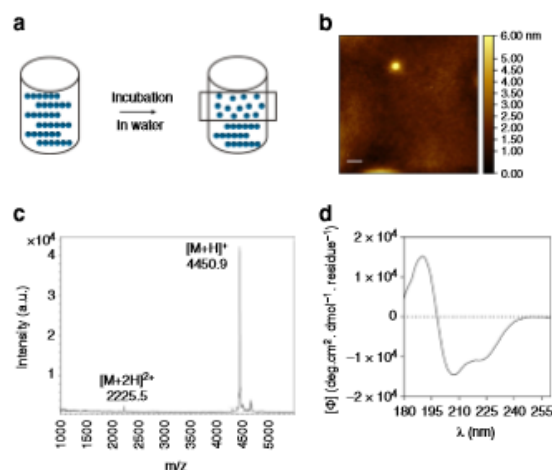
as a prominent shoulder at 1641 cm^{-1}, which indicate that peptide conformation is composed of β-sheet structure. The presence of a band at 1662 cm^{-1} can indicate the presence of β-turn or 3_{10}-helix structures [30, 31].

When the probe thioflavin T (ThT) was applied to fibrillar Oxm, a characteristic fluorescence emission at 480 nm confirmed that the peptide had adopted a cross-β-sheet conformation (Fig. 2c) [32]. As expected, no emission was observed in the presence of freshly prepared Oxm. Finally, dynamic light scattering analysis of free and fibrillar Oxm showed a significant shift in the size of species present in solution (Fig. 2d). For the free peptide solution, the size distribution shows a major sub-population of species with a mean diameter of 3.6 nm. In contrast, the fibrillar Oxm sample contained significantly larger species, with a mean diameter of 825 nm. Altogether, we show that Oxm can be converted, under mild conditions and with a high yield, into fibrillar nanostructures displaying amyloid-like features.

Oxm nanofibrils dissociate to release intact peptide. To assess the stability of fibrillar Oxm, 1 mg mL^{-1} nanofibrils were incubated in five media: phosphate buffer (25 mM, pH 7.5), Tris-HCl buffer (25 mM, pH 7.5), 0.09% saline, water and aqueous HCl (10 mM, pH 2). After 48 h in 0.09% saline, fibrillar Oxm was stable and no release of peptide was detected from the fibrils (Supplementary Table 1). As the stability of hormone fibrils has been described to depend on the presence of salts of monoprotic or polyprotic acids [33], the stability of fibrillar Oxm was assessed in phosphate and Tris-HCl buffers. In both buffers, fibrillar Oxm was stable with less than 1.5% of released peptide detected after 48 h. By contrast, in water 37% of peptide was released after 4 h incubation, and 53% was released by 48 h (Supplementary Table 1). Moreover, in aqueous HCl, a 77% release was observed after only 4 h. This shows that electrostatic interactions play a major role in the stability of fibrillar Oxm—the positive charge of the peptide at both acidic and neutral conditions induced an electrostatic repulsion between peptide molecules, which rendered the fibrillar state unstable. The presence of salts such as NaCl, phosphate or Tris-HCl stabilizes the fibrillar state at 1 mg mL^{-1}. We therefore anticipate that different equilibrium states are reached depending on the solution conditions, such as the peptide concentration, the presence of various salts and pH.
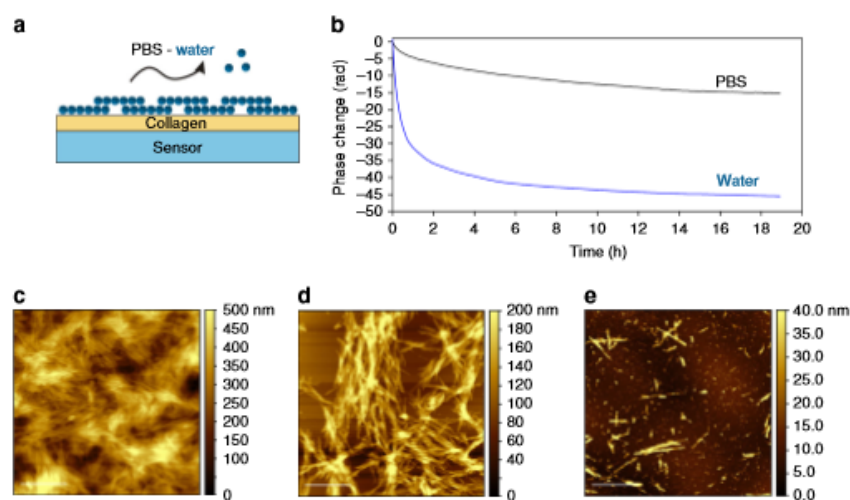
Fig. 4 Dissociation profile of Oxm nanofibrils under physiological conditions. **a** Schematic of the dissociation study using the DPI biosensing technique. **b** Phase changes as a function of time on top of the DPI sensor coated with collagen and fibrillar Oxm in water (blue) and PBS (black). **c-e** Representative AFM images of Oxm nanofibrils deposited onto a collagen layer before **c** and after incubation in PBS **d** and water **e**. Scale bar, 1 μm

Investigations to further characterize the equilibrium properties of the system under various conditions are ongoing.

The AFM images of released peptide in water show a smooth layer of peptide spread onto mica (Fig. 3a, b). As measured by mass spectrometry, the peptide remained chemically intact after release from the nanofibrils ($[M + H]^+ = 4450.9$, Fig. 3a, c). Furthermore, the far-UV CD spectrum of released Oxm in water shows that the peptide recovered its initial conformation, which is characterized by helical and disordered structures in proportions similar to free peptides (Fig. 3a, d and Supplementary Fig. 2). These results highlight the ability of self-assembled peptide nanofibrils to release intact peptides that can fold from a cross-β-sheet structure back to their initial helical conformation, which is a key structural element for the activation of cell receptors[34].

A surface-based technique, dual polarization interferometry (DPI), was used to assess the dissociation profile of Oxm nanofibrils under conditions mimicking physiological pH, ionic strength and temperature, with the fibrils in interaction with one main component of the s.c. space, and with peptide cleared upon release from the fibrils. DPI is one of the most powerful label-free biosensing techniques available; it can be used to monitor the real-time phase changes resulting from the variation in thickness and refractive index of layers deposited on the top of a sensor[35, 36]. In this study, DPI was used to characterize the dissociation process of fibrillar nanostructures in conditions mimicking the s.c. compartment (with continuous flow to clear released peptide upon fibril dissociation and fibrils deposited on a collagen layer; Fig. 4a)[37]. A decrease in phase changes as a function of time is observed under these conditions, indicating the removal of material from the surface, with a sharper decrease during the first 4 h in water than in phosphate-buffered saline pH 7.4 (PBS; Fig. 4b). AFM images of the surface before (Fig. 4c) treatment, and after flowing with PBS (Fig. 4d) or water (Fig. 4e) for 20 h, show that the removal of materials corresponded to a dissociation of the nanofibrils. This result is indicated visually by less fibril coverage on the surface of the sensor, with only a few residual short fibrils imaged after incubation in water. Quantification of the change in thickness, density and mass after 4 h incubation shows that 42% of the deposited material was removed from the surface in water, whereas only 10% was

removed in PBS (Supplementary Table 2 and Supplementary Fig. 3). Therefore, under physiological conditions in PBS, Oxm nanofibrils dissociate with a sustained release profile. This finding contrasts with the trend observed for amyloid-like fibrils, which are known to be stable under various solution conditions. For instance, glucagon fibrils are generally stable even under the harsh conditions of thermal and chemical denaturation, but their stability appears to be related to the structure of fibrils and self-assembly conditions (salts, peptide concentration and temperature)[38]. In those experiments, the trend observed implied that complete dissociation of glucagon fibrils can occur upon high dilution, given time.

The released peptide is active and nontoxic in vitro. Having shown the chemical stability of the released Oxm, we assessed its functional potency in comparison to that of free and fibrillar Oxm. Agonist potency determination for all samples was performed using cAMP accumulation assays in Chinese hamster ovary (CHO) cells expressing recombinant human GLP-1 (hGLP-1R) or glucagon (hGCGR) receptors (Fig. 5a, b). Free, released and fibrillar Oxm all acted as full agonists in hGLP-1R- and hGCGR-expressing cells, compared to the maximum effects of GLP-1 or glucagon peptides in GLP-1R and GCGR assays, respectively.

Released and free Oxm had comparable potencies against hGLP-1R, with EC_{50} values of 96.6 ± 31.0 (geometric mean ± s.e.m.) and 72.4 ± 17.9 pM, respectively, whereas fibrillar Oxm was approximately 40-fold less potent with an EC_{50} of 2938.3 ± 655.7 pM (Supplementary Table 3). In the hGCGR-expressing line released and free Oxm also showed similar potencies, with EC_{50} values of 26.0 ± 5.2 and 18.2 ± 4.2 pM, respectively, whereas fibrillar Oxm was ~62-fold less potent, EC_{50} 1120.5 ± 302.2 pM (Supplementary Table 3). Formation of nanofibrillar structures is expected to preclude pharmacological activity of the peptide, therefore any measured in vitro activity of the fibrillar material is likely to be due to release of small amounts of non-fibrillated peptide in the assay conditions.

To assess the in vitro cytotoxicity of Oxm species, a cell viability assay was performed in the presence of free, released, and fibrillar Oxm. Metabolic bioactivity of living cells was measured
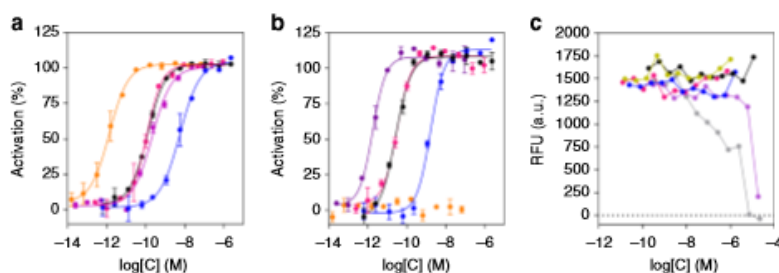
Fig. 5 Agonist potency and cytotoxicity profiles of Oxm species. **a**, **b** In vitro potencies determined in cAMP accumulation assays in CHO cell lines expressing human GLP-1 **a** and GCG **b** receptors of free Oxm (black), released Oxm (magenta), fibrillar Oxm (blue), glucagon (violet), GLP-1 (orange). Data show representative curves of >5 independent experiments. Curve data are the arithmetic mean ± s.d. of duplicate data points. **c** 48 h cytotoxicity prolife in CHO-GLP-1R cells of vehicle (yellow), free Oxm (black), released Oxm (magenta), fibrillar Oxm (blue), Ro-318220 (violet), Staurosporine (gray). RFU = Relative fluorescence units. Data show representative curves of three independent experiments
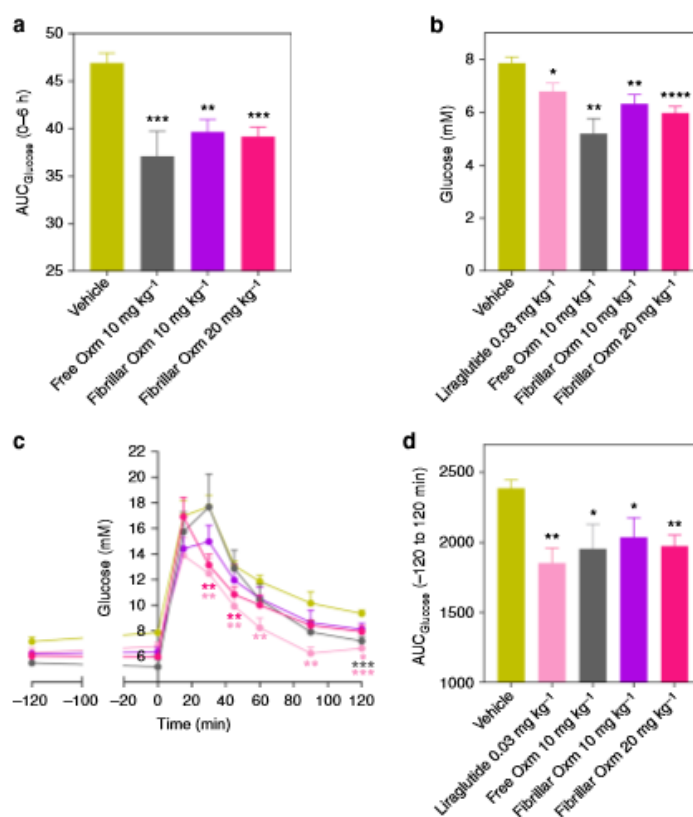
Fig. 6 Effect of fibrillar Oxm on blood glucose lowering. Glucose lowering demonstrated after 6 h of administration with either vehicle or free and fibrillar Oxm by either AUC **a**, or blood glucose concentration at 6 h **b**. A glucose tolerance test (GTT) was conducted at 6 h post-dose **c** and efficacy was also expressed by AUC **d**. Liraglutide was used as positive control and administrated 2 h prior to GTT. Data are mean ± s.e.m. ($n = 7$–8 animals per group). *$P < 0.05$, **$P < 0.01$, ***$P < 0.001$, ****$P < 0.0001$, vs. vehicle, two-sided, unpaired t-test

through bioreduction of a resazurin-based dye (Fig. 5c). None of the forms of Oxm were cytotoxic at concentrations up to 1000-fold above the EC_{50} value in the CHO-hGLP-1R cell line. Two positive control cytotoxic agents, Ro-318220 and staurosporine, both protein kinase C inhibitors, showed the expected curves of concentration vs. loss of cell viability. These studies show that the

fibrillar state of Oxm is not acutely cytotoxic at the concentrations tested and can be used as a reservoir in which active and nontoxic peptides can be stored and released upon dissociation of the nanofibrils under physiological conditions. Our result is in agreement with studies describing mature fibrils as harmless reservoirs of polypeptides with the toxic species being the non-

ARTICLE

Dynamic light scattering analysis. The intensity distribution profiles of freshly prepared and fibrillar Oxm (1 mg mL^{-1}) in 0.09% saline at 25 °C were determined by DLS using a Zetasizer Nano ZS (Malvern Instruments, UK) at a back-scattering angle of 173°.

Stability studies. Solutions of fibrillar Oxm at 1 mg mL^{-1} in phosphate buffer (25 mM, pH 7.5), Tris-HCl buffer (25 mM, pH 7.5), water (pH 5.9–6.2), 0.09% saline (pH 5.9–6.2) and aqueous HCl (10 mM, pH 2) were incubated for 4 and 48 h under quiescent conditions at 37 °C. The samples were first centrifuged at 16,200×g for 30 min. The collected supernatant was then filtered through a 50 kDa molecular weight cutoff membrane. The concentration of peptide was measured in the filtrate and compared to the initial peptide concentration to assess the percentage release. Released peptides in water were used for further studies. Mass spectra were obtained by matrix-assisted laser desorption ionization (MALDI) on a Bruker ultrafleXtreme mass spectrometer. The net charge of the peptide vs. pH was calculated using GPMAW 9.52a software.

Dissociation study of fibrillar Oxm using DPI. A dual polarization interferometer (Farfield Analight 4D, Biolin Scientific AB) was used to optically characterize the dissociation profile of fibrillar Oxm deposited onto collagen-coated sensor chips. Details of the instrumentation has been described previously[51]. Human collagen, diluted to 0.2 mg mL^{-1} in water, was first deposited onto the unmodified oxynitride sensor chip and left to dry at room temperature before being briefly rinsed with water. Then, fibrillar Oxm (1 mg mL^{-1}, 10 μL) in 0.09% saline was deposited onto the collagen layer and left to dry at room temperature without rinsing. Water or PBS solutions were continuously flowed over the deposited fibrillar Oxm layer at a rate of 20 μL min^{-1} at 37 °C. After incubation, aqueous 10 mM HCl (pH 2) and 2% Hellmanex in water were injected to remove any residual materials (including the collagen layer) before proceeding to the chip calibration using 80% (w/w) ethanol in water. Data were analyzed using the Analight Explorer 1.6.0.27583 (Farfield-Biolin Scientific AB, Sweden) to calculate the layer refractive index, density, thickness, and mass[51]. Variations in the layer properties were calculated from the maximum values at the start of incubation. As blood is almost phosphate free, the dissociation of fibrillar Oxm was also monitored in a Tris-buffered saline (TBS) and compared to water (Supplementary Fig. 3). Similarly to PBS, slower dissociation was observed in TBS compared to water. Finally, removal of materials from a collagen layer was assessed in water and PBS (Supplementary Fig. 3). A negligible amount of collagen was removed from the surface in water. In PBS, the phase change stabilized after an initial decrease.

Potency assay. In vitro agonist potencies of free, released, and fibrillated Oxm were determined in cAMP accumulation assays in CHO cells that were stably transfected with human GLP1R or human GCGR receptor[52–54]. In brief, peptide samples were incubated with cells plated at 500 cells per well in 384-well black shallow microtiter plates (Corning, USA) for 30 min prior to lysis and detection using the HTRF cAMP dynamic 2 assay kit (Cisbio, France). Plates were then incubated for 1 h prior to reading on an Envision plate reader (Perkin Elmer, USA). Eleven-point duplicate concentration-response curves were generated for three independent experiments, and data were represented as the percent activation of the maximum reference ligand. Curves were fitted using nonlinear regression analysis in GraphPad Prism software 6.03 (GraphPad, USA).

Cell viability assay. CHO-hGLP-1R cells in growth medium (DMEM, 10%FBS Sigma-Aldrich) were plated at 10,000 cells per well in 96-well black clear-bottom poly-D-lysine-coated microtiter plates (Corning, USA). Cells were pretreated with Oxm or cytotoxic standards (staurosporine, Ro-318220 Sigma-Aldrich) for 48 h, followed by incubation for 5 h with resazurin dye (in vitro toxicological assay kit, Sigma-Aldrich) at 37 °C in a 5% CO$_2$ atmosphere. Fluorescence emission was measured at 590 nm (560 nm excitation).

Pharmacodynamic studies. All in vivo procedures were conducted under the authority of a UK Project license which had been reviewed and approved by an Animal Welfare and Ethical Review Body (AWERB) in compliance with EU Directive 2010/63/EU before any work was carried out. Mice were housed under standard conditions with a 12 h light/dark cycle and ad libitum access to food and water. Thirty-nine C57BL/6 wild-type mice were sourced from MRC Harwell, Oxford, UK and randomized into five groups based on body weight (average body weight 33.8 g). Free and fibrillar Oxm were formulated at 1 mg mL^{-1} stock in 0.09% saline. Food was removed from animals at 8 AM, at a time when all animals had a blood glucose measurement made from a drop of blood obtained from a tail prick sample at baseline, 45 min, 2, 4, and 6 h using a hand-held glucometer (Contour NXT, Bayer). Group 1 ($n = 7$) received vehicle 0.09% saline, Group 2 ($n = 8$) received positive control liraglutide 0.03 mg kg^{-1} (4 h later, such that the first injection was 2 h prior to the glucose tolerance test), Group 3 ($n = 8$) received free Oxm at 10 mg kg^{-1} (10 mL kg^{-1}), Group 4 ($n = 8$) received fibrillar Oxm 10 mg kg^{-1} (10 mL kg^{-1}), and Group 5 ($n = 8$) received fibrillar Oxm at 20 mg kg^{-1} (20 mL kg^{-1}) via s.c. injection. After 6 h, animals were injected with glucose i.p at 2 g kg^{-1} and glucose measured at 15, 30, 45, 60, 90, and 120 min post-injection. All

data are mean ± s.e.m. Significances were determined using two-sided, unpaired Student's t-test vs. vehicle.

Pharmacokinetic studies. All in vivo procedures were conducted under the authority of a UK Project license which had been reviewed and approved by an Animal Welfare and Ethical Review Body (AWERB) in compliance with EU Directive 2010/63/EU before any work was carried out. Lean male CD rats (Charles River Sprague Dawley substrain rats[55]) weighing 200–250 g at the start of the study (Charles River, UK) were housed under standard conditions with a 12 h light/dark cycle and ad libitum access to food and water. Free and fibrillar Oxm were formulated at 1 mg mL^{-1} stock in 0.09% saline. Groups of three animals were injected with either free Oxm at 5 mg kg^{-1} i.v. (5 mL kg^{-1}), free Oxm at 5 or 10 mg kg^{-1} s.c. (5 or 10 mL kg^{-1}) or fibrillar Oxm at 5 or 10 mg kg^{-1} s.c. (5 or 10 mL kg^{-1}). Serum samples were collected from i.v.-injected animals at 5, 10, 15, 20, 30, 45 min and 1, 2, 4, 6, and 24 h and from s.c.-injected animals at 5, 10, 15, 30, 45 min, 1, 2, 4, 6, and 24 h and 2, 3, and 5 days. Blood samples were taken into serum collecting tubes containing DPP4 inhibitor (Millipore, UK), allowed to clot for 30 min and then spun to obtain serum, which was stored at −80 °C until the assays were performed. Serum peptide content was determined as apparent concentration measured by ex vivo bioactivity in serum using an in vitro cell-based cAMP bioassay (Cisbio, France) for determining agonist bioactivity at human GLP1R and human glucagon receptor as described in potency assay above[21, 56]. In brief, CHO K1 cells stably transfected with either human GLP1R or human glucagon receptor were used to determine peptide concentrations in serum by comparing the degree of cAMP accumulation in serum samples from treated animals against a standard curve generated by spiking peptide into naïve pooled male rat serum (Seralabs, West Sussex, UK) using acoustic dispensing. Bioactivity data were analyzed using nonlinear regression analysis in GraphPad Prism. SAAM II software (The Epsilon Group, Charlottesville, VA; version 2.1) was used for the pharmacokinetic analysis. Naïve pooling and model-based weights were used for nonlinear regression. The final model is shown in Supplementary Fig. 6.

Data availability. All data supporting the findings of this study are available within the article and Supplementary Information file, or available from the authors upon request.

References

1. Kaspar, A. A. & Reichert, J. M. Future directions for peptide therapeutics development. *Drug Discov. Today* **18**, 807–817 (2013).
2. Fosgerau, K. & Hoffmann, T. Peptide therapeutics: current status and future directions. *Drug Discov. Today* **20**, 122–128 (2014).
3. Sleep, D., Cameron, J. & Evans, L. R. Albumin as a versatile platform for drug half-life extension. *Biochim. Biophys. Acta* **1830**, 5526–5534 (2013).
4. Kontermann, R. E. Strategies for extended serum half-life of protein therapeutics. *Curr. Opin. Biotechnol.* **22**, 868–876 (2011).
5. Kovalainen, M. et al. Novel delivery systems for improving the clinical use of peptides. *Pharmacol. Rev.* **67**, 541–561 (2015).
6. Penchala, S. C. et al. A biomimetic approach for enhancing the in vivo half-life of peptides. *Nat. Chem. Biol.* **11**, 793–798 (2015).
7. Schwendeman, S. P., Shah, R. B., Bailey, B. A. & Schwendeman, A. S. Injectable controlled release depots for large molecules. *J. Control Release* **190**, 240–253 (2014).
8. Adler-Abramovich, L. & Gazit, E. The physical properties of supramolecular peptide assemblies: from building block association to technological applications. *Chem. Soc. Rev.* **43**, 6881–6893 (2014).
9. Mandal, D., Nasrolahi Shirazi, A. & Parang, K. Self-assembly of peptides to nanostructures. *Org. Biomol. Chem.* **12**, 3544–3561 (2014).
10. Knowles, T. P. et al. Role of intermolecular forces in defining material properties of protein nanofibrils. *Science* **318**, 1900–1903 (2007).
11. Knowles, T. P. J., Oppenheim, T. W., Buell, A. K., Chirgadze, D. Y. & Welland, M. E. Nanostructured films from hierarchical self-assembly of amyloidogenic proteins. *Nat. Nanotechnol.* **5**, 204–207 (2010).
12. Hauser, C. a. E., Maurer-Stroh, S. & Martins, I. C. Amyloid-based nanosensors and nanodevices. *Chem. Soc. Rev.* **43**, 5326–5345 (2014).
13. Loo, Y., Zhang, S. & Hauser, C. A. E. From short peptides to nanofibers to macromolecular assemblies in biomedicine. *Biotechnol. Adv.* **30**, 593–603 (2012).
14. Knowles, T. P. J. & Buehler, M. J. Nanomechanics of functional and pathological amyloid materials. *Nat. Nanotechnol.* **6**, 469–479 (2011).
15. Maji, S. K. et al. Functional amyloids as natural storage of peptide hormones in pituitary secretory granules. *Science* **325**, 328–332 (2009).

16. Maji, S. K. et al. Amyloid as a depot for the formulation of long-acting drugs. *PLoS Biol.* **6**, 0240–0252 (2008).
17. Jadhav, P. R., Agersø, H., Tornøe, C. W. & Gobburu, J. V. S. Semi-mechanistic pharmacodynamic modeling for degarelix, a novel gonadotropin releasing hormone (GnRH) blocker. *J. Pharmacokinet. Pharmacodyn.* **33**, 609–634 (2006).
18. Bataille, D. & Dalle, S. The forgotten members of the glucagon family. *Diabetes Res. Clin. Pract.* **6**, 1–10 (2014).
19. Pocai, A. Action and therapeutic potential of oxyntomodulin. *Mol. Metab.* **3**, 241–251 (2014).
20. Wynne, K. et al. Subcutaneous oxyntomodulin reduces body weight in overweight and obese subjects: a double-blind, randomized, controlled trial. *Diabetes* **54**, 2390–2395 (2005).
21. Kosinski, J. R. et al. The Glucagon receptor is involved in mediating the body weight-lowering effects of oxyntomodulin. *Obesity* **20**, 1566–1571 (2012).
22. Pocai, A. Unraveling oxyntomodulin, GLP1's enigmatic brother. *J. Endocrinol.* **215**, 335–346 (2012).
23. Chakradhar, S. All in one: researchers create combination drugs for diabetes and obesity. *Nat. Med.* **22**, 694–696 (2016).
24. Druce, M. R. et al. Investigation of structure-activity relationships of oxyntomodulin (Oxm) using Oxm analogs. *Endocrinology* **150**, 1712–1722 (2009).
25. Schjoldager, B. T., Baldissera, F. G., Mortensen, P. E., Holst, J. J. & Christiansen, J. Oxyntomodulin: a potential hormone from the distal gut. Pharmacokinetics and effects on gastric acid and insulin secretion in man. *Eur. J. Clin. Invest.* **18**, 499–503 (1988).
26. Bianchi, E. et al. A PEGylated analog of the gut hormone oxyntomodulin with long-lasting antihyperglycemic, insulinotropic and anorexigenic activity. *Bioorg. Med. Chem.* **21**, 7064–7073 (2013).
27. Muppidi, A. et al. Design of potent and proteolytically stable oxyntomodulin analogs. *ACS Chem. Biol.* **11**, 324–328 (2016).
28. Price, S. L., Minnion, J. S. & Bloom, S. R. Increased food intake with oxyntomodulin analogues. *Peptides* **73**, 95–100 (2015).
29. Andersen, C. B. et al. Glucagon fibril polymorphism reflects differences in protofilament backbone structure. *J. Mol. Biol.* **397**, 932–946 (2010).
30. Yang, H., Yang, S., Kong, J., Dong, A. & Yu, S. Obtaining information about protein secondary structures in aqueous solution using Fourier transform IR spectroscopy. *Nat. Protoc.* **10**, 382–396 (2015).
31. Barth, A. Infrared spectroscopy of proteins. *Biochim. Biophys.* **1767**, 1073–1101 (2007).
32. Amdursky, N., Erez, Y. & Huppert, D. Molecular rotors: what lies behind the high sensitivity of the thioflavin-T fluorescent marker. *Acc. Chem. Res.* **45**, 1548–1557 (2012).
33. Nespovitaya, N. et al. Dynamic assembly and disassembly of functional β-endorphin amyloid fibrils. *J. Am. Chem. Soc.* **138**, 846–856 (2016).
34. Neumann, J. M. et al. Class-B GPCR activation: is ligand helix-capping the key? *Trends Biochem. Sci.* **33**, 314–319 (2008).
35. Escorihuela, J. et al. Dual-polarization interferometry: a novel technique to light up the nanomolecular world. *Chem. Rev.* **115**, 265–294 (2015).
36. Ouberai, M. M., Xu, K. & Welland, M. E. Effect of the interplay between protein and surface on the properties of adsorbed protein layers. *Biomaterials* **35**, 6157–6163 (2014).
37. Kinnunen, H. M. & Mrsny, R. J. Improving the outcomes of biopharmaceutical delivery via the subcutaneous route by understanding the chemical, physical and physiological properties of the subcutaneous injection site. *J. Control Release* **182**, 22–32 (2014).
38. Pedersen, J. S. et al. The changing face of glucagon fibrillation: structural polymorphism and conformational imprinting. *J. Mol. Biol.* **355**, 501–523 (2006).
39. Chen, S. W. et al. Structural characterization of toxic oligomers that are kinetically trapped during α-synuclein fibril formation. *Proc. Natl Acad. Sci. USA* **112**, E1994–E2003 (2015).
40. Fändrich, M. Oligomeric intermediates in amyloid formation: structure determination and mechanisms of toxicity. *J. Mol. Biol.* **421**, 427–440 (2012).
41. Campioni, S. et al. A causative link between the structure of aberrant protein oligomers and their toxicity. *Nat. Chem. Biol.* **6**, 140–147 (2010).
42. Wang, Y., Lomakin, A., Kanai, S., Alex, R. & Benedek, G. B. Transformation of oligomers of lipidated peptide induced by change in pH. *Mol. Pharm.* **12**, 411–419 (2015).
43. Rudra, J. S. et al. Modulating adaptive immune responses to peptide self-assemblies. *ACS Nano* **6**, 1557–1564 (2012).
44. Du, X., Zhou, J., Shi, J. & Xu, B. Supramolecular hydrogelators and hydrogels: from soft matter to molecular biomaterials. *Chem. Rev.* **115**, 13165–13307 (2015).

45. Li, Y. et al. Variant fatty acid-like molecules conjugation, novel approaches for extending the stability of therapeutic peptides. *Sci. Rep.* **5**, 18039 (2015).
46. Zhu, L. et al. The role of dipeptidyl peptidase IV in the cleavage of glucagon family peptides: in vivo metabolism of pituitary adenylate cyclase-activating polypeptide-(1-38). *J. Biol. Chem.* **278**, 22418–22423 (2003).
47. Knowles, T. P. J., Vendruscolo, M. & Dobson, C. M. The amyloid state and its association with protein misfolding diseases. *Nat. Rev. Mol. Cell Biol.* **15**, 384–396 (2014).
48. Zapadka, K. L. et al. A pH-induced switch in human glucagon-like peptide-1 aggregation kinetics. *J. Am. Chem. Soc.* **138**, 16259–16265 (2016).
49. Sreerama, N. & Woody, R. W. Estimation of protein secondary structure from circular dichroism spectra: comparison of CONTIN, SELCON, and CDSSTR methods with an expanded reference set. *Anal. Biochem.* **287**, 252–260 (2000).
50. Johnson, W. C. Analyzing protein circular dichroism spectra for accurate secondary structures. *Proteins Struct. Funct. Genet.* **35**, 307–312 (1999).
51. Xu, K., Ouberai, M. M. & Welland, M. E. A comprehensive study of lysozyme adsorption using dual polarization interferometry and quartz crystal microbalance with dissipation. *Biomaterials* **34**, 1461–1470 (2013).
52. Butler, R. et al. Use of the site-specific retargeting jump-in platform cell line to support biologic drug discovery. *J. Biomol. Screen* **20**, 528–535 (2015).
53. Naylor, J., Rossi, A. & Hornigold, D. C. Acoustic dispensing preserves the potency of therapeutic peptides throughout the entire drug discovery workflow. *J. Lab. Autom.* **21**, 90–96 (2016).
54. Henderson, S. J. et al. Robust anti-obesity and metabolic effects of a dual GLP-1/glucagon receptor peptide agonist in rodents and non-human primates. *Diabetes Obes. Metab.* **18**, 1176–1190 (2016).
55. Uchino, E., Tsuzuki, T. & Inoue, K. The effects of age and sex on seven elements of sprague-dawley rat organs. *Lab. Anim.* **24**, 253–264 (1990).
56. Pocai, A. et al. Glucagon-like peptide 1/glucagon receptor dual agonism reverses obesity in mice. *Diabetes* **58**, 2258–2266 (2009).

Author contributions

M.M.O., A.L.G.D.S. and M.E.W. conceived the project. M.M.O., A.L.G.D.S., D.C.H., D.B., D.J.C. and P.V. conceived and designed the experiments. M.M.O., S.K., S.M., D.C.H., D.B., J.N. and I.S. performed the experiments. M.M.O., A.L.G.D.S., S.M., D.C.H., D.B., J.N., D.J.C., J.H. and P.V. Analyzed the data. M.M.O., A.L.G.D.S., S.K., S.M., D.C.H., D.B., D.J.C., J.H., P.V. and M.E.W. wrote the paper. All authors discussed the results and commented on the manuscript.

Additional information

Supplementary Information accompanies this paper at doi:10.1038/s41467-017-01114-1.

Competing interests: The authors declare no competing financial interests.

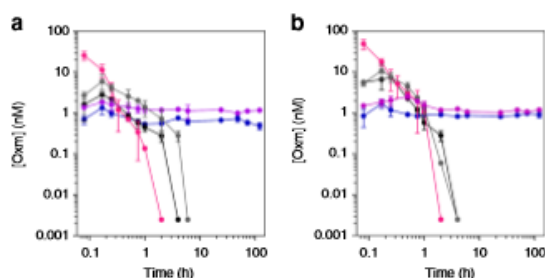**Reprints and permission** information is available online at http://npg.nature.com/reprintsandpermissions/

Publisher's note: Springer Nature remains neutral with regard to jurisdictional claims in published maps and institutional affiliations.

ARTICLE

Fig. 7 Pharmacokinetic profiles following administration of free and fibrillar Oxm. Oxm bioactivity in rat serum determined using in vitro cell-based cAMP bioassay for determining GLP-1 **a** and GCG **b** receptor agonist bioactivity after administration of 5 mg kg^{-1} of free Oxm i.v. (magenta), s.c. (black), and fibrillar Oxm s.c. (blue) and 10 mg kg^{-1} of free Oxm s.c. (gray) and fibrillar Oxm s.c. (violet). The data correspond to the average measurements from 3 rats ± s.d

fibrillar oligomeric assemblies[39–41]. Nonetheless, peptide oligomerization can also be beneficial to extent the half-life of peptide therapeutics as described for Liraglutide (Victoza)[42]. Potential immunogenicity of protein aggregates is a subject of intense research, and it appears that some self-assembled peptides elicit a wide range of immune response from no detectable to strong antibody responses[43, 44]. Even if the molecular determinants have yet to be established, it has been reported that immunogenicity of self-assembled peptide can be significantly attenuated by modulating the peptide sequence recognized by T cells[43]. Therefore, further studies will be required to fully characterize in vivo toxicity and immunogenicity profiles of fibrillar Oxm.

Oxm nanofibrils produce a pharmacological effect in vivo.

To understand if fibrillar Oxm can act as a pharmacological depot, we followed glucose levels in wild-type C57BL/6 mice following administration of either 0.09% saline vehicle, free Oxm (10 mg kg^{-1} s.c), or fibrillar Oxm (10 and 20 mg kg^{-1} s.c). Blood glucose was measured in blood samples taken from tail prick using a hand-held glucometer at either baseline, 45 min, 4 or 6 h post-dose. Area under the curve (AUC) analysis for this 6 h time period showed that both doses of fibrillar Oxm as well as free Oxm had a significant glucose lowering effect vs. vehicle (Fig. 6a). Indeed at 6 h, vehicle blood glucose concentration was 7.8 mM, whereas free Oxm, fibrillar Oxm 10 mg kg^{-1}, and fibrillar Oxm 20 mg kg^{-1} were 5.2, 6.3, and 6 mM respectively, all of which were significantly lower than vehicle 6 h after the subcutaneous administration (Fig. 6b). Six hours after administration, an intraperitoneal glucose tolerance test (GTT) was conducted and showed that glucose levels during the test were significantly lower in the fibrillar Oxm group at 20 mg kg^{-1} vs. vehicle at times 45 and 60 min, demonstrating improved glucose tolerance (Fig. 6c). The AUC's calculated during the GTT showed that there was a significant difference vs. vehicle in free and fibrillar groups at both doses (Fig. 6d). The GLP-1 agonist Liraglutide at 0.03 mg kg^{-1} was used as a positive control. These data provide an early insight that nanofibrils of Oxm when dosed in vivo can produce a glucose lowering pharmacodynamic effect, therefore warranting further investigation and optimization as to the therapeutic potential of such formulations.

Oxm nanofibrils prolong peptide serum bioactivity in vivo.

To investigate the application of fibrillar Oxm as a reservoir from which peptide can be released in vivo, we administered the nanofibrils at 5 and 10 mg kg^{-1} s.c. in CD rats and took serum

samples for up to 5 days post-injection. Serum Oxm content was determined as in vitro bioactivity using cell-based hGLP-1R and hGCGR cAMP bioassays, and compared with free Oxm dosed at 5 and 10 mg kg^{-1} s.c. and at 5 mg kg^{-1} i.v. (Fig. 7a, b). At 10 min, Oxm serum concentrations showed an initial peak of 1.34 and 1.85 nM for 5 and 10 mg kg^{-1} of the nanofibrils, respectively, (hGLP-1R cAMP assay), probably due to the presence of free Oxm in the fibrillar sample. This was followed by a steady-state with a constant bioactivity equivalent of 1 nM for 5 days. The hGLP-1R cAMP assay revealed Oxm bioactivity in serum even at 5 days, the final time point we analyzed, at 0.48 nM (after 5 mg kg^{-1}) and 1.16 nM (after 10 mg kg^{-1}; Fig. 7a). Similarly, using the hGCGR cAMP assay, Oxm concentration in serum was 0.91 and 1.19 nM at 5 days after a single injection of 5 and 10 mg kg^{-1}, respectively (Fig. 7b). Overall, with an equivalent of 1 nM Oxm bioactivity detected for 5 days, this study shows a sustained release of Oxm from the nanofibrils in vivo that is characterized by a significantly longer bioactivity than free Oxm. Indeed, Oxm bioactivity is not detected after 2 h post-injection of 5 mg free peptide kg^{-1} (i.v.) or 4 h post-injection of 5 and 10 mg free peptide kg^{-1} (s.c.) (Fig. 7a, b).

The prolongation of Oxm bioactivity is remarkable when considering that no modification has been performed such as engineering poly(ethylene glycol)- and lipid-modified Oxm analogs[4, 24, 26, 45]. The activity of Oxm is limited in vivo by both excretion (i.e., clearance through the kidneys) and enzymatic inactivation through the activity of, for example, dipeptidyl peptidase 4 (DPP4)[46]. Recently, enhanced proteolytic stability was achieved by synthesizing crosslinked Oxm analogs[27]. Even though these analogs showed higher serum stability, their half-life was only prolonged from 0.6 h for the native sequence to 1.9 h for the analogs after s.c. injection.

To further characterize the pharmacokinetic profiles of free and fibrillar Oxm in our rats, a two-compartment model was initially fitted to the i.v. free Oxm hGLP-1R data (5 mg kg^{-1}; Supplementary Fig. 4). Pharmacokinetic parameter estimates (Supplementary Table 4) suggest an elimination half-life of ~13 min for free Oxm, similar to what has been reported in humans[25]. Subsequently, hGLP-1R data for free Oxm following s.c. administration (5 and 10 mg kg^{-1}) were fitted to an absorption model including two parallel routes of absorption, with and without a delay (lag time; Supplementary Fig. 5). Parameters for the i.v. phase were fixed from the previous analysis of i.v. data. Parameter estimates using the hGLP-1R assay data (Supplementary Table 5) suggested that the bioavailability of free Oxm is ~34% (21% using hGCGR data), and the absorption half-lives of the parallel routes, with and without a lag time, calculated as the ratio of ln (2) and the rate constants, were 3.29 (6.78 using hGCGR assay data) and 1.57 (0.86 using hGCGR assay data) h, respectively. These estimates support the notion that free Oxm is absorbed at a slower rate than it is eliminated.

hGLP-1R data from fibrillar Oxm administration (5 and 10 mg kg^{-1}) were fitted to an expanded model that accounts for an additional absorption phase and fibril dissociation, also with two parallel routes with and without a lag time (Supplementary Fig. 6). The possibility of free Oxm being immediately available in the central compartment was also considered, to account for the rapid appearance of a peak of bioactivity in serum (Supplementary Fig. 7). Parameter estimates (Supplementary Table 6) suggest that the absorption phase of fibrillar Oxm was even more rate limiting, with absorption half-lives of up to several days. Given the length of the experiment (5 days), these numerical estimates need to be considered in light of the duration of the experiment, which was shorter than the estimated half-life, but point to a significantly prolonged bioactivity. Interestingly, the data could only be fitted if the central volume of distribution (V_c) was

As discussed above, protein aggregation is a potentially widespread phenomenon with a range of implications in various pharmaceutical and biomedical applications. Consequently, by better understanding the exact mechanism of aggregation it may be possible to develop new, more stable protein based-drugs with higher therapeutic activities. Zapadka and co-workers indicated that in addition to aggregation, formation of amyloid fibril was also an important factor that contributed to structural changes and loss of properties of peptide-based formulations (Zapadka, et al., 2016, p. 1). The research group indicated that the aggregation of proteins and peptides into amyloid fibrils rich with beta-sheets was a common transformation process that could be observed in peptide containing solutions. The formation of these structures substantially reduced the effectiveness of various pharmaceutical products and contributed to yield reduction in the development of new drugs. A considerable number of research efforts were focused on better understanding of the underlying mechanisms resulting in the formation of such amyloid fibrils for specific proteins, however the overall level of understanding remains low. Nevertheless, it was established that agglomeration of proteins as well as formation of amyloid-fibrils proceeded via sigmoidal-like kinetics characterised by a nucleation-polymerisation mechanism. The process was also characterised by the presence of a lag phase during which formation of nucleating species was observed. This lag phase was subsequently followed by a phase of rapid growth with the formation of a plateau in cases where the system reaches equilibrium. Chiti and Dobson indicated that formation of oligomers at low concentrations was also possible along with the formation of fibrils (Chiti & Dobson, 2006, p. 333). A considerable amount of progress was made in describing factors that affect system aggregation. Key factors included internal parameters such as molecular volume, ionic strength, pH, concentration and conformation of monomer and rate of nucleation. Other highly important factors included agitation and changes in temperature. The number of factors that affect formation of oligomers is not limited to those outlined above which highlights the necessity of additional investigations in the area (Zapadka, et al., 2016, p. 2).

Zapadka and co-workers have described how human glucagon-like peptide-1 or GLP-1 is an important biopharmaceutical product. This peptide has found a range of applications in the drug industry in the development of type-2 diabetes drugs. Buell, Dobson and Knowles suggest that formation of GLP-1 based aggregates with the formation of amyloid fibrils occurs at acidic pH and physiological conditions (Buell, et al., 2014, p. 11). From a structural perspective, GLP-1 presents a hormone peptide, containing 31 amino acid residues. The peptide regulates glucose levels in blood through glucose-dependent secretion of insulin. In turn, structural changes in the peptide as well as the impact that pH changes have on these changes can be established using various analytical techniques including far-UV

CD (far-UV circular dichroism), SEC (size-exclusion chromatography), DLS (Dynamic light scattering), MALS (Multiangle light scattering detector) and analytical ultracentrifugation (AUC). Changes in the protein structure as well as its stability and fibrils morphology may be confirmed by using other instrumental techniques including TEM (Transmission Electron Microscopy) and AFM (Atomic Force Microscopy) (Zapadka, et al., 2016, p. 2).

Aggregation kinetics of GLP-1 at various pH were described in the publication by Zapadka and co-workers (Zapadka, et al., 2016, p. 2). The report explains how experimental data could be obtained by using thioflavin T based monitoring of fluorescence. This reagent was shown to increase its fluorescence levels upon forming bonds with beta-sheets of amyloid fibrils. Analysis of the resulting experimental data was focused on the determination of the apparent growth rate as well as lag time that was associated with different concentrations of the peptide and pH. During the conducted experiments it was established that pH had a considerable impact on the overall aggregation kinetics. The research group indicated that the observed results did not correlate with other kinetics patterns, established in the case of similar proteins (Zapadka, et al., 2016, p. 2). Thus, it was established that at pH 8.5 the observed aggregation kinetics could be explained with the aid of a nucleation/polymerisation fibril formation mechanism, however at pH 7.5 it was observed that increases in the peptide concentration were associated with increase in the lag time of aggregation. The obtained results can be explained by the formation of additional intermediary species and oligomers through slow uni-molecular pathways. Both the structure and stability of the corresponding intermediary formations as well as the initial point of the aggregation process can be established using the indicated methods of analysis. Comparing the obtained findings with the previously discussed publications, a range of factors influence the behaviour of proteins in solutions and the impact of each factor is dependent on the structure of the analysed protein or peptide. The process of aggregation involves formation of various intermediary species what may reduce the area of potential applications of the analysed peptides (Zapadka, et al., 2016, p. 3). The results of this study are discussed in section 3.5 below.

A pH-Induced Switch in Human Glucagon-like Peptide-1 Aggregation Kinetics

Karolina L. Zapadka,[†] Frederik J. Becher,[†] Shahid Uddin,[‡] Paul G. Varley,[‡] Steve Bishop,[‖] A. L. Gomes dos Santos,[‡] and Sophie E. Jackson*,[†]

[†]Department of Chemistry, University of Cambridge, Cambridge CB2 1EW, U.K.

[‡]Formulation Sciences, MedImmune Ltd., Granta Park, Cambridge CB21 6GH, U.K.

[‖]Formulation Sciences, MedImmune, One MedImmune Way, Gaithersburg, Maryland 20878, United States

Ⓢ *Supporting Information*

ABSTRACT: Aggregation and amyloid fibril formation of peptides and proteins is a widespread phenomenon. It has serious implications in a range of areas from biotechnological and pharmaceutical applications to medical disorders. The aim of this study was to develop a better understanding of the mechanism of aggregation and amyloid fibrillation of an important pharmaceutical, human glucagon-like peptide-1 (GLP-1). GLP-1 is a 31-residue hormone peptide that plays an important role regulating blood glucose levels, analogues of which are used for treatment of type 2 diabetes. Amyloid fibril formation of GLP-1 was monitored using thioflavin T fluorescence as a function of peptide concentration between pH 7.5 and 8.2. Results from these studies establish that there is a highly unusual pH-induced switch in GLP-1 aggregation kinetics. At pH 8.2, the kinetics are consistent with a nucleation–polymerization mechanism for fibril formation. However, at pH 7.5, highly unusual kinetics are observed, where the lag time increases with increasing peptide concentration. We attribute this result to the formation of off-pathway species together with an initial slow, unimolecular step where monomer converts to a different monomeric form that forms on-pathway oligomers and ultimately fibrils. Estimation of the pK_a values of all the ionizable groups in GLP-1 suggest it is the protonation/deprotonation of the N-terminus that is responsible for the switch with pH. In addition, a range of biophysical techniques were used to characterize (1) the start point of the aggregation reaction and (2) the structure and stability of the fibrils formed. These results show that the off-pathway species form under conditions where GLP-1 is most prone to form oligomers.
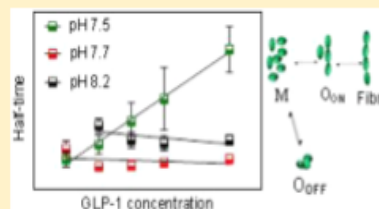
■ INTRODUCTION

The aggregation of peptides and proteins into β-sheet rich amyloid fibrils is a common process increasingly associated with problems in drug development and pharmaceutical applications, as well as many disease states.[1] Although significant progress has been made over the past 15 years in elucidating the structure[2] and morphology[3] of amyloid fibrils and their mechanism of formation,[4,5] our current understanding of how peptides and proteins aggregate into fibrils remains incomplete. It has been shown that amyloid fibrils are commonly formed through a nucleation–polymerization (N–P) mechanism with characteristic sigmoidal-like kinetics. There is an initial lag phase, during which critical nucleating species are formed, which is followed by a rapid growth phase, and then a plateau as either the system reaches equilibrium or the monomer levels are completely depleted.[6,5]

Oligomers have often been observed to form during fibril formation, albeit at sometimes very low concentrations.[7,8] However, many aspects of the relationship between oligomers and the mechanism of fibril formation are not yet fully understood.[8] Considerable progress has been made in understanding some of the factors affecting the aggregation propensity of a system, which has been shown to depend upon sequence,

monomer conformation, nucleation rate, effective monomer concentration, pH, ionic strength, small molecules, and external factors such as temperature or agitation.[5,9,10]

In this work, we focus on the human glucagon-like peptide-1, GLP-1(7–37), which is a 31-residue hormone peptide.[11] GLP-1 plays an important role in our body regulating blood glucose levels through regulation of glucose-dependent insulin secretion, inhibition of glucagon secretion, and gastric emptying together with reduction of food intake.[11] It is an important pharmaceutical molecule, analogues of which are used for the treatment of type 2 diabetes.[11,12] It has previously been reported that GLP-1 aggregates into amyloid fibrils under physiological conditions[13] and at pH 5.8.[14]

Here, we present the results of a detailed study of the pH dependence of the aggregation kinetics of GLP-1. Aggregation kinetics were monitored by thioflavin T (ThT), which increases its fluorescence upon binding to β-sheet rich amyloid fibrils.[5] Kinetic data from these experiments were analyzed to obtain the apparent growth rate, $t_{1/2}$, and lag time at different peptide concentrations and pH values.

We report an unusual pH-induced switch in GLP-1 aggregation kinetics.

In order to understand the complex, pH-dependent aggregation kinetics obtained, a detailed characterization of freshly prepared samples of GLP-1 was undertaken using a range of biophysical techniques to obtain information on the size, structure, and oligomeric state of species present. This included analytical ultracentrifugation (AUC), asymmetric flow field-flow fractionation (AF4) with multiangle light scattering detector (MALS), dynamic light scattering (DLS), size-exclusion chromatography (SEC), far-UV circular dichroism (far-UV CD), and ANS-binding assays. In all cases, fibrils formed were confirmed using atomic force microscopy (AFM) and transmission electron microscopy (TEM) providing information on the structure, stability, and morphology of the fibrils and how this depends upon pH.

■ EXPERIMENTAL SECTION

Materials. The 31-residue GLP-1(7−37) (HAEGTFTSDVSSYLE-GQAAKEFIAWLVKGRG) was purchased from Bachem (98.5% pure), with a molecular weight of 3.36 kDa and used without further purification. GLP-1 powder was dissolved in buffer (25 mM sodium phosphate at pH 7.5 or 25 mM Tris-HCl at pH 8.0 or 8.5) to a final concentration of 298 μM. The solution was filtered (0.22 μm filter) prior to use, and the concentration was determined spectrophotometrically using a NanoDrop spectrophotometer (ND 2000, Thermo Scientific) and a theoretical extinction coefficient of 6990 M^{-1} cm^{-1} at 280 nm. All other chemicals were of analytical grade.

Kinetics of Aggregation: Thioflavin T Binding Assays. For kinetic experiments, a stock solution of 298 μM GLP-1 in buffer was prepared, as described above. Final concentrations of GLP-1 were 25, 50, 75, 100, and 150 μM, and the samples were incubated with 50 μM ThT and 0.01% NaN$_3$ (added to prevent bacterial growth). The 50 μM concentration for ThT was chosen as the aggregation kinetics were shown to be independent of ThT concentration between 10 and 80 μM ThT, Figure S1. The peptide/ThT samples (120 μL) were pipetted into a 96-well half-area plate made of black polystyrene with a clear bottom and a nonbinding surface (Corning 3881, USA). A sealing tape (Costar Thermowell) was used to protect samples from evaporation. Fluorescence measurements were carried out on a Fluorostar Optima Microplate Reader (BMG Labtech, Offenburg, Germany), which was thermostated at 37 °C. ThT binding to fibrils was monitored by using an excitation filter at 440 nm and recording the fluorescence emission at 480 nm. Bottom reading of the plate every 30 min with 5 min of shaking prior to each measurement was performed. Each cycle was executed with the orbital shaker at 350 rpm, 5 flashes per well, and fluorescence measurements were made at a gain of 1000.

Each individual ThT data set was fit to eq 1,

$$y = y_0 + A/(1 + \exp(-k(t - t_{1/2}))) + bt \qquad (1)$$

where y_0 is the starting fluorescence, A is the amplitude of the transition, $t_{1/2}$ is the half-time, which is defined as the time at which the ThT fluorescence has reached 50% of its final baseline value, k is the apparent growth rate, and b is the slope of the final baseline. Note in many other studies, data are normalized prior to fitting such that the inclusion of this additional term is not needed. The lag time was calculated from the kinetic parameters obtained using eq 2:[15,20]

$$t_{lag} = t_{1/2} - 2/k \qquad (2)$$

All measurements were made in triplicate for each peptide concentration in a single 96-well plate, and each experiment was repeated at least three times on different days with freshly prepared samples.

Analytical Ultracentrifugation (AUC) Sedimentation Velocity Experiment. Sedimentation velocity measurements were performed at 20 °C, 60 000 rpm using a Beckman Optima XL-I analysis

ultracentrifuge equipped with an An-60Ti rotor. The instrument was equipped with a UV−visible absorbance detector. GLP-1 (150 μM) was prepared in buffer and incubated at room temperature for 2 h before the start of the experiment. The sample (400 μL) was loaded into the AUC cell. The SEDFIT program was used to correct the sedimentation coefficient distributions to standard conditions, and the c(s) method was implemented (www.analyticalultracentrifugation.com/default.htm).

Asymmetric Flow Field-Flow Fractionation with Multiangle Light Scattering (AF4-MALS). AF4-MALS was used to separate and estimate the size of species in a 1500 μM solution of freshly prepared GLP-1 sample in buffer using an Eclipse (Wyatt Technology Europe GmbH, Dernbach, Germany). The AF4 was controlled by a high-performance liquid chromatography system (HPLC, Agilent) equipped with UV/vis and MALS detectors (Wyatt Technology Europe GmbH, Dernbach, Germany). A 1 kDa cutoff poly(ether sulfone) (PES) membrane was used in the Eclipse SC channel for optimal separation of species (Pall, New York, USA). Buffer was used as the mobile phase, and the system was equilibrated overnight prior to the experiment. The channel flow was maintained at 1 mL min^{-1}, and the cross-flow was varied: 4.5 mL min^{-1} from 0 to 2 min, 2.5 mL min^{-1} from 2 to 5 min, 4.5 mL min^{-1} from 5 to 15 min, 4 mL min^{-1} from 15 to 20 min then 1 mL min^{-1} from 20 to 30 min. Detection was accomplished using UV absorbance at 280 nm and multiangle light scattering. Data from MALS were analyzed by ASTRA (Wyatt Technology Europe GmbH, Dernbach, Germany). The detectors were calibrated using BSA standards (Thermo Scientific). The calibration was validated by separation of 25 μL of 2 mg mL^{-1} BSA in an appropriate mobile phase.

Dynamic Light Scattering (DLS). The intensity-weighted mean hydrodynamic diameter distribution and the number size distribution of freshly prepared GLP-1 (1500 μM) and fibrillar GLP-1 (1500 μM) in buffer at room temperature (20−25 °C) were determined by DLS using a Zetasizer Nano ZS (Malvern Instruments, Malvern, U.K.). A Zen 2112 cuvette and a scattering angle of 173° were used. The average values of the polydispersity index (PdI) were obtained from the cumulants analysis of the intensity autocorrelation function that was performed by the Zetasizer Software provided by the manufacturer. Reported parameters were determined from an average of at least three measurements.

Atomic Force Microscopy (AFM). GLP-1, from either (i) a freshly prepared solution or (ii) mature fibrils, was spread onto freshly cleaved mica (SPI supplies, West Chester, PA). The samples were then incubated for 20 min, followed by washing with 200 μL of deionized water, and dried under a stream of nitrogen. Images were acquired in air at room temperature (20−25 °C) with a PicoPlus AFM instrument with a PicoSPM II controller from Molecular Imaging (Agilent Technologies, USA) in AC mode, equipped with a MikoMasch NSC26/No Al cantilever, between 65 and 130 Hz frequency, force constant varying from 0.6 to 2.0 N m^{-1} (Innovative Solutions Bulgaria Ltd., Sofia, Bulgaria). The images were analyzed with the open source software Gwyddin (http://gwyddion.net/).[16]

■ RESULTS AND DISCUSSION

Aggregation Kinetics. The aggregation kinetics of amyloid fibril formation were measured starting from freshly prepared samples of GLP-1 at three different pH values using ThT fluorescence. The aggregation was monitored over a range of peptide concentrations from 25 to 150 μM. Typical results are shown in Figure 1. Kinetic parameters were determined by fitting the data to eq 1, and a lag time was then calculated for each data set using eq 2. Standard sigmoidal curves were obtained for GLP-1 aggregation under all the conditions used; however, the kinetic parameters obtained from the fitting varied with pH and peptide concentration, Figure 1. See SI2, Table S1, for further details.

At higher pH ($\geq$8.2), the $t_{1/2}$ is found to decrease with increasing peptide concentration characteristic of a process
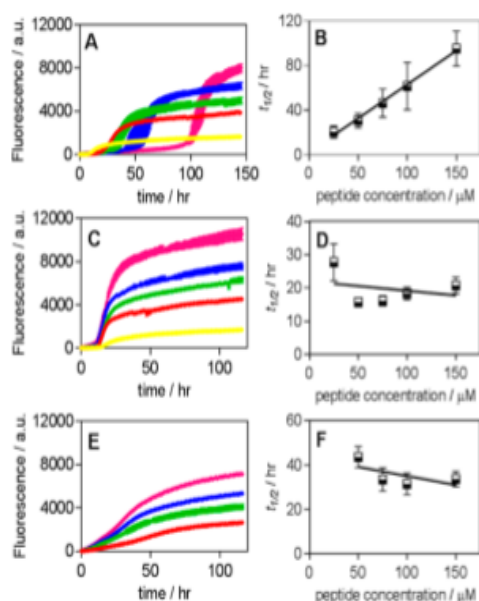
Figure 1. Aggregation kinetics of GLP-1 as a function of peptide concentration at different pHs. GLP-1 aggregation kinetics at pH 7.5 (A,B), pH 7.7 (C,D), and pH 8.2 (E,F). Panels A, C, and E show typical traces for the fibrillation of GLP-1 followed by ThT fluorescence at different GLP-1 concentrations. Each peptide concentration was run in triplicate. Panels D, E, and F show the dependence of the $t_{1/2}$ on the concentration of GLP-1. The error bars shown in panels A, C, and E are the standard deviation from the mean for a single experiment in which each peptide concentration was run in triplicate. In panels B, D and F, the error bars correspond to the standard deviations of the kinetic parameters determined from three independent experiments each of which was run in triplicate.

following a nucleation–polymerization mechanism for fibril formation, Figure 1F. Surprisingly at lower pH values there is either very little dependence on peptide concentration or the $t_{1/2}$ increases with increasing peptide concentration, Figure 1D,B. These results were very reproducible. The highly unusual kinetics were observed for GLP-1 aggregation at pH 7.5 where the $t_{1/2}$ increases with increasing peptide concentration (the opposite of what is expected for a N–P model) suggesting that other processes come into play, Figure 1B. These unusual results have, to the best of our knowledge, been observed for just two other systems: ribosomal protein S6 (where a model involving an off-pathway oligomerization process was proposed)[17] and immunoglobulin light chain (where an increase in concentration leads to a monotonic decrease in fibrillation propensity, which has been related to dimer formation in the native state).[18]

In order to assess the degree to which GLP-1 monomer is converted into amyloid fibrils in the ThT assays, monomer depletion experiments were also undertaken, SI3. Using UPLC methods (ultrapressure liquid chromatography), the loss in signal corresponding to monomeric or small soluble oligomers of GLP-1 was monitored with time, Figure S2. After 120 h at pH 7.7 at 37 °C, a solution of 75 μM GLP-1 was almost completely converted into high molecular weight species, Figure S3.

Characterization of Freshly Prepared Samples of GLP-1 in Buffer, at the Starting Point of the Kinetic Assays, at Different pH Values. A wide range of biophysical techniques were used to fully characterize the structure and properties of

freshly prepared samples of GLP-1 at pH 7.5, 8.0, and 8.5. The structure of species in solution was probed using far-UV CD, and the hydrophobic surface area was probed using ANS-binding assays, while the size of species in solution was investigated using SEC, AF4, AUC, DLS, AFM, and TEM; see the following sections.

Characterization of the Structure and Hydrophobicity of Freshly Prepared GLP-1 Samples. The far-UV CD spectra of freshly prepared samples of GLP-1 show that there is no change in the secondary structure with pH, Figure S4. The average secondary structure is predicted to be approximately 30% α-helix, 20% β-strand, 20% turns, and 30% disordered between pH 7.5 and 8.5. ANS binding was also used to probe the exposed hydrophobic surface area.[19] ANS binding to freshly prepared samples of GLP-1 at different pH values was assessed using fluorescence measurements over a range of peptide concentrations, see SI5 Figure S5. The data clearly indicate that GLP-1 is more highly prone to form oligomers with exposed hydrophobic surface area at pH 7.5 relative to pH 8.0 or 8.5.

Characterization of the Size Distribution of Species in Freshly Prepared GLP-1 Samples. The size distribution of species in freshly prepared samples of GLP-1 was performed using a range of biophysical techniques from pH 7.5 to 8.5. Although standard size-exclusion chromatography was useful to give an initial assessment of the size of the major species in solution for GLP-1 at different pH values (see SI6, Figure S6), this method was unable to detect small populations of larger species. To do this, more sophisticated methods of analysis were required. Using AF4, we were successfully able to detect and separate monomeric GLP-1 from small oligomers present in the samples at both pH 8.0 and 8.5 (Figure 2C and E).
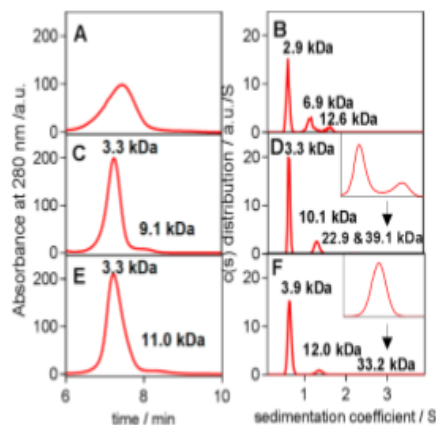
Figure 2. Size distribution of species in freshly prepared GLP-1 samples at different pHs determined using AF4 and AUC: (A,B) pH 7.5, (C,D) pH 8.0, and (E,F) pH 8.5. The left-hand column shows the AF4 results (A, C, and E) along with the M_w of monomers and small oligomers estimated using MALS (see section SI7, Figure S7, for more detail). The right-hand column shows the results of the AUC sedimentation velocity analysis of the GLP-1 samples illustrating the size distribution of sedimenting species obtained by c(s) analysis.

At pH 8.0 and 8.5, the distinct peaks observed likely correspond to a monomer and trimer with molecular weights of, 3.3 and 9.1 kDa at pH 8.0 and 3.3 and 11 kDa at pH 8.5. However, at pH 7.5, a single broad peak was observed suggesting a high level of heterogeneity of species in solution at this pH compared with the higher pHs, Figure 2A. See SI7, Figure S7, for further detail.

Analytical centrifugation measurements of sedimentation velocities were also performed, and as with the AF4 data, similar velocity profiles were obtained at pH 8.0 and 8.5, (Figure 2D,F). In these cases, the samples are mainly monomeric; however, small populations of both small and larger oligomers are present, Figure 2D,F, inset figures, and Table 1. Interestingly, the

Table 1. Percentage of Oligomeric Species Present in Freshly Prepared GLP-1 Samples[a]

	percentage of the species present (%)		
pH	monomer	small oligomers	larger oligomers
7.5	64	36	b
8.0	77	21.5	1.5
8.5	90	9.7	0.3

[a]For more information, see section SI10, Table S4. [b]Not observed.

sedimentation velocity profile at pH 7.5 shows mainly monomer, Figure 2B; however, the sample is much more polydisperse in comparison to the results at higher pH values. At pH 7.5, larger oligomers are not present, Table 1 and Figure 2B. Molecular masses corresponding to a trimer determined using AUC were 12 kDa at pH 8.5 and 10 kDa at pH 8.0. At 7.5, oligomeric species ranged from 6.9 to 12.6 kDa corresponding to a mix of dimer, trimer, and tetramer, Figure 2. See SI7, Figure S7, for further detail.

Dynamic light scattering (DLS), a technique that is sensitive to large particles in solution, was also used to probe whether larger oligomeric species not detectable by AF4 or AUC are present in solution. The DLS results (Figure 3) confirmed that
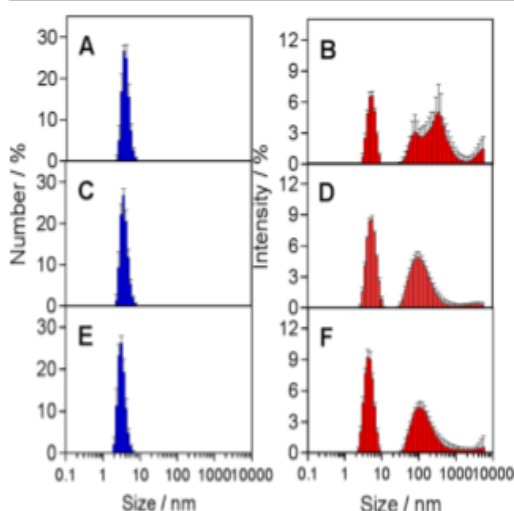

Figure 3. Dynamic light scattering results of freshly prepared GLP-1 at three different pHs: (A,B) pH 7.5, (C,D) pH 8.0, and (E,F) pH 8.5. The left-hand column shows the size distribution by number (A, C, and E), and the right-hand column shows the size distribution by intensity (B, D, and F). See section SI8, Figure S8, for more detail.

the main population has a small hydrodynamic radius that likely corresponds to GLP-1 monomer and the small oligomers detected by AF4 and AUC, Figure 2. However, larger particles were also found to be present under all conditions, Figure 3. These were also observed in both AFM and TEM images (see SI9, Figure S9).

Fibril Structure and Morphology. The structure of the fibrils formed at the end of the ThT assays was investigated by

far-UV CD, Figure S4C. Although the spectra recorded at the three pH values are slightly different, they all show a broad minima around 218 nm characteristic of amyloid fibrils, Figure S4C. AFM was also used to verify and characterize the fibrils formed under different conditions, Figure 4. In these cases, 150 μM
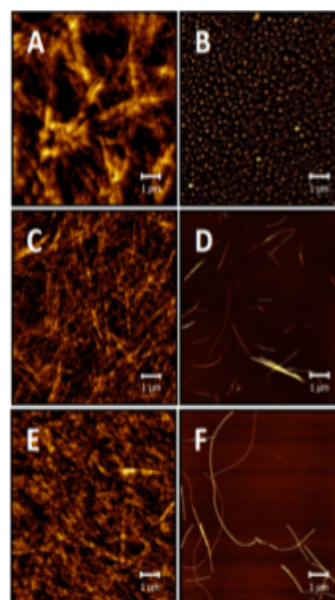

Figure 4. Atomic force microscopy images of typical GLP-1 fibrils formed under different conditions: (A,B) pH 7.5, (C,D) pH 8.0, and (E,F) pH 8.5. The left-hand column shows AFM images of samples of 150 μM GLP-1 aggregated for 200 h at 37 °C. The right-hand column shows AFM images of the fibrils diluted 100 times into deionized water prior to imaging (see section SI11, Figure S10, for more details).

GLP-1 samples at pH 7.5, 7.7, and 8.2 were allowed to aggregate at 37 °C for 200 h in the presence of 50 μM ThT and 0.01% NaN₃. Fibrils were then retrieved and imaged using AFM, Figure 4.

Fibrils formed at 37 °C, pH 7.7 and 8.2, are stable and typically 1−3 μm in length and 10−15 nm in height, and have a twist (Figure 4 and SI11, Figure S10). In contrast, the fibrils formed at pH 7.5 are short, thin, sticky, and considerably more heterogeneous, Figure 4. In addition, at pH 7.5, fibrils are unstable and dissociate after dilution (100-fold) either in water or buffer, Figure 4B (see SI11, Figure S10, for more detail). After dilution spherical-like morphologies are observed with diameters ranging from 0.1 to 0.4 μm and heights ranging between 10 and 60 nm, Figure 4B.

A Model for GLP-1 Aggregation under Different Conditions. The concentration of peptide[20,21] and the presence of on-pathway oligomers[22] are both known to be important in the formation of amyloid fibrils. Increasing peptide concentration usually leads to an increase in the rate of fibrillation as observed by a reduction in lag time,[6,20] a feature that is typical of a nucleation−polymerization mechanism.[20] For GLP-1 at pH values over 8.0, an inverse relationship between lag time and peptide concentration is observed, and in this case, a simple nucleation−polymerization mechanism can be proposed where monomer (M) first associates into oligomers (O_on) that are on-pathway to fibril formation, Figure 5. For GLP-1, under these conditions, this is a slow nucleated
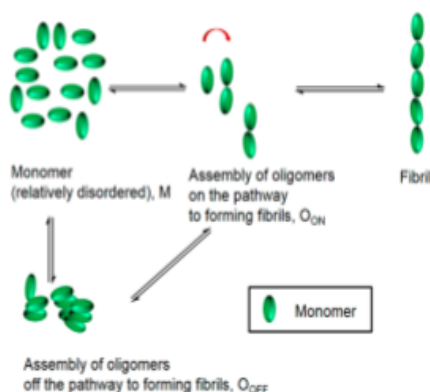
Figure 5. Proposed mechanism for GLP-1 fibril formation. There are two pathways, one in which the monomer (M) associates to form on-pathway oligomers (O_{ON}), which can convert directly into fibrils. On the second pathway, monomers can form a different oligomeric state (O_{OFF}), which is not on the direct pathway to fibril formation. The on- and off-pathway oligomers may be able to interconvert; however, the energy barriers to interconversion are likely high and the kinetics slow.

process, which leads to the specific formation of stable fibrils, which are long, stable, and twisted, Figure 4.

However, the simple nucleation–polymerization model does not explain the unusual kinetic data obtained at pH 7.5. Under these conditions, we propose a more complex model in which there is competition between the formation of on-pathway oligomers leading to fibrils and the formation of a different form of oligomer, which has to be off-pathway, Figure 5. Powers and Powers have elegantly modeled such a mechanism mathematically.[23] They have shown that, under specific kinetic conditions where a set of assumptions can be applied, a positive slope is obtained for a plot of $t_{1/2}$ versus the concentration of monomer.[23] They propose that this is an essential piece of evidence consistent with their off-pathway model.[23] This is what we observe for GLP-1 at pH 7.5, Figure 1B.

We are not the first to observe such dependence experimentally and propose a kinetic scheme in which off-pathway as well as on-pathway oligomeric species form. This has also been observed in the fibrillation of immunoglobulin light chain LEN[18] and S6 ribosomal protein.[17] In both these cases, the polypeptide starts as a globular folded protein rather than a relatively unstructured and dynamic short peptide such as GLP-1. Here, we present strong evidence that off-pathway oligomers are also populated during the fibrillation of GLP-1 at pH 7.5, highlighting this as a more general phenomenon and putting the concept proposed some years ago on firm experimental ground.

Kinetic Modeling of On- and Off-Pathway Oligomer Models. In order to verify that an off-pathway species would give rise to the difference in aggregation kinetics observed, three models for the fibrillation of GLP-1 were created within the program KinTek (see SI12 for further details). In the first model (model 1), we used a simple model of nucleation–polymerization and demonstrated that the kinetic parameter $t_{1/2}$ decreases with increasing peptide concentration as expected, Figure S11A,C. We then added an off-pathway reaction where monomer converts through monomer addition to create a series of off-pathway oligomers and added this to our starting nucleation-polymerization model to generate model 2. This model also shows a decrease in $t_{1/2}$ with increasing peptide concentration, Figure S11B,D. However, addition of the off-pathway oligomers to the reaction scheme in model 1 resulted

in a delay in $t_{1/2}$ as shown in Figure S11E,F, which shows the amount of fibril formation (in terms of monomer concentration) with time at 25 and 150 μM monomer starting concentrations. The value of $t_{1/2}$ increased on addition of the off-pathway species, from 53 to 94 h at 25 μM and from 8.6 to 16 h at 150 μM monomer. These results confirm that the presence of off-pathway species results in an increase in the length of time it takes for sufficient nuclei to be formed; however, model 2 does not fully explain the results obtained for GLP-1. A third model, model 3, which was essentially the same as model 2 except an additional unimolecular step was included where monomers M interconvert with a different form of monomer, M*, and only M* forms the on-pathway oligomers required for fibril formation, was created. In this case, the dependence of the $t_{1/2}$ on initial monomer concentration switches such that it increases with increasing starting concentration, Figure S11H, as we observe experimentally for GLP-1 at pH 7.5.

Thus, our results on GLP-1 at pH 7.5 are consistent with the presence of off-pathway oligomeric species as well as a unimolecular step on-pathway to fibril formation.

Studies on rat and human isoforms of the amyloidogenic protein IAPP, associated with diabetes in humans, have recently established that various oligomeric species can be found under conditions where human IAPP forms amyloid fibrils.[24] In this case, a detailed analysis of the structure and properties of the different oligomers revealed that only the globally flexible, low-order oligomers, which did not bind ANS nor have extensive β-sheet secondary structure, were toxic to cells.[24] These results raise the interesting question of whether the on- and off-pathway oligomers that we have shown form at different pH values for GLP-1 may also have different properties including potentially different cell toxicity.

Origin of the pH-Induced Switch in Mechanism for GLP-1 Aggregation. *Net Charge on the Peptide in Its Monomeric State.* It is well established that the total charge on a peptide or protein can play an important role in determining its propensity toward aggregation.[25,26] Normally, the closer the net charge is to zero the higher propensity to aggregate, as there are little or no unfavorable electrostatic interactions to overcome to form oligomeric species and nuclei.[25]

In order to better understand our results, we used PropKa in the Schrodinger Suite to calculate the pK_a values and therefore the charge on each ionizable group in GLP-1 as a function of pH, SI13. Two structures were used as starting points: 1D0R, which is an ensemble of structures calculated from NMR experiments performed in trifluoroethanol (TFE), Figure S12A,B, and 3IOL, the structure of GLP-1 bound to its receptor. In both cases, GLP-1 is highly helical with more residues involved in α-helix formation than our far-UV CD data in aqueous buffer suggest, Figure S4. However, as no unbound structure for GLP-1 in water is available, these structures were used. Both structures gave very similar results, SI13, Figures S12 and S13. The charge on each ionizable group and the overall net charge on the peptide are shown in Figure S12C,D, respectively. The results show that there are two ionizable groups that change ionization state between pH 7.5 and 8.5: the N-terminus and the side chain of His1. The pK_a of His1 is <7, while that of the N-terminus is approximately 8. The pK_a of the N-terminus is affected by the fact that it can form hydrogen bonds with backbone amide groups as observed in the ensemble of structures generated from the NMR data, Figure S12B. On the basis of these results, we propose that the protonation state of the N-terminus plays a

Article

critical role in the formation of off-pathway oligomers. When positively charged, that is, at pH values below its pK_a of approximately 8, off-pathway oligomers are favored over on-pathway oligomers. In contrast, at pH values above its pK_a, when it is uncharged, on-pathway oligomers are favored. Thus, analogs of GLP-1 that are N-terminally acetylated may well not show this unusual behavior.

Do the aggregation kinetics of GLP-1 follow the general rule that aggregation propensity increases the lower the net charge on the peptide?[25,26] The pK_a calculations suggest that GLP-1 has no overall net charge at approximately pH 5.5, Figure S12D and S13B. However, aggregation kinetics cannot be measured at this pH due to solubility problems. The net charge is predicted to increase between pH 7.5 and 8.5 due to the deprotonation of the N-terminus (from an overall net charge of approximately $-1/-2$ to $-2/-3$, Figure S12D and S13B). Experimentally, we observe an increase in the propensity of GLP-1 to form fibrils, counter to what might be expected. However, one can argue that there is an increase in the aggregation propensity of GLP-1 as its overall charge reduces, i.e., moving toward pH 5.5, but that it is an increased tendency to form off-pathway oligomers not on-pathway oligomers that would lead to amyloid fibril formation. In this regard, it is important to define specifically the aggregation state, as many such states (on- and off-pathway oligomers, fibrils, etc.) may exist.

Net Charge on the Peptide in the Oligomers. The discussion above relates to the net charge and pK_a values of ionizable groups in a highly helical, monomeric form of GLP-1. We cannot rule out that it is not the net charge of the monomer that is important, but the net charge and pK_a values of ionizable groups in the different oligomeric species that play the dominant role in the pH effects observed. Our results suggest that differences in the size and structure of the on- and off-pathway oligomers may lead to different responses to changes in pH over the range studied. In particular, the stability or the kinetics of formation/dissociation of the two oligomeric species may have different pH dependencies.

CONCLUSIONS

In conclusion, we have presented unusual aggregation kinetic data for GLP-1 at pH 7.5, where the lag time increases with increasing peptide concentration. These results indicate the likely existence of off-pathway oligomeric species, which we believe form rapidly relative to the on-pathway oligomers and which therefore act as a sink of monomers. These off-pathway oligomers will slowly dissociate and can therefore, in time, form on-pathway oligomers and ultimately fibrils. However, in addition there has to be an initial unimolecular conversion of the monomer to a different monomeric species, which can form on-pathway oligomers and ultimately fibrils. At pH 7.5, the fibrils formed by GLP-1 are short and unstable. At slightly higher pH values, pH $\geq$ 8.2, the aggregation kinetics of GLP-1 revert back to the simple and frequently observed nucleation–polymerization mechanism where only on-pathway oligomers are formed to any extent.

Using a number of biophysical techniques, we were successfully able to detect a range of small oligomers present in GLP-1 samples at all the pH values studied, establishing that monomeric GLP-1 is in equilibrium with either a dimer or a trimer, as well as and other slightly larger oligomeric species even in freshly prepared samples of very pure peptide. The results demonstrate that at pH 7.5, GLP-1 has a higher propensity to form oligomeric species, consistent with our proposed

mechanism under these conditions where there is a rapid and nonspecific aggregation of GLP-1 into oligomers that are off-pathway.

It is also of interest to note that, under conditions where GLP-1 is very prone to forming oligomers (pH 7.5), the fibrils that it forms are short and relatively unstable. In contrast, increasing the pH by as little as 0.5 has a dramatic effect. Slightly higher pH values, where the monomeric form is more stable and therefore small oligomers much less prevalent at the beginning of the reaction, favors the formation of on-pathway oligomers and ultimately the formation of much more stable fibrils, which are long and twisted.

ASSOCIATED CONTENT

Supporting Information

The Supporting Information is available free of charge on the ACS Publications website at DOI: 10.1021/jacs.6b05025.

> Supplementary results on the design and control of experiments to confirm the presence of small oligomers in freshly prepared samples of GLP-1, together with detailed aggregation kinetic data, experimental procedures for AFM imaging and the determination of fibril morphology, and supplementary figures and tables described in the paper (PDF)

AUTHOR INFORMATION

Corresponding Author
*sej13@cam.ac.uk

Notes
The authors declare no competing financial interest.

ACKNOWLEDGMENTS

REFERENCES

(1) Frokjaer, S.; Otzen, D. E. *Nat. Rev. Drug Discovery* **2005**, *4* (4), 298.

(2) Greenwald, J.; Riek, R. *Structure (Oxford, U. K.)* **2010**, *18* (10), 1244.

(3) Tycko, R.; Wickner, R. B. *Acc. Chem. Res.* **2013**, *46* (7), 1487.

(4) Eichner, T.; Radford, S. E. *Mol. Cell* **2011**, *43* (1), 8.

(5) Arosio, P.; Knowles, T. P. J.; Linse, S. *Phys. Chem. Chem. Phys.* **2015**, *17*, 7606.

(6) Cohen, S. I. A; Vendruscolo, M.; Dobson, C. M.; Knowles, T. P. J. *J. Mol. Biol.* **2012**, *421*, 160.

(7) Chiti, F.; Dobson, C. M. *Annu. Rev. Biochem.* **2006**, *75* (1), 333.

(8) Fändrich, M. *J. Mol. Biol.* **2012**, *421* (4–5), 427.

(9) Buell, A. K.; Galvagnion, C.; Gaspar, R.; Sparr, E.; Vendruscolo, M.; Knowles, T. P. J.; Linse, S.; Dobson, C. M. *Proc. Natl. Acad. Sci. U. S. A.* **2014**, *111* (21), 7671.

Article

(10) Buell, A. K.; Dobson, C. M.; Knowles, T. P. J. *Essays Biochem.* **2014**, *56* (1), 11.

(11) Drucker, D. J. *Nat. Clin. Pract. Endocrinol. Metab.* **2005**, *1* (1), 22.

(12) Drucker, D. J. *Diabetes* **2015**, *64* (2), 317.

(13) Poon, S.; Birkett, N. R.; Fowler, S. B.; Luisi, B. F.; Dobson, C. M.; Zurdo, J. *Protein Pept. Lett.* **2009**, *16* (12), 1548.

(14) Jha, N. N.; Anoop, A.; Ranganathan, S.; Mohite, G. M.; Padinhateeri, R.; Maji, S. K. *Biochemistry* **2013**, *52* (49), 8800.

(15) Alvarez-Martinez, M. T.; Fontes, P.; Zomosa-Signoret, V.; Arnaud, J. D.; Hingant, E.; Pujo-Menjouet, L.; Liautard, J. P. *Biochim. Biophys. Acta, Proteins Proteomics* **2011**, *1814* (10), 1305.

(16) Nečas, D.; Klapetek, P. *Open Physics* **2012**, *10* (1), 181.

(17) Deva, T.; Lorenzen, N.; Vad, B. S.; Petersen, S. V.; Thørgersen, I.; Enghild, J. J.; Kristensen, T.; Otzen, D. E. *Biochim. Biophys. Acta, Proteins Proteomics* **2013**, *1834* (3), 677.

(18) Souillac, P. O.; Uversky, V. N.; Fink, A. L. *Biochemistry* **2003**, *42* (26), 8094.

(19) Lindgren, M.; Sörgjerd, K.; Hammarström, P. *Biophys. J.* **2005**, *88* (6), 4200.

(20) Nielsen, L.; Khurana, R.; Coats, A.; Frokjaer, S.; Brange, J.; Vyas, S.; Uversky, V. N.; Fink, A. L. *Biochemistry* **2001**, *40* (20), 6036.

(21) Powers, E. T.; Powers, D. L. *Biophys. J.* **2006**, *91* (1), 122.

(22) Lorenzen, N.; Nielsen, S. B.; Buell, A. K.; Kaspersen, J. D.; Arosio, P.; Vad, B. S.; Paslawski, W.; Christiansen, G.; Valnickova-Hansen, Z.; Andreasen, M.; Enghild, J. J.; Pedersen, J. S.; Dobson, C. M.; Knowles, T. P. J.; Otzen, D. E. *J. Am. Chem. Soc.* **2014**, *136* (10), 3859.

(23) Powers, E. T.; Powers, D. L. *Biophys. J.* **2008**, *94* (2), 379.

(24) Abedini, A.; Plesner, A.; Cao, P.; Ridgway, Z.; Zhang, J.; Tu, L.-H.; Middleton, C. T.; Chao, B.; Sartori, D.; Meng, F.; Wang, H.; Wong, A. G.; Zanni, M. T.; Verchere, C. B.; Raleigh, D. P.; Schmidt, A. M. *eLife* **2016**, *5*, e12977.

(25) Chiti, F. In *Protein Misfolding, Aggregation and Conformational Diseases: Part A: Protein Aggregation and Conformational Diseases*; Uversky, V., Fink, A., Eds.; Springer: New York, 2007; pp 47−50.

(26) Roberts, C. J. *Trends Biotechnol.* **2014**, *32* (7), 372.

3.0 Results

The key results from each publication submitted for consideration under this thesis are described below.

3.1 Application of NMR spectroscopy in characterisation of monoclonal antibodies

Kheddo and co-workers applied the methods described in the previous sections based on proton NMR spectroscopy to characterise formulations containing monoclonal antibodies in arginine glutamate-based solutions (Kheddo, et al., 2014, p. 1246). Thus, in the first section of the experimental work it was required to use one dimensional proton NMR spectroscopy to establish stability of monoclonal antibodies with the addition of arginine glutamate. The results obtained by the research group are summarised on the figure 3.1 below:
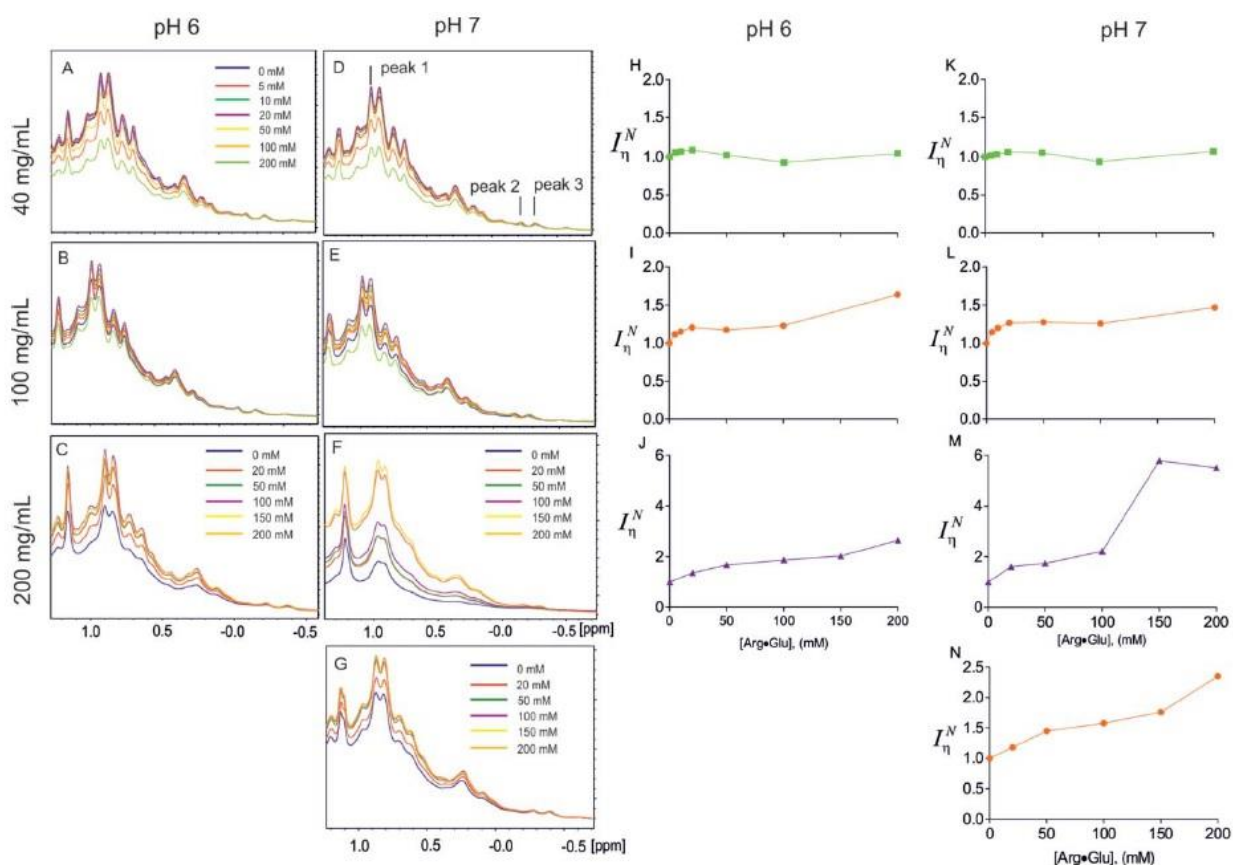
Figure 3.1: Correlation between the addition of arginine glutamate and NMR signals of monoclonal antibodies, adapted from (Kheddo, et al., 2016, p. 1246).

In figure 3.1 above, slides A-G represent selected regions of proton NMR spectra of monoclonal antibodies at tow pH values with corresponding concentrations of components. In cases A-F CP (10 mM) buffer was used to produce the corresponding solutions. For comparison purposes, panel G included spectral data of 100 mg/mL monoclonal antibodies, obtained with no addition of arginine

glutamate. Dependencies between intensities of the recorded peaks and corresponding viscosity of the tested solutions are represented in figures H-N, figure 3.1. Trends represented in figure 3.1 indicated that at protein concentrations below 40 mg/mL self-association of the tested protein samples was low. In turn, intensities of the signals marginally decreased with increasing concentrations of arginine glutamate. The observed decrease was proportional to increasing viscosity of the solution.

During a second set of experiments, Kheddo and co-workers aimed to carry out stability investigations on monoclonal antibodies by combining proton NMR with size-exclusion chromatography. The corresponding investigations suggest, that with the aid of proton NMR, it was possible to quantify the amounts of both monomeric and low oligomeric protein concentrations that remain in the solution. As the result it was decided to employ the same method of analysis to monitor possible changes with monoclonal antibodies as well as the corresponding degradation with time in various formulations. The obtained results are summarised in figure 3.2 and 3.3.
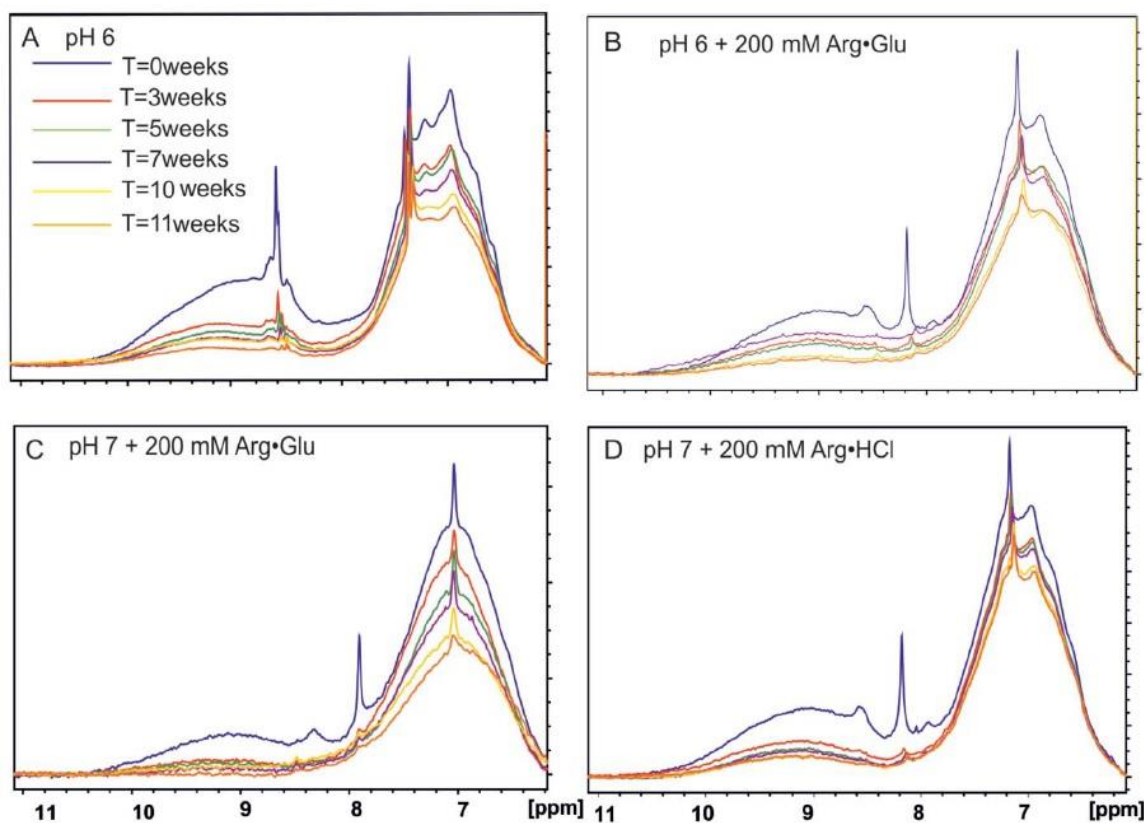

Figure 3.2: Representation of NMR long-term data, describing changes in monoclonal antibodies in the analysed formulations, adapted from (Kheddo, et al., 2016, p. 1248).
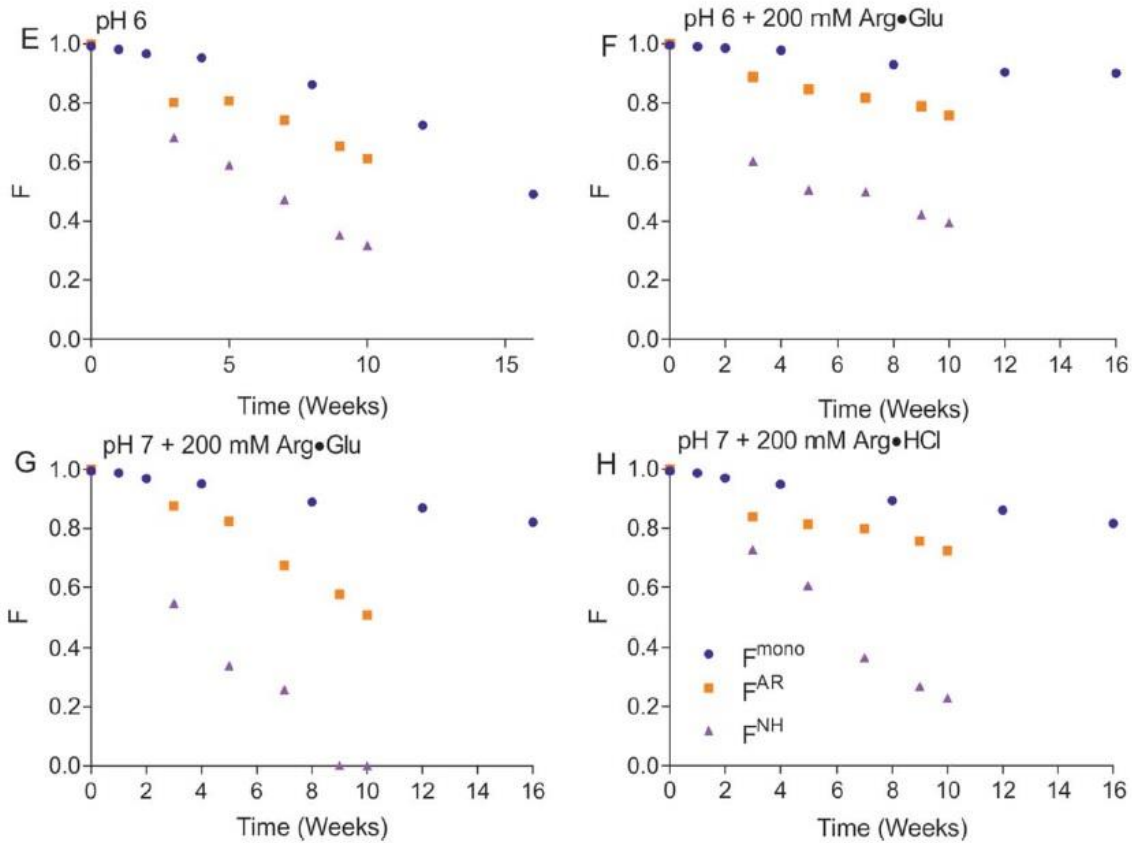
Figure 3.3: Representation of NMR long-term data, describing changes in monoclonal antibodies in the analysed formulations, adapted from (Kheddo, et al., 2016, p. 1248).

Figures 3.2 and 3.3 above show alterations in the analysed monoclonal antibody formulations in various arginine glutamate concentrations with time. In the figures 3.3, F represented changes in stability over time. As indicated by the observed trends addition of 200 mM of arginine glutamate substantially increased storage stability but only at pH 6, Figures 3.3E and F. As evident from the figures 3.3G and H at pH 7 introduction of arginine glutamate was similar to the addition of arginine hydrochloride. Long term stability was outlined on the figures 3.3G and F. It can be stated that arginine glutamate was not as effective as arginine hydrochloride in providing long-term protein stabilisation.

In addition to the assessment above of formulation stability, proton NMR was employed to measure translational self-diffusion and rheometry. The results generated by Kheddo and co-workers indicated that protein aggregation could be reduced with the addition of arginine-glutamate to concentration dependent formulations (Kheddo, et al., 2016, p. 1249). The obtained stabilisation trends were supported by other publications (Golovanov, et al., 2004, p. 8933) (Hautbergue & Golovanov, 2008, p. 336).

3.2 Application of orthogonal techniques in Characterisation of stress-induced antibody aggregates

The work described by Hamrang and co-workers on the application of orthogonal techniques for the analysis of stress-induced distributions and morphological changes in protein aggregates complement the work described by Kheddo and co-workers (Hamrang, et al., 2015, p. 2473) and discussed previously. In the work by Hamrang and co-workers it was suggested that physical methods of analysis could be used to determine correlations between thermal stress, particle concentration, aggregate morphology and distribution of particle sizes. In order to establish if there is any effect of thermal stress on concentration of sub-visible particles the research used two different concentrations of monoclonal antibodies, 1 and 10 mg/ml, in both treated and non-treated (temperature changes, changes in pH and buffer addition) monoclonal antibodies. Dynamic light scattering data showed lower number of detected protein particles in non-treated samples of monoclonal antibodies, compared with the corresponding samples that were stressed overnight at approximately $60^{\circ}C$.

Hamrang et al then further investigated the correlation between distribution of particles and thermal stress. The corresponding particle size distributions were obtained using both MFI and RICS methods based on monoclonal antibodies. Subsequent statistical analysis of the data suggested that there were statistically significant differences between size distributions in the analysed particles, suggesting that thermal stress had an effect on the distribution of the thermally treated protein particles as expected. Finally, Hamrang and co-workers carried out a series of experiments aiming to characterise particle concentrations in terms of freeze-thaw treatment. Particle counts generated from the corresponding MFI analysis were compared with the generated freeze-thaw treatments that manifested substantial differences in sizes of the generated particles and their number. A considerable concentration dependent correlation was observed in the case of applying uncontrolled freeze-thaw stress. Thus, it was observed that in the case of 10 mg/mL protein samples a higher number of particles was observed when compared to the corresponding monoclonal antibody 1 mg/mL samples. The results obtained by Hamrang and co-workers complement previously discussed publication by Kheddo and co-workers in terms of monoclonal antibody stability at various conditions (Hamrang, et al., 2015, p. 2477).

By applying the analysis techniques outlined in the methodology section, it was possible to establish the culture viability effect that introduction of arginine glutamate has on both cell lines as well as primary fibroblast cells. This study indicated that it was necessary to investigate specific correlation between osmolality and viability of cell lines (Kheddo, et al., 2016, p. 91). In order to produce osmolalities ranging from 280 to 525 mOsm/kg, various excipients, such as arginine glutamate, sodium chloride, arginine chloride and sodium glutamate were employed. These salts were added to the corresponding cell containing solutions and results were obtained in the form of percentages of surviving cells. The results are summarised in Figure 3.4 below:
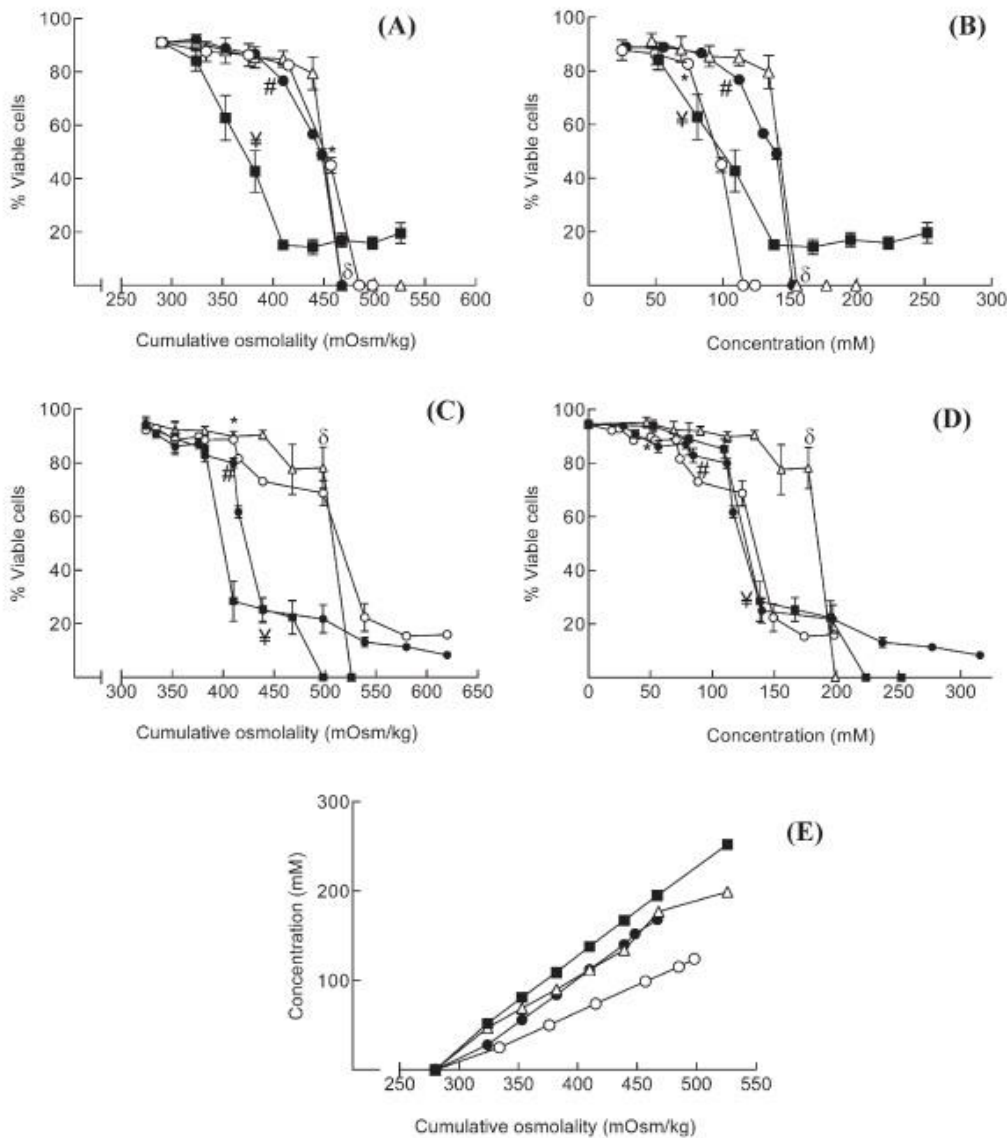
Figure 3.4: The correlations between percentages of surviving cells and osmolality of the tested solutions (Kheddo, et al., 2016, p. 91) Trends were presented as correlations between percentage of viable cells versus cumulative osmolality (A, C) or solution concentration (B, D). The correlation between the tested salt concentrations and cumulative osmolality was represented on the figure E. In figure 3.4 above, the corresponding correlation between concentration of the introduced salts and the observed osmolality levels are outlined in plot E. In turn, culture viability was established with the aid of a flow cytometer and is presented in the format of the proportion of cells that survive. Correlations between the percentage of surviving cells and osmolality are outlined in figure 3.4A, while the effect of solution concentration on culture viability is represented in figure 3.4B.

While assessing culture viability as represented in figure 3.4, the baseline level of viability was established as 90% of surviving cells. Looking at the data in figure 3.4, from the trends presented it was observed that osmolarity increases with the addition of arginine glutamate, sodium chloride and sodium

glutamate and results in a reduction in culture viability to approximately 50% and rising osmolarity to a level of 450 mOsm/kg. In turn, implementation of arginine hydrochloride to change osmolality had a much more negative effect on culture viability with a reduction to 45% at osmolality levels of approximately 380 mOsm/kg.

Trends presented in figure 3.4B suggest that during the assessment on a mole of salt per mole basis it is possible to superimpose the cytotoxicity profiles of arginine glutamate and sodium glutamate, while addition of sodium chloride and arginine hydrochloride resulted in the highest impact on culture viability with reduction of viable cells below 50% at a concentration of 100 mM. Finally, the data presented in figure 3.4 suggested that arginine glutamate had the lowest impact on viability of culture. Nevertheless, a different pattern was observed in the case when human fibroblasts were cultured in the presence of arginine glutamate and the described above salts. For instance, according to the data presented in figure 3.4C and 3.4D, introduction of higher doses of reagents had a negative effect on culture viability (Kheddo, et al., 2016, p. 91).

3.3 Investigation of dynamical allostery effects in mutated scFV antibody fragments and stabilising/destabilising effects

In the study reported by Ramaprasad and co-workers, various computational methods were employed to investigate dynamical allostery observed in mutated scFv antibody fragments as well as the corresponding stabilising and destabilising effects that influence the integrity of the analysed protein (Ramaprasad et al., 2017, p. 2). Previous reports in the area have identified that, in many cases, mutated scFv antibodies shared similar activity (Miller, et al., 2010, p. 550). From a structural perspective the corresponding mutants contained a heavy and a light domain, connected through a flexible linker composed of 116-132 amino acid residues. As indicated and discussed in the previous sections of this thesis, dynamical allostery may be established through MSF changes, associated with external perturbations with subsequent comparison of response/perturbation profiles (Miller, et al., 2010, p. 550).

3.4. Oxm self-assembles into fibrillar nanostructures

Immediately after thioflavin was applied to Oxm, there was a characteristic fluruoscece emmited at 480 nm confirming adoption of of crossβsheet conformation as in the figure below.
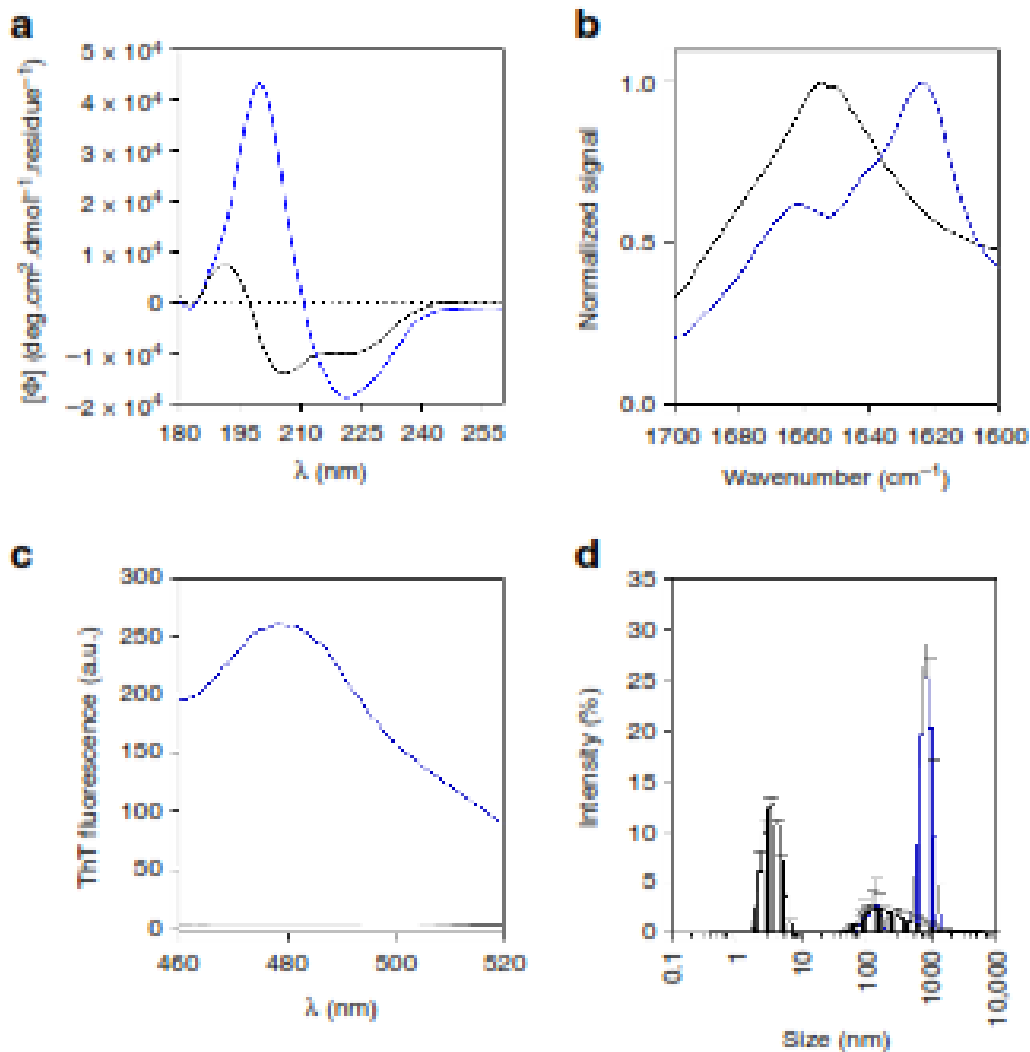
Structural property of free and fibrillar Oxm, Adapted from (Ouberai et al., 2017, P. 3).

Structural properties of free and fibrillar Oxm. a–d Free (black) and fibrillar (blue) Oxm at 1 mg mL−1 in 0.09% saline. Far-UV CD a, ATR-FT-IR, b and ThT emission spectra c, and DLS analysis (Error bars represent standard deviations obtained from eight measurements of the same sample) d

However, there was no omission observed in the presence of a freshly prepared Oxm. In contrast, the fibrillar Oxm sample contained significantly larger species, with a mean diameter of 825 nm. The group tends to show that Oxm can as well be converted, under very mild conditions and with a high yield, into fibrillar nanostructures displaying amyloid-like features. In figure 2c abover, there was a clear shift in of the size of species present in the solution.

3.5. Protein concentration effects on albumin solution viscosity

Perturbations in proteins (particularly mutations of specific residues) resulting in stabilising and destabilising effects are also expected to change rheology of the corresponding protein solutions. Thus, Goncalves and co-workers subsequently showed that the rheology of human albumin solutions was

substantially affected by concentration of the protein in solution. The results describing solution rheology experimentation are summarised in figure 3.6 below.
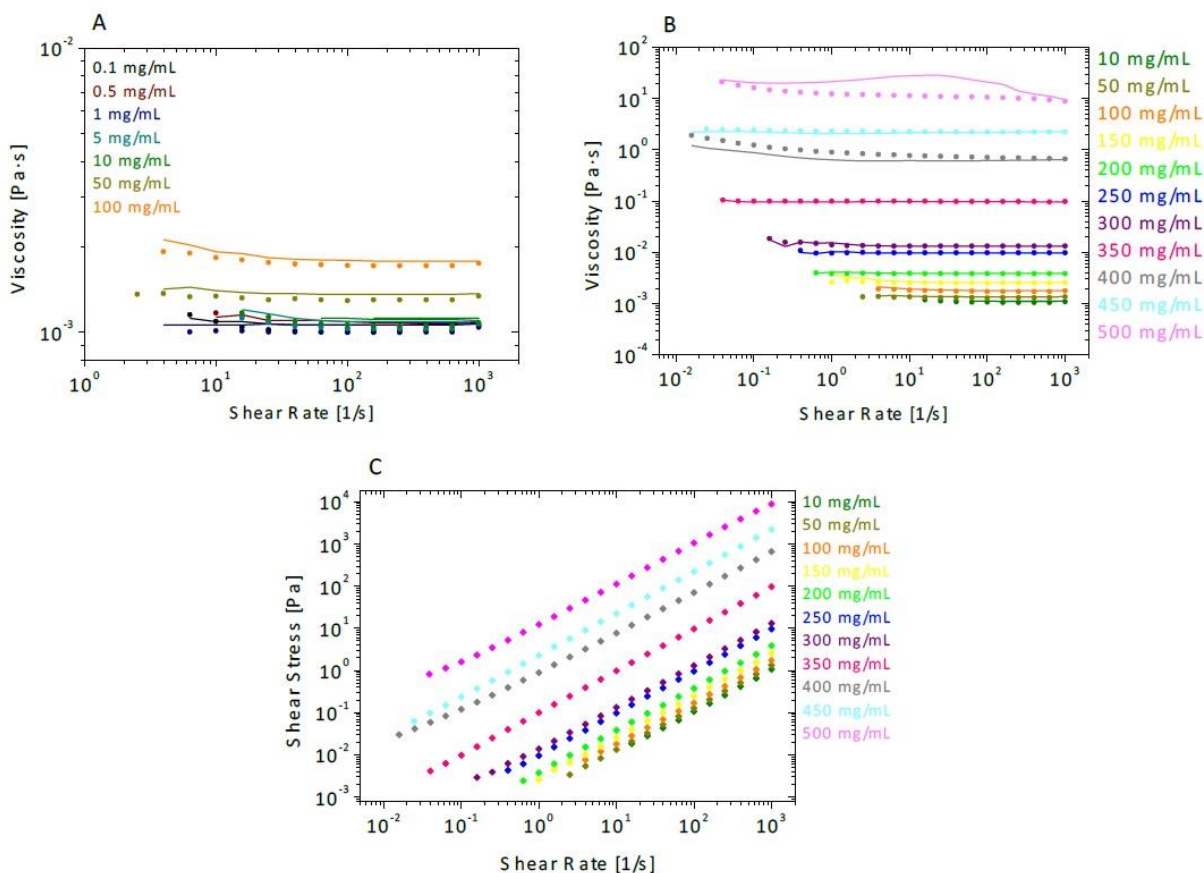
Figure 3.6: Rheology data of human recombinant albumin solutions, adapted from (Goncalves, et al., 2013, p. 10)

In figure 3.6A above, rheology investigations on recombinant albumin samples were carried out at protein concentrations ranging from 0.1 to 100 mg/mL. In turn, in figure 3.6B protein concentrations ranging from 10 mg/mL to 500 mg/mL were used. In figure 3.6C, flow curves describing the rheology of albumin solutions with concentrations ranging from 10 mg/mL to 500 mg/mL are shown (Goncalves, et al., 2013, p. 10).

Based on the data represented in figure 3.6, it can be seen that solutions of recombinant albumin manifest constant sheer viscosities at shear rates rising from 0.01 to 1000 s^{-1}. In turn, a linear increase in the shear stress was observed with the application of higher shear rates as may be expected. Additionally, increases in viscosity were observed with increasing concentrations of the tested protein solution. Correlations between protein concentrations and viscosity of the corresponding solutions as well as correlations between protein concentrations and peak areas were therefore investigated and these data are outlined in figure 3.7 below.
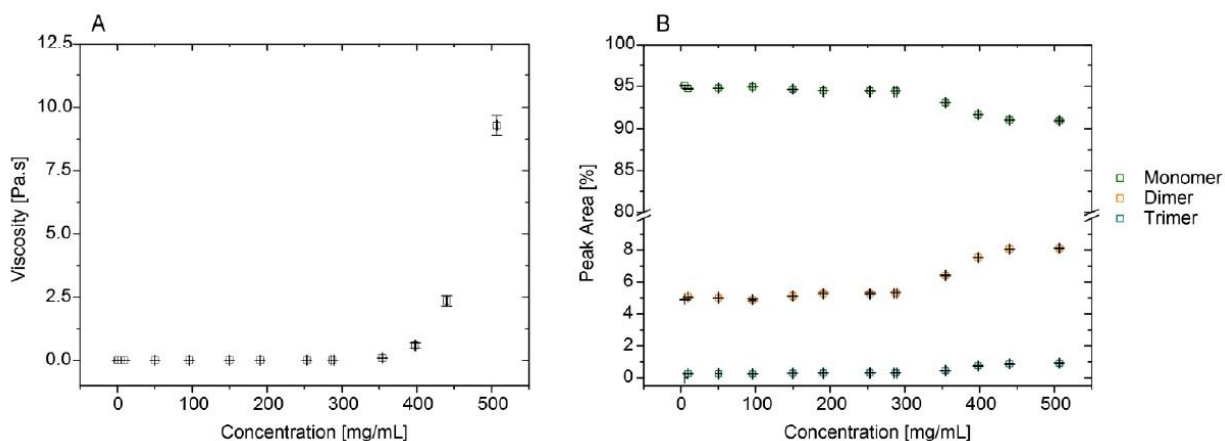
Figure 3.7: Correlation plots between protein concentration, viscosity and peak area, adapted from (Goncalves, et al., 2013, p. 10).

In figure 3.7 above it can be seen that viscosity of protein solutions increased with increase in the concentration of the tested protein as expected. Thus, chromatography experiments suggested that higher aggregation levels were detected at higher protein concentrations (Goncalves, et al., 2013, p. 10) in agreement with other studies.

3.5 Aggregation kinetics of a pH-induced switch of human glucagon-like peptide 1

In addition to aggregation due to increases in protein concentration, work by Zapadka and co-workers indicated that aggregation kinetics were affected by changes in pH of the corresponding protein solutions (Zapadka, et al., 2016, p. 2). By application of the experimental procedures outlined in the methods section, it was possible to describe aggregation kinetics of GLP-1 and present the findings as correlations between peptide concentrations at various pH levels. Zapadka and co-workers were also able to describe size distributions of the analysed species in the prepared protein samples (Zapadka, et al., 2016, p. 2). The obtained results are summarised in figure 3.8 below.
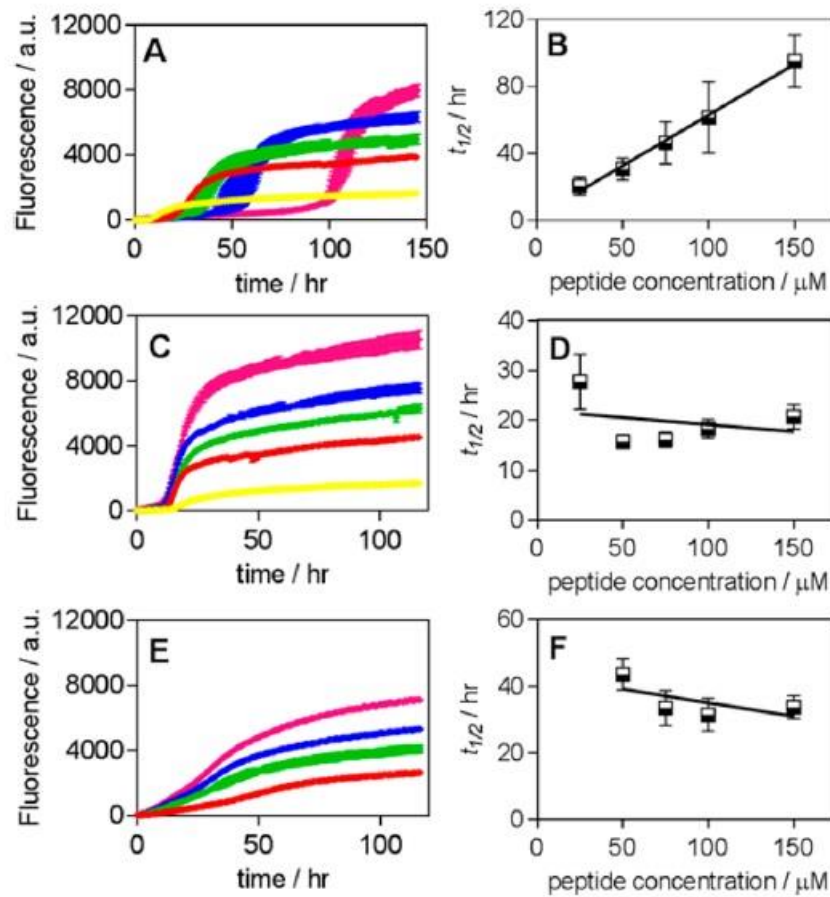
Figure 3.8: GLP-1 aggregation kinetics represented as a function between various pH levels and protein concentrations, adapted from (Zapadka, et al., 2016, p. 3)

In figure 3.8 above, aggregation kinetics of GLP-1 at pH 7.5 are presented in figure 3.8A and 3.8B, at pH 7.7 in figures 3.8C and 3.8D, and at pH 8.2 in figures 3.8E and 3.8F. Figures 3.8A, C and E represent fibrillation traces of GLP-1 that was followed by fluorescence of the obtained samples at various concentrations of GLP-1. In all concentrations triplet runs describing the behaviour of the analysed samples were obtained. Finally, in figures 3.8D, E and F the corresponding correlation between GLP-1 concentration and aggregation half-time ($t_{1/2}$) is described. Standard deviations that corresponded to the established aggregation kinetics parameters were outlined in the form of errors bars (Zapadka, et al., 2016, p. 3).
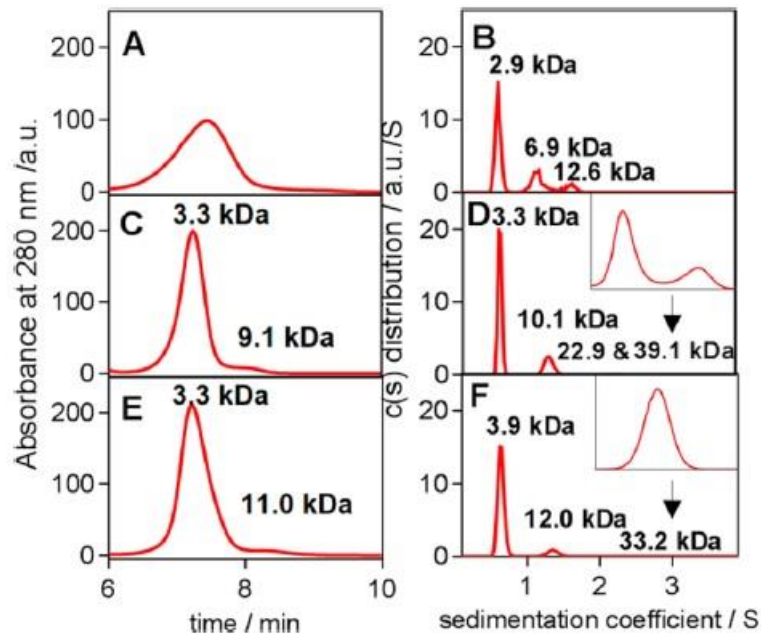
Figure 3.9: Representation of size distributions of protein samples at various pH levels, adapted from (Zapadka, et al., 2016, p. 3)

In figure 3.9 above, size distributions were assessed at various pH values, including 7.5 (figure 3.9A and B), 8.0 (figure 3.9C and D) and 8.5 (figure 3.9E and F). The right-hand column represents the sedimentation results obtained by using AUC analysis of sedimentation velocity while the left-hand column outlines size distribution data based on AF4 results (Zapadka, et al., 2016, p. 3).

4.0 General Discussion

Monoclonal antibody-based drugs have been established as novel and highly effective type of modern pharmaceutical product that have the potential to substantially increase the efficiency of the available treatment methods and develop novel methods of treatment for a variety of diseases. Publications, discussed in the work presented here, as well as the corresponding experimental findings outlined in these publications, indicate that various instrumental methods of analysis could be employed to characterise monoclonal antibody-based formulations, investigate interactions of individual proteins and draw conclusions regarding possible agglomeration as the result of changes in concentration, temperature and pH of the analysed solution (Kheddo, et al., 2016, p. 1246) (Kheddo, et al., 2016, p. 88) (Zapadka, et al., 2016, p. 2) (ScienceDirect, 2018).

Proton NMR spectroscopy was found to be highly effective in the characterisation of protein interactions in monoclonal antibody-based formulations containing various concentrations of arginine glutamate and arginine hydrochloride (Kheddo, et al., 2016, p. 1257) (Kheddo, et al., 2016, p. 88). In addition to the application to proton NMR for the characterisation of monoclonal antibody formulations, literature sources (Hamrang, et al., 2015, p. 2475) suggest that characterisation of the corresponding stress-induced protein aggregates along with determination of size distributions and description of morphological changes may be conducted with the aid of orthogonal analysis techniques, including combinations of thermal stress protocols, freeze-thaw protocols, confocal microscopy and application of dynamic light scattering (Hamrang, et al., 2015, p. 2475). Kheddo and co-workers showed that introduction of arginine glutamate (section 2.3) as well as arginine-based salts had a positive effect on the stabilisation of the corresponding monoclonal antibody-based formulations (Kheddo, et al., 2016, p. 1257) (Kheddo, et al., 2016, p. 88). However, when considering the established effects of arginine glutamate as well as sodium chloride on viability of cells (i.e. addition during cell culture, not just during final formulation of the product) it was determined that with the introduction of higher concentrations of these additives, culture viability was reduced. In turn, analysis of the observed viability reduction indicated that the reduced culture viability was primarily associated with osmolality changes with no cell mortality due to inflammation. These findings, as well as the corresponding techniques employed during the assessment of culture viability, may subsequently be extrapolated to other analytical studies (Kheddo, et al., 2016, p. 88) (Kheddo, et al., 2016, p. 1257).

The work by Kheddo and co-workers and that describe by Hamrang and co-workers were focused on the application of different methods of instrumental analysis in the assessment of culture viability as well as characterisation of physical processes placed upon monoclonal antibodies during their formulation and introduction into biological systems (Kheddo, et al., 2016, p. 88) (Kheddo, et al., 2016, p. 1257) (Hamrang, et al., 2015, p. 2473). The experimental finding presented here also suggest

that protein stabilising and destabilising effects were of paramount importance to the assessment of dynamical allostery processes taking place in mutated scFv antibody fragments (Ramaprasad et al., 2017, p. 1). Thus, Hamrang and co-workers showed that even minor alterations in the analysed antibody fragments had a considerable effect on the resulting agglomeration of proteins in the respective formulations. Similarly, as outlined in the work by Kheddo and co-workers and of Hamrang and co-workers, it was determined that physical methods of analysis were highly effective in monitoring and undertaking stability assessments as well as determination of conformational changes to provide an indication of the most significant factors affecting stabilisation of monoclonal antibody formulations (Kheddo, et al., 2014, p. 127) (Kheddo, et al., 2016, p. 88) (Kheddo, et al., 2014, p. 127) (Ramaprasad et al., 2017, p. 3) (Hamrang, et al., 2015, p. 2473).

The remaining publications presented and analysed in this thesis were focused on the determination of the effects that changes in concentration of proteins had on viscosity of albumin formulations and investigations of the effects that changes in pH had on protein agglomeration and stability. Both publications presented are fundamentally important as they explore and describe the behaviour of proteins under various physiological conditions and formulations relevant to the biopharmaceutical industry. The corresponding findings may subsequently be extrapolated to monoclonal antibody-based formulations with the possibility of developing novel, more stable and more potent drugs (Goncalves, et al., 2013, p. 1) (Zapadka, et al., 2016, p. 2). Considering the effect that protein concentration had on alteration in viscosity of the final protein solution, Goncalves and co-workers indicated that the biophysical characteristics and correlations could be expanded to the description of the rheological behaviour as well as the content of protein species in both dilute, as well as highly concentrated, albumin solutions (Goncalves, et al., 2013, p. 2). This is particularly important as in most cases biotherapeutic proteins are formulated at high concentrations but many measurements on aggregation of such formulations are undertaken on diluted samples that can result in a changing of the aggregates present. Thus, approaches such as NMR and rheology that can study the protein solutions in the final formulation and concentration are likely to unravel and reveal insights into the behaviour of such proteins that is not revealed when analysing these in diluted samples.

Analysis of the shear rheology results suggests that the observed patterns followed a Newtonian behaviour. The observed trends and correlations can be explained by the presence of polysorbate-80 in the protein solutions. Introduction of this surfactant is common in pharmaceutical practice and its addition results in negation of rheological properties as well as surfactant tension that is expected with the addition of water and formation of protein films on the interface between air and water (Goncalves, et al., 2013, p. 2).

The results obtained in the study by Goncalves and co-workers clearly demonstrated that protein concentration had an effect on the viscosity which increased with protein concentration (Goncalves, et al., 2013, p. 2). In particular, this study established that the highest viscosity increase was detected in cases when protein concentration was increased from 250 to 500 mg/mL. At the concentration of approximately 500 mg/ml, the highest sample viscosity was observed. As mentioned in the previous sections, the indicated patterns could be employed in the design of monoclonal antibody-based formulations and design more stable and more concentrated biopharmaceutical formulations but that can ensure that viscosity does not become problematic or 'too high' (Goncalves, et al., 2013, p. 3). The findings are further supported by the corresponding data obtained using high pressure size exclusion chromatography. It was initially presumed that increases in viscosity were associated with protein agglomeration through protein-protein interactions. Whilst this may indeed be the case, the observed viscosity was affected by additional environmental factors including temperature of the solution, flow rate and nature of the mobile phase buffer (Goncalves, et al., 2013, p. 3).

The work reported by Goncalves and co-workers is of importance to the development of modern biopharmaceutical products because principles applied to the analysis of albumin formulations can be expanded to monoclonal antibody-based formulations and other types of pharmaceutical products where protein agglomeration is observed (Goncalves, et al., 2013, p. 3). In summarising the experimental data that were obtained from this research, it should be indicated that at high protein concentrations, in addition to protein-protein interactions, additional formulation and storage/environmental specific factors should be taken into consideration during the assessment of correlations between viscosity and protein concentration. Consequently, during the development of monoclonal antibody-based drugs, factors such as possible interaction areas in the globular structure of proteins and their volume should be considered (Goncalves, et al., 2013, p. 3).

Looking at specific cases of developing monoclonal antibody formulations, Kheddo and co-workers indicated that undesired high viscosity in various mAb formulations may considerably promote reversible self-association of the corresponding proteins which may result in irreversible structural changes at high concentrations (Kheddo, et al., 2016, p. 1252). Irreversible agglomeration may considerably reduce the activity of the formulations and for this reason implementation of analytical monitoring and analysis techniques is essential in order to maintain the initial product activity and prevent agglomeration. Nuclear magnetic resonance spectroscopy was found to be a highly potent and versatile analytical technique that may be employed in various cases when speed and precision are required. Kheddo and co-workers showed that this technique was highly sensitive towards analysis of monoclonal antibodies and determination of possible formation of agglomerates (Kheddo, et al., 2016, p. 1252). Nevertheless, sample preparation conditions and considerations need to be followed in order

to obtain data of adequate accuracy. These conditions include specific pH of the sample, temperature of the media and possible presence of additives. It was shown that proton NMR was highly effective during the analysis and characterisation of unlabelled and large monoclonal antibody proteins. The research indicated that the corresponding production of NMR data may be carried out automatically and conclusions on possible formation of agglomerates could be drawn based on maximisation of the signal intensity. It should also be noted that the application of traditional assays (e.g. testing of new drugs determined based on qualitative structure-activity relationships) may be highly beneficial at early stages of the analysis of monoclonal antibody-based formulations and the implementation of NMR techniques may be beneficial at later stages when detailed understanding of protein-protein and protein-solvent interactions are required (Kheddo, et al., 2016, p. 1252).

In addition to the 1D NMR signals, Kheddo and co-workers suggested that NMR long-range data was also important in the assessment of formulation stabilities and optimisation of formulations. The NMR spectroscopy approach may be employed to determine various NMR measurements, including relaxation rates and translational diffusion data. The work in the publication by Kheddo and co-workers complements previously reported literature findings on correlations between viscosity of protein and concentration. The unique feature of NMR spectroscopy was to provide highly diverse information, covering *in situ* sample behaviour. Also, the discussed analytical technique can be employed to characterise conformational states of the analysed proteins, quantities of both monomeric and oligomeric protein species in the solution as well as complement corresponding chromatography data and light scattering. The data describe in the here highlights the importance of investigation into the possibility of using other instrumental methods of analysis in the characterisation of monoclonal antibodies (Kheddo, et al., 2014, p. 129) (Kheddo, et al., 2016, p. 89) (Kheddo, et al., 2014, p. 127) (Hamrang, et al., 2015, p. 2473) (Ramaprasad et al., 2017, p. 3).

5.0 Conclusions

In analysing the data and papers presented here it is important to note that the formulation of antibodies for use in the clinic is the last step between production of the drug and administration into humans. Being able to stabilise an antibody and provide it in a suitable form for delivery is therefore an important part of the whole manufacturing of such drugs. A range of physical and chemical methods can be employed to study conformational changes in the corresponding monoclonal antibody-based formulations and how changes to formulations impact on various attributes indicative of antibody stability (e.g. aggregation, fragmentation, activity). The outlined work detailed here suggests that characterisation of monoclonal antibody-based formulations could effectively be enhanced with the aid of proton NMR spectroscopy. It can also be suggested that in addition to the discussed stable monoclonal antibodies, the corresponding NMR techniques may also be expanded to other less stable materials to aid in formulation development.

In addition to proton NMR spectroscopy, the work described here has shown that various analytical techniques may also be used to complement analysis of monoclonal antibodies and determine aggregate size ranges in response to the application of various external factors. For example, by applying the RICS technique to the generation of particle size data it is possible to obtain information not biased to specific range of particle sizes, which highlights the importance of the corresponding technique in sizing of protein-based aggregates. From the data presented it can also be concluded that sizing characterisation of monoclonal antibody-based formulations is of paramount importance for adequate description of various novel and highly perspective pro-drugs.

In addition to investigating the impact of excipients on the final formulation of antibodies, the work presented here investigated the ability of excipients to maintain the stability of a monoclonal antibody whilst in culture in the cell culture media and the impact on the culture viability and protein product stability. Assessing the behaviour of both adherent and non-adherent cell lines the findings of this work indicated that in all cases similar toxicity patterns were observed upon introduction of arginine glutamate. Thus, it can be concluded that changes in toxicity were primarily dictated by osmolarity changes. The data also suggests that non-inflammatory processes dictate cellular death upon introduction of sodium chloride. Comparing the activity of arginine glutamate with sodium chloride it was found that both compounds manifest similar cellular toxicity but at different concentrations. Introduction of both osmolarity-forming compounds is not expected to result in inflammations. Analysis of the stabilising and destabilising effects in both normal and mutated ScFv antibodies suggested that the corresponding responses were based on the nature of the perturbations taking place in the analysed formations. Locations of specific perturbations are expected to vary from protein to protein, however

stabilisation of individual fragments is expected to take place as the result of interaction with solute molecules.

The studies on human recombinant albumin highlight the importance of protein-protein interactions during formulation of the corresponding pharmaceutical product. The results of studies that were carried out on recombinant human albumin and the corresponding correlations between protein concentration, viscosity and agglomeration can potentially be expanded to monoclonal antibodies during the development of mAb-based formulations. Finally, analysis of the kinetics of GLP-1 aggregation was monitored at pH 7.5. It was observed that the lag time increased with increases in the peptide concentration. For this reason, it can be concluded that formation of unexpected and uncharacterised oligomeric species took place at the indicated pH level, which promoted further agglomeration of monomers. Development of the described agglomeration and aggregation pathway may lead to the transformation of the initial off-pathway oligomers into the corresponding on-pathway oligomers with subsequent development of fibrils. It is clear that due to intrinsic structural features of GLP-1, fibrils that are formed at pH=7.5 are unstable and short. Subsequent increase in the pH level results in the disruption of the formed bonds and development of aggregation pathways proceeding according to traditional nucleation mechanisms.

Collectively, the discussed papers and work presented here reinforces the fact that the development of monoclonal antibody-based drugs is a highly challenging, but perspective field of the modern pharmaceutical industry. Thus, implementation of monoclonal antibodies in the treatment of diseases has the potential to considerably increase the effectiveness of the employed treatment and reduce costs.

Reference list

Alfaleh, M., Jones, M., Howard, C. & Mahler, S., 2017. Strategies for selecting membrane protein-specific antibodies using phase display with cell-based planning. *Antibodies,* 6(10), pp. 1-19.

Arakawa, T. et al., 2007. Suppression of protein interactions by arginine: a proposed mechanism of arginine effects. *Biophysics and chemistry,* Volume 127, pp. 1-8.

Bruno, V., Battaglia, G. & Nicoletti, F., 2011. The advent of monoclonal antibodies in the treatment of chronic autoimmune diseases. *Neurological Science,* 3(January), pp. 283-288.

Buell, A., Dobson, C. & Knowles, T., 2014. The physical chemistry of the amyloid phenomenon: thermodynamics and kinetics of filamentous protein aggregation. *Essays in Biochemistry,* Volume August, pp. 11-39.

Bye, J., Platts, L. & Falconer, R., 2014. Biopharmaceutical liquid formulation: a review of the science of protein stability and solubility in aqueous environments. *Biotechnology Letters,* Volume 36, pp. 869-875.

Byrne, P., 2013. Role of monoclonal antibodies in the treatment of asthma. *Can Respir J.,* 20(1), pp. 23-25.

Cavanagh, J., Fairbrother, W., Palmer, A. & Skelton, N., 2006. *Protein NMR Spectroscopy: Principles and Practice.* 2nd ed. London: Academic Press.

Chiti, F. & Dobson, C., 2006. Protein misfolding, functional amyloid, and human disease. *Annual Reviews in Biochemistry,* Volume 75, pp. 333-366.

Clark, D. & Pazdernik, N., 2015. *Biotechnology.* 2nd ed. London: Academic Cell.

Farhadfar, N. & Litzow, M., 2016. New monoclonal antibodies for the treatment of acute lymphoblastic leukemia. *Leukemia Research,* 49(October), pp. 13-21.

Ferri, N. et al., 2016. Pharmacokinetics interactions of monoclonal antibodies. *Pharmacological Research,* 111(September), pp. 592-599.

Golovanov, A., Hautbergue, G., Wilson, S. & Lian, L., 2004. A simple method for improving protein solubility and long-term stability. *Journal of American Chemical Society,* Volume 126, pp. 8933-8939.

Goncalves, A. et al., 2013. The effect of protein concentration on the viscosity of a recombinant albumin solution formulation. *The Royal Society of Chemistry,* Volume 1-3, pp. 1-16.

Hamrang, Z. et al., 2015. Characterisation of Stress-Induced Aggregate Size Distributions and Morphological Changes of a Bi-Specific Antibody Using Orthogonal Techniques. *Journal of Pharmaceutical Sciences,* Volume 104, pp. 2473-2481.

Hautbergue, G. & Golovanov, A., 2008. Increasing the sensetivity of cryoprobe protein NMR experiments by using the sole low-conductivity arginine glutamate salt. *Journal of Magnetic Resonance,* Volume 191, pp. 335-339.

Kheddo, P. et al., 2016. Characterizing monoclonal antibody formulations in arginine glutamate solutions using 1H NMR spectroscopy. *MABS,* 8(7), pp. 1245-1258.

Kheddo, P. et al., 2016. The effects of arginine glutamate, a promising excipient for protein formulation, on cell viability: Comparisons with NaCl. *Toxicology in Vitro,* Volume 33, pp. 88-98.

Kheddo, P. et al., 2014. The effect of arginine glutamate on the stability of monoclonal antibodies in solution. *International Journal of Pharmaceutics,* 473(1-2), pp. 126-133.

Loveday, S., Creamer, L., Singh, H. & Rao, M., 2007. Phase and rheological behavior of high-concentration colloidal hard-sphere and protein dispersions. *Journal of Food Science,* 72(7), pp. R101-R107.

Merck KGaA, 2015. *An Introduction to Antibodies and Their Applications,* Darmstadt: Merck KGaA.

Miller, B. et al., 2010. Stability engineering of scFvs for the development of bispecific and multivalent antibodies. *Protein Engineering, Design and Selection,* 23(7), pp. 549-557.

Minton, A., 2012. Hard Quasispherical Particle Models for the Viscosity of Solutions of Protein Mixtures. *Journal of Physical Chemistry,* 116(31), pp. 9310-9315.

Ordonez, N., 1999. The immunohistochemical diagnosis of epithelial mesothelioma. *Human Pathology,* Volume 30, pp. 313-323.

Ren, C. et al., 2017. Development of monoclonal antibodies against Sj29 and its possible application for schistosomiasis diagnosis. *International Journal of Infectious Diseases,* 61(August), pp. 74-78.

Santos, R. & Galvao, V., 2017. Monoclonal Antibodies Hypersensitivity: Prevalence and Management. *Immunology and Allergy Clinics of North America,* 37(4), pp. 696-711.

ScienceDirect, 2018. *ScienceDirect.* [Online]
Available at: http://www.sciencedirect.com/
[Accessed 23 February 2018].

Singam, A., Uddin, S., Casas-Finet, J. & Jacobs, D., 2017. Decomposing dynamical allosterity in mutated scFv antibody fragments into stabilizing and destabilizing effects. *ASC publications,* pp. 1-8.

Smith, G., 1985. Filamentous fusion phage: Novel expression vectors that display cloned antigens on the virion surface. *Science,* Volume 228, pp. 1315-1317.

Teo, E., Chew, Y. & Phipps, C., 2016. A review of monoclonal antibody therapies in lymphoma. *Critical Reviews in Oncology/Hematology,* 97(January), pp. 72-84.

Watts, J., Fowler, L., Whitton, P. & Pearce, B., 2005. Release of arginine, glutamate and glutamine in the hippocampus of freely moving rats: Involvement of nitric oxide. *Brain Research Bulletin,* 65(6), pp. 521-528.

Yamada, T., Yamamoto, K., Ishihara, T. & Ohta, S., 2017. Purification of monoclonal antibodies entirely in flow-through mode. *Journal of Chromatography B,* 1061-1062(September), pp. 110-116.

Zapadka, K. et al., 2016. A pH-Induced Switch in Human Glucagon-like Peptide-1 Aggregation Kinetics. *Journal of the American Chemical Society,* Volume November, pp. 1-7.

Zheng, J.Y. and Janis, L.J., 2006. Influence of pH, buffer species, and storage temperature on physicochemical stability of a humanized monoclonal antibody LA298. *International Journal of Pharmaceutics*, *308*(1-2), pp.46-51.